

Electronic Theses and Dissertations, 2004-2019

2015

Mathematical Modeling of Carbon Removal in the A-Stage Activated Sludge System

Thomas Nogaj
University of Central Florida

 Part of the [Environmental Engineering Commons](#)
Find similar works at: <https://stars.library.ucf.edu/etd>
University of Central Florida Libraries <http://library.ucf.edu>

This Doctoral Dissertation (Open Access) is brought to you for free and open access by STARS. It has been accepted for inclusion in Electronic Theses and Dissertations, 2004-2019 by an authorized administrator of STARS. For more information, please contact STARS@ucf.edu.

STARS Citation

Nogaj, Thomas, "Mathematical Modeling of Carbon Removal in the A-Stage Activated Sludge System" (2015). *Electronic Theses and Dissertations, 2004-2019*. 1161.
<https://stars.library.ucf.edu/etd/1161>

MATHEMATICAL MODELING OF CARBON REMOVAL IN THE A-STAGE
ACTIVATED SLUDGE SYSTEM

by

THOMAS M. NOGAJ
B.S. University of Illinois, 1983
M.S. University of Iowa, 1985

A dissertation submitted in partial fulfillment of the requirements
for the degree of Doctor of Philosophy
in the Department of Civil, Environmental and Construction Engineering
in the College of Engineering and Computer Science
at the University of Central Florida
Orlando, Florida

Spring Term
2015

Major Professor: Andrew A. Randall

© 2015 Thomas M. Nogaj

ABSTRACT

This research developed a dynamic activated sludge model (ASM) to better describe the overall removal of organic substrate, quantified as chemical oxygen demand (COD), from A-stage high rate activated sludge (HRAS) systems. This dynamic computer model is based on a modified ASM1 (Henze et al., 2000) model. It was determined early in the project that influent soluble COD, which is normally represented by a single state variable in ASM1, had to be subdivided into two state variables (S_{Bs} and S_{Bf} , or slow and fast fractions) to simulate the performance of A-stage systems. Also, the addition of state variables differentiating colloidal COD from suspended COD was necessary due to short hydraulic residence times in A-stage systems which do not allow for complete enmeshment and bioflocculation of these particles as occurs in conventional activated sludge systems (which have longer solid retention times and hydraulic retention times). It was necessary to add several processes (both stoichiometry and kinetic equations) to the original ASM1 model including heterotrophic growth on both soluble substrate fractions and bioflocculation of colloidal solids. How to properly quantify heterotrophic growth on S_{Bs} and S_{Bf} resulted in two separate approaches with respect to process kinetic equations. In one approach the S_{Bf} was metabolized preferentially over S_{Bs} which was only utilized when S_{Bf} was not available. This is referred to as the Diauxic Model. In the other approach S_{Bf} and S_{Bs} were metabolized simultaneously, and this is referred to as the Dual Substrate Model. The Dual Substrate Model calibrated slightly better than the Diauxic Model for one of the two available pilot studies data sets (the other set was used for model verification).

The Dual Substrate A-stage model was used to describe the effects of varying specific operating parameters including solids retention time (SRT), dissolved oxygen (DO), influent COD and temperature on the effluent COD:N ratio. The effluent COD:N ratio target was based on its suitability for a downstream nitrite shunt (i.e. nitrification/denitrification) process. In the downstream process the goal is to eliminate nitrite oxidizing bacteria (NOB) from the reactor while selecting for ammonia oxidizing bacteria (AOB). The results showed that a low SRT (<0.25 d) can produce high effluent substrates (S_B and C_B), and elevated COD:N ratios consistent with NOB out-selection downstream, the HRAS model was able to predict the measured higher fraction of C_B in the A-stage effluent at lower SRTs and DO concentrations, and to achieve the benefits of operating an A-stage process, while maintaining an effluent COD:N ratio suitable for a downstream nitrification/denitrification process, an A-stage SRT in the range of 0.1 to 0.25 d should be maintained.

This research also included an analysis of A-stage pilot data using stoichiometry to determine the bio-products formed from soluble substrate removed in an A-stage reactor. The results were used to further refine the process components and stoichiometric parameters to be used in the A-stage dynamic computer model, which includes process mechanisms for flocculation and enmeshment of particulate and colloidal substrate, hydrolysis, production of extracellular polymeric substances (EPS) and storage of soluble biodegradable substrate. Analysis of pilot data and simulations with the dynamic computer model implied (indirectly) that storage products were probably significant in A-stage COD removal.

To my wife Laura, my children Adam, Allyson, Kelsey, and Taylor, and my parents, for your
love and unwavering support over the years.

ACKNOWLEDGMENTS

I would like to thank Hampton Roads Sanitation District and Dr. Charles Bott for funding and providing the resources required to complete this doctoral research. I would also like to thank Mark Miller for his diligence in operating the HRSD A-stage pilot plant which provide essential data to support this doctoral research effort.

I would like to express my deep appreciation and gratitude to my primary advisor Dr. Andrew Randall for accepting the challenge associated with supporting an “older” graduate student. His flexibility and faith in me during the dissertation process enabled me to attend to life while also earning my Ph.D. He’s been motivating, encouraging, and enlightening. His patience and commitment to our weekly meetings proved to be an invaluable learning experience.

I would sincerely like to thank Dr. Jose Jimenez for initiating the contact with Dr. Bott which led to my involvement in developing the A-stage model. In addition, Dr. Jimenez made available supporting data which was vital to this doctoral research effort. I am grateful to Dr. Jimenez for his contribution, participation and dedication in support of this effort.

I would like to thank my committee members Drs. Steven Duranceau and Manoj Chopra for their guidance and thought-provoking suggestions.

I would also like to thank Drs. Sudhir Murthy, Imre Takacs, and Bernhard Wett for their guidance and support in developing the model. I would especially like to thank Dr. Imre Takacs for providing the dynamic solver used to analyze my model framework.

I would like to thank Dr. David Cooper who saw enough in me to give me this opportunity. Thank you Dr. Cooper.

I am deeply indebted to my family, my wife, my children and my parents, their love and support provided me with the energy to complete this journey.

Finally, I would like to acknowledge the innumerable sacrifices made by my wife Laura, who shoulder the day-to-day burden while allowing me to dedicate myself to pursue this doctoral degree. To you Laura I will always be grateful.

TABLE OF CONTENTS

LIST OF FIGURES	xiv
LIST OF TABLES	xviii
NOMENCLATURE	xxi
CHAPTER 1 INTRODUCTION	1
1.1 General	1
1.2 Research Objectives	2
1.2.1 Problem Statement.....	2
1.2.2 Statement of Research Objectives	3
CHAPTER 2 LITERATURE REVIEW	5
2.1 ASM Modelling.....	5
2.2 High Rate System for Carbon Removal.....	12
2.2.1 Wastewater Characterization.....	14
2.2.3 Storage Polymers.....	17
2.3 Stoichiometry	21
2.4 Mainstream Nitrogen Removal	22
2.4.1 Nitritation/Denitritation.....	24
2.4.2 Deammonification	26

2.4.3 Importance of C:N Ratio for B-stage nitrite shunt and/or anammox	28
2.5 Diauxic Growth	30
CHAPTER 3 MATERIALS AND METHODS	32
3.1 Data for Model Calibration and Validation.....	32
3.1.1 Pilot Scale Data Used for Model Calibration	32
3.1.2 Hampton Roads Sanitation District (HRSD) Pilot Data (used for A-stage Model Validation and Stoichiometric Analysis).....	36
3.1.3 Sample Collection and Monitoring	37
3.2 Model Development	41
3.3 Mathematical Model IDE and Calibration/Validation Procedure.....	44
3.3.1 A-stage Model Calibration using NO Dataset.....	45
3.3.2 A-stage Model Validation using HRSD Dataset	47
CHAPTER 4 MATHEMATICAL MODELING OF CARBON REMOVAL IN THE HIGH- RATE ACTIVATED SLUDGE SYSTEM: MODEL PRESENTATION AND APPLICATION	49
4.1 Introduction	49
4.2 Materials and Methods	51
4.2.1 Sample Collection and Monitoring	53
4.3 Results and Discussion.....	53

4.3.1 High-Rate Activated Sludge (HRAS) System for Carbon Removal.....	53
4.3.2 HRAS Model Matrix	60
4.3.3 Fate of the Influent Substrate (S_{BF} & S_{Bs}).....	65
4.3.4 Flocculation	69
4.3.5 Mathematical Model Calibration.....	70
4.4 Conclusions	76
 CHAPTER 5 MODELLING OF ORGANIC SUBSTRATE TRANSFORMATION IN THE HIGH-RATE ACTIVATED SLUDGE PROCESS	 77
5.1 Introduction	77
5.1.1 ASM1 Model	79
5.2 Materials and Methods	80
5.3 Modified Model Description	83
5.3.1 Fate of Soluble Substrate.....	83
5.3.2 Adsorption of Colloidal COD	85
5.3.3 EPS Production.....	87
5.3.4 Production of Storage Products	88
5.4 Results and Discussion.....	90
5.4.1 Model Calibration.....	90
5.4.2 Modified Model Validation.....	91

5.4.3 Effect of Influent Biomass.....	93
5.5 Conclusions	94
CHAPTER 6 MATHEMATICAL MODELING OF THE HIGH RATE ACTIVATED SLUDGE SYSTEM: OPTIMIZING THE COD:N RATIO IN THE PROCESS EFFLUENT	
	96
6.1 Introduction	96
6.2 Materials and Methods	98
6.3 Results and Discussion.....	100
6.3.1 Variable SRT	102
6.3.2 Variable Dissolved Oxygen.....	104
6.3.3 Effect of Storage.....	106
6.3.4 Temperature Effect on the COD:N Ratio.....	108
6.3.5 Optimal HRAS Operating Parameters.....	108
6.4 Conclusion.....	114
CHAPTER 7 USING A STOICHIOMETRIC MASS BALANCE APPROACH TO IDENTIFY SOLUBLE SUBSTRATE REMOVAL PATHWAYS IN THE HIGH RATE ACTIVATED SLUDGE PROCESS	
	115
7.1 Introduction	115
7.2 Objective	117

7.3 Materials and Methods	117
7.4 COD Mass Balance	123
7.5 Stoichiometry	125
7.5.1 Half Reaction Approach	127
7.5.2 Substrate Partitioning Approach.....	130
7.6 Results and Discussion:.....	137
7.6.1 Dataset Analysis	137
7.7 Aggregate Stoichiometric Results	140
7.8 Conclusions	141
CHAPTER 8 CONCLUSIONS AND FUTURE RESEARCH	142
8.1 Conclusions	142
8.2 Recommendations for Future Research	145
APPENDIX A: STOICHIOMETRY SAMPLE CALCULATIONS.....	146
APPENDIX B: HRAS MODEL FRAMEWORK – DUAL SUBSTRATE	151
APPENDIX C: NO DATASET CALIBRATION RESULTS.....	163
Effect of Variable SRT	164
Readily Biodegradable COD.....	164
EPS Production.....	165
Colloidal COD Removal Efficiency.....	166

Effect of Variable DO	167
Readily Biodegradable COD.....	167
EPS Production.....	168
Colloidal COD Removal Efficiency.....	169
Modified Parameter Values.....	170
APPENDIX D: HRSD STATE VARIABLE DATASET	171
APPENDIX E: HYDROLYSIS	186
Hydrolysis	187
Lysis Regrowth	187
APPENDIX F: PARTIAL PETERSON MATRIX.....	189
APPENDIX G: STOICHIOMETRY TABLES	192
APPENDIX H: HRSD PILOT OFF-GAS DATA	197
REFERENCES	202

LIST OF FIGURES

Figure 1: Non steady state material balance equations for each state variable in Table 1	9
Figure 2: Stoichiometric development of Equation 2	10
Figure 3: Typical plot of the relationship between the specific growth rate coefficient and the concentration of a non-inhibitory substrate (Grady et al., 2011)	11
Figure 4: COD Fractionation for particulate (pCOD), colloidal (cCOD) and soluble (readily biodegradable) COD (ffCOD) adopted for this work (Jimenez, 2002)	15
Figure 5: Stoichiometry of PHB formation (Van Aalst-Van Leeuwen et al., 1997)	18
Figure 6: Conventional Nitrogen Removal	23
Figure 7: Nitrite Shunt	24
Figure 8: Nitrification/Anammox process	27
Figure 9: Diauxic growth of Escherichia coli on a mixture of glucose and lactose (Clark, 2012).	30
Figure 10: University of New Orleans pilot plant configuration	32
Figure 11: HRAS model Calibration data (Jimenez, 2002)	35
Figure 12: Process flow diagram of the HRSD A-stage process pilot plant	36
Figure 13: SUMO Integrated Development Environment – HRSD A-stage Pilot Configuration (Takacs, 2013)	44
Figure 14: A-stage Model Calibration Results – NO Dataset	47
Figure 15: A-stage Model Validation Results – HRSD Dataset	48
Figure 16: Process flow diagram of the HRSD A/B process pilot plant	52

Figure 17: COD Fractionation for particulate (pCOD), colloidal (cCOD) and soluble COD (ffCOD) adopted for this work	56
Figure 18: Proposed mathematical model modifications for the HRAS carbon removal model	61
Figure 19: S_{Bs} electron flow schematic for HRAS model	66
Figure 20: S_{Bf} electron flow schematic for HRAS model.....	67
Figure 21: HRAS model calibration results.....	75
Figure 22: ASM1 Prediction for the HRAS System [Aerobic SRT = 0.25 d, DO = 0.2 mg/L, HRT = 30 min, $\mu_{max} = 6.0$ d-1 ; $K_s = 20$ mg/L; $K_{O,H} = 0.2$ mg/L; $b_H = 0.62$ d-1; $Y_H = 0.67$]	79
Figure 23: HRSD A-stage pilot plant configuration	80
Figure 24: University of New Orleans pilot plant configuration	81
Figure 25: Dual Substrate Model calibration results	91
Figure 26: Validation Results for the Diauxic and Dual Substrate models	93
Figure 27: Effect of Influent Biomass Concentration.....	94
Figure 28: Conventional Nitrogen Removal.....	96
Figure 29: Nitrite Shunt	98
Figure 30: HRAS Process Configuration in SUMO	99
Figure 31: Effect of variable SRT on A-stage effluent COD:N ratios (a), TCOD fractions (b), EPS production (c) and active biomass concentration (d) (HRAS model), $S_T = S_U + S_{Bf} + S_{Bs}$ where S_U is the inert fraction.	103

Figure 32: Effect of variable DO on A –stage effluent COD:N ratios (a), TCOD fractions (b), EPS production (c) and active biomass concentration (d) at SRT = 1.5 days (HRAS Model), $S_T = S_U + S_{Bf} + S_{Bs}$ where S_U is the inert fraction.....	105
Figure 33: Effect of variable DO on effluent COD:N ratios (a), TCOD fractions (b), EPS production (c) and active biomass concentration (d) at SRT = 0.13 days (HRAS Model), $S_T = S_U + S_{Bf} + S_{Bs}$ where S_U is the inert fraction.	106
Figure 34: Comparison of the effect of variable SRT and DO on COD removal in the HRAS model (a) variable SRT DO >1.0, (b) variable DO at SRT = 1.5 d. Influent TCOD= 301 mg/L.....	107
Figure 35: Effect of Temperature on COD:N ratio at (a) variable SRT, (b) SRT = 1.5 d and variable DO.....	108
Figure 36: Comparison of COD:N ratios at constant SRT and variable DO, TCOD = 361 mg/L(), Influent COD:N ratio = 8.5:1 (HRAS model).....	110
Figure 37: Comparison of COD:N ratios at constant SRT and variable DO, TCOD = 600 mg/L, influent COD:N = 15:1 (HRAS model)	111
Figure 38: Comparison of A-stage effluent COD:N ratio	113
Figure 39: Comparison of TCOD fractions between the pilot data and the HRAS model..	113
Figure 40: HRAS Model substrate partitioning pathways (for electron and carbon flow)..	119
Figure 41: Calculated COD mass balances based on off-gas data.....	124
Figure 42: Rate of change in the CO ₂ :O ₂ ratio as electrons are shunted away from fe and towards fs. Using domestic wastewater (S_{Bs}) as the electron donor (Table 19).	129

Figure 43: Procedure for determining stoichiometric coefficients for S_{Bf} at varying $CO_2:O_2$ ratios using the stoichiometry shown in Table 20.	135
Figure 44: Procedure for determining stoichiometric coefficients for S_{Bs} using the stoichiometry shown in Table 19.....	136
Figure 45: Comparison of off-gas $CO_2:O_2$ ratio to stoichiometric substrate partition fractions based on single substrate using stoichiometry defined in Table 19 and Table 20.....	137
Figure 46: Composite substrate partition fractions based on combined S_{Bf} (acetic acid) and S_{Bs} (domestic wastewater) stoichiometry	138
Figure 47: Substrate Partitioning coefficients $k_{EPS,PC}$ (f_{EPS}) and $k_{STO,PC}$ (f_{STO}) generated from the A-stage model at variable SRT and DO (SRT=1.5 days).	140
Figure 48: Schematic representation of the lysis: regrowth approach to modeling biomass decay	188

LIST OF TABLES

Table 1 Process kinetics and stoichiometry for aerobic growth of heterotrophs (Henze et al., 2000)	8
Table 2 Typical HRAS model calibration, process operating parameters used to generate model output to compare to data in Figure 11.	34
Table 3 A-stage model influent wastewater constituent concentrations.....	34
Table 4 HRSD A-stage HRAS sampling plan (Miller, 2013)	39
Table 5 SUMO Peterson Matrix for ASM1 (Takacs, 2013).....	42
Table 6 ASM1 kinetic and stoichiometric parameters used in the Peterson matrix (Takacs, 2013)	43
Table 7 Partial list of parameter values for the mass balance equations	45
Table 8 HRSD A-stage HRAS experimental data	55
Table 9 Partial list of state variables	61
Table 10 Partial Peterson matrix for the HRAS model.....	63
Table 11 Partial Peterson matrix process rate equations for the HRAS model	64
Table 12 HRAS model calibration, process operating parameters	71
Table 13 HRAS model influent wastewater constituent concentrations	72
Table 14 Partial list of parameter values for the mass-balance equations	73
Table 15 Partial list of state variables (gCOD.m ⁻³).....	85
Table 16 Influent state variables for model validation	92

Table 17 Partial Peterson matrix processes and stoichiometric coefficients for the HRAS model.....	121
Table 18 Partial Peterson matrix process rate equations for the HRAS model	122
Table 19 Stoichiometry for the slow fraction (S_{Bs}) of the readily biodegradable soluble substrate (i.e. equivalent to F-rbCOD from ASM2d)	131
Table 20 Stoichiometry for the fast fraction (S_{Bf}) of the readily biodegradable soluble substrate	132
Table 21 Summary of equations used in the Substrate Partitioning Approach (NCEES, 2011)	133
Table 22 Average aggregate COD based stoichiometric yield coefficients based on combined stoichiometry.....	139
Table 23 HRAS model framework	152
Table 24 HRAS model framework rate expressions.....	154
Table 25 HRAS model state variables	156
Table 26 HRAS model kinetic parameters for Hydrolysis	158
Table 27 HRAS model kinetic parameters for Heterotrophic growth and decay	158
Table 28 HRAS model kinetic parameters for Autotrophic growth and decay	159
Table 29 HRAS model kinetic parameters for other conversion reactions	159
Table 30 HRAS model kinetic parameters for temperature dependency	159
Table 31 HRAS model kinetic parameters for operational inputs	159
Table 32 HRAS model stoichiometric parameters for growth yields.....	159
Table 33 HRAS model stoichiometric parameters for nitrogen fractions	160

Table 34 HRAS model stoichiometric parameters for charge and electron equivalence	160
Table 35 HRAS model stoichiometric parameters for calculated variable conversions	160
Table 36 HRAS model stoichiometric parameters for EPS and Storage Products (STO)....	160
Table 37 Calculated stoichiometric parameter values for oxygen demands.....	161
Table 38 Calculated stoichiometric parameter values for suspended solids.....	161
Table 39 Calculated stoichiometric parameter values for other variables	161
Table 40 Calculated kinetic parameter values for OUR and Temperature dependency	162
Table 41 Calculated kinetic parameter values for Growth Rate and Proportionality	
Coefficients	162
Table 42 Calculated kinetic parameter values for saturation concentrations	162
Table 43 NO calibration modified parameter list	170
Table 44 HRSD pilot influent state variables	172
Table 45 HRSD pilot reactor state variables.....	176
Table 46 HRSD pilot effluent state variables	181
Table 47 Partial Peterson matrix processes and stoichiometric coefficients for the HRAS	
model.....	190
Table 48 Partial Peterson matrix process rate equations for the HRAS model	190
Table 49 Partial list of default parameter values for the mass-balance equations	191
Table 50 Stoichiometry dataset.....	193
Table 51 S_{Bf} substrate partition fractions.....	195
Table 52 HRSD pilot off-gas data	198

NOMENCLATURE

AOB	Ammonia Oxidizing Bacteria
ASM	Activated Sludge Model
ATP	Adenosine Triphosphate
BOD	Biochemical Oxygen Demand
CO ₂ _PR	Carbon Dioxide Production Rate
COD	Chemical Oxygen Demand
DO	Dissolved Oxygen
F/M	Food-to-Microorganism
HRAS	High Rate Activated Sludge
HRT	Hydraulic Retention Time
MLSS	Mixed Liquor Suspended Solids
N	Nitrogen
NAD	Nicotinamide Adenine Dinucleotide
NADH	Reduced Nicotinamide Adenine Dinucleotide
NOB	Nitrite Oxidizing Bacteria
OHO	Ordinary Heterotrophic Bacteria
OUR	Oxygen Utilization Rate
PC	Proportionality Coefficient
PHA	Polyhydroxyalkanoate

PHB	Poly - β - hydroxybutyrate
RAS	Return Activated Sludge
rbCOD	Readily Biodegradable COD
SBR	Sequential Batch Reactor
SRT	Solids Retention Time
sbCOD	Slowly Biodegradable COD
SLPM	Standard Liters per Minute
SOP	Soluble Orthophosphorus
TKN	Total Kjeldahl Nitrogen
TN	Total Nitrogen
TP	Total Phosphorus
TVSS	Total Volatile Suspended Solids
WAS	Waste Activated Sludge
VFA	Volatile Fatty Acid
VSS	Volatile Suspended Solids
$K_{B,HYD}$	Saturation coefficient for X_B/X_{OHO}
b_{ANO}	Decay rate for X_{ANO}
b_{OHO}	Decay rate for X_{OHO}
f_e	Fraction of electrons shunted to Energy
f_s	Fraction of electrons shunted to biomass synthesis
f_{EPS}	Fraction of electrons shunted to EPS production
f_{STO}	Fraction of electrons shunted to the formation of storage products

f_U	Fraction of X_U generated in biomass decay
i_{CB}	Biomass COD to VSS ratio
i_{Charge_SNHx}	Conversion factor for NH_x in charge
i_{Charge_SNOx}	Conversion factor for NO_3 in charge
i_{COD_N2}	NH_3 to N_2 oxidation electron equivalence
i_{COD_NO3}	NH_3 to NO_3 oxidation electron equivalence
i_{CV}	Particulate COD to VSS ratio
$i_{N,EPS}$	N content EPS
$i_{N,XB}$	N content of biomass (X_{OHO} , X_{PAO} , X_{ANO})
$i_{N,XU}$	N content of products from biomass
$i_{NO3,N2}$	NO_3 reduction to N_2 electron equivalence
$K_{B,STO}$	Half-saturation coefficient for storage of S_B
K_{Bf}	Half-saturation coefficient for S_B
K_{Bs}	Half-saturation coefficient for S_{Bs}
K_{EPS}	Half-saturation coefficient for EPS
$k_{EPS,MAX}$	EPS formation coefficient
K_{NHx}	Substrate Half-saturation coefficient for ANOs
$K_{NHx,nut}$	Nutrient half-saturation coefficient
K_{NOx}	Half-saturation coefficient for S_{NOx}
$K_{O,ANO}$	Half-saturation coefficient for S_{O2}
$K_{O,EPS}$	EPS Half-saturation coefficient for S_{O2}
$K_{O,OHO}$	Half-saturation coefficient for S_{O2}

$K_{O,STO}$	Half-Saturation Coefficient STO for S_{O_2}
K_{SL}	Half-saturation coefficient for surface limitation
$K_{STO,HYD}$	Hydrolysis Half-saturation coefficient for STO
q_{ADS}	Rate constant for adsorption
q_{AMM}	Rate constant for ammonification
$q_{EPS,HYD}$	EPS hydrolysis
q_{STO}	Rate constant for growth on X_{STO}
$q_{STO,HYD}$	Storage Hydrolysis Rate Constant
$q_{XB,HYD}$	Rate Constant
T	Temperature
T_{base}	Arrhenius base temperature
Y_{ANO}	Yield of X_{ANO} growth per S_{NO_3}
$Y_{OHO,AER}$	Yield for aerobic X_{OHO} growth
$Y_{OHO,ANOX}$	Yield for anoxic X_{OHO} growth
Y_{STO}	Yield for S_B storage and enmeshment
$\eta_{GRO,ANOX}$	Reduction factor for anoxic growth of X_{OHO}
η_{HYD}	Correction factor for hydrolysis under anoxic conditions
$\theta_{\mu,OHO}$	Arrhenius coefficient
$\theta_{b,O_2,OHO}$	Arrhenius coefficient
μ_{ANO}	Maximum growth rate of X_{ANO}
μ_{OHO}	Maximum growth rate of X_{OHO}

CHAPTER 1 INTRODUCTION

1.1 General

Mathematical modeling of the activated sludge process has become an essential part of the design and operation of wastewater treatment plants. These models were developed to analyze the biochemical transformations that occur in wastewater treatment facilities. These biochemical operations modify or destroy materials that microorganisms can act upon via mineralization or biotransformation (Grady et al., 2011). Biochemical operations in activated sludge employ two major cycles: carbon and nitrogen. The microorganisms involved in each cycle derive their energy and reducing power from oxidation reactions, involving the transfer of electrons. Organisms that use organic compounds as their electron donor and source of carbon for cell synthesis are heterotrophic bacteria. Those organisms that used inorganic compounds (e.g. NH_3) as their electron donor and carbon dioxide as the carbon source are referred to as autotrophic bacteria.

In this dissertation activated sludge systems are defined as follows:

- A conventional activated sludge system is defined by an SRT of 3-15 days, an HRT of 4-8 hours, and a DO of 2 mg/L.
- A typical HRAS system is defined by an SRT of 1-3 days, an HRT of 1.5 to 3 hours, and a DO of 2 mg/L.
- An A-stage HRAS system is defined by an SRT of 4-12 hours, an HRT of 30 minutes, and a DO of <1 mg/L.

This research will develop mathematical models which evaluate the carbon cycle as it pertains to an A-stage HRAS system. This research will develop a carbon removal model using ASM1 as the initial framework. The framework will be modified adding the required removal mechanisms to accurately predict the performance of a HRAS system.

1.2 Research Objectives

1.2.1 Problem Statement

Hampton Roads Sanitation District (HRSD) is implementing a pilot plant program to develop recommendations to improve the performance of seven wastewater treatment plants that discharge to the James River Basin, Virginia. This effort is in response to the Total Maximum Daily Load (TMDL) limits imposed by the U.S. Environmental Protection Agency (EPA) to restore clean water in the Chesapeake Bay and the region's streams, creeks and rivers (December 2010). In response, the State of Virginia established a Watershed Improvement Plan (WIP) to comply with these limits. Under the WIP, HRSD is required to do the following (Hingley, 2012):

- Reduce total nitrogen discharged by 1.6 million pounds annually by 12/31/2016.
- Reduce total nitrogen discharged by an additional 1 million pounds annually by 12/31/2021.

As part of the pilot program, HRSD is conducting pilot testing of several nitrogen removal processes including a novel deammonification process. The study was initiated in March 2011, and the pilot testing work is ongoing. HRSD has contracted with UCF to develop a mathematical model of the HRAS (A-stage, activated sludge system operated to

remove organic carbon from influent wastewater at low SRTs, typically less than 1 day and no measurable dissolved oxygen) pilot plant to accurately predict carbon and nitrogen removal. The challenge is that HRSD is evaluating processes, e.g. HRAS, simultaneous nitrification/denitrification (SND), and mainstream deammonification, which could be considered non-conventional.

1.2.2 Statement of Research Objectives

This research will develop a modified ASM1 model to better describe the overall removal of organic substrate from the high rate activated sludge process. Organic substrate removal in the A-stage HRAS process can be primarily attributed to microbial storage of readily biodegradable soluble substrate and removal of colloidal and particulate substrate through the production of extracellular polymeric substances (EPS) and bioflocculation. Biomass is wasted before significant hydrolysis and mineralization can occur. This modified model will incorporate those substrate removal mechanisms that best simulate the performance of the A-stage. The modified model will be calibrated using the HRAS data collected by Jimenez (2002); Jimenez et al. (2005) including EPS production at varying SRT's and DO concentrations. The HRSD pilot plant will evaluate the performance of the A/B process which, for this research, will include an initial "A-stage" high rate activated sludge process followed by either a "B-stage" Nitritation/Denitritation or a Mainstream Deammonification process without bioaugmentation from a sidestream process. Model validation will be conducted using data from the existing HRSD A-stage pilot plant. The research objectives are summarized below:

1. Develop a mathematical model that accurately predicts the removal of carbon substrate for HRAS, i.e. valid at low HRT and SRT's from 2 days to washout.
2. The model will simulate the removal of both particulate and colloidal material separately. The mechanisms developed should simulate effluent quality and EPS production in accordance with existing data from Jimenez (2002), and Jimenez (personal communication).

The HRAS (A-stage) system is operated to remove organic carbon from influent wastewater with as little oxidation as possible and yield a waste activated sludge (WAS) with high methane (CH_4) production potential i.e. to reduce energy requirements.

3. This research will evaluate, using experimental data from a typical HRAS pilot and A-stage HRAS pilot, the removal mechanisms which affect the removal efficiency of organic carbon from an A-stage system to determine which mechanisms should be included in the A-stage model.

CHAPTER 2 LITERATURE REVIEW

2.1 ASM Modelling

The IWA task group on mathematical modeling for design and operation of biological wastewater treatment processes has introduced activated-sludge models ASM No. 1, 2, 2D, and 3 (Henze et al., 2000). ASM1 simulates the removal of organic matter (carbon) and nitrogen. Carbon removal occurs through the biological oxidation of organic matter and assimilation via biosynthesis. Nitrogen removal occurs through biological nitrification and denitrification, plus assimilation. The ASM2 models (2, 2d) are an extension of ASM1 incorporating biological nutrient (nitrogen and phosphorus) removal. ASM3 was developed as a possible replacement for ASM1 with the significant difference being the importance of storage polymers in the heterotrophic conversion of organics in activated sludge systems (Krishna & Van Loosdrecht, 1999).

The ASM1 and ASM3 models were developed to simulate the aerobic and anoxic treatment of domestic wastewater based on typical operating conditions, e.g. Solids Retention Time (SRT) greater than 3 days. These models were not developed to model activated sludge systems with low SRTs (less than 1 day) where bioflocculation/adsorption of particulate and colloidal (slowly biodegradable) substrate and storage may become limiting (Henze et al., 2000).

The ASM1 and ASM3 models implicitly assume that the removal of slowly biodegradable substrate (primarily particulate substrate and colloidal substrate) is from instantaneous enmeshment and hydrolysis of particulate and colloidal substrate followed by

oxidation of soluble biodegradable substrate. However, researchers have overlooked the effect of the kinetics of bioflocculation on the overall particulate and colloidal substrate removal process and have concentrated their attention on the kinetics of hydrolysis and oxidation when modeling carbon removal in activated-sludge systems.

Jimenez et al. (2005, 2007) revealed that flocculation plays a major role in the removal of particulate and colloidal COD and many operational parameters such as solids retention time (SRT), dissolved oxygen (DO) and hydraulic retention times (HRT) can affect their removal in the activated sludge process. At low SRT (less than 2 days) and low HRT (less than 1 hour) some of the particulate and (especially) colloidal COD may not be removed since the kinetic rate of flocculation may not result in complete enmeshment and hydrolysis. Hence, flocculation should be considered as an important mechanism when modeling activated sludge systems, especially high-rate activated sludge (HRAS) processes (i.e. systems with low SRT and HRT).

Developing a mathematical model to simulate the behavior of activated sludge systems; integrates biological phenomena for carbon oxidation, nitrification and denitrification that results in multiple complex reactions (Henze et al., 2000). These equations are mass balance equations developed for each component of interest in the reactor. Each component is referred to as a state variable, e.g. S_s is the state variable for soluble substrate. The reactions involved are referred to as processes and may affect multiple state variables (Henze et al., 2000). At a minimum, the deterministic models for activated sludge consist of the following elements (Henze et al., 2000):

- A list of components (state variables)

- The transformation processes involved including a stoichiometric matrix (v_{ij}) and process rate constants(ρ_j).
- Wastewater treatment facility process schematic.
- Internal transport and mixing, including settling, return and waste flow rates.

The models implement a fundamental approach by first identifying specific processes involved in accomplishing a certain level of biochemical treatment, carbon and nitrogen removal in ASM1 to nutrient removal (N and P removal) in ASM2d. Each process in the biokinetic matrix is defined by the specific stoichiometry of the reaction involved in the biochemical operation. Typically these stoichiometric reactions are developed based on molar units; however, these units do not facilitate comparison of, through mass balances, the fate of the participating constituents. Thus, evaluating the biochemical operations would be better accomplished by converting to mass based stoichiometry using COD for organics, and “as N” and “as P” units for nutrients (Grady et al., 2011).

The ASM models use matrix notation for the presentation of biokinetic models. This approach for heterotrophic growth in an aerobic environment is shown in Table 1. Henze et al. (1999) summarized the matrix approach, the components (state variables) which are to be considered in the model and the transformation processes are defined by the indices i and j respectively. The stoichiometric coefficients are presented in the form of a matrix defined by v_{ij} . The process rate constants form a vector p_j . The matrix is often referred to as the Peterson matrix (Peterson, 1965) and will be referred to as such throughout this research.

Table 1 Process kinetics and stoichiometry for aerobic growth of heterotrophs (Henze et al., 2000)

		Continuity →			Process Rate, ρ_j [ML ⁻³ T ⁻¹]
Component →	i	1 X _{OH0}	2 S _S	3 S _O	
j Process ↓					
Material Balance	1 Growth	1	$-\frac{1}{Y_H}$	$-\frac{1 - Y_H}{Y_H}$	$\frac{\mu S_S}{K_S + S_S} X_{OH0}$
	2 Decay	-1		-1	bX_{OH0}
Observed Conversion Rates ML ⁻³ T ⁻¹		$r_j = \sum_j r_{ij} = \sum_j v_{ij} \rho_j$			Kinetic Parameters: Maximum specific growth rate: $\hat{\mu}$ Half-velocity constant: K_S Specific decay rate: b
Stoichiometric Parameters: True growth yield: Y_H		Biomass [M(COD)L ⁻³]	Substrate [M(COD)L ⁻³]	Oxygen (negative COD) [M(-COD)L ⁻³]	

The stoichiometric matrix relates to a material balance in the vertical direction. A material balance can be written for each component i (state variable) which may be affected by one or all of the processes j . The observed transfer rate is the sum of the transformation rates from each process (Gujer & Henze, 1991): The rate of production of each component (state variable) i , r_i , can be computed by

$$r_i = \sum v_{ji} \rho_j \quad \text{for all processes } j \quad (1)$$

For state variables shown in Table 1 the material balance equations are shown in Figure 1.

Mass Balance Equation for Soluble Substrate:

$$\frac{dS_S}{dt} = -\frac{1}{Y_H} * \left(\mu_{m,H} * \frac{S_S}{K_S + S_S} X_{OHO} \right)$$

Mass Balance Equation for particulate substrate:

$$\frac{dX_{OHO}}{dt} = -\frac{1}{Y_H} * \left(\mu_{m,H} * \frac{S_S}{K_S + S_S} X_{OHO} \right) - bX_{OHO}$$

Mass Balance Equation for dissolved oxygen:

$$\frac{dS_O}{dt} = -\left(\frac{1 - Y_H}{Y_H} \right) * \left(\mu_{m,H} * \frac{S_S}{K_S + S_S} X_{OHO} \right) - bX_{OHO}$$

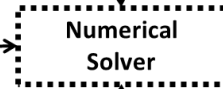


Figure 1: Non steady state material balance equations for each state variable in Table 1

The material balance equations shown in Figure 1 are used as input to a numerical solver which generates either static (based on a snapshot of the system) or dynamic (time dependent variation) results.

In the development of the ASM models substrate utilization and biomass growth have been coupled (Process 1, Table 1) such that the generalized equation can be written as

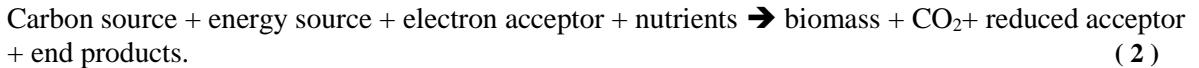
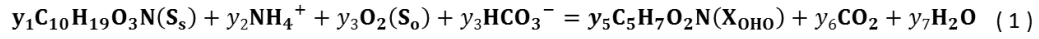
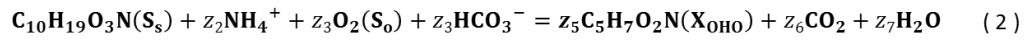


Figure 2 shows the stoichiometric development of Equation 2 starting with a mole based equation (1) converted to a mass based equation (1 → 2) then to a COD based equation (2 → 3 → 4) normalized to the carbon source and finally to a COD based equation normalized to biomass (4 → 5).



$\frac{y_i * MW_i}{y_1 * MW_1} \Downarrow$ Mass based



$\frac{y_i * MW_i * COD_i}{y_1 * MW_1 * COD_1} \Downarrow$ COD based, since HCO_3^- , CO_2 , and H_2O do not change their oxidation state these constituents drop out

$$(1)\text{S}_s + -x\text{S}_o = Y_H \text{X}_{\text{OHO}} \quad (3)$$

\Downarrow Continuity – Solve for x

$$(-1)\text{S}_s + (-1)(-(1 - Y_H))\text{S}_o + Y_H \text{X}_{\text{OHO}} = 0 \quad (4)$$

\Downarrow Normalize for X_{OHO}

$$\left(-\frac{1}{Y_H}\right)\text{S}_s + (-1)\left(\frac{-(1 - Y_H)}{Y_H}\right)\text{S}_o + \text{X}_{\text{OHO}} = 0 \quad (5)$$

S_s = Soluble substrate concentration (mgCOD/L) → Carbon Source
 S_o = Dissolve oxygen concentration (mgCOD/L) → Electron acceptor
 Y_H = Biomass yield coefficient (mgCOD/mgCOD)
 X_{OHO} = Biomass Concentration (mgCOD/L)
 x = stoichiometric coefficient for O_2
 Continuity - sum of the coefficients for the reactants = sum of the coefficients of the products
 COD_i = COD Mass Equivalents

Figure 2: Stoichiometric development of Equation 2

As part of the COD based transformation (Figure 2(Equation 2)), since HCO_3^- , CO_2 , and H_2O do not change their oxidation state these constituents drop out of the equation. This is also the case with NH_4^+ , there is no change in the oxidation state of N (-III) in ammonia and biomass N (-III). The biomass (X_{OHO}) coefficient is considered the true yield (Y_H). The stoichiometric coefficient for oxygen (S_o) is negative, indicating that oxygen is consumed in the reaction (Grady et al., 2011).

Continuity is maintained by applying conservation equations based on the principal that in chemical reactions, elements, electrons, and COD are neither created nor destroyed (i.e. for the mass based and COD based stoichiometric coefficients, $\sum \text{products} = \sum \text{reactants}$)

The stoichiometric coefficients in Figure 2 (Equation 5) are the same as those in Table 1 for Process 1. The process rate equations rely on a hyperbolic inhibition (switching) function ($K_O/(K_O + S_O)$) to determine when a particular process would become active based on specific environmental conditions. Aerobic growth, defined by process 1 in Table 1 has a kinetic rate affected by the concentration of readily biodegradable substrate and DO (S_s, S_O respectively) according to the Monod expressions ($S_s/(K_S + S_s)$) and ($S_O/(K_O + S_O)$), where K_S and K_O are the half-rate saturation coefficients. The half-rate saturation coefficient determines how rapidly μ (biomass specific growth rate d^{-1}) approaches $\hat{\mu}$ (maximum specific growth rate d^{-1}) and is defined as the concentration at which μ is equal to half of $\hat{\mu}$, as shown in Figure 3.

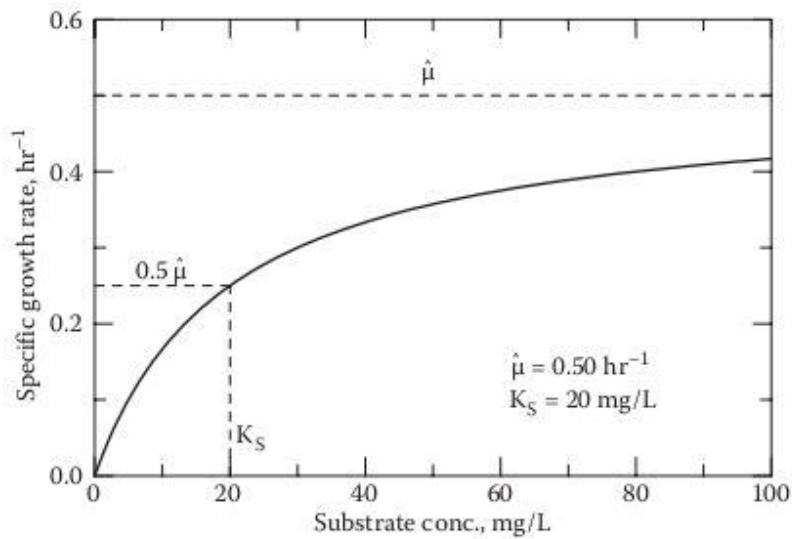


Figure 3: Typical plot of the relationship between the specific growth rate coefficient and the concentration of a non-inhibitory substrate (Grady et al., 2011)

2.2 High Rate System for Carbon Removal

The need to develop a treatment technology that reduced energy consumption in treating influent wastewater, along with the need for nutrient removal, led to the development of the high rate activated sludge (HRAS) process. A typical HRAS process can be defined by an SRT of 1-3 days, an HRT of 1.5 to 3 hours, and a DO of 2 mg/L.

The Adsorption/Bio-oxidation process or A/B process, is an HRAS process which can be categorized as a two-stage, dual activated sludge process. The first stage (A-stage, high F:M ratio) is design to reduce the influent total COD upstream of the B-stage (bio-oxidation) for nitrification and denitrification (Boehnke et al., 1997). The A-stage is a HRAS process which can be defined by an SRT of 4-12 hours, an HRT of 30 minutes, and a DO of <1 mg/L.

Boehnke et al. (1997) suggested that experiments using municipal wastewater showed a 40 percent removal of the influent organic load within the first minute and 70 percent removal within 10 minutes. This removal is attributed to physical/chemical causes as opposed to biological removal mechanisms, suggesting that adsorption, flocculation and coagulation play a significant role. This observation was true for both high and low F:M ratios.

Boehnke et al. (1997) also determined that a critical operating aspect of the A-stage is that it builds on the microbial population that exists in the sewer system. This is significant in modeling this type of system since the influent active biomass concentration is a key parameter in accurately predicting the performance on the A-stage. In addition, although anaerobic conditions need to be avoided, the oxygen content in the A-stage reactor

is non-measurable. The lower SRT in the A-stage promotes the growth of bacteria in the reactor which have the highest metabolism per unit weight, and as a result, are more efficient at reducing soluble organic substrate. The A-stage has also been shown to modify hard to decompose (refractory) organics, passing more easily biodegradable organics to the B-stage, which significantly reduces the treatment burden on the downstream B-stage, especially if denitrification is required.

The soluble organic substrate (COD) removal efficiency of the A-stage is a critical design parameter in achieving the target nitrogen removal efficiency in the B-stage. The theoretical BOD:N ratio required for denitrification is >3.0 (COD:N >4.8). Higher ratios would improve the stability of the denitrification process. To accommodate B-stage nitrogen removal the COD removal efficiency in the A-stage should be low, however, higher COD removal are preferred due to the low cost per gram of COD removed. The target COD removal efficiency for the A-stage would be determined based on treatment objectives established in order to comply with regulatory requirements.

The objective of a HRAS is to remove organic carbon from influent wastewater at low SRTs, typically less than 1 day. In the A-stage, the primary removal mechanisms for removal of colloidal and readily biodegradable COD include biomass synthesis, adsorption, and storage. In addition, energy production and the production of extracellular polymeric substances (EPS) can be significant (Lapidou & Rittmann, 2002a; Ni, Zeng, et al., 2009). EPS aids in the adsorption mechanism. Formation of storage products (Beun et al., 2002; Krishna & Van Loosdrecht, 1999; Ni & Yu, 2008; Third et al., 2003) occurs under high food/microorganism (F/M) ratios and low DO environments.

2.2.1 Wastewater Characterization

Typical characteristics for any municipal wastewater include both soluble and particulate organics. Total chemical oxygen demand (TCOD) can be defined as the sum of particulate COD (pCOD) and soluble COD (sCOD) present in the wastewater. Jimenez et al. (2005) stated that the pCOD consists of organic suspended solids (ssCOD) and organic colloids (cCOD) in the wastewater ($pCOD = ssCOD + cCOD$). The ssCOD is quantified with a 934AH glass fiber filter. Soluble COD was quantified by floc filtered COD (ffCOD,(Mamais et al., 1993)). Colloidal COD was the difference between ssCOD filtrate (TCOD – ssCOD) and ffCOD filtrate.

Figure 4 shows the COD breakdown of Jimenez (2002) adopted for this study. The most important aspect is the differentiation of particulate and colloidal COD, which have not traditionally been considered separately in most studies or in the ASM derived models. The reason for this is that in higher HRT and SRT systems there is plenty of time for both colloidal and particulate COD to flocculate completely and to be degraded (Jimenez, 2002). However in low HRT/SRT systems (HRAS) there is not always time for this to occur. This also means that effluent CODs in HRAS systems are higher than would be expected in higher HRT and SRT systems (Miller et al., 2013) .

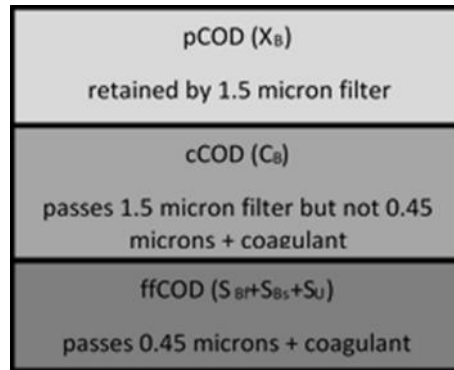


Figure 4: COD Fractionation for particulate (pCOD), colloidal (cCOD) and soluble (readily biodegradable) COD (ffCOD) adopted for this work (Jimenez, 2002)

2.2.2 Extracellular Polymer Substances (EPS)

EPS is considered the prerequisite for the existence of all microbial aggregates (Flemming & Wingender, 2001). It is the construction material responsible for the cell to cell adhesion or bacterial aggregation (Ehlers & Turner, 2011; Higgins & Novak, 1997; Jorand et al., 1995). The composition of EPS has been studied extensively and is believed to consist primarily of polysaccharides and proteins (Flemming & Wingender, 2001; Park & Novak, 2007). Earlier studies suggest that polysaccharides were the most abundant and important constituent, however, more recent studies have shown that protein may be the most abundant constituent by ratio, i.e., protein/polysaccharide ratio in the range of 2 to 5 (Higgins & Novak, 1997; Jorand et al., 1995; Park & Novak, 2007). Higgins and Novak (1997) studied the role of protein in bioflocculation and found that since cation concentration mainly affects the bound protein and not the bound polysaccharide, that the protein not only plays an important role in bioflocculation of activated sludge, but it may in fact be dominant. The role of cations is significant in the development of a stabilized biopolymer network. Higgins and Novak (1997) found that divalent cations bind exocellular protein within the biological floc

resulting in a stable biopolymer network with good settling and dewatering characteristics. High concentrations of monovalent cations displaced the divalent cations from within the floc reducing the bound protein content which deteriorated the settling characteristics of the sludge.

2.2.2.1 Modelling EPS

Laspidou and Rittmann (2002b) stated that EPS is microbially produced organic material that contains both electrons and carbon, but are not active cells. This is significant since the diversion of electrons and carbon away from biosynthesis to EPS formation affects both the cell yield and growth rate. The traditional view of activated sludge systems is that the substrate electrons are shunted along two pathways either to the electron acceptor to create energy or to biomass synthesis (Rittmann & McCarty, 2001). When a significant portion of the electrons are shunted to EPS production, less is available for biomass synthesis and biomass yield and specific growth rate decreases. Laspidou and Rittmann (2002a) developed a unified theory, which attempts to quantify the relationships among extracellular polymeric substances (EPS), soluble microbial products (SMP), original substrate, and an electron acceptor. In this theory, the rate of EPS formation is proportional to the substrate utilization rate.

2.2.2.2 Operational Factors Affecting EPS Production

Extracellular Polymer Substances (EPS) production impacts the bioflocculation removal efficiency for particulate and colloidal substrate. Past models assume instantaneous enmeshment where recent research data shows that this assumption may not be valid for high

rate systems. For this research EPS production calibration data, collected by (Jimenez, 2002, 2013), unpublished), indicates EPS is a function of growth (as volatile suspended solids VSS), hydrolysis rate of X_B (slowly biodegradable substrate), DO concentration in the reactor and EPS hydrolysis rate. The data shows that EPS production increases with an increase in both SRT (0.3 to 2 days) and DO (.01 to 2 mg/L at an SRT of 1.5 days).

Ehlers and Turner (2011) evaluated the impact of EPS on bioflocculation in HRAS (HRT = 1.1 d, SRT from 0.7 to 1.4 d) systems using domestic wastewater and found an inverse relationship between the F:M ratio and EPS production rate. The results suggested that as the F:M ratio increased the EPS production rate decreased. In addition, in a continuous feed reactor during low COD influent feed, an efficient aggregating population was not formed which may be due to limiting nutrients and competing microorganisms resulting in washout. Ni, Zeng, et al. (2009) compared the EPS formation coefficient values reported in the literature and found that the when using acetate as the electron donor the k_{EPS} values ranged from 0.18 to 0.23 (gCOD_{EPS}/g COD_{Ac}). The true biomass yield (Y_{OHO}) ranged from 0.49-.61 on acetate. These values are based on a sludge age \gg 3d.

2.2.3 Storage Polymers

2.2.3.1 PHB Formation on Acetic Acid

In the presence of external substrate, organisms may use the substrate for growth or form storage products (Van Loosdrecht & Heijnen, 2002). Van Aalst-Van Leeuwen et al. (1997) developed a metabolic model for PHB production and consumption in bacterial cells

in a pure culture subject to feast/famine conditions. The stoichiometry is described by seven internal reactions (Figure 5).

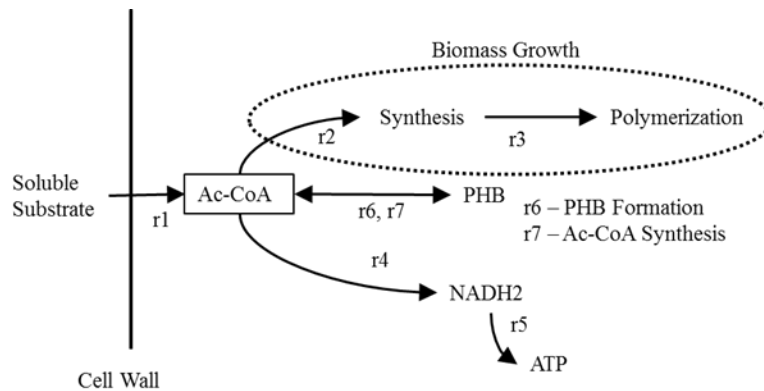


Figure 5: Stoichiometry of PHB formation (Van Aalst-Van Leeuwen et al., 1997)

Poly- β -hydroxybutyrate (PHB) was the dominant storage polymer under excess acetate conditions (Smolders et al., 1995; Van Aalst-Van Leeuwen et al., 1997). Under conditions of carbon surplus the rate of substrate uptake will be larger than that needed for growth. The formation of NADH₂ results from the uptake of substrate which is consumed by oxidative phosphorylation resulting in the formation of adenosine triphosphate (ATP) and NAD⁺. Should the consumption of ATP be limited then ATP will accumulate resulting in subsequent accumulation of NAD⁺. As a result, the production of PHB is highly likely since PHB formation requires NADH₂. A key premise of the metabolic model states that the composition of the biomass consists of two compartments (Roels, 1983; Van Aalst-Van Leeuwen et al., 1997) an active biomass compartment and a PHB compartment. The active biomass is capable of reproduction and growth, and the PHB compartment for storage of carbon and energy. The fraction of PHB in the biomass is represented by f_{PHB} . The fraction of active biomass in the total biomass is then $1 - f_{PHB}$. Van Aalst-Van Leeuwen et al. (1997)

developed a kinetic model for PHB production where there is a linear relationship (Equation 3) between the steady state growth rate (dilution rate) and the maximum fraction of PHB stored in the cell ($f_{\text{PHB,Max}}$).

$$f_{\text{PHB}}^{\text{max}} = 0.38 - 0.78\mu \quad (3)$$

Based on this relationship, no PHB accumulation occurs as the dilution rate approaches the maximum growth rate. Should the specific growth rate reach zero, the maximum obtainable PHB content ($f_{\text{PHB,Max}}$) becomes 0.39 (C mol/C mol).

As an alternative to the metabolic model, Ni 2007 developed a growth/storage based model using a modified ASM3 framework. ASM3 is a growth based model expanded to include the storage phenomena. Studies have shown that the ASM3 model developed inconsistencies when used to interpret data from short-term respirometric batch experiments (Krishna & Van Loosdrecht, 1999; Ni & Yu, 2008). ASM3 assumes that all the soluble substrate is first converted to storage products before it is used for growth. Krishna and Van Loosdrecht (1999) determined that using a simplified version of ASM3 (only aerobic heterotrophic conversions and acetate as the sole substrate) was inconsistent under two conditions; one being the inconsistencies in the biomass growth rate observed experimentally during feast and famine conditions, and second the elevated levels of internal storage polymers predicted (SRT of 2.5 days and an HRT of 8h) which were inconsistent with the measures oxygen consumption (Ni & Yu, 2008). Ni and Yu (2008) developed a modified ASM3 model incorporating a simultaneous substrate, storage, and growth concept along with consideration for microbial maintenance processes and oxygen transfer. Processes were included for hydrolysis of slowly biodegradable substrate, growth on readily biodegradable

substrate, formation of storage products, growth on storage products, maintenance on readily biodegradable substrate, maintenance on storage products, and biomass decay and oxygen transfer. Growth on either external substrate (S_s) or internal substrate (X_{STO}) is managed using a substrate switching function controlled by the substrate half saturation coefficient K_s . Growth stops when all the external and internal substrate are consumed. Kinetic parameters were added to describe maximum growth rate on storage products, production rate of storage products and maintenance rate. Results showed that these parameters along with the substrate affinity constant were vital to the models ability to effectively predict the simultaneous heterotrophic growth and storage in an activated sludge system under aerobic conditions.

Review of the literature suggests that systems operated at low DO concentrations (<0.9 mg/L; according to Third et al., 2003), typical of an A-stage system, result in the microbial uptake of readily biodegradable soluble COD and could result in the formation of storage polymers. Third et al. (2003) showed that during the fill phase of an SBR, using a synthetic wastewater with acetate as the organic carbon substrate and at low DO (< 0.01 mg.L⁻¹), 20% of the substrate goes to oxidation, 5% goes to assimilation, and 75% to PHB production. At higher DO (> 0.9 mg.L⁻¹), 20% of the substrate goes to oxidation, 20% goes to assimilation, and 60% to PHB production.

2.2.3.2 PHB Formation on Domestic Wastewater

As discussed in the previous section, there is an abundance of research supporting aerobic storage product production under dynamic conditions in a laboratory plant, using synthetic substrate and pure cultures. There is also significant research studying storage product formation using real sludge and real wastewater. Carucci et al. (2001) evaluated the

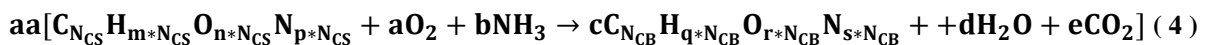
formation of storage products when real sludge is mixed with real wastewater. Respirometric batch tests were run using pure acetate, flocculated and filtered wastewater, and influent unsettled wastewater using a F/M ratio of 0.05 – 0.3 gCOD/gVSS to separate the high-OUR rbCOD from the low-OUR sbCOD. The experimental results show a significant production of PHB when using only acetic acid as the carbon source (0.55 gCOD_{PHB}/gCOD_{AC}). When using raw (domestic) wastewater PHB production increased (0.74 vs 0.55 gCOD/gCOD). Confirming that PHB is stored from other substrates, however, acetate is still the major contributor. This study only identified PHB analytically, but in order to explain the OURs generated either other storage products are being formed or other removal mechanism (non-storage) must be active.

2.3 Stoichiometry

Chemical stoichiometric equations have been used ((McCarty, 1975; Sherrard & Schroeder, 1976) to describe the activated sludge bio-oxidation process. This approach has proven effective in understanding how these treatment processes function. Typical equations written to describe aerobic processes are written qualitatively as follows (Sherrard & Schroeder, 1976):

Bacteria + Organics + Nutrients + Oxygen → New Bacteria + CO₂ + H₂O + Residual organics and Inorganics

This equation could be represented by a chemical stoichiometric equation for an aerobic system using domestic wastewater as the organic substrate as follows:



Equation 4 represents a typical activated sludge system operating at an SRT > 3 d where the available electrons are shunted primarily to biomass growth (f_s) or energy (f_e). McCarty (1975) was able to demonstrate that for suspended growth systems, the fraction of electrons going to mineralization (energy, f_e) increases as the sludge age (SRT) increases. Using the half reaction approach, McCarty (1975) showed that, using domestic wastewater as the electron donor and oxygen as the electron acceptor, the production of CO_2 would decrease and the consumption of O_2 would also decrease as electrons are shunted away from energy production towards synthesis of new biomass.

2.4 Mainstream Nitrogen Removal

The conventional approach to Nitrogen removal includes two primary mechanisms, Nitrification and Denitrification as shown in Figure 6. The nitrification pathway is a two-step oxidation of ammonia ($\text{NH}_3/\text{NH}_4^+$). The first step oxidizes ammonia to nitrite (NO_2^-) by Ammonia Oxidizing Bacteria (AOB) (Nitritation), the second step oxidizes nitrite to nitrate (NO_3^-) by Nitrite Oxidizing Bacteria (NOB) (Nitrataion).

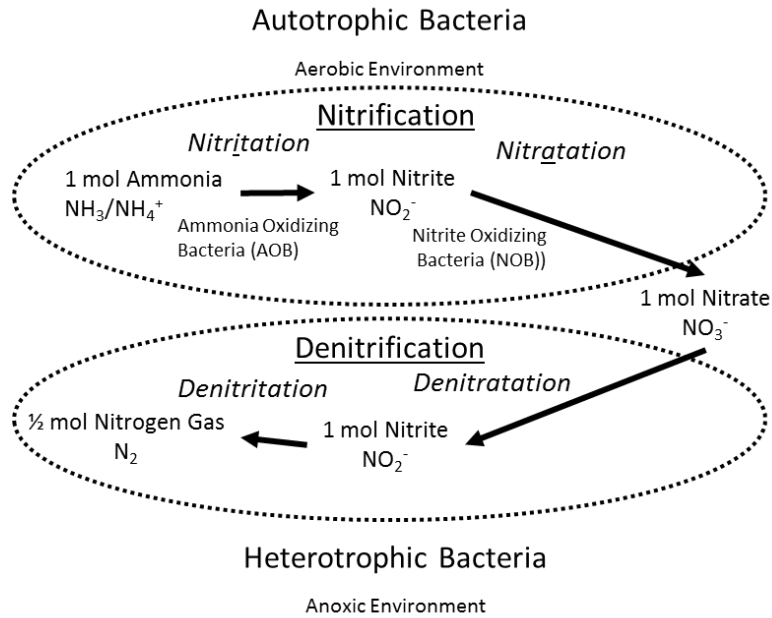


Figure 6: Conventional Nitrogen Removal

The first step (Nitritation) consumes 75 percent of the oxygen (energy) and approximately 100 percent of the alkalinity required for the two step process. The remaining 25 percent of the overall energy requirement is consumed in the second step (Nitratation). The oxidation of ammonia is carried out in an aerobic environment by autotrophic bacteria. The denitrification pathway again, is the two step reduction of nitrate to nitrogen gas in an anoxic environment (negligible dissolved oxygen) by ordinary heterotrophic bacteria (OHO). In the first step (denitratation) the OHOs oxidize organic substrate (COD) using NO_3^- as the electron acceptor which is reduced to NO_2^- . This consumes approximately 40 percent of the total organic substrate needed to complete the denitrification process. In the second step (denitritation) NO_2^- is converted to nitrogen gas consuming the remaining 60 percent of the total organic substrate needed for the reaction. The process described above

(nitrification/denitrification) would be considered the conventional approach to removing nitrogen from wastewater. The industry has introduced alternative approaches to nitrogen removal several of which are being evaluated by HRSD including Nitritation/Denitritation and Mainstream Deammonification.

2.4.1 Nitritation/Denitritation

This approach is a modification of the conventional process where the NO_2^- resulting from the first step in the nitrification pathway is shunted to the second step of the denitrification pathway, in other words the second step of nitrification (Nitratation) and the first step of denitrification (Denitratation) are eliminated. The elimination of these two steps is referred to as “Nitrite Shunt”. To achieve this, the goal is to eliminate NOB from the reactor while selecting for AOB (Regmi et al., 2012). This process is illustrated in Figure 7.

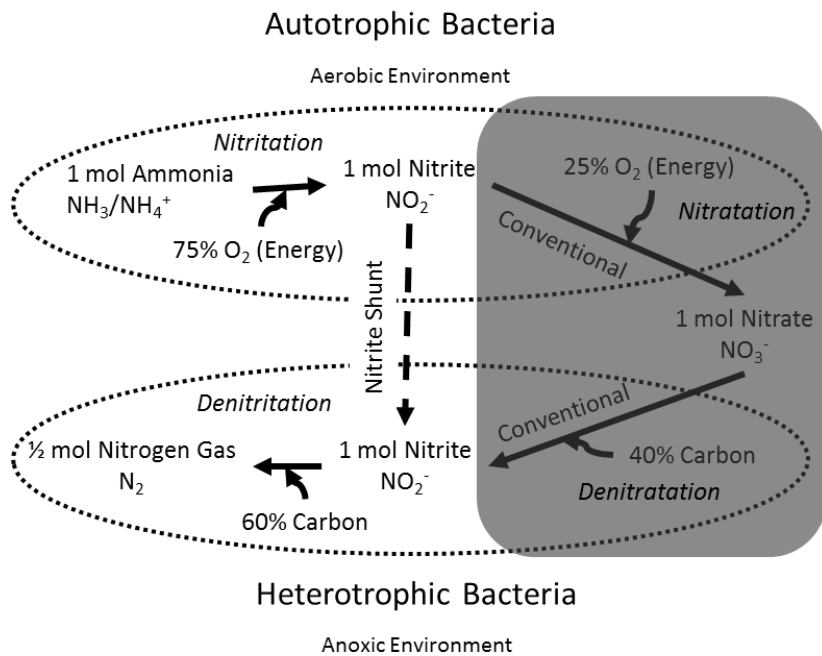


Figure 7: Nitrite Shunt

This is the Nitrite Shunt process where the first step is referred to as the nitrification step and the second is denitrification. The SHARON process has been used successfully to treat ammonium rich sidestream flows i.e. reject water from a digester dewatering process (Hellings et al., 1998). The sidestream flows also have elevated temperatures (30 °C) which the SHARON process takes advantage of, operating at high specific growth rates with minimal or no sludge retention required. When compared to a mainstream system elevated temperature provides a second advantage in that, at normal temperatures (i.e. as in a wastewater treatment plant 5 to 20°C) the nitrite oxidizing bacteria grow faster than the ammonium oxidizers. The result is that ammonium is completely oxidized to nitrate. The reverse is true at the elevated temperatures. This introduces one of the key challenges of implementing mainstream “nitrite shunt”, NOB suppression since the main wastewater stream rarely has elevated temperatures. The advantages of the sidestream (SHARON) approach include (Jubany et al., 2009);

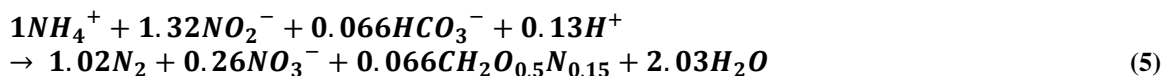
- A 25% reduction in oxygen demand (energy)
- A 40% reduction in supplemental carbon (electron donor) demand)
- A reduction in biomass production

These advantages can result in lower capital investment as the result of a decrease in required mainstream reactor volumes, and a savings in annual operational costs. However, these advantages most likely would not be realized in a mainstream application, primarily due to the fact that COD and Nitrogen removal are still coupled together. In a mainstream application there are several operational challenges, the most critical being able to attain nitrification through NOB suppression. One approach to attain NOB suppression is DO control

(Jubany et al., 2009). Research has shown that NOB have a lower affinity for oxygen than the AOB (Guisasola et al., 2005; Jubany et al., 2009). As a result, NOB suppression and nitrite accumulation are favored at low DO concentration (Garrido et al., 1997; Jubany et al., 2009; Pollice et al., 2002; Ruiz et al., 2003) . Regmi et al. (2012) induced NOB suppression using ammonia based DO control. The aeration in the activated sludge reactor is controlled based on the reactor ammonia concentration. A solenoid valve regulates the reactor HDO (high DO) and LDO (low DO) set points. The objective is to control the growth rate of NOBs by reducing the concentration of the electron acceptor (DO) available. The denitrification pathway converts the NO_2^- to nitrogen gas using organic substrate as the carbon source. The challenge is to operate the A-stage process to reduce the carbon passed to the B-stage to a level that favors the growth of autotrophic biomass, but still having enough organics to drive the denitrification process by heterotrophic biomass. This would avoid having to provide an exogenous carbon source, e.g. methanol or acetate, to drive denitrification.

2.4.2 Deammonification

Deammonification is a two-step process with partial nitrification as the first step followed by an anaerobic reactor with anammox biomass. Anaerobic ammonium oxidation (anammox) is the biological conversion (Figure 8) of ammonium and nitrite to dinitrogen gas (Strous et al., 1999). Anammox bacteria are obligate anaerobes that convert ammonia and nitrite to dinitrogen gas and biomass according to the following overall Equation 5 (Strous et al., 1998)



The nitrification reactor is operated to produce an effluent with equal amounts of ammonia and nitrite which is required for the downstream anammox process. Ammonia – oxidizing bacteria (AOB) aerobically convert about half the ammonia to nitrite and the anammox bacteria anaerobically oxidize the remaining ammonia using nitrite to nitrogen gas (Wett et al., 2013). This process has been used successfully to treat ammonia rich waste streams such as dewatering sidestreams from anaerobically digested sludge (Wett, 2007; Wett et al., 2013)

In mainstream processes this is accomplished using transient anoxia where the aeration is cycled ON/OFF to control the growth of NOB and create an environment that favors the growth of AOBs. (Regmi et al., 2012). Regmi et al. (2014) developed a nitrification DO control strategy to produce equal amounts of ammonia-N and nitrite-N based by comparing the $\text{NH}_3\text{-N}$ concentration to the $\text{NO}_x\text{-N}$ ($\text{NO}_2^- \text{-N} + \text{NO}_3^- \text{-N}$) concentration. If $\text{NH}_3\text{-N}$ is greater than $\text{NO}_x\text{-N}$, aeration is increased, if it is less than aeration is decreased.

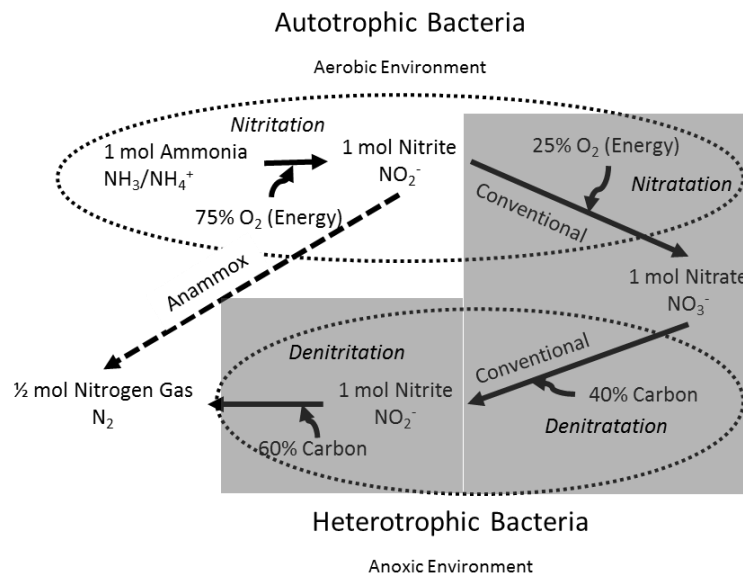


Figure 8: Nitritation/Anammox process

The mainstream deammonification process does have several operational challenges (Bott, 2012)

- The Anammox bacteria are sensitive to temperature, they preferred temperatures > 30°C. Typically domestic wastewaters average 20°C which results in a slow growth rate, e.g. 10 day doubling time, requiring long SRTs (30 – 50 days).

Deammonification has been successfully used for sidestream treatment of recycle streams (typically centrate from anaerobic digesters) which is warm and nitrogen rich (low C/N ratio).

- Sensitive to nitrite concentration ($\text{NH}_4^+:\text{NO}_2^-$ ratio 1:1.3), causes irreversible loss of activity and the toxicity is a function of concentration and exposure time.
- Sensitive to DO, however, this inhibition is reversible.
- Sensitive to free ammonia concentrations > 10 mg/l.

2.4.3 Importance of C:N Ratio for B-stage nitrite shunt and/or anammox

Daigger et al. (2011) performed a desktop analysis of several biological nitrogen removal processes including nitrification, nitritation, and anammox using standard biological process calculations. It is well documented that there are oxygen and carbon savings associated with the treatment of ammonia-rich sidestreams using either nitritation (SHARON[®] process) or anammox (DEMON[®] process). Daigger et al. (2011) evaluated the application of these process to estimate the minimum carbon: nitrogen ratio (C:N) needed for total nitrogen removal and the associated oxygen requirements as follows:

- -Nitrification/denitrification ($\text{mgCOD}\cdot\text{mg N}^{-1}$) = 3.5-4.0

- Nitritation/denitritation ($\text{mgCOD} \cdot \text{mg N}^{-1}$) = 2.0-2.5
- Partial nitritation/denitritation ($\text{mgCOD} \cdot \text{mg N}^{-1}$) = 0.5

The net oxygen requirement for each removal process is the same ($1.71 \text{ mg O}_2 \cdot \text{mg N}$ converted to N_2). Daigger et al. (2011) demonstrated that when using nitritation and partial nitritation, with the associated mainstream nitrogen removal process, significantly reduced the influent wastewater C:N ratio required for nitrogen removal. In addition, for each mainstream nitrogen removal process the oxygen requirement is the same provided that enough organic material is available to convert the oxidized nitrogen to nitrogen gas.

Lemaire et al. (2008) adjusted the influent readily biodegradable COD (rbCOD) concentration feeding a single lab scale SBR providing biological nutrient removal. They found that by reducing the influent rbCOD concentration; the NO_x^- (nitrite + nitrate) started to accumulate in the effluent apparently caused by incomplete denitrification due to lack of COD supply. They found that the COD:N ratio required for conventional nitrification (active nitrate pathway) was approximately 9:1, whereas, when the system was operating via the nitrite shunt pathway the COD:N ratio was around 7:1. The relatively high COD:N ratio (7:1) reported by Lemaire et al. (2008) may be due to the specificity of the wastewater treated (i.e., high levels of slowly biodegradable particulate COD and non-biodegradable COD).

The significance of the colloidal fraction of COD on the downstream B-stage using nitrite shunt cannot be ignored when modeling HRAS systems. The removal efficiency of the colloidal fraction of COD (C_B) is a function of the active biomass and EPS concentrations in the reactor; both of which are a function of the SRT (Jimenez, 2002). Longer SRTs (≥ 0.5

days) result in an increase in active biomass and EPS concentrations in the reactor, resulting in an increase in C_B removal efficiency. Regmi et al. (2014) hypothesized that the type and quantity of COD is important in inducing and maintaining NOB suppression and AOB activity. A rise in the soluble COD fraction in the HRAS effluent would result in a larger portion of the influent COD being rapidly removed in the downstream B-stage reactor, making less COD available for denitrification. The ideal effluent from the HRAS (A-stage) system would consist primarily of colloidal COD.

Depending on how the HRAS process is operated the removal efficiency of the colloidal fraction of COD can have a significant impact on the TCOD in the reactor effluent, which impacts the colloidal COD fraction and the COD:N ratio received downstream.

2.5 Diauxic Growth

The preferential use of some substrates over others present in a mixture describes the diauxic behavior of many bacteria. “The diauxie refers to the phenomenon in which a batch culture of bacteria growing on a mixture of two substrates preferentially utilizes only one of the substrates”. This phenomenon is illustrated in Figure 9.

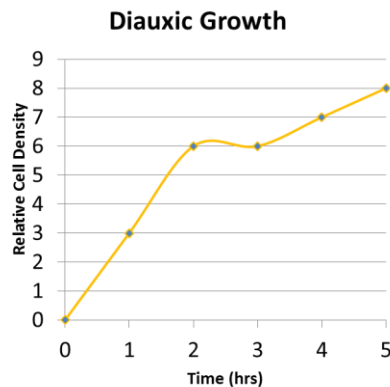


Figure 9: Diauxic growth of *Escherichia coli* on a mixture of glucose and lactose (Clark, 2012).

Such a substrate utilization pattern results in the appearance of two successive exponential growth phases, with each growth phase corresponding to the consumption of only one of the two substrates (Narang et al., 1997).

CHAPTER 3 MATERIALS AND METHODS

3.1 Data for Model Calibration and Validation

3.1.1 Pilot Scale Data Used for Model Calibration

The New Orleans (NO) is a HRAS pilot plant comprised of the following components: a rotating screen, an inlet mechanism (30 gal mixing tank), an aeration tank (40 gal), a mechanical flocculator and a secondary clarifier (70 gal) (Figure 10). The unit was designed for a flow rate of 7.5 m³/d (2000gal/d) and a hydraulic retention time in the aeration tank of 30 minutes. The SRT ranged from 0.3 days to 2.0 days

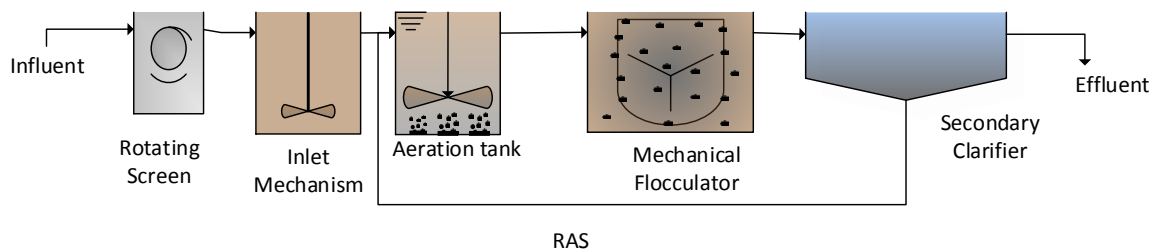


Figure 10: University of New Orleans pilot plant configuration

The sampling plan for the NO pilot plant involved collecting grab samples several times per week. The sampling points included the effluent from the rotary screen (plant influent), the supernatant and MLSS from the aeration tank, the return activated sludge and secondary effluent. Samples were analysed for total COD, soluble COD (i.e. ffCOD is truly soluble COD) using a 0.45 micron Hach No. 300 glass qualitative filter paper, floc filtered COD using flocculated samples filtered using a 0.45 micron Hach No. 300 glass qualitative filter paper, and total and volatile suspended solids (Jimenez, 2002). EPS was extracted by

using the extraction method developed by Frolund et al. (1995) and is summarized as follows:

- Transfer 300 ml of sludge to an extraction beaker with baffles and the cation exchange resin (CER) was added (70g CER/g VSS).
- Stir suspension for 3 hours at 1000 rpm.
- The extracted EPS were harvested by centrifugation of a sample of the CER-sludge suspension for 1 minute at 12,000g to remove the CER.
- The supernatant was centrifuged twice for 15 minutes at 12,000g in order to remove remaining floc components.
- Quantify EPS by measuring the total organic carbon content of the sample by using an Apollo 9000HS-TOC analyzer (Tekmar-Dohrmann, Mason, Ohio).
- EPS was extracted at least three times per SRT. Triplicate values were averaged.

The data collected by Jimenez et al. (2013), at varying SRTs and dissolved oxygen (DO) concentrations, are based on the pilot plant operating parameters summarized in Table 2. The SRT and DO concentration were varied in order to evaluate the effect on the production of EPS and the subsequent effect in the removal efficacy of particulate and colloidal organics. A qualitative dataset was generated establishing the relationship between SRT, EPS production, and particulate COD removal and DO concentration, EPS production and particulate COD removal.

Table 2 Typical HRAS model calibration, process operating parameters used to generate model output to compare to data in Figure 11.

SRT	Influent Flow (m ³ /d)	WAS Flow (m ³ /d)	Reactor Volume (m ³)	RAS Flow (m ³ /d)	Reactor DO (mg/l)
0.3	5	0.2	0.15	3.75	1.5
0.5	7.5	0.15	0.22	3.75	2.0
1.0	3.75	0.11	0.22	3.75	1.25
1.5	3.75	0.12	0.35	3.75	1.5
2.0	3.75	0.09	0.35	3.75	1.5

SRT – Solids Retention Time, DO – Dissolved Oxygen concentration in the reactor

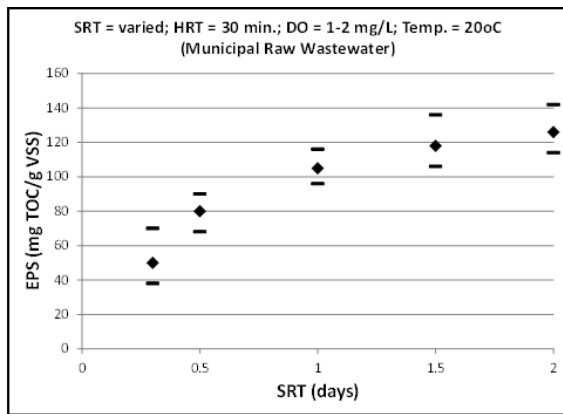
The feed source for the pilot was raw influent from the local municipal treatment facility.

The average influent constituent concentrations are summarized in Table 3.

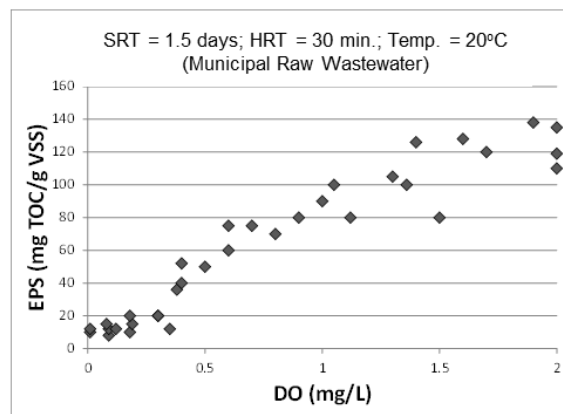
Table 3 A-stage model influent wastewater constituent concentrations

Symbol	Description	Value	Units
S _I	Soluble undegradable organics	10	g COD.m-3
S _{BF}	Soluble biodegradable organics	60	g COD.m-3
S _{Bs}	Slowly biodegradable organics	30	g COD.m-3
C _B	Colloidal biodegradable organics	60	g COD.m-3
X _U	Particulate undegradable organics from the influent	30	g COD.m-3
X _B	Particulate biodegradable organics	150	g COD.m-3
X _{OHO,ACT}	Active Ordinary heterotrophic organisms	10	g COD.m-3
X _E	Particulate undegradable endogenous products	0	g COD.m-3
S _{NOx}	Nitrate and nitrite (NO ₃ + NO ₂)	0	g N.m-3
S _{NHx}	Ammonia (NH ₄ + NH ₃)	35	g N.m-3
S _{NB}	Soluble biodegradable organic N	5	g N.m-3
X _{NB}	Particulate biodegradable organic N	10	g N.m-3
S _{ALK}	Alkalinity	6	meq/L
X _{INORG}	Inorganic suspended solids	40	g TSS.m-3
X _{EPS}	Extracellular Polymer Substances	1	g COD.m-3
X _{STO}	Storage Polymer Substances	1	g COD.m-3
pH	pH	7	-

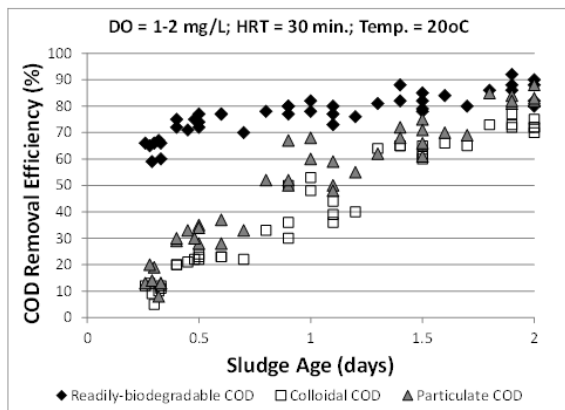
Figure 11 shows data used to calibrate the HRAS model for rbCOD removal, EPS production and colloidal removal which was collected by (Jimenez, 2002). This data includes EPS production as a function of SRT (Figure 11a), the effect of DO concentration on EPS production (Figure 11b), the effect of SRT on the removal efficiency of readily biodegradable and colloidal COD (Figure 11c), and impact of DO on the removal efficiency of readily biodegradable and colloidal COD (Figure 11d).



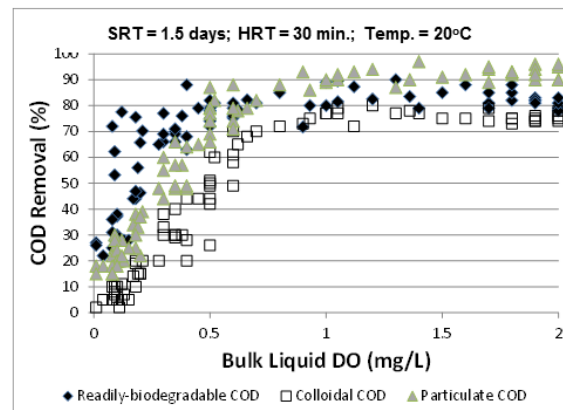
a) Impact of SRT on EPS Production



b) Impact of DO on EPS Production



c) Impact of SRT on the COD removal efficiency



d) Impact of DO on the COD removal efficiency

Figure 11: HRAS model Calibration data (Jimenez, 2002)

3.1.2 Hampton Roads Sanitation District (HRSD) Pilot Data (used for A-stage Model Validation and Stoichiometric Analysis)

HRSD owns and operates an A/B (adsorption/bio-oxidation) pilot plant located at the Chesapeake-Elizabeth treatment plant in Virginia Beach, Virginia. The pilot plant consists of an A-stage reactor for carbon removal followed by a B-stage for nitrogen removal. Currently, the A-stage includes three reactors (45 gal per reactor), operated at a 0.2 day SRT and a combined 0.5 hour HRT, and is fed screened and dewatered raw municipal wastewater at 4.5 gpm (24.53 m³/d) (Figure 12).

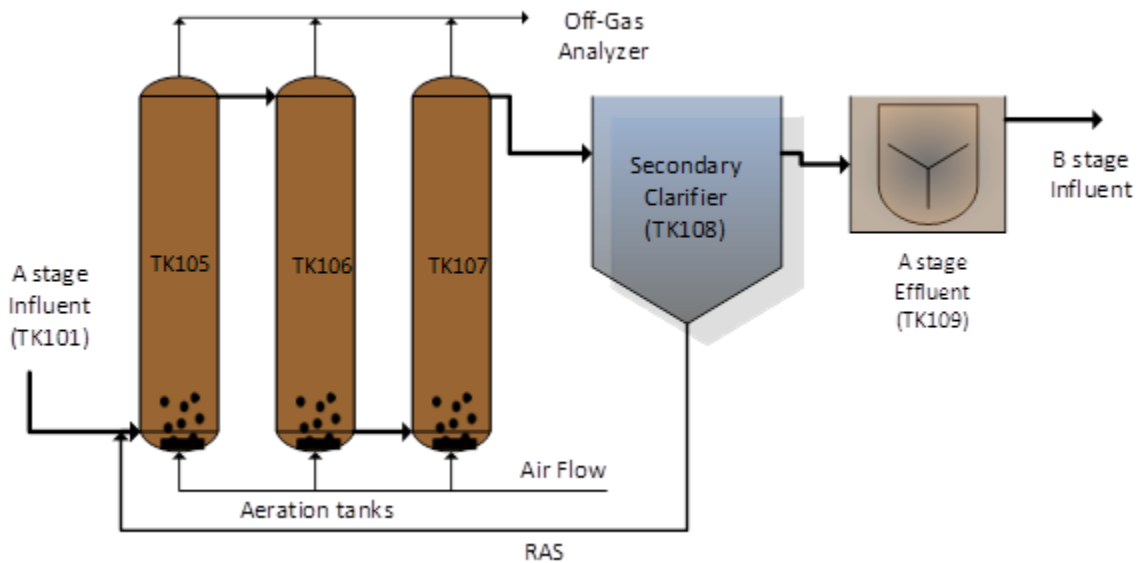


Figure 12: Process flow diagram of the HRSD A-stage process pilot plant

Operational data from the A-stage pilot plant was used to validate (not calibrate) the new carbon A-stage removal model and the stoichiometric analysis.

The 24 MGD Chesapeake-Elizabeth Treatment Plant (CETP) in Norfolk Virginia provides an important opportunity for the potential application of the mainstream deammonification process. CETP does not currently perform nitrogen removal, but Hampton Roads Sanitation

District (HRSD) anticipates a future treatment objective of 4–5 mg/L Total Nitrogen (TN). HRSD is currently operating a pilot study at CETP (Figure 12) to evaluate mainstream deammonification.

The A-stage or adsorption stage utilizes an SRT and HRT lower than most high rate activated sludge (HRAS) processes. The idea is to remove COD without oxidizing it by adsorption and assimilation. However the bioflocculation of particulate (pCOD) and colloidal COD (cCOD) may only be partial at these low SRTs and HRTs.

3.1.3 Sample Collection and Monitoring

Treatment efficiency of both the A-stage and B-stage were monitored by collecting 24-hr flow-weighted composite samples from the influent and effluent of each stage and analyzing it for TSS, total volatile suspended solids (TVSS), COD, sCOD, floc-filtered COD, total Kjeldahl nitrogen (TKN), soluble TKN, total phosphorus (TP) soluble orthophosphorus (SOP), and alkalinity. Grab samples are also routinely collected from the influent and effluent of each stage and from all activated sludge reactors. The grab samples were analyzed for TSS and the soluble species such as NO_3^- -N, NO_2^- -N, PO_4^{3-} -P (same as SOP), and total ammonia nitrogen (NH_3 -N + NH_4^+ -N = TAN). The sum of nitrate and nitrite was given the term NO_x -N or oxidized nitrogen species (Miller et al., 2012).

Table 4 shows the sampling plan used to collect the data from the HRSD pilot. EPS and storage products were not measured in the HRSD study, but O_2 and CO_2 off-gas was in the later part of the study. Each of the three A-stage reactors were covered, with the off-gas collected and analyzed using a Servomex Model 1440 gas analyzer. Data collected at 10 second intervals included % CO_2 , % O_2 and the standard airflow rates (SLPM). By comparing

this data to the ambient air concentrations, the change in CO₂ and O₂ concentrations in the off-gas were calculated. The change in CO₂ along with airflow data allowed the calculation of the CO₂ production rate (CO₂_PR) and the oxygen utilization rate (OUR).

Table 4 HRSD A-stage HRAS sampling plan (Miller, 2013)

Parameter	Units	RWI TK-101	HRAS Inf/Eff TK-103 and TK-109	HRAS TK-105	HRAS RAS	HRAS Effluent TK-107
CEL						
TSS	mg/L		2x/Wk/Composite	2x/Wk/Grab		2x/Wk/Composite
VSS	mg/L		2x/Wk/Composite	2x/Wk/Grab		2x/Wk/Composite
TCOD	mg/L			1x/Wk/Grab		
sCOD	mg/L					
VFA, Distillation	mg/L		2x/Wk/Composite			2x/Wk/Composite
VFA, GC	mg/L		1x/Wk/Composite			1x/Wk/Composite
TcBOD ₅	mg/L		1x/Wk/Composite			1x/Wk/Composite
ScBOD ₅	mg/L		1x/Wk/Composite			1x/Wk/Composite
TKN	mg N/L		2x/Wk/Composite	1x/Wk/Grab		2x/Wk/Composite
SKN	mg N/L		1x/Wk/Composite			1x/Wk/Composite
Pilot Plant						
Ammonia	mg N/L		5x/Wk/Composite			5x/Wk/Composite
Nitrate	mg N/L		5x/Wk/Composite			5x/Wk/Composite
Nitrite	mg N/L		5x/Wk/Composite			5x/Wk/Composite
COD	mg/L		5x/Wk/Composite			5x/Wk/Composite
Sol COD, GF	mg/L		5x/Wk/Composite			5x/Wk/Composite
Sol COD, CM	mg/L		1x/Wk/Composite			1x/Wk/Composite
ffCOD	mg/L		1x/Wk/Composite			1x/Wk/Composite
TSS	mg/L			3x/Wk/Grab	3x/Wk/Grab	3x/Wk/Comp
SVI	mL/g			3x/Wk/Grab		
Temperature	°C	5x/Week	5x/Week	5x/Week		5x/Week
pH		5x/Week	5x/Week	5x/Week		5x/Week
DO	mg O ₂ /L		5x/Week	5x/Week		5x/Week
Online Monitoring						

Parameter	Units	RWI TK-101	HRAS Inf/Eff TK-103 and TK-109	HRAS TK-105	HRAS RAS	HRAS Effluent TK-107
TSS	mg/L					Continuous
Temperature	°C	Continuous	Continuous	Continuous		Continuous
pH						Continuous
DO	mg O ₂ /L			Continuous		

CEL – Certified Environmental Laboratory

Pilot Plant – On-site sample analysis

Online Monitoring – Instrumentation and Telemetry system

RWI – Raw Water Influent

HRAS Inf/Eff – Pilot influent and effluent

HRAS RAS – Pilot Return Activated Sludge

3.2 Model Development

The base model to be used for the development of the A-stage HRAS model as part of this research is the Activated Sludge Model No.1 (ASM1) (Henze et al., 2000). This model consists of 14 state variables and 8 processes (Table 5). Although this model has been developed for both carbon (r1 and r2) and nitrogen (r3) removal; in meeting our objective of developing a model capable of integrating with a full plant model, we will incorporate nitrogen transformation by coupling them to carbon transformations. The stoichiometric coefficients which represent heterotrophic biomass growth on soluble substrate are shown in the biokinetic matrix (Table 5) as coefficients for transformation process 1.

The elemental composition matrix shown in Table 5 are the conversion values i for the state variables to be used. The parameters listed in Table 6 are the default parameters used for the model. These parameters are adjusted to calibrate the model to a specific operating condition. Data should be calibrated with as little change to the default values as possible.

Table 5 SUMO Peterson Matrix for ASM1 (Takacs, 2013)

j	Symbol	Name	S_I	S_S	X_U	X_B	$X_{B,H}$	$X_{B,A}$	X_E	S_O	S_{NO}	S_{NH}	S_{ND}	X_{ND}	S_{ALK}	S_{N2}	Rate expression (r_j)
1	r1	Aerobic growth of heterotrophs		$-1/Y_H$			1			$-(1-Y_H)/Y_H$		$-i_{XB}$			$-i_{XB} * i_{Charge_SNHx}$		$\mu_H * (S_S / (K_S + S_S)) * (S_O / (K_{O,H} + S_O)) * (S_{NH} / (K_{NH,H} + S_{NH})) * (S_{ALK} / (K_{ALK} + S_{ALK})) * X_{B,H}$
2	r2	Anoxic growth of heterotrophs		$-1/Y_H$			1				$-(1-Y_H) / (i_{NO3,N2} * Y_H)$	$-i_{XB}$			$-(1-Y_H) / (i_{NO3,N2} * Y_H) * i_{Charge_SNOx} - i_{XB} * i_{Charge_SNHx}$	$(1-Y_H) / (i_{NO3,N2} * Y_H)$	$\mu_H * (S_S / (K_S + S_S)) * (K_{O,H} / (K_{O,H} + S_O)) * (S_{NO} / (K_{NO} + S_{NO})) * (S_{NH} / (K_{NH,H} + S_{NH})) * \eta_g * X_{B,H}$
3	r3	Aerobic growth of autotrophs						1		$-(i_{COD_NO3} - Y_A) / Y_A$	$1/Y_A$	$-i_{XB} - 1/Y_A$			$(i_{XB} + 1/Y_A) * i_{Charge_SNHx} + (1/Y_A) * i_{Charge_SNOx}$		$\mu_A * (S_{NH} / (K_{NH} + S_{NH})) * (S_O / (K_{O,A} + S_O)) * (S_{ALK} / (K_{ALK} + S_{ALK})) * X_{B,A}$
4	r4	Decay of heterotrophs				$1-f_P$	-1		f_P					$i_{XB} - f_P * i_{XP}$			$b_H * X_{B,H}$
5	r5	Decay of autotrophs				$1-f_P$		-1	f_P					$i_{XB} - f_P * i_{XP}$			$b_A * X_{B,A}$
6	r6	Ammonification of soluble organic Nitrogen										1	-1		i_{Charge_SNHx}		$k_a * S_{ND} * X_{B,H}$
7	r7	Hydrolysis of entrapped organics		1		-1											$k_h * ((X_S / X_{B,H}) / (K_X + X_S / X_{B,H})) * ((S_O / (K_{O,H} + S_O)) + \eta_h * (K_{O,H} / (K_{O,H} + S_O))) * (S_{NO} / (K_{NO} + S_{NO})) * X_{B,H}$
8	r8	Hydrolysis of entrapped organic nitrogen											1	-1			$k_h * (X_{ND} / X_S) * ((X_S / X_{B,H}) / (K_X + X_S / X_{B,H})) * ((S_O / (K_{O,H} + S_O)) + \eta_h * (K_{O,H} / (K_{O,H} + S_O))) * (S_{NO} / (K_{NO} + S_{NO})) * X_{B,H}$

Elemental composition

COD	1	1	1	1	1	1	1	1	-1	i_{COD_NO3}	0	0	0	0	0		i_{COD_N2}
N	0	0	0	0	i_{XB}	i_{XB}	i_{XP}	0	0	1	1	1	1	0	0		1
Charge	0	0	0	0	0	0	0	0	0	i_{Charge_SNOx}	i_{Charge_SNHx}	0	0	-1	0		0

Table 6 ASM1 kinetic and stoichiometric parameters used in the Peterson matrix (Takacs, 2013)

Symbol	Name	Default value	Unit
k_h	Maximum specific hydrolysis rate	3	$\text{g X}_{\text{CB}} \cdot \text{g X}_{\text{OHO}}^{-1} \cdot \text{d}^{-1}$
K_X	Saturation coefficient for $\text{X}_B/\text{X}_{\text{OHO}}$	0.03	$\text{g X}_{\text{CB}} \cdot \text{g X}_{\text{OHO}}^{-1}$
η_h	Correction factor for hydrolysis under anoxic conditions	0.4	-
μ_H	Maximum growth rate of X_{OHO}	6	d^{-1}
η_g	Reduction factor for anoxic growth of X_{OHO}	0.8	-
K_S	Half-saturation coefficient for S_B	20	$\text{g S}_B \cdot \text{m}^{-3}$
b_H	Decay rate for X_{OHO}	0.62	d^{-1}
$K_{\text{O,H}}$	Half-saturation coefficient for S_{O_2}	0.2	$\text{g S}_{\text{O}_2} \cdot \text{m}^{-3}$
K_{NO}	Half-saturation coefficient for S_{NO_x}	0.5	$\text{g S}_{\text{NO}_x} \cdot \text{m}^{-3}$
$K_{\text{NH,H}}$	Half-saturation coefficient for NH_4^*	0.05	$\text{g S}_{\text{NH}_x} \cdot \text{m}^{-3}$
μ_A	Maximum growth rate of X_{ANO}	0.8	d^{-1}
b_A	Decay rate for X_{ANO}	0.15	d^{-1}
k_a	Rate constant for ammonification	0.08	$\text{m}^3 \cdot \text{g X}_{\text{CB,N}}^{-1} \cdot \text{d}^{-1}$
$K_{\text{O,A}}$	Half-saturation coefficient for S_{O_2}	0.4	$\text{g S}_{\text{O}_2} \cdot \text{m}^{-3}$
K_{NH}	Half-saturation coefficient for S_{NH_x}	1	$\text{g S}_{\text{NH}_x} \cdot \text{m}^{-3}$
K_{ALK}	Half-saturation coefficient for alkalinity	0.001	meq/L
Stoichiometric parameters			
Y_H	Yield for X_{OHO} growth	0.67	$\text{g X}_{\text{OHO}} \cdot \text{g X}_{\text{CB}}^{-1}$
f_P	Fraction of X_U generated in biomass decay	0.08	$\text{g X}_U \cdot \text{g X}_{\text{Bio}}^{-1}$
Y_A	Yield of X_{ANO} growth per S_{NO_3}	0.24	$\text{g X}_{\text{AUT}} \cdot \text{g S}_{\text{NO}_3}^{-1}$
i_{XB}	N content of biomass (X_{OHO} , X_{PAO} , X_{ANO})	0.086	$\text{g N} \cdot \text{g X}_{\text{Bio}}^{-1}$
i_{XP}	N content of products from biomass	0.06	$\text{g N} \cdot \text{g X}_{\text{UE}}^{-1}$
$i_{\text{NO}_3, \text{N}_2}$	NO_3 reduction to N_2 electron equivalence	2.857	$\text{g COD} \cdot \text{g N}^{-1}$
$i_{\text{COD}_, \text{NO}_3}$	NH_3 to NO_3 oxidation electron equivalence	-4.571	$\text{g COD} \cdot \text{g N}^{-1}$
$i_{\text{COD}_, \text{N}_2}$	NH_3 to N_2 oxidation electron equivalence	1.7142857	$\text{g COD} \cdot \text{g N}^{-1}$
$i_{\text{Charge}_, \text{SNH}_x}$	Conversion factor for NH_x in charge	0	$\text{kCharge} \cdot \text{g N}^{-1}$
$i_{\text{Charge}_, \text{SNO}_x}$	Conversion factor for NO_3 in charge	-7.14E-05	$\text{kCharge} \cdot \text{g N}^{-1}$
i_{CV}	Particulate COD to VSS ratio	1.48	$\text{g COD} \cdot \text{g VSS}^{-1}$

3.3 Mathematical Model IDE and Calibration/Validation Procedure

The software used for model simulation is SUMO version 0.9.15.0 developed by Dynamita SARL Nyons, France. SUMO includes an integrated development environment (IDE) used to define the process configuration to be modeled. This process configuration along with the model matrix are analyzed by the SUMO analysis engine to generate the performance data. The analysis can be run as a static simulation using the baseline data entered into the model or as a dynamic simulation using variable input for specific state variables. Each pilot configuration (HRSD and NO) was developed using the SUMO IDE (Figure 13).

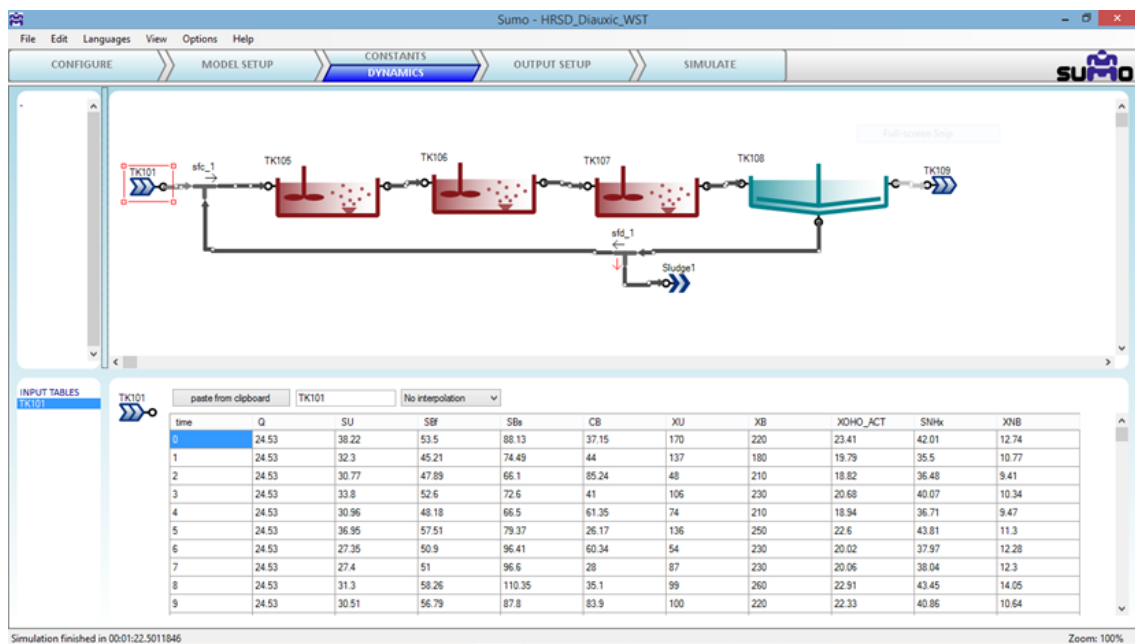


Figure 13: SUMO Integrated Development Environment – HRSD A-stage Pilot Configuration (Takacs, 2013)

3.3.1 A-stage Model Calibration using NO Dataset

Table 7 shows the model parameter values used to generate the model output. The calibration results shown in Table 7 were generated using the current A-stage model matrix which is a dual substrate (S_{Bf} and S_{Bs}) model based on a single heterotrophic population. Growth on the external substrate (S_{Bs}) is managed using a substrate switching function controlled by the substrate half saturation coefficient K_{Bs} (Appendix B). Calibration results discussed in subsequent Chapters may differ from the results in Table 7 since those efforts used an earlier version of the model matrix.

Table 7 Partial list of parameter values for the mass balance equations

Symbol	Name	Value	Unit
μ_{OHO}	Maximum growth rate of X_{OHO}	8	d^{-1}
K_{Bf}	Half-saturation coefficient for S_B	20	$g S_{Bf}.m^{-3}$
K_{Bs}	Half-saturation coefficient for S_{Bs}	40	$g S_{Bs}.m^{-3}$
b_{OHO}	Decay rate for X_{OHO}	0.62	d^{-1}
$K_{O,OHO}$	Half-saturation coefficient for S_{O_2}	0.1	$g S_{O_2}.m^{-3}$
q_{ADS}	Rate constant for adsorption	0.065	d^{-1}
K_{SL}	Half-saturation coefficient for surface limitation	0.009	-
q_{STO}	Rate constant for growth on X_{STO}	2	d^{-1}
$k_{EPS,MAX}$	EPS formation coefficient	0.225	$g COD_{EPS}.gVSS^{-1}$
$q_{EPS,HYD}$	EPS hydrolysis	0.25	d^{-1}
K_{EPS}	Half-saturation coefficient for EPS	100	$gX_{EPS}.m^{-3}$
$q_{XB,HYD}$	Rate Constant	2.75	d^{-1}
$k_{STO,MAX}$	Maximum Production Rate for Storage Polymers	0.58	$g X_{STO}.gS_{Bf}^{-1}$
f_{STO}	Fraction of X_{STO} in Active Biomass	0.15	-
$q_{STO,HYD}$	Storage Hydrolysis Rate Constant	3	d^{-1}
$K_{STO,HYD}$	Hydrolysis Half-saturation coefficient for STO	0.15	$gX_{STO}.gX_{OHO}^{-1}$
$K_{O,EPS}$	Half-saturation coefficient for S_{O_2}	1	$g S_{O_2}.m^{-3}$

The model was calibrated by adjusting the kinetic parameters associated with each process. For soluble substrate removal, the maximum specific growth rate (μ_{OHO}) was

adjusted (to 8 day^{-1}) so that the utilization rate for the S_{Bf} fraction was fast enough to initiate the uptake of S_{Bs} . This is consistent with work by Insel et al. (2012) who established in a bench-scale activated sludge SBR, fed acetate as the sole carbon source, that the maximum specific growth rate (μ_{OHO}) increased from 3.9 to 7 day^{-1} when the SRT was changed from 10 to 2 days. The half saturation coefficients (K_{Bf} and K_{Bs}) were then adjusted to better control the utilization of S_{Bf} and S_{Bs} to simulate the removal of soluble COD to fit the data (Figure 11c, d). The elevated half saturation coefficients K_{Bf} (20 gCOD/m^3) and K_{Bs} (40 gCOD/m^3) at an SRT ranging from 0.3 to 2 days are consistent with results obtained by Insel et al. (2012). Insel et al. (2012) established that the half saturation coefficient for growth (K_S) increased from 5 to $25 \text{ g COD}_S/\text{m}^3$ when the SRT was changed from 10 to 2 days. This suggests that K_S could be even higher in shorter SRT systems like the A-stage.

EPS removal (Figure 11a, b) was calibrated by adjusting the EPS formation parameter $k_{EPS,MAX}$ ($0.225 \text{ gCOD}_{EPS}\cdot\text{gVSS}$) and the EPS hydrolysis parameter $q_{EPS,HYD}$ (0.25 d^{-1}). Colloidal substrate removal (Figure 11c, d) was calibrated by adjusting the adsorption rate parameter q_{ADS} (0.065 d^{-1}) and the surface limitation parameter K_{SL} (0.009) until the HRAS model results trended well with the experimental data. The A-stage model calibration results are summarized in Figure 14 with the detailed results included in Appendix C.

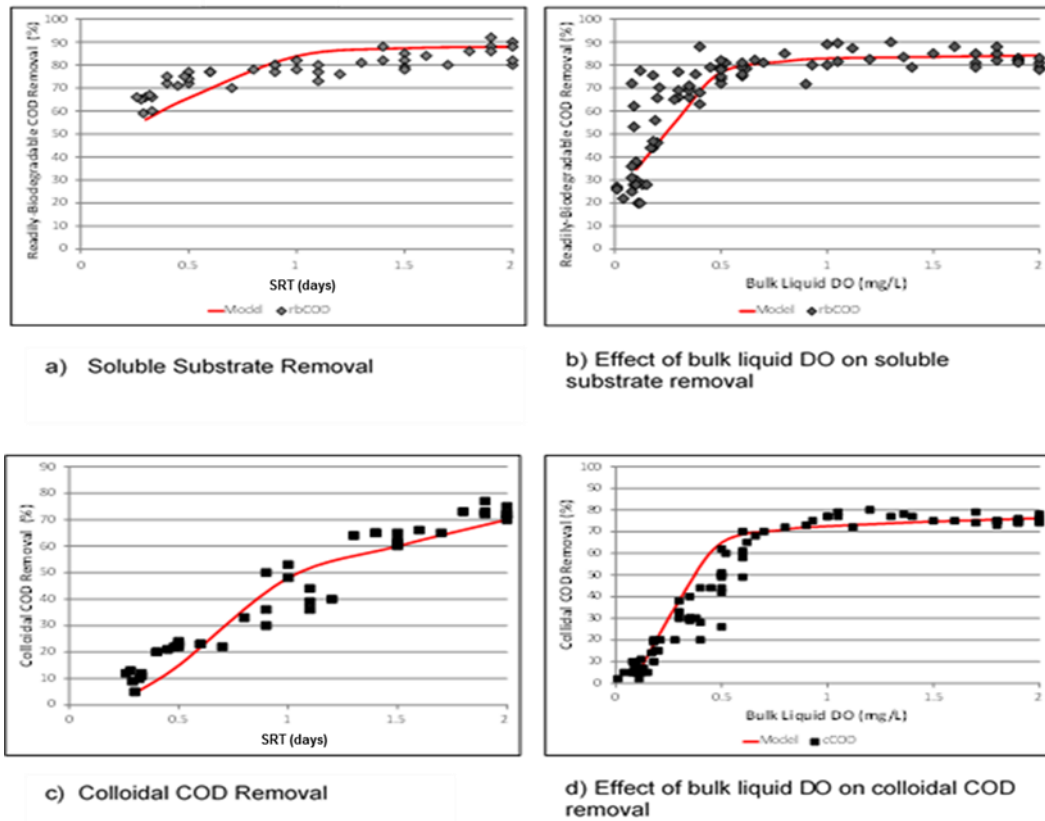


Figure 14: A-stage Model Calibration Results – NO Dataset

3.3.2 A-stage Model Validation using HRSD Dataset

The HRSD configuration was validated against the A-stage model matrix shown in Appendix B, using a subset of the pilot data collected (Appendix D). This dataset includes dynamic influent and effluent data for state variables including S_{Bf} , S_{Bs} , C_B , X_B , influent biomass, and reactor DO (SO_2). Dynamic input into the SUMO IDE also includes influent flow, the return activated sludge (RAS) flow, and waste activated sludge (WAS) flow. The default parameter values were obtained from the calibration results (Table 7). The validation procedure involved adjusting the select parameters to improve the model results fit with the

HRSD pilot data. It was found that the A-stage model results were highly sensitive to variations in the dissolved oxygen half saturation coefficient K_{O,OH_2O} (adjusted to 0.02 g $SO_2 \cdot m^{-3}$) and the initial fraction of storage products in the cell f_{STO} (adjusted to 0.1). Modifying these parameters generated results that trended well with the observed HRSD pilot data for soluble substrate (S_{Bf} and S_{Bs}) and reactor volatile suspended solids (VSS) (Figure 15)

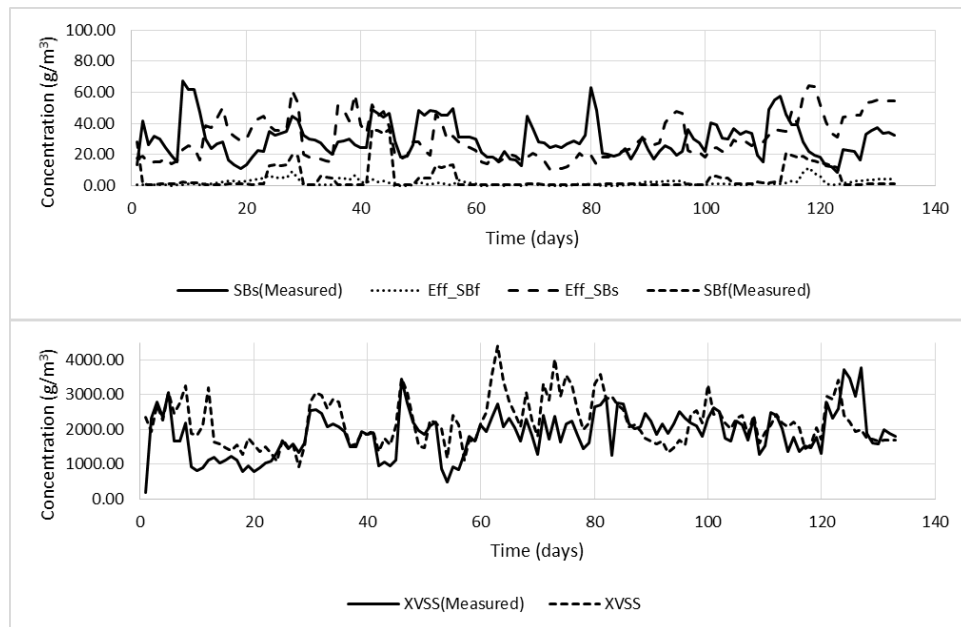


Figure 15: A-stage Model Validation Results – HRSD Dataset

The results shown in Figure 15 for reactor VSS are based on a revised particulate COD conversion factor of 1.86 gVSS/gCOD (default value is 1.48 gVSS/gCOD). This revised conversion factor was determined based on COD mass balances generated using the HRSD dataset (Appendix G). The procedure for determining this revised conversion factor is discussed in Chapter 7.

CHAPTER 4

MATHEMATICAL MODELING OF CARBON REMOVAL IN THE HIGH-RATE ACTIVATED SLUDGE SYSTEM: MODEL PRESENTATION AND APPLICATION

Note: The contents of this chapter will be submitted for publication in Water Research.

Thomas M. Nogaj, Andrew A. Randall, Jose A. Jimenez, Imre Takacs, Charles B. Bott, Mark W. Miller, Sudhir Murthy and Bernhard Wett; Mathematical Modeling Of Carbon Removal In The High-Rate Activated Sludge System: Model Presentation And Application

4.1 Introduction

Mathematical modeling of the activated sludge process has become an essential part of the design and operation of wastewater treatment plants. These models were developed to analyze the biochemical transformations that occur in wastewater treatment facilities. These biochemical operations alter or destroy materials that microorganisms can act upon via mineralization or biotransformation(Grady et al., 2011). Biochemical operations in activated sludge employ two major cycles: carbon and nitrogen. The microorganisms involved in each cycle derive their energy and reducing power from oxidation reactions, involving the transfer of electrons. Organisms that use organic compounds as their electron donor and source of carbon for cell synthesis are heterotrophic bacteria.

The IWA task group on mathematical modeling for design and operation of biological wastewater treatment processes has introduced activated-sludge models ASM No. 1, 2, 2D, and 3(Henze et al., 2000). ASM1 simulates the removal of organic matter (carbon) and nitrogen. Carbon removal occurs through the biological oxidation of organic matter and assimilation via biosynthesis, nitrogen removal occurs through biological nitrification and

denitrification, plus assimilation. The ASM 2 models (2, 2d) are an extension of ASM 1 incorporating biological nutrient (nitrogen and phosphorus) removal. ASM3 was developed as a possible replacement for ASM1 with the significant difference being the importance of storage polymers in the heterotrophic conversion of organics in activated sludge systems (Krishna & Van Loosdrecht, 1999).

The ASM1 and ASM3 models were developed to simulate the aerobic and anoxic treatment of domestic wastewater based on typical operating conditions, e.g. Solids Retention Time (SRT) greater than 3 days. These models were not developed to model activated sludge systems with very high organic loads or low SRTs (less than 1 day) where bioflocculation/adsorption of particulate and colloidal (slowly biodegradable) substrate and storage may become limiting (Henze et al., 2000). In addition, the very short hydraulic retention times of some HRAS systems may result in differences in predicted performance since the implicit assumption that substrate reactions can proceed to completion may no longer be true.

These models assume a two-step process for the removal of slowly biodegradable substrate (primarily particulate substrate and colloidal substrate): instantaneous enmeshment and hydrolysis of particulate and colloidal substrate followed by oxidation of soluble biodegradable substrate. However, researchers have overlooked the effect of the kinetics of bioflocculation on the overall particulate and colloidal substrate removal process and have concentrated their attention on the kinetics of hydrolysis and oxidation when modeling carbon removal in activated-sludge systems.

Jimenez et al. (2005, 2007) revealed that flocculation plays a major role in the removal of particulate and colloidal COD and many operational parameters such as solids retention time (SRT), dissolved oxygen (DO) and hydraulic retention times (HRT) can affect their removal in the activated sludge process. At low SRT (less than 2 days) and low HRT (less than 1 hour) some of the particulate and (especially) colloidal COD may not be removed since the kinetic rate of flocculation may not result in complete enmeshment and hydrolysis. Hence, flocculation should be considered as an important mechanism when modeling activated sludge systems, especially high-rate activated sludge (HRAS) processes (i.e. systems with low SRT and HRT).

This paper will discuss a mathematical modeling approach which evaluates the carbon cycle as it pertains to High Rate Activated Sludge (HRAS) systems. HRAS are operated at low SRTs (typically less than 1 day) where past ASM models are not adequate. This approach uses the ASM 1 as the initial framework. The framework will be modified adding the required removal mechanisms to accurately predict the performance of a HRAS system.

4.2 Materials and Methods

The 24 MGD Chesapeake-Elizabeth Treatment Plant (CETP) provides a unique opportunity for the potential application of the mainstream deammonification process. CETP does not currently perform nitrogen removal, but Hampton Roads Sanitation District (HRSD) anticipates a future treatment objective of 4–5 mg/L Total Nitrogen (TN). HRSD is currently operating a pilot study at CETP (Figure 16) to evaluate mainstream deammonification.

Hampton Roads Sanitation District (HRSD) owns and operates an A/B (adsorption/bio-oxidation) pilot plant located at the Chesapeake-Elizabeth treatment plant in Virginia Beach, Virginia. The pilot plant consists of a HRAS reactor for carbon removal followed by a B-stage for nitrogen removal. Currently, the HRAS A-stage is a single reactor, operated at a 0.5 day SRT and 0.5 hour HRT, and is fed screened and de gritted raw municipal wastewater at 1.5 gpm (Figure 16).

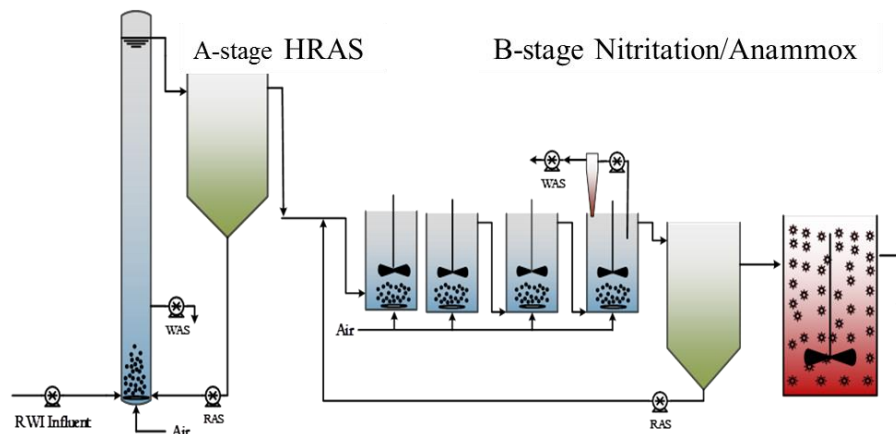


Figure 16: Process flow diagram of the HRSD A/B process pilot plant

HRSD is in the process of modifying the A stage configuration to include a parallel process train to include three AS columns. This configuration would provide flexibility in the process to be operated as either CSTR or plug flow type reactor. Operational data from the HRAS pilot plant will be used to further develop and to validate the new carbon HRAS removal model discussed in this paper.

4.2.1 Sample Collection and Monitoring

Treatment efficiency of both the A-stage and B-stage are monitored by collecting 24-hr flow-weighted composite samples from the influent and effluent of each stage and analyzed for TSS, total volatile suspended solids (TVSS), COD, sCOD, floc-filtered COD, total Kjeldahl nitrogen (TKN), soluble TKN, nitrate, nitrite, total phosphorus (TP), soluble phosphorus (SOP), and alkalinity. Grab samples are also routinely collected from the influent and effluent of each stage and from all activated sludge reactors. The grab samples are analyzed for TSS and the dissolved fractions of NO_3^- -N, NO_2^- -N, PO_4^{3-} -P, and total ammonia nitrogen (NH_3 -N + NH_4^+ -N = TAN). The sum of nitrate and nitrite is given the term NO_x -N or oxidized nitrogen species. The data collected through the sampling and monitoring program will be supplemented by extracellular polymeric substances EPS data collected by Jimenez as part of his dissertation (Jimenez, 2002).

4.3 Results and Discussion

4.3.1 High-Rate Activated Sludge (HRAS) System for Carbon Removal

The objective of a HRAS process is to remove organic carbon from influent wastewater at low SRTs, typically less than 1 day, which minimizes the oxygen required to remove influent organics and prevents nitrification. Detailed observations of preliminary results from the HRAS pilot system have led to the following modifications of existing models:

1. Preliminary results from the pilot show a higher effluent soluble COD than the B-stage where it is removed at a significantly longer SRT (Table 8). Normally, the method to quantify the non-biodegradable soluble COD is to operate a lab or pilot scale activated sludge system and use the effluent soluble COD as the non-biodegradable fraction. However, at the low SRT (and low HRT) of the HRAS system there is a fraction of the effluent COD that is biodegradable in the higher SRT B stage, but not biodegradable in the A (HRAS) stage. This has led to the establishment of two state variables for soluble biodegradable substrate designated as S_{Bf} (S_B fast) and S_{Bs} (S_B slow). S_{Bf} is the soluble COD that is biodegradable in both the HRAS and also in the B stage. S_{Bs} is the soluble COD that is non-biodegradable in the HRAS system, but is biodegradable in the B stage. In the HRAS model S_{Bf} is biodegraded first, and it is only when S_{Bf} runs out that biodegradation of S_{Bs} becomes significant. This is analogous to diauxic growth in which one substrate is biodegraded immediately by constitutive enzymes, and only when it runs out are enzymes induced for metabolism of the second substrate. The data does not show, or disprove, this mechanism, but this approach is at least plausible mechanistically. There are several other plausible approaches, however, such as simply running out of time to complete the biodegradation of S_{Bf} due to the low HRT.

Table 8 HRSD A-stage HRAS experimental data

Tank ID	TCOD	sCOD	pCOD	ffCOD	cCOD
A-stage (SRT < 1 d)					
Influent	455	260	195	188	72
Effluent	260	113	147	56	57
% Removed	43%	57%	25%	70%	21%
B-stage (SRT >= 6 d)					
Influent	260	113	147	56	57
Effluent	63	33	30	22	11
% Removed	76%	71%	80%	61%	81%

Typical characteristics for any municipal wastewater include both soluble and particulate organics. Before developing modifications to the mathematical model it is important to define the soluble, particulate and colloidal fractions of the influent COD. In Table 8 total chemical oxygen demand (TCOD) can be defined as the sum of particulate COD (pCOD) and soluble COD (sCOD) present in the wastewater. For the purpose of this investigation, the pCOD consists of organic suspended solids (ssCOD) retained by a 1.5 micron filter excluding the soluble COD (sCOD) in the wastewater ($pCOD = TCOD - sCOD$). The state variable X_B represents pCOD in the A-stage HRAS model. The colloidal COD (cCOD) consists of the fraction of the soluble COD (sCOD, fraction passing the 1.5 micron filter) retained by the 0.45 micron filter plus coagulant. The state variable C_B represents cCOD in the A-stage HRAS model. The dissolved COD excluding colloids is the truly soluble organic material in the wastewater and this was quantified by coagulation/flocculation

followed by filtration (i.e. ffCOD) (Jimenez et al., 2005). The truly soluble COD is defined in the HRAS model as the sum of the state variables S_{Bf} , S_{Bs} and S_I .

Figure 17 shows the COD breakdown adopted for the purpose of developing the HRAS carbon removal model (Jimenez, 2002). The most important aspect is the differentiation of particulate and colloidal COD, which has not traditionally been done in most studies nor in the ASM derived models. The reason for this is that in higher HRT and SRT systems there is plenty of time for both colloidal and particulate COD to flocculate completely and to be degraded. However, in low HRT/SRT systems (HRAS) there is not always time for this to occur. This also means that effluent CODs in HRAS systems are higher than would be predicted by existing models.

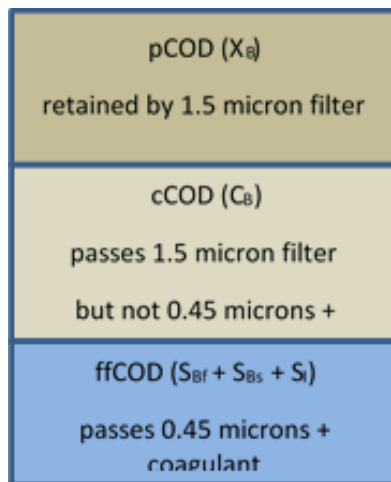


Figure 17: COD Fractionation for particulate (pCOD), colloidal (cCOD) and soluble COD (ffCOD) adopted for this work

The effluent from the pilot A-stage is the influent feed to the B-stage (Figure 16).

Experimental results from the pilot reveal a sCOD removal efficiency of approximately

57%, oxidation of the truly soluble COD accounts for most of the sCOD removal. The results (Table 8) show a 25% reduction in pCOD and 21% reduction in cCOD, which demonstrates that the assumption that the pCOD and cCOD are instantaneously enmeshed may not be accurate. In addition, even the effluent ffCOD in the A-stage was higher than the B-stage effluent suggesting that there is a fraction of the ffCOD that degrades slower than the rest.

2. Extracellular Polymer Substances (EPS) production impacts the bioflocculation removal efficiency for particulate and colloidal substrate (Jimenez, 2002). Past models assume instantaneous enmeshment whereas the data from Jimenez (2002 and 2013) shows that this assumption may not be valid for high rate systems. The EPS data produced by Jimenez (2002) and Jimenez et al. (2013) was used as calibration data for this study. The data indicates EPS production increased with SRT (thus decreased with growth) over a range of 0.3 to 2.0 days. In addition, EPS increased with the DO concentration over the same range of SRT values. Laspidou and Rittmann (2002a) hypothesized that the net EPS concentration is a function of the portion of influent soluble substrate (substrate electron pool) shunted to EPS formation versus the EPS hydrolysis rate. Our HRAS model incorporates EPS production as part of the aerobic growth process on S_{Bf} and S_{Bs} . The proportionality coefficient $k_{EPS,PC}$ quantifies the portion of influent electrons shunted to EPS formation. The portion of substrate electrons that are shunted to EPS formations ($k_{EPS,PC}$) are then subtracted from the biomass yield coefficient Y_{OHO} , i.e. $Y_{OHO}*(1 - k_{EPS,PC})$, reducing the electrons available for biomass synthesis. As substrate concentration decreases, the growth rate

decrease subsequently reduces EPS production. EPS formation is first driven by S_{Bf} during aerobic growth, although some influent electrons are lost to storage products. EPS formation on S_{Bs} does not occur until S_{Bf} starts to run out. In the model EPS formation driven by influent S_{Bs} does not have to compete with the formation of storage products (which only occurs through S_{Bf}). Additional S_{Bs} becomes available through hydrolysis of X_B (Carucci et al., 2001). $K_{O,EPS}$ was estimated using a nonlinear regression analysis of the EPS production data vs DO concentration data provided by Jimenez et al. (2000). The value $k_{EPS,MAX}$ (maximum EPS production) was determined by developing a least square logarithmic fit of the dataset provided by Jimenez et al. (2000) resulting in an estimated $k_{EPS,MAX}$ value of 0.25 (gCOD_{EPS}/gVSS).

$$k_{EPS,SC} = \left(\frac{k_{EPS,MAX}}{i_{CB}} \right) \times \left(\frac{S_{O_2}}{(K_{O,EPS} + S_{O_2})} \right) \quad (6)$$

Equation 6 shows how $k_{EPS,PC}$ was calculated; The term i_{CB} is a stoichiometric conversion factor that converts $k_{EPS,MAX}$ from units of gCOD_{EPS}/gVSS to gCOD_{EPS}/gCOD_{VSS}.

3. The production of storage polymers during the growth phase. Past studies have shown that the production of storage polymers at low SRT's (typical of a HRAS system) indicate that storage is dependent on the growth rate of the biomass (Sin et al., 2005; Van Aalst-Van Leeuwen et al., 1997). A linear correlation was developed for the accumulation rate of storage polymers based on the difference between the maximum substrate uptake rate and the uptake rate required for growth. When the system is

operated close to its maximum uptake rate (which exceeds the possible growth rate) then minimal storage is observed (Sin et al., 2005; Van Aalst-Van Leeuwen et al., 1997).

Since most WWTP's are operated at high SRT's (i.e. low growth rates relative to HRAS) it is hypothesized that the maximum substrate uptake rate is higher than the amount needed for growth. Therefore, the maximum flux into the cell (substrate electron pool) exceeds the amount that can be utilized for biomass synthesis, resulting in a portion of the influent electrons/carbon being diverted to formation of storage polymers (Sin et al., 2005).

The diversion of substrate electrons to storage in our HRAS model is represented by the proportionality constant $k_{STO,PC}$. Only S_{Bf} can be utilized to form storage products in the model. The portion of substrate electrons that are shunted to storage product formation ($k_{STO,PC}$) are also subtracted from the biomass yield coefficient Y_{OHO} , i.e. ($Y_{OHO} * (1 - k_{EPS,PC} - k_{STO,PC})$), for aerobic growth using S_{Bf} , further reducing the electrons available for biomass synthesis. Similar to how our HRAS model simulates EPS formation our model incorporates the formation of storage products into the process for aerobic growth. However, only S_{Bf} is used to form storage products. As the HRAS model evolves during the duration of this research it may be necessary to incorporate the formation of storage products in the process for aerobic growth on S_{Bs} (Carucci et al., 2001).

4.3.2 HRAS Model Matrix

The ASM models uses matrix notation for the presentation of biokinetic models. The matrix approach summarizes the components (state variables) and the transformation processes which are to be considered in the model. The stoichiometric coefficients and process rate equations are presented in the matrix. The matrix is often referred to as the Peterson matrix and will be referred to as such throughout this paper. Using the ASM1 Peterson matrix as our reference model, proposed modifications to the mathematical model for the HRAS model are defined in Figure 18. A partial list of state variables used is shown in Table 9. The modified stoichiometric matrix is shown in Table 10 with the associated process rate equations shown in Table 11. It must be noted that the pathways emanating from S_{Bf} and S_{Bs} will never both be significant at the same time due to the model kinetic equations being such that S_{Bs} transformations will not be significant until S_{Bf} runs out (i.e. when $S_{Bf} < K_{Bf}$; see Table 11). The colloidal substrate (C_B) is added as a new state variable. The C_B and slowly biodegradable particulate COD (X_B) are enmeshed which represents the colloidal and particulate COD adsorbed through the bioflocculation- removal mechanism. The adsorbed organics are then converted through hydrolysis to the slow fraction of soluble readily biodegradable substrate S_{Bs} .

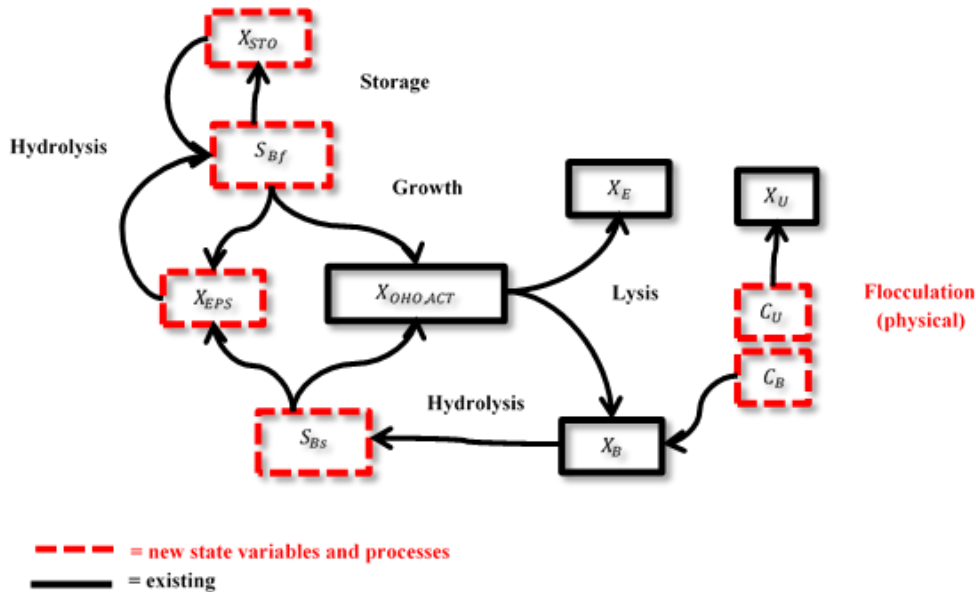


Figure 18: Proposed mathematical model modifications for the HRAS carbon removal model

Table 9 Partial list of state variables

Symbol	Name	Units
S_U	Soluble non-biodegradable organics	g COD.m^{-3}
S_{Bf}	Soluble biodegradable organics	g COD.m^{-3}
S_{Bs}	Slowly biodegradable organics	g COD.m^{-3}
C_U	Colloidal non-biodegradable organics from the influent	g COD.m^{-3}
C_B	Colloidal biodegradable organics	g COD.m^{-3}
X_U	Particulate non-biodegradable organics from the influent	g COD.m^{-3}
X_B	Particulate biodegradable organics	g COD.m^{-3}
$X_{OHO,ACT}$	Active Ordinary heterotrophic organisms	g COD.m^{-3}
X_{ANO}	Autotrophic nitrifying organisms (NH_4^+ to NO_3^-)	g COD.m^{-3}
X_E	Particulate non-biodegradable endogenous products	g COD.m^{-3}
S_{O_2}	Dissolved oxygen	$\text{g O}_2.\text{m}^{-3}$
S_{ALK}	Alkalinity	meq/L
X_{EPS}	Extracellular Polymer Substances	g COD.m^{-3}
X_{STO}	Storage Polymer Substances	g COD.m^{-3}

A new state variable (X_{STO}) was added for storage products. Gujer et al. (1999) in ASM 3 defines X_{STO} as a cell internal storage product of heterotrophic organisms (COD). It occurs only associated with X_{OHO} and is not included in the mass of X_{OHO} . X_{STO} cannot be directly compared with analytically measured PHA or glycogen. ASM 3 hypothesized, that all heterotrophic microorganisms (X_{OHO}) can store substrate. In contrast, Hanada et al. (2002) studied the possibility of combining the characteristics of ASM 1 and ASM 3, assuming there are two types of heterotrophic biomass, those that use storage material and those that don't. This was called the dual biomass model. Hanada et al. (2002) concluded that the ratio of heterotrophs to PHA producing heterotrophs ($X_{OHO/PHA}$) varied from 15-35% between facilities; based on operational and environmental conditions. The results revealed that the storage rate constant as defined in ASM 3 was not universally applicable. As part of this study, both concepts will be considered in developing the HRAS mathematical model.

Table 10 Partial Peterson matrix for the HRAS model

j	Symbol	Name	S_I	S_{BF}	S_{Bs}	C_U	C_B	X_U	X_B	$X_{OHO,ACT}$	X_E	S_{O_2}	X_{EPS}	X_{STO}
1	r1	Aerobic growth of heterotrophs - Fast		$1/(Y_{OHO,AER}*(1-k_{EPS,PC}-k_{STO,PC}))$						1		$-(1-Y_H)/Y_H$	$k_{EPS,PC}/(Y_{OHO,AER}*(1-k_{EPS,PC}-k_{STO,PC}))$	$k_{STO}/(Y_{OHO,AER}*(1-k_{EPS,PC}-k_{STO,PC}))$
2	r2	Aerobic growth of heterotrophs - Slow			$-1/(Y_{OHO,AER}*(1-k_{EPS,PC}))$					1		$-(1-Y_H)/Y_H$	$k_{EPS,PC}/(Y_{OHO,AER}*(1-k_{EPS,PC}))$	
3	r3	Decay of heterotrophs						$1-f_U$		-1	f_U			
4	r4	Hydrolysis of entrapped organics			1				-1					
5	r5	flocculation of colloidal substrate					-1		1					
6	r6	flocculation of colloidal inerts				-1		1						
7	r7	Hydrolysis of storage products		1										-1
8	r8	EPS hydrolysis		1									-1	

Table 11 Partial Peterson matrix process rate equations for the HRAS model

j	Symbol	Name	Rate expression (r _j)
1	r1	Aerobic growth of heterotrophs - Fast	$\mu_{OHO} * (S_{Bf} / (K_{Bf} + S_{Bf})) * (S_{O2} / (K_{O,OHO} + S_{O2})) * (S_{O2} / (K_{O,EPS} + S_{O2})) * (S_{NHx} / (K_{NHx,nut} + S_{NHx})) * X_{OHO}$
2	r2	Aerobic growth of heterotrophs - Slow	$\mu_{OHO,SLOW} * (S_{Bs} / (K_{Bs} + S_{Bs})) * (K_{Bf} / (K_{Bf} + S_{Bf})) * (S_{O2} / (K_{O,OHO} + S_{O2})) * (S_{O2} / (K_{O,EPS} + S_{O2})) * (S_{NHx} / (K_{NHx,nut} + S_{NHx})) * X_{OHO}$
3	r3	Decay of heterotrophs	$b_{OHO} * X_{OHO,ACT}$
4	r4	Hydrolysis of entrapped organics	$q_{XB,HYD} * ((X_B / X_{OHO}) / (K_{B,HYD} + X_B / X_{OHO})) * ((S_{O2} / (K_{O,OHO} + S_{O2})) + \eta_{HYD} * (K_{O,OHO} / (K_{O,OHO} + S_{O2}))) * (S_{NOx} / (K_{NOx} + S_{NOx})) * X_{OHO}$
5	r5	flocculation of colloidal substrate	$q_{ADS} * C_B * (X_{OHO} + X_{ANO}) * (K_{SL} / ((C_B / (X_{OHO} + X_{ANO})) + K_{SL})) * (X_{EPS} / (K_{EPS} + X_{EPS}))$
6	r6	flocculation of colloidal inerts	$q_{ADS} * C_U * (X_{OHO} + X_{ANO}) * (K_{SL} / ((C_U / (X_{OHO} + X_{ANO})) + K_{SL})) * (X_{EPS} / (K_{EPS} + X_{EPS}))$
7	r7	Hydrolysis of storage products	$q_{STO,HYD} * (X_{STO} / X_{OHO} / (K_{STO,HYD} + X_{STO} / X_{OHO})) * (K_{Bf} / (K_{Bf} + S_{Bf})) * (K_{Bs} / (K_{Bs} + S_{Bs})) * (S_{O2} / (K_{O,OHO} + S_{O2})) * X_{OHO}$
8	r8	EPS hydrolysis	$q_{EPA,HYD} * X_{EPS}$

Mathematical model modifications taking into account the effect of low sludge age (SRT) on the wastewater fractions of S_S and S_I resulted in the inclusion of three new state variables, inert colloidal COD (C_U), organic molecules available to the fast growing biomass associated with low SRT/HRT systems (S_{Bf}) and a fraction of the biodegradable COD concentration that is not utilized at low SRT's (SRT < 1 d) and HRT's (S_{Bs}) but biodegrades at high SRT/high HRT. Low SRT and HRT result in only partial degradation of the soluble substrate in the wastewater; the rest of the biodegradable soluble substrate is removed in the B-stage. The ffCOD experimental data supports this hypothesis. The A-stage obtained an ffCOD percent removal of 70% (SRT < 1 d) with an additional 18% removal in the B-stage (SRT \geq 6 d). The data reveals that the A-stage effluent ffCOD still contains readily biodegradable COD unlike effluents at greater SRTs. The biodegradable fraction remaining in A-stage effluent is designated as S_{Bs} which is further biodegraded in the B-stage. So the S_S of ASM1 is split into two fractions to model HRAS, i.e. S_{Bf} and S_{Bs} .

4.3.3 Fate of the Influent Substrate (S_{Bf} & S_{Bs})

Laspidou and Rittmann (2002b) developed a unified theory, which attempts to quantify the relationships among extracellular polymeric substances (EPS), soluble microbial products (SMP), original substrate, and an electron acceptor. We have adopted this theory in part by developing a model consistent in the way it describes the metabolism of all biomass types (De Silva & Rittmann, 2000). This approach, illustrated in Figure 19 and Figure 20, shows the fate of the COD (electron flow) as the substrate enters the cell.

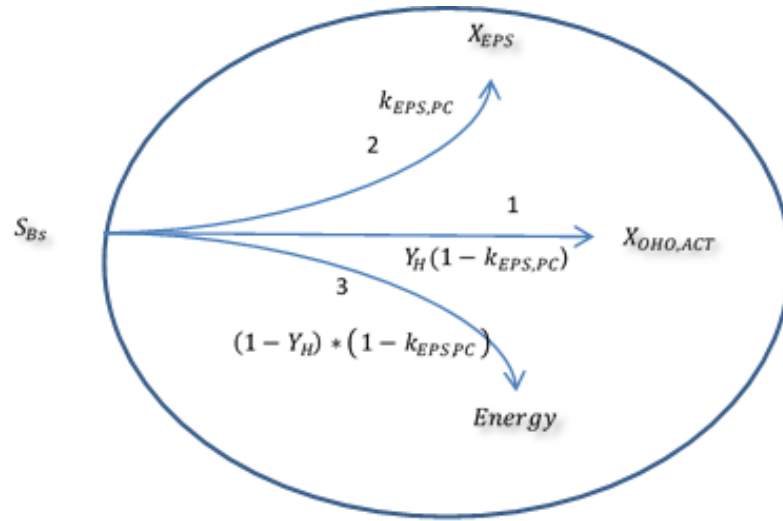


Figure 19: S_{Bs} electron flow schematic for HRAS model

For S_{Bs} , three (3) pathways were identified for which the COD (electrons) entering the cell could flow. A portion of the electrons are used by the cell for biomass synthesis (pathway No.1), while pathway No. 2 is for the production of EPS and pathway No. 3 are electrons sent to the electron acceptor to generate energy. The distribution of electrons for each pathway is defined by a proportionality coefficient (PC); $k_{EPS,PC}$ is the proportionality coefficient for the production of EPS ($Mass_{EPS}/Mass_{Ss}$) and Y_H is the true yield if all the influent substrate were used for biomass synthesis. Since this not the case in our model, Y_H is decreased by the factor $(1 - k_{EPS,PC})$.

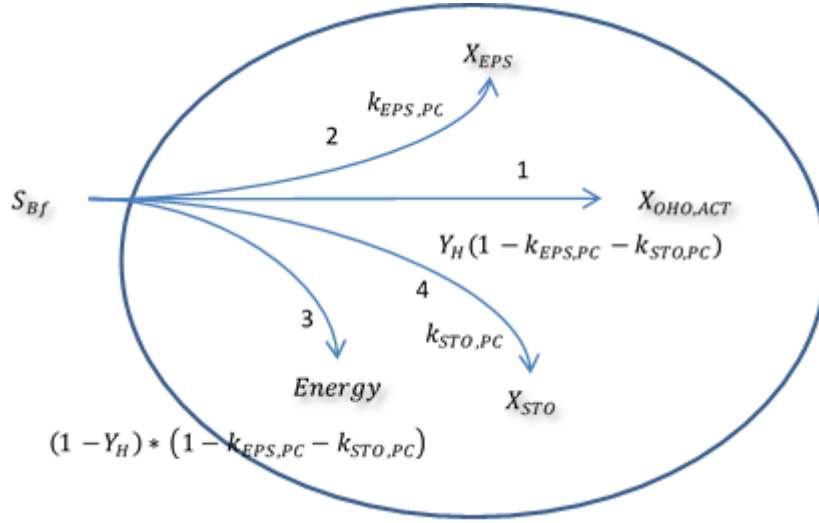


Figure 20: S_{Bf} electron flow schematic for HRAS model

For S_{Bf} , the HRAS model has been expanded to include a 4th pathway for which the COD (electrons) entering the cell could flow. A portion of the electrons are used by the cell for the production of STO (pathway No. 4). The proportionality coefficient $k_{STO,PC}$ has been added for the production of storage polymers (M_{STO}/M_S). Y_H is discounted by the factor $(1 - k_{EPS,PC} - k_{STO,PC})$.

This electron scheme can be incorporated into the Peterson matrix by modifying the stoichiometry for the aerobic growth of heterotrophs to account for the portion of electrons that are shunted to EPS resulting in:

$$(1)S_{B_s} + -x_{S_{B_s}}S_O = Y_H(1 - k_{EPS,PC})X_{OHO} + k_{EPS,PC}X_{EPS} \quad (7)$$

$$(1)S_{B_f} + -x_{S_{B_f}}S_O = Y_H(1 - k_{EPS,PC} - k_{STO,PC})X_{OHO} + k_{EPS,PC}X_{EPS} + k_{STO,PC}X_{STO} \quad (8)$$

We can do a continuity check of the COD based coefficients since

$$\sum COD \text{ Based Coefficients(Reactants)} = \sum COD \text{ Based Coefficients(Products)}$$

and solve for x (stoichiometric coefficient for dissolved oxygen S_O)

$$X_{S_{Bs}} = (1 - Y_H) * (1 - k_{EPS,PC}) \quad (9)$$

$$X_{S_{Bf}} = (1 - Y_H) * (1 - k_{EPS,PC} - k_{STO,PC}) \quad (10)$$

Substituting Equation (9) into Equation (7) and rearranging maintaining continuity

$$(-1)S_{Bs} + (-1) \left(\left((1 - Y_H) * (1 - k_{EPS,PC}) \right) \right) S_O + Y_H(1 - k_{EPS,PC})X_{OHO} + k_{EPS,PC}X_{EPS} = 0 \quad (11)$$

and Equation (10) into Equation (8) and rearranging maintaining continuity

$$(-1)S_{Bf} + (-1)(1 - Y_H) * (1 - k_{EPS,PC} - k_{STO,PC})S_O + Y_H(1 - k_{EPS,PC} - k_{STO,PC})X_{OHO} + k_{EPS,PC}X_{EPS} + k_{STO,PC}X_{STO} = 0 \quad (12)$$

Using X_{OHO} as the reference constituent, Equation (11) can be written as

$$\left(-\frac{1}{Y_H(1 - k_{EPS,PC})} \right) S_{Bs} + (-1) \left(\frac{(1 - Y_H)}{Y_H} \right) S_O + X_{OHO} + \frac{k_{EPS,PC}}{(1 - k_{EPS,PC})Y_H} X_{EPS} = 0 \quad (13)$$

and Equation (12) can be written as

$$\left(-\frac{1}{Y_H(1 - k_{EPS,PC} - k_{STO,PC})} \right) S_{Bf} + (-1) \left(\frac{(1 - Y_H)}{Y_H} \right) S_O + X_{OHO} + \frac{k_{EPS,PC}}{(1 - k_{EPS,PC} - k_{STO,PC})Y_H} X_{EPS} = 0 \quad (14)$$

In addition to the stoichiometric modifications two (2) new state variables X_{EPS} (g COD_{EPS}/L) and X_{STO} (g COD_{STO}/L) have been added to the matrix.

A hydrolysis process (r8) has been added to the HRAS Peterson matrix for the hydrolysis of X_{EPS} to S_{Bf} . A simple but reliable approach for EPS hydrolysis has been added to the HRAS model (Table 11); the EPS rate expression is a first order relationship with

respect to EPS (X_{EPS}) with $q_{EPS, HYD}$ as the hydrolysis rate constant (Laspidou & Rittmann, 2002a).

The framework for the storage component of the HRAS model is in the preliminary development phase. The storage proportionality coefficient $k_{STO, PC}$ is estimated based on the kinetic model for the storage product (STO) production phase presented by (Van Aalst-Van Leeuwen et al., 1997). It is assumed that bacterial biomass consists of two primary compartments, one for the active biomass and the other for storage products. The active biomass is capable of reproduction and growth; the storage products are used as storage for carbon and energy (Roels, 1983). Further evaluation, e.g. STO product consumption, and validation through a review of previous pilot studies and literature will be required to confirm which process components and parameters are to be included in the HRAS model.

4.3.4 Flocculation

Experimental results from the HRSD pilot plant (Table 8) reveal that a large fraction of the effluent COD from the A-stage comprises particulate and colloidal COD. Based on this data, particulate and colloidal COD removal efficiencies of 25% and 21%, respectively, were accomplished. This data demonstrates that the assumptions included in the existing activated sludge models, i.e. that particulate and colloidal COD are instantaneously enmeshed into the bio-floc, are not accurate.

Proposed modifications to the mathematical model for the HRAS process are shown in Table 10 (Jimenez, 2002; Jimenez et al., 2005). The model to date incorporates two new process components; r_5 flocculation of colloidal substrate (C_B) and r_6 flocculation of colloidal inerts (C_U). The kinetic rate expression for each process

$$r_5: \mathbf{q}_{\text{ADS}} \times \mathbf{C}_B \times (\mathbf{X}_{\text{OHO}} + \mathbf{X}_{\text{ANO}}) \times \left(\frac{\mathbf{K}_{\text{SL}}}{\left(\frac{\mathbf{C}_B}{(\mathbf{X}_{\text{OHO}} + \mathbf{X}_{\text{ANO}})} \right) + \mathbf{K}_{\text{SL}}} \right) \times \left(\frac{\mathbf{X}_{\text{EPS}}}{\mathbf{K}_{\text{EPS}} + \mathbf{X}_{\text{EPS}}} \right) \quad (15)$$

$$r_6: \mathbf{q}_{\text{ADS}} \times \mathbf{C}_U \times (\mathbf{X}_{\text{OHO}} + \mathbf{X}_{\text{ANO}}) \times \left(\frac{\mathbf{K}_{\text{SL}}}{\left(\frac{\mathbf{C}_U}{(\mathbf{X}_{\text{OHO}} + \mathbf{X}_{\text{ANO}})} \right) + \mathbf{K}_{\text{SL}}} \right) \times \left(\frac{\mathbf{X}_{\text{EPS}}}{\mathbf{K}_{\text{EPS}} + \mathbf{X}_{\text{EPS}}} \right) \quad (16)$$

is a first order rate expression with respect to the colloidal concentration. The kinetic parameter q_{ADS} is the adsorption rate constant and K_{SL} is the surface limitation coefficient. The colloidal substrate (C_B) is flocculated onto the particulate substrate (X_B). The adsorbed organics are then converted through hydrolysis to the slow fraction of the soluble readily biodegradable substrate (S_{Bs}) which can then be oxidized or stored by the biomass. The inert colloids (C_U) are flocculated onto the inert particulates (X_U) and removed from the system through wasting.

The work to-date forms a solid framework for the removal of colloids from a HRAS system. Additional pilot scale studies will be required to confirm this framework including the evaluation of the colloidal and particulate COD through the flocculation-removal mechanism forming X_{ADS} which defines the aggregation (adsorption) of the colloidal and suspended (particulate) solids onto the microbial floc.

4.3.5 Mathematical Model Calibration

The software used for model simulation is SUMO version 0.9.15.0 developed by Dynamita SARL Nyons, France. The process consists of influent flow, aeration basin

(reactor), clarifier (solids separation), return activated sludge flow to the reactor (RAS), waste activated sludge flow (WAS) and effluent.

The data collected by Jimenez et al. (2013), at varying SRTs and dissolved oxygen (DO) concentrations, are based on the pilot plant operating parameters summarized in Table 12. The SRT and DO concentration were varied in order to evaluate the effect on the production of EPS and the subsequent effect in the removal efficacy of particulate and colloidal organics. A qualitative dataset was generated establishing the relationship between SRT, EPS production, and particulate COD removal and DO concentration, EPS production and particulate COD removal.

Table 12 HRAS model calibration, process operating parameters

SRT	Influent Flow (m ³ /d)	WAS Flow (m ³ /d)	Reactor Volume (m ³)	RAS Flow (m ³ /d)	Reactor DO (mg/l)
0.3	5	0.2	0.15	3.75	1.5
0.5	7.5	0.15	0.22	3.75	2.0
1.0	3.75	0.11	0.22	3.75	1.25
1.5	3.75	0.12	0.35	3.75	1.5
2.0	3.75	0.09	0.35	3.75	1.5

The feed source for the pilot was raw influent from the local municipal treatment facility.

The average influent constituent concentrations are summarized in Table 13.

Table 13 HRAS model influent wastewater constituent concentrations

Symbol	Description	Value	Units
S _I	Soluble undegradable organics	10	g COD.m-3
S _{Bf}	Soluble biodegradable organics	60	g COD.m-3
S _{Bs}	Slowly biodegradable organics	30	g COD.m-3
C _U	Colloidal undegradable organics from the influent	20	g COD.m-3
C _B	Colloidal biodegradable organics	40	g COD.m-3
X _U	Particulate undegradable organics from the influent	30	g COD.m-3
X _B	Particulate biodegradable organics	150	g COD.m-3
X _{OHO,ACT}	Active Ordinary heterotrophic organisms	10	g COD.m-3
X _E	Particulate undegradable endogenous products	0	g COD.m-3
S _{NOx}	Nitrate and nitrite (NO ₃ + NO ₂)	0	g N.m-3
S _{NHx}	Ammonia (NH ₄ + NH ₃)	35	g N.m-3
S _{NB}	Soluble biodegradable organic N	5	g N.m-3
X _{NB}	Particulate biodegradable organic N	10	g N.m-3
S _{ALK}	Alkalinity	6	meq/L
X _{INORG}	Inorganic suspended solids	40	g TSS.m-3
X _{EPS}	Extracellular Polymer Substances	1	g COD.m-3
X _{STO}	Storage Polymer Substances	1	g COD.m-3
pH	pH	7	-

The model was calibrated by adjusting the kinetic parameters associated with each process.

Table 14 shows the model parameter values used to generate the model output.

Table 14 Partial list of parameter values for the mass-balance equations

Symbol	Name	Value	Unit
$K_{B,HYD}$	Saturation coefficient for X_B/X_{OHO}	0.03	$g X_{CB}.g X_{OHO}^{-1}$
μ_{OHO}	Maximum growth rate of X_{OHO}	7	d^{-1}
K_{Bf}	Half-saturation coefficient for S_B	2	$g S_{Bf}.m^{-3}$
K_{Bs}	Half-saturation coefficient for S_{Bs}	3	$g S_{Bs}.m^{-3}$
b_{OHO}	Decay rate for X_{OHO}	0.62	d^{-1}
$K_{O,OHO}$	Half-saturation coefficient for S_{O2}	0.1	$g S_{O2}.m^{-3}$
K_{NOx}	Half-saturation coefficient for S_{NOx}	0.5	$g S_{NOx}.m^{-3}$
$K_{NHx,nut}$	Nutrient half-saturation coefficient	0.05	$g S_{NHx}.m^{-3}$
q_{ADS}	Rate constant for adsorption	0.08	d^{-1}
K_{SL}	Half-saturation coefficient for surface limitation	0.002	-
q_{STO}	Rate constant for growth on X_{STO}	2	d^{-1}
K_{NHx}	Substrate Half-saturation coefficient for ANOs	1	$g S_{NHx}.m^{-3}$
$k_{EPS,MAX}$	EPS formation coefficient	0.25	$g COD_{EPS}.gVSS^{-1}$
$q_{EPS,HYD}$	EPS hydrolysis	0.12	d^{-1}
K_{EPS}	Half-saturation coefficient for EPS	100	$gX_{EPS}.m^{-3}$
$q_{XB,HYD}$	Rate Constant	2.75	d^{-1}
$k_{STO,MAX}$	Maximum Production Rate for Storage Polymers	0.58	$g X_{STO}.gS_{Bf}^{-1}$
f_{STO}	Fraction of X_{STO} in Active Biomass	0.2	-
$q_{STO,HYD}$	Storage Hydrolysis Rate Constant	3	d^{-1}
$K_{STO,HYD}$	Hydrolysis Half-saturation coefficient for STO	0.15	$gX_{STO}.gX_{OHO}^{-1}$
$K_{O,EPS}$	Half-saturation coefficient for S_{O2}	1	$g S_{O2}.m^{-3}$
$\mu_{OHO,SLOW}$	Maximum growth rate of X_{OHO} on S_{SLOW}	1.5	d^{-1}

Figure 21 presents the HRAS model output as either a function of SRT, or as a function of DO concentration. The parameters affected by SRT and DO were ffCOD removal ($S_{Bf} + S_{Bs} + S_I$), and colloidal COD removal. These predictions are compared to the corresponding experimental data from Jimenez et al., 2002. Overall, the model outputs capture all the experimental trends.

For the removal of soluble readily biodegradable substrate (Figure 21a,b) the maximum growth rates used for S_{Bf} and S_{Bs} were 7 d^{-1} and 1.5 d^{-1} respectively. One challenge that had to be overcome during calibration involved developing the matrix so that the model would accurately predict results at low DO's. Initially, the matrix was designed to hydrolyze the particulate biodegradable substrate (X_B) to S_{Bf} . At a maximum growth rate for S_{Bf} greater than or equal to 3 d^{-1} , the HRAS model over predicted the readily biodegradable COD removal at low DO but trended well at the higher DO (greater than or equal to 1.0 mg/l). Since S_{Bf} is considered to consist of the most biodegradable fraction of the influent organics (e.g. due to low molecular weights, functional groups that facilitate biodegradation, compounds with constitutive enzymes corresponding to them, etc.) we expect a high growth rate. Lapidou et al. (2002a) used a growth rate of 7.5 d^{-1} . In order to lower the removal efficiency of soluble organics in the HRAS model to those that were observed, the HRAS matrix was modified so that X_B is hydrolyzed to S_{Bs} . However, this modification alone did not improve the model accuracy, in fact, it had the opposite effect. This was due to two factors, one X_B was now hydrolyzing to produce more S_{Bs} and second the utilization of S_{Bs} was slowed by a switching function preventing S_{Bs} uptake until all the S_{Bf} was utilized. The solution was to increase the growth rate on S_{Bf} to 7 d^{-1} (which was a value that also agreed

better with Laspidou et al., 2002a) which accelerated the utilization of S_{Bf} and initiated the uptake of S_{Bs} sooner. The utilization of S_{Bs} was controlled by the maximum growth rate on S_{Bs} , and this value was adjusted to 1.5 d^{-1} so that the simulated removal of soluble COD fit the data. Using this value and the revised maximum growth rate for S_{Bf} , the HRAS model results trended well with the experimental data (Figure 21a, b).

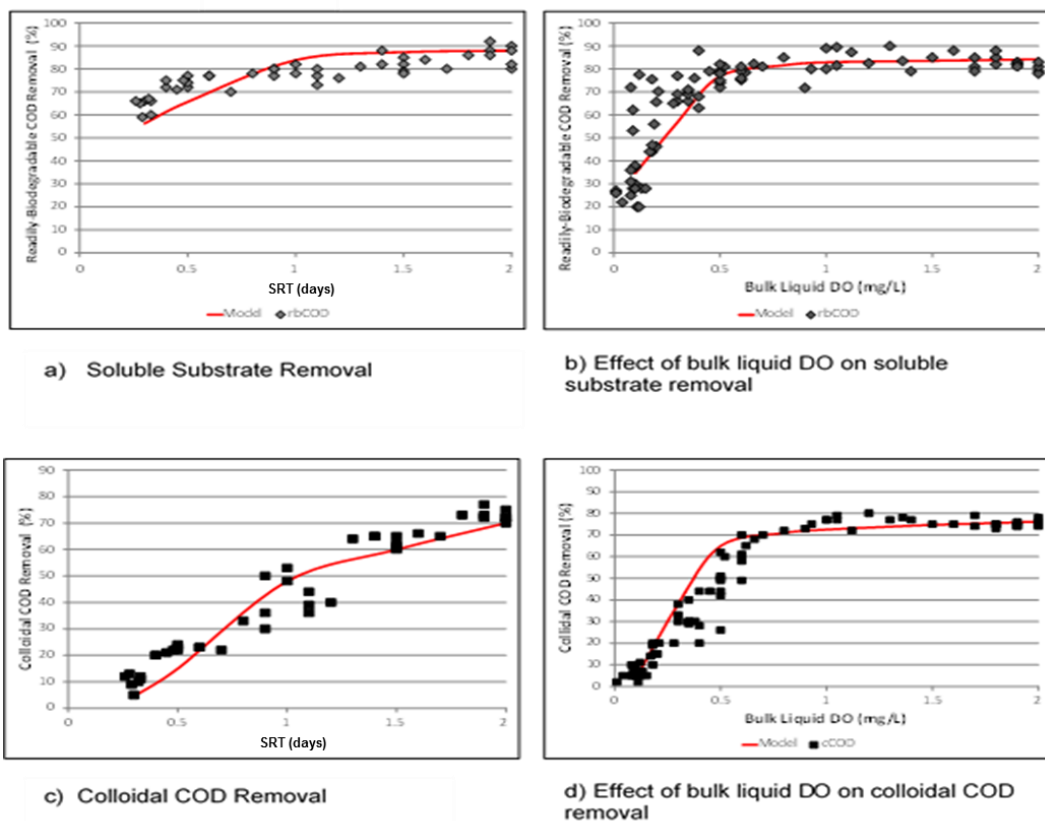


Figure 21: HRAS model calibration results.

Colloidal substrate removal (Figure 21c,d) was calibrated by adjusting the adsorption rate parameter q_{ADS} (0.08 d^{-1}) and the surface limitation parameter K_{SL} (0.002) until the HRAS model results trended well with the experimental data (Figure 21c, d). Future research includes experiments to further validate these parameter values

4.4 Conclusions

Simulation of the HRAS system was accomplished by including the kinetics of flocculation on the overall particulate and colloidal substrate removal process. In addition, the removal of soluble substrate in an HRAS system was simulated by differentiating the COD that is non-biodegradable in the HRAS system but biodegradable in longer SRT/HRT systems. The biosynthesis and hydrolysis/biodegradation of EPS and storage products were also included. All of the changes made were driven by observed data with the exception of including storage products.

The following list summarizes the preliminary conclusions based on the work completed to date:

1. Differentiating S_S into S_{Bf} and S_{Bs} allowed simulation of the difference in the effluent soluble COD of the HRAS (A stage) effluent versus the higher SRT/HRT B stage.
2. Differentiating colloidal COD from particulate COD allowed better simulation of the partial removal of this wastewater constituent observed in HRAS and B stage effluent.
3. The model framework presented in this paper is preliminary and just one approach that our team is evaluating. Future research efforts will evaluate alternatives, e.g. single substrate, in order to develop a reliable and efficient HRAS mathematical model.

CHAPTER 5

MODELLING OF ORGANIC SUBSTRATE TRANSFORMATION IN THE HIGH-RATE ACTIVATED SLUDGE PROCESS

Note: The contents of this chapter has been approved for publication in Water Science & Technology. Thomas M. Nogaj, Andrew A. Randall, Jose A. Jimenez, Imre Takacs, Charles B. Bott, Mark W. Miller, Sudhir Murthy and Bernhard Wett; Modelling Of Organic Substrate Transformation In The High-Rate Activated Sludge Process

5.1 Introduction

The high-rate activated sludge (HRAS) process for carbon removal uses high food-to-microorganism ratios and low solids and hydraulic retention times (SRT and HRT) for the biological transformation and removal of wastewater organics (COD). When a HRAS system is the first step in the Adsorption-Bio-oxidation (A/B) process(Bohnke & Diering, 1986), the general objectives are to maximize the removal of organics through adsorption/absorption while minimizing the energy input required for treatment and to produce large amounts of waste sludge that can be converted to biogas by anaerobic digestion (Schulze-Rettmer & Zuckut, 1998). A key mechanism in the adsorption of colloidal and particulate COD is the production of extracellular polymeric substances (EPS) produced as part of the aerobic growth transformation process. It is argued that the production of EPS is essential to sludge floc formation (Li & Yang, 2007). A key mechanism in the absorption of soluble substrate is the production of cellular storage products. The literature (Beun et al., 2000; Third et al., 2003) suggests that the operating environment of HRAS systems, high F/M ratios and low DO, is conducive to the production of storage products which allows for the redirection of COD to downstream processes e.g. anaerobic digestion for energy recovery. Hence, accurate

modelling of this system is of importance to design, control, and optimize the performance of not only HRAS systems but of the A/B process as a whole.

The modelling of the activated sludge process, particularly the COD transformations, has significantly evolved towards fundamental principles in the past decades from simple single-substrate models to more complex multiple-substrate models involving the processes of oxidation, hydrolysis and storage (Dold et al., 1980; Sin et al., 2005). However, these models have evolved to describe COD removal in systems operating at long SRT (i.e. > 3 days) where the biodegradable soluble organic substrate (S_B) can be modelled as a single substrate with a single kinetic expression. However, full-scale and pilot-scale results from HRAS (Haider et al., 2003; Jimenez, 2002; Miller et al., 2012) show that very low SRT (i.e. < 1 day) may result in a selection of fast growing bacteria, which are only able to biodegrade the most readily degradable organics in the process conditions of the A-stage (i.e. low SRT and short contact time). Haider et al. (2003) showed that the inert soluble COD fraction (S_U) in the effluent from a HRAS with an SRT of 0.5 days was always higher than the same COD fraction from a system with an SRT of 20 days. Hence, they recommended that for modelling, the S_B fraction of the wastewater should be split into two distinct biodegradable fractions. In addition, current models assume that flocculation and adsorption of colloidal and particulate substrate (C_B and X_B) is complete and instantaneous; hence, flocculation can be ignored in these models (Haider et al., 2003; Jimenez, 2002). However, in HRAS systems such as those employed in the A/B process, these assumptions with respect to organic substrate flocculation are no longer applicable (Jimenez et al., 2005) and removal of X_B and C_B is only partial.

5.1.1 ASM1 Model

The ASM1 model framework as presented by (Henze et al., 2000) was used as a first step to simulate the performance of the HRAS system and the results are depicted in Figure 22. In summary, the ASM1 model does not properly predict the removal of organic substrate at low SRTs. The ASM1 model under predicts the performance of the HRAS system with respect to effluent soluble COD and does not address the higher effluent colloidal CODs observed for the HRAS.

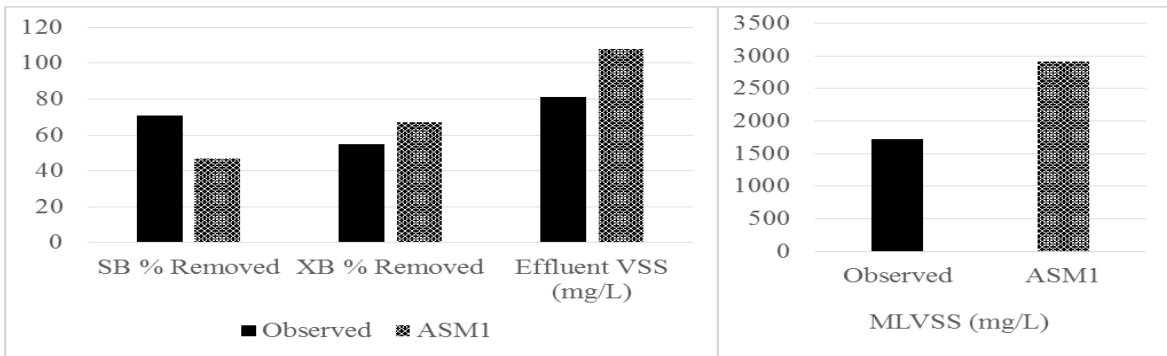


Figure 22: ASM1 Prediction for the HRAS System [Aerobic SRT = 0.25 d, DO = 0.2 mg/L, HRT = 30 min, $\mu_{max} = 6.0 \text{ d}^{-1}$; $K_s = 20 \text{ mg/L}$; $K_{O,H} = 0.2 \text{ mg/L}$; $b_H = 0.62 \text{ d}^{-1}$; $Y_H = 0.67$]

This study discusses a modelling approach which evaluates the organic substrate transformations as it pertains to HRAS systems. This approach uses the Activated Sludge Model No.1 (ASM1) (Henze et al., 2000) as the initial framework. The original framework was modified to describe the proper mechanisms required to accurately describe the performance of the HRAS system.

5.2 Materials and Methods

Historical operating data from two pilot systems were evaluated to understand the organic substrate transformation mechanisms in HRAS and used to calibrate and validate the proposed process model. The data used during this study includes operating data from an A-stage pilot plant owned and operated by the Hampton Roads Sanitation District (HRSD) (Miller et al., 2013) and from a HRAS pilot plant operated at the University of New Orleans (Jimenez et al. unpublished data).

HRSD owns and operates an A/B (adsorption/bio-oxidation) pilot plant located at the Chesapeake-Elizabeth treatment plant in Virginia Beach, Virginia. The pilot plant consists of a HRAS reactor for carbon removal followed by a B-stage for nitrogen removal (Figure 23). Currently, the HRAS A-stage includes three reactors (45 gal per reactor), operated at a 0.2 day SRT and 0.5 hour HRT, and is fed screened and degritted raw municipal wastewater at 4.5 gpm (24.53 m³/d).

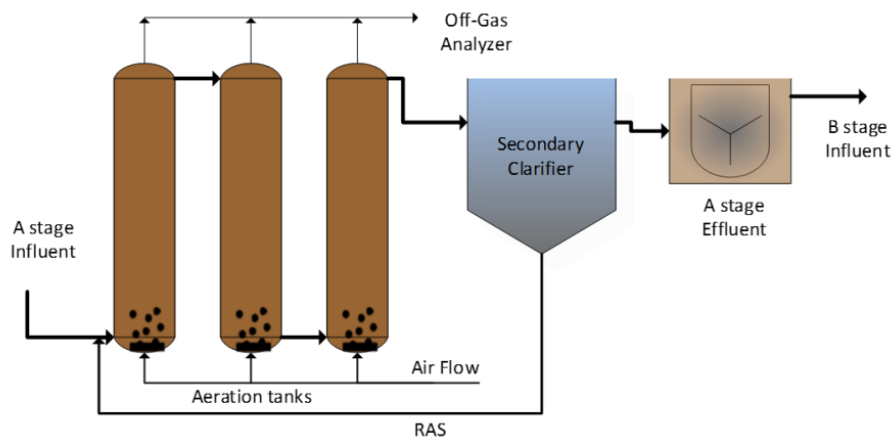


Figure 23: HRSD A-stage pilot plant configuration

The dataset used to calibrate the modified models was collected by Jimenez (unpublished data) and is referred to as the New Orleans (NO) dataset. The SRT and DO concentration were varied by Jimenez in order to evaluate the effect of these operating parameters on the production of EPS and the removal of organic substrate, and the same parameters were varied in the models presented in this paper during calibration using the NO dataset.

A partial list of the kinetic parameter values established through model calibration is summarized in Table 49 in Appendix F. The kinetic parameters added represent the pathways incorporated in the modified models for soluble substrate, EPS production, adsorption/flocculation and creation of storage polymers.

The New Orleans (NO) is a HRAS pilot plant comprised of the following components: a rotating screen, an inlet mechanism (30 gal mixing tank), an aeration tank (40 gal), a mechanical flocculator and a secondary clarifier (70 gal) (Figure 24). The unit was designed for a flow rate of $7.5\text{m}^3/\text{d}$ ($2000\text{gal}/\text{d}$), a hydraulic retention time in the aeration tank of 30 minutes, and the SRT varied from 0.3 days to 2 days.

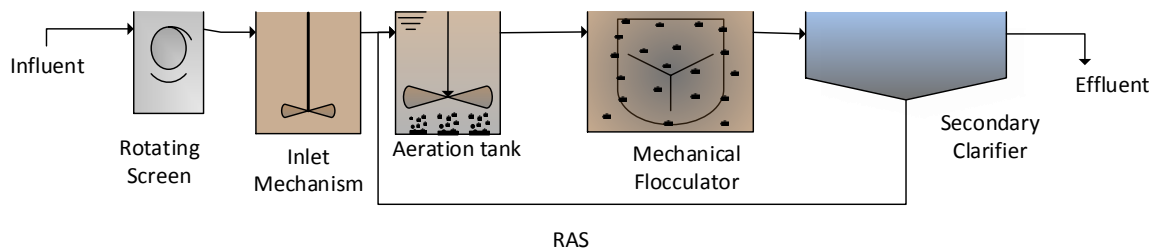


Figure 24: University of New Orleans pilot plant configuration

The sampling plan for the NO pilot plant involved collecting grab samples several times per week. The sampling points include the effluent from the rotary screen (plant influent), the supernatant and MLSS from the solids contact tank, the return activated sludge and secondary effluent. Samples were analysed for total COD, filtered COD using a 0.45 micron Hach No. 300 glass qualitative filter paper, dissolved COD using flocculated samples filtered using a 0.45 micron Hach No. 300 glass qualitative filter paper, total and volatile suspended solids. EPS was extracted by using the extraction method developed by Frolund et al. (1995) and is summarized as follows:

- 300 ml of sludge were transferred to an extraction beaker with baffles and the CER was added (70g CER/g VS).
- The suspension was stirred for 3 hours at 1000 rpm.
- The extracted EPS were harvested by centrifugation of a sample of the CER-sludge suspension for 1 minute at 12,000g to remove the CER.
- The supernatant was centrifuged twice for 15 minutes at 12,000g in order to remove remaining floc components.
- EPS was quantified by measuring the total organic carbon content of the sample by using an Apollo 9000HS-TOC analyzer fabricated by Tekmar-Dohrmann.

EPS was extracted at least three times per SRT. Triplicate values were averaged.

Dynamic simulations were run to calibrate and validate the HRAS model framework. The model was calibrated against the NO dataset based on the removal efficiency of the soluble (S_B) and colloidal COD and the EPS production rate. These parameters were evaluated under variable SRT and variable DO (constant SRT) conditions. Model validation was based on the removal efficiency of the soluble substrate (S_B) using a subset of the HRSD dataset spanning a 4 week period. Weekly averages were used as input parameters generated from daily composite samples.

5.3 Modified Model Description

To describe the behavior of the HRAS pilot plants, the ASM1 model was modified to incorporate non-steady state material balance equations for dual soluble substrate (S_{Bf} , S_{Bs}) utilization, production of EPS (X_{EPS}), production of storage products (X_{STO}), and adsorption of inert and biodegradable colloidal COD (C_U and C_B). The modifications were also influenced by the literature (Jimenez, 2002; Laspidou & Rittmann, 2002b; Miller et al., 2013).

5.3.1 Fate of Soluble Substrate

Conventionally, the method to quantify the non-biodegradable soluble COD from an activated sludge plant is to operate a laboratory or pilot scale system at an SRT longer than 3 days (Ekama et al., 1986) and use the effluent soluble COD as the non-biodegradable soluble fraction. However, at the low SRT (and low HRT) of the HRAS system, this method is no longer valid since there is a fraction of the effluent COD that is biodegradable in the higher SRT B-stage, but not biodegradable in the A-stage. This led to the establishment of two state

variables for S_B designated as S_{Bf} (S_B fast) and S_{Bs} (S_B slow). S_{Bf} corresponds to the high affinity soluble COD that is biodegradable in the HRAS system at low SRT and HRT (Haider et al., 2003; Pala-Ozkok et al., 2013). The high affinity substrate is defined as the raw influent SCVFA concentration. To further support this fractionation; in our model S_{Bf} is removed in the A-stage which is validated by the experimental results from the HRSD A-stage pilot which shows, on average, 95 percent removal of influent SCVFAs. S_{Bs} is the lower affinity fraction of the soluble COD that is biodegradable at a slower rate in the HRAS system and thus only partially biodegraded in the A-stage. Two modified models were developed. In one model, S_{Bf} is biodegraded first, and it is only when S_{Bf} is fully utilized that biodegradation of S_{Bs} becomes significant. This is analogous to diauxic growth in which one substrate is biodegraded immediately by constitutive enzymes, and only when the first substrate runs out are enzymes induced for metabolism of the second substrate. The data does not show, or disprove, this mechanism, but this model is at least plausible mechanistically. This is referred to in this study as the Diauxic Model. The second model is a dual substrate model where S_{Bf} and S_{Bs} are utilized simultaneously with the growth on S_{Bf} occurring at a higher maximum specific substrate utilization rate than growth on S_{Bs} . This model is referred to as the Dual Substrate Model in this study. The difference between the two model frameworks is the addition of an inhibition function in the Diauxic Model ($K_{Bf}/(K_{Bf}+S_{Bf})$) which applies to heterotrophic growth on S_{Bs} . There are significant differences in the kinetics between each model with the diauxic model including maximum growth rates and half saturation coefficients for each soluble substrate fraction. The Dual Substrate Model uses a single maximum growth rates with specific half saturation coefficients for each fraction.

Using ASM1 as the template for the development of both models several new state variables were added to the matrix, a list of the state variables added to both models is shown in Table 15. The stoichiometric and kinetic matrices were also modified with the changes included in Appendix F. Further details are discussed in the following sections.

Table 15 Partial list of state variables (gCOD.m⁻³)

Symbol	Name
S_U	Soluble non-biodegradable organics
S_{Bf}	Rapidly biodegradable soluble organics
S_{Bs}	Slowly biodegradable soluble organics
C_U	Colloidal non-biodegradable organics
C_B	Colloidal biodegradable organics
X_U	Particulate non-biodegradable organics
X_B	Particulate biodegradable organics
X_{OHO}	Active ordinary heterotrophic organisms
X_E	Particulate non-biodegradable endogenous products
X_{EPS}	Extracellular polymeric substances
X_{STO}	Intracellular storage polymeric substances

5.3.2 Adsorption of Colloidal COD

For the purpose of this investigation, the particulate COD (pCOD) consists of organic suspended solids (ssCOD) in the wastewater (pCOD =TCOD + sCOD). The soluble COD

(sCOD) excluding colloids is the truly soluble organic material in the wastewater and this was quantified by coagulation/flocculation followed by filtration (i.e. ffCOD) (Mamais et al., 1993). The sCOD is the sum of the state variables S_{Bf} , S_{Bs} and S_U .

In the Diauxic model it must be noted that the growth rates from S_{Bf} and S_{Bs} will never both be significant at the same time. This is due to the model kinetic equations being such that S_{Bs} transformations will not be significant until S_{Bf} runs out (i.e. when $S_{Bf} < K_{Bf}$).

The colloidal substrate is distinguished from suspended material in the HRAS model since flocculation and enmeshment of colloidal solids may not be complete in low SRT and HRT HRAS systems. The colloidal fraction is separated into its' biodegradable fraction (C_B) and its' non-biodegradable fraction (C_U) and added as new state variables. The C_B are enmeshed into X_B via bio-flocculation (see process r5 in Table 47 of the Appendix F) and when this occurs in the model they become part of the X_B which can subsequently be hydrolyzed (process r4) to form S_{Bs} . The kinetic rate expression for flocculation is a first-order rate expression with respect to the colloidal concentration (See Table 48 in Appendix F). The C_B is flocculated onto the X_B , becoming part of that category of organics. The adsorbed organics are then converted through hydrolysis to S_{Bs} which can then be oxidized or converted to EPS or biomass by the microorganisms. The C_U is flocculated onto the X_U and removed from the system through wasting. The A-stage influent C_U concentration is defined as the B-stage effluent C_U concentration. Due to flocculation and adsorption in the B-stage, this definition could result in the model under estimating the influent C_U concentration, just as current methods for estimating S_I for ASM1 and ASM2 type-models may over-estimate S_I since soluble microbial products are not explicitly accounted for because it is not practical to

do so. This is the same reason we do not explicitly account for the bio-flocculative/adsorptive removal of influent C_U . However, better methods for determining these COD fractions may be developed in future investigations, with the major difficulty being developing something still suitable for practical use (as the current method we propose is), as opposed to methods only possible in a handful of academic labs

5.3.3 EPS Production

Extracellular polymeric substances (EPS) production impacts the bioflocculation removal efficiency for particulate and colloidal substrate (Jimenez, 2002). The EPS data produced by Jimenez et al. (unpublished data) was used as calibration data for the models. This dataset shows a linear correlation between substrate utilization rate and EPS production and an increase in EPS production with SRT over a range of 0.3 to 2.0 days. In addition, EPS increased with the DO concentration over the same range of SRT values. Laspidou and Rittmann (2002a) indicated that the net EPS concentration is a function of the portion of influent soluble substrate (substrate electron pool) shunted to EPS formation versus the EPS hydrolysis rate. Hence, the modified models incorporate EPS production as part of the aerobic growth process on S_{Bf} and S_{Bs} . The proportionality coefficient $k_{EPS,PC}$ (Equation 18) quantifies the portion of influent electrons shunted to EPS formation. The portion of substrate electrons that are shunted to EPS formations ($k_{EPS,PC}$) are then subtracted from the biomass yield coefficient $Y_{OHO,AER}$, i.e. $Y_{OHO,AER}*(1 - k_{EPS,PC})$, reducing the electrons available for biomass synthesis. In the Diauxic model, EPS formation is first driven by S_{Bf} during aerobic growth. EPS formation on S_{Bs} does not occur until S_{Bf} starts to run out. In contrast, the EPS formation in the Dual Substrate model occurs simultaneously on both soluble substrate

fractions. Additional S_{Bs} becomes available through hydrolysis of X_B (Carucci et al., 2001). The values for $k_{EPS,MAX}$ (maximum EPS production) and $K_{O,EPS}$ were estimated using a nonlinear regression analysis of the EPS production data vs DO concentration data provided by (Jimenez, 2002). This analysis resulted in an estimated $k_{EPS,MAX}$ value of 0.25 (g COD_{EPS}/g VSS) and $K_{O,EPS}$ value of 1.5 (g S_{O_2}/m^3). The proportionality coefficient $k_{EPS,PC}$ is calculated as shown in Equation 17 and Equation 18.

$$k_{EPS,SC} = \left(\frac{k_{EPS,MAX}}{i_{CB}} \right) \times \left(\frac{S_{O_2}}{(K_{O,EPS} + S_{O_2})} \right) \quad (17)$$

The value $k_{EPS,SC}$ is the stoichiometric coefficient (SC) normalized to the biomass concentration (g $COD_{EPS}/gCOD_{XOHO}$). The term i_{CB} (1.48 g $COD_{XOHO}/gVSS$) is a stoichiometric conversion factor that converts $k_{EPS,MAX}$ from units of g $COD_{EPS}/gVSS$ to g $COD_{EPS}/gCOD_{XOHO}$. Since EPS is produced as a function of growth rate, and EPS hydrolysis is first order with respect to the amount of EPS available, EPS increases at very low SRTs. But as SRT increases a point is reached where the EPS hydrolysis rate exceeds EPS production, and beyond that point EPS decreases with increasing SRT. For the current models that occurred at an SRT greater than 2.0 days.

$$k_{EPS,PC} = \frac{(k_{EPS,SC} \times Y_{OHO,AER}) \times (1 - k_{STO,PC})}{(1 + (k_{EPS,SC} \times Y_{OHO,AER}))} \quad (18)$$

5.3.4 Production of Storage Products

Review of the literature suggests that systems operated at low DO concentrations (<0.9 mg/L; according to Third et al., 2003), typical of a HRAS system, the microbial uptake of rapidly biodegradable soluble COD (S_{Bf}) could result in the formation of storage

polymers. Third et al. (2003) found using acetate as the substrate for COD, the microbial uptake of acetate and its conversion to storage polymers was strictly oxygen dependent. At low DO, the flow of electrons was used for acetate uptake and production of storage polymers. Higher DO supply rates resulted in higher growth rates with the flow of electrons mainly going to biomass production with approximately 20% of the substrate being oxidized, independent of the DO concentration. The following expression was added to both the Diauxic and Dual Substrate models to simulate the flow of electrons to storage as a function of DO concentration.

$$f_{STO} = (f_{shunt,max}) \times \left(\frac{S_{O_2}}{(K_{O,STO} + S_{O_2})} \right) \quad (19)$$

Where f_{STO} represents the fraction of storage products in the active biomass, $f_{shunt,max}$ represents the maximum flow of electrons as a function of dissolved oxygen concentration and $K_{O,STO}$ is the half-saturation coefficient for S_{O_2} .

The diversion of substrate electrons to storage in the modified models is represented by the proportionality constant $k_{STO,PC}$. The portion of electrons that are shunted to $k_{STO,PC}$ are also subtracted from the biomass yield coefficient $Y_{OHO,AER}$, i.e. ($Y_{OHO,AER} * (1 - k_{EPS,PC} - k_{STO,PC})$), for aerobic growth using S_{Bf} and S_{Bs} , further reducing the electrons available for biomass synthesis. Storage products are biodegraded in the model when both S_{Bf} and S_{Bs} are depleted. X_{STO} is hydrolyzed directly to S_{Bs} and used for aerobic growth in such cases.

5.4 Results and Discussion

The Diauxic and Dual Substrate models were analyzed using the process simulator software SUMO version 0.9.15.0 developed by Dynamita (Nyons, France). The experimental datasets from New Orleans and HRSD were used to calibrate and validate the modified models.

5.4.1 Model Calibration

The soluble substrate (S_B) removal efficiency for the NO dataset of 70 percent compared to 69 percent for the Dual Substrate Model and 64 percent for the Diauxic Model indicates that, although both models were effective in predicting the removal efficiency, the dual substrate model results were slightly closer to the NO data. Figure 25 presents calibration curves comparing the Dual Substrate Model results, as a function of SRT and DO, with the NO experimental data. The model fit the NO data reasonably well.

Colloidal substrate removal was calibrated by adjusting the adsorption rate parameter q_{ADS} (0.07 d^{-1}) and the surface limitation parameter K_{SL} (0.002) until the Dual Substrate Model results trended well with the experimental data. Ongoing research includes analysis of independent datasets to validate these parameter values.

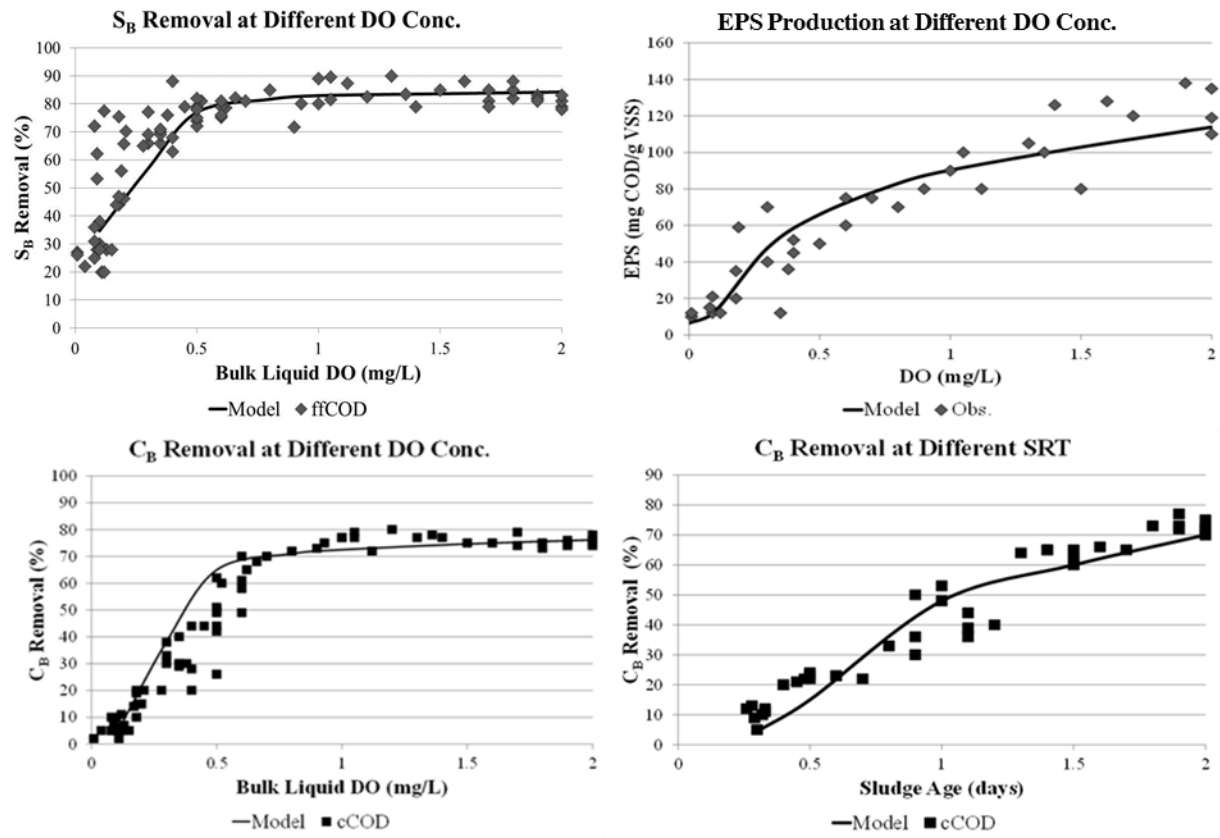


Figure 25: Dual Substrate Model calibration results

5.4.2 Modified Model Validation

The HRSD dataset used for validation spanned a four week period where the pilot plant had reached steady-state operating conditions. Weekly averages, based on daily composite samples, were calculated for that period and the data reduced to a format compatible with the models. Influent values for select state variables are shown in Table 16. S_U , S_{Bs} , C_B and C_U were obtained by comparing the A-stage (low SRT) and B-stage (high SRT) effluent COD fractions, including 1.5 micron filtration, ffCOD (0.45 micron membrane filters plus coagulant) and VFAs. Dynamic input data for model validation also included weekly DO concentrations, and return and waste activated sludge (RAS and WAS) flow.

Table 16 Influent state variables for model validation

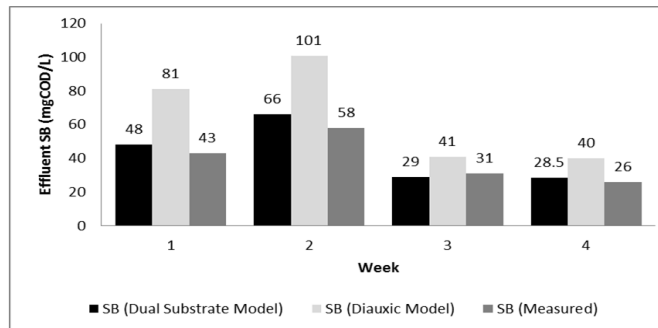
Time (week)	Q (m ³ /d)	S _U (g/m ³)	S _{Bf} (g/m ³)	S _{Bs} (g/m ³)	C _U (g/m ³)	C _B (g/m ³)	X _U (g/m ³)	X _B (g/m ³)	X _{OHO} (g/m ³)
1	24.53	28±1.2	53±2.7	76±3.0	4±0.5	44±4.5	31±5.5	312±34	20±1.0
2	24.53	19±1.03	50±3.12	89±5.4	11±1.5	40±3.5	38±6.5	278±58.7	20±1.34
3	24.53	19±0.22	51±0.6	89±1.01	10±1.75	324.0±	53±3	355±2.89	40±0.25
4	24.53	27±0.31	48±0.72	83±0.94	2±0.2	53±7.0	20±1.5	362±13.2	40±0.25

Ranges shown are ± one standard deviation.

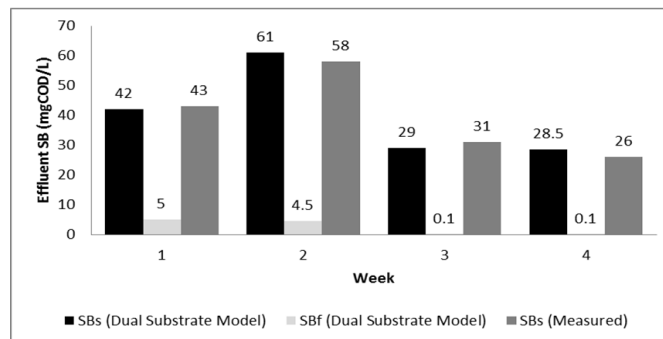
Dynamic simulations were performed in order to compare the predicted effluent values with those of the HRSD pilot plant. Figure 26a presents a comparison of the effluent soluble biodegradable fraction ($S_{Bf} + S_{Bs}$) for both the Diauxic and Dual Substrate models. Based on these results, the Dual Substrate model better predicts the performance of the HRSD pilot plant, however this may be due to the specific process configuration (especially HRT) in combination with the specific value of the switching function parameter in the Diauxic Model. This will be further evaluated in the future. Figure 26b shows the Dual Substrate Model predicted values for S_{Bf} and S_{Bs} . Based on the definition of the S_{Bf} and S_{Bs} fractions discussed previously, the model predicts almost full removal of S_{Bf} whereas a significant part of the S_{Bs} fraction passes through the biological reactor operated at an SRT of approximately 0.2 days.

The A-stage typically removed 68 to 77% of the influent S_{Bs} with the remainder being removed in the B-stage. The lower removal efficiencies/higher effluent S_B in the A-stage

during weeks 1 and 2 can be attributed to lower SRTs (0.086 and 0.126 days respectively) when compared to weeks 3 and 4 (0.236 and 0.23 days respectively).



a) Comparison of the effluent SB concentration from the Diauxic and Dual Substrate models



b) Dual Substrate model validation for SBf and SBs concentrations

Figure 26: Validation Results for the Diauxic and Dual Substrate models

5.4.3 Effect of Influent Biomass

The HRSD pilot operates at an SRT approaching the washout SRT condition based on the maximum growth rate for the heterotrophic biomass population. This results in a biomass population that varies significantly depending on the influent biomass concentration. Figure 27 shows the effect of influent biomass concentration at various SRT's on the reactor biomass concentration. The results show that as the SRT increases above 0.3 d, the biomass

concentration in the reactor approaches a condition where the influent biomass concentration no longer determines the reactor biomass concentration. However, at the lower SRT (typical of the HRSD pilot) the biomass concentration varies significantly depending on the influent biomass concentration. Therefore, the influent biomass concentration is essential to the model's ability to predict the MLVSS and the removal of soluble COD. This is consistent with the results in Figure 26 where the influent biomass concentration increased for weeks 3 and 4 (Table 16).

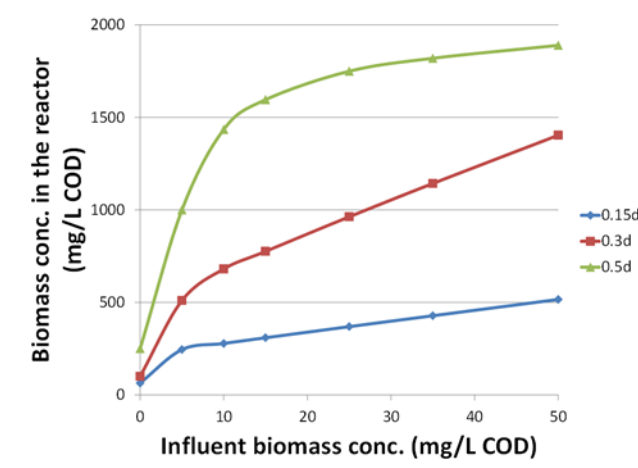


Figure 27: Effect of Influent Biomass Concentration

5.5 Conclusions

A modified ASM1 model was developed to describe the organic substrate transformation in the high-rate activated sludge (HRAS) process. Data from two HRAS pilot plants was used to calibrate and to validate the proposed model for HRAS systems. Two soluble substrate models were evaluated during this study, i.e. the Dual Substrate and the Diauxic Models. Both models used two state variables for biodegradable soluble substrate

(S_{BF} and S_{BS}) and a single biomass population. The Dual Substrate model provided better results than the Diauxic model and therefore it was adopted during this study. Overall;

- The Dual Substrate model described successfully the higher effluent soluble COD observed in the HRAS systems due to the partial removal of S_{BS} , which is almost completely removed in higher SRT systems.
- The Dual Substrate Model was able to accurately predict the elevated (compared to $SRT \gg 1$ day) effluent soluble COD for the HRSD A-stage.
- The Dual Substrate Model was more accurate than the Diauxic Model with respect to effluent soluble COD during the validation phase using HRSD A-stage data.

CHAPTER 6
MATHEMATICAL MODELING OF THE HIGH RATE ACTIVATED SLUDGE
SYSTEM: OPTIMIZING THE COD:N RATIO IN THE PROCESS EFFLUENT

Note: The contents of this chapter will be submitted for publication in Water Research.

Thomas M. Nogaj, Andrew A. Randall, Jose A. Jimenez, Imre Takacs, Charles B. Bott, Mark W. Miller, Sudhir Murthy and Bernhard Wett; Mathematical Modeling Of The High Rate Activated Sludge System: Optimizing The COD:N Ratio In The Process Effluent

6.1 Introduction

The industry has shown a considerable amount of interest in alternative approaches to nitrogen removal; one such approach is partial nitrification, i.e. the oxidation of ammonium to nitrite (nitrite pathway). This approach is a modification of the conventional process (Figure 28) where the second step in the nitrification pathway is shunted to the second step of the denitrification pathway, in other words, the second step of nitrification (Nitratation) and the first step of denitrification (Denitratation) are eliminated. The elimination of these two steps is referred to as “Nitrite Shunt”.

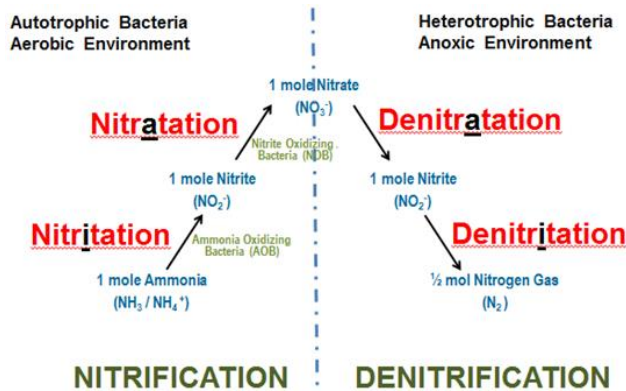


Figure 28: Conventional Nitrogen Removal

The goal is to eliminate nitrite oxidizing bacteria (NOB) from the reactor while selecting for ammonia oxidizing bacteria (AOB) (Regmi et al., 2012) . This process is illustrated Figure 29, where the first step is referred to as the nitrification step and the second is denitrification. This paper evaluates a mainstream A/B (Adsorption/Bio-oxidation) process focusing on the performance of the A-stage, specifically, the factors effecting the COD:N (total COD:TKN) ratio in the A-stage effluent. The advantages of this approach include:

- A reduction in oxygen demand (energy)
- No supplemental carbon source is needed (use COD in the A-stage effluent)

These advantages would result in lower capital investment as the result of a decrease in required reactor volumes, and a savings in annual operational costs. Along with the advantages to this approach there are several operational challenges, the most critical being able to attain nitrification through NOB suppression. The challenge is to reduce the carbon passed to the activated sludge reactor to a level that favors the growth of autotrophic biomass, but also drives the denitrification process by heterotrophic biomass. This would avoid having to provide an exogenous carbon source, e.g. methanol or acetate, to drive denitrification. The optimal amount of carbon passed to the activated sludge process is measured based on the COD:N ratio. The COD:N ratio in the B-stage influent (A-stage effluent) needed to support nitrogen removal in the B-stage is dependent on the type treatment provided in the B-stage. More influent COD may be needed due to the control strategy employed in the B-stage. One strategy used is transient anoxia (Regmi et al., 2014) , where the air flow is cycled on/off based on select set points, the COD is needed to drive down the residual DO concentration in the reactor (when air flow is off) to suppress NOB

activity. Current research suggests that conventional nitrification/denitrification may require a COD:N ratio of $\geq 9:1$ (Grady et al., 2011; Lemaire et al., 2008), nitrification/ anammox may require a COD:N ratio $\leq 3:1$ (Desloover et al., 2011; Jenni et al., 2014), and nitrification/denitrification a COD:N ratio of 7:1(Lemaire et al., 2008; Regmi et al., 2014).

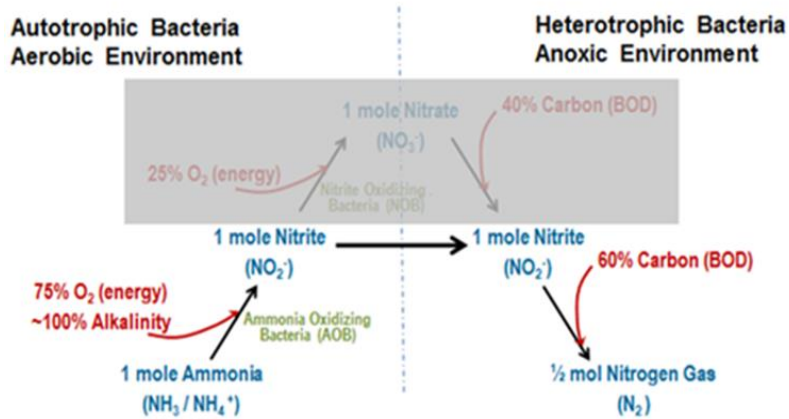


Figure 29: Nitrite Shunt

6.2 Materials and Methods

A calibrated process model(Nogaj et al., 2013), using SUMO (developed by Dynamita, Nyons, France) was used to evaluate the impact of process operating parameters on the effluent COD:N ratio. The process matrix used for this analysis was developed to model a HRAS system (Nogaj et al., 2013). The process configuration is shown in Figure 30.

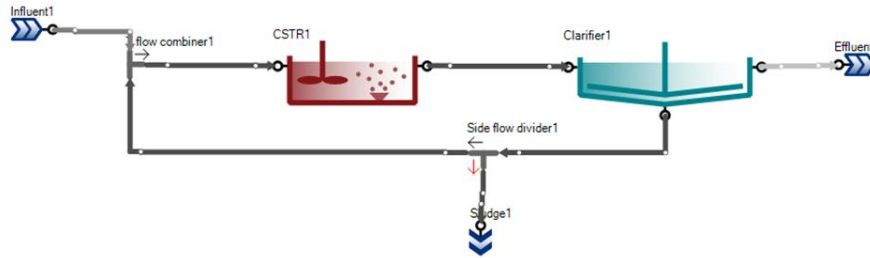


Figure 30: HRAS Process Configuration in SUMO

Historical operating data from two pilot systems were used to understand the effect of varying specific HRAS operating parameters on the soluble substrate removal and bioflocculation mechanisms in the HRAS model. The data used during this study includes operating data from an A-stage pilot plant owned and operated by the Hampton Roads Sanitation District (HRSD) (Miller et al., 2013) and from a HRAS pilot plant operated by the University of New Orleans (Jimenez, 2014).

The HRAS model process matrix subdivided the readily biodegradable fraction into S_{Bf} (VFAs) and S_{Bs} (the same as ASM2 F-rbCOD). Biodegradable non-soluble COD is subdivided into particulate COD (X_{COD}) and colloidal (C_B). The HRAS model also includes storage of soluble biodegradable substrate, hydrolysis and oxidation.

The stoichiometry for the aerobic growth of heterotrophic biomass on both S_{Bf} and S_{Bs} shunts influent electrons (COD), not just for growth and maintenance, but also for the production of extracellular polymeric substances (X_{EPS}) and cellular storage products (X_{STO}). The rate of bioflocculation is a function of the concentration of colloidal substrate, the total active biomass and EPS in the reactor.

6.3 Results and Discussion

One of the benefits of nitrite shunt is the lower operating costs associated with the reduction in COD required to complete the denitrification process. Lemaire et al. (2008) demonstrated this concept by adjusting the influent readily biodegradable COD (rbCOD) concentration feeding a single lab scale SBR providing biological nutrient removal. They found that by reducing the influent rbCOD concentration; the NO_x^- (nitrite + nitrate) started to accumulate in the effluent apparently caused by incomplete denitrification due to lack of COD supply. They found that the COD:N ratio required for conventional nitrification (active nitrate pathway) was approximately 9:1, whereas, when the system was operating via the nitrite pathway the COD:N ratio was around 7:1. These results support the reduced COD requirement for nitrite shunt. The relatively high COD:N ratio reported by Lemaire et al. (2008) may be due to the specificity of the wastewater treated (i.e., high levels of slowly biodegradable particulate COD and non-biodegradable COD). Also, additional nutrient removal (biological P) was achieved in their experiments.

The significance of the colloidal fraction of COD cannot be ignored when modeling HRAS systems. The removal efficiency of the colloidal fraction of COD is a function of the active biomass and EPS concentrations in the reactor; both of which are a function of the SRT. Longer SRTs (≥ 0.5 days) result in an increase in active biomass and EPS concentrations in the reactor, resulting in an increase in C_B removal efficiency. Regmi et al. (2014) hypothesized that the type and quantity of COD is important in inducing and maintaining NOB suppression and AOB activity. A rise in the soluble COD fraction in the HRAS effluent would result in a larger portion of the influent COD being rapidly removal

downstream, making less COD available for denitrification. The ideal effluent from the HRAS system would consist primarily of colloidal COD. Colloidal COD can be better managed downstream in the B-stage due the slower kinetics associated with hydrolysis.

The International Water Association (IWA) task group on mathematical modeling for design and operation of biological wastewater treatment processes has introduced activated-sludge models ASM No. 1, 2, 2D, and 3 (Henze et al., 2000). ASM1, which targets the removal of carbon and nitrogen, assumes a two-step process for the removal of slowly biodegradable substrate (primarily particulate substrate and colloidal substrate): instantaneous enmeshment and hydrolysis of particulate and colloidal substrate followed by oxidation of soluble biodegradable substrate. Flocculation plays a major role in the removal of particulate and colloidal COD and many operational parameters such as SRT, DO and HRT can affect their removal in the activated sludge process (Jimenez et al., 2005, 2007). The HRAS model includes mechanisms for the removal of the colloidal fraction of COD through the bioflocculation transformation process. Depending on how the HRAS process is operated the removal efficiency of the colloidal fraction of COD can have a significant impact on the TCOD in the reactor effluent, which impacts the colloidal COD fraction of the COD:N ratio received downstream.

A number of HRAS model (Nogaj et al., 2013) simulations were run in order to determine the effect of varying on the A-stage operating parameters on the effluent COD:N ratio. The model predictions for S_B removal, EPS production, C_B removal and storage products (X_{STO}) were compared to support the model results. These results are based on the New Orleans data set which has an influent COD:N(TKN) ratio of 8.5:1.

It is important to keep in mind, the COD:N ratio in the influent to the B-stage is only one of the criteria used for the out selection of NOBs, additional parameters include low SRT and intermittent aeration. The focus of this paper is on the operational factors effecting the COD:N ratio in the A-stage effluent.

6.3.1 Variable SRT

Preliminary results using the HRAS model at variable SRT ($DO > 1$ mg/l) are shown Figure 31. The results (Figure 31a) show that the COD:N(TKN) ratio decreases as the SRT increases from 0.3 days to 2 days. The most significant reduction occurs between 0.5 and 1.5 days which correlates well with the production of EPS (Figure 31c), the removal of the colloidal fraction of the influent COD, and the increase in active biomass (MLVSS) concentration (Figure 31d) in the reactor.

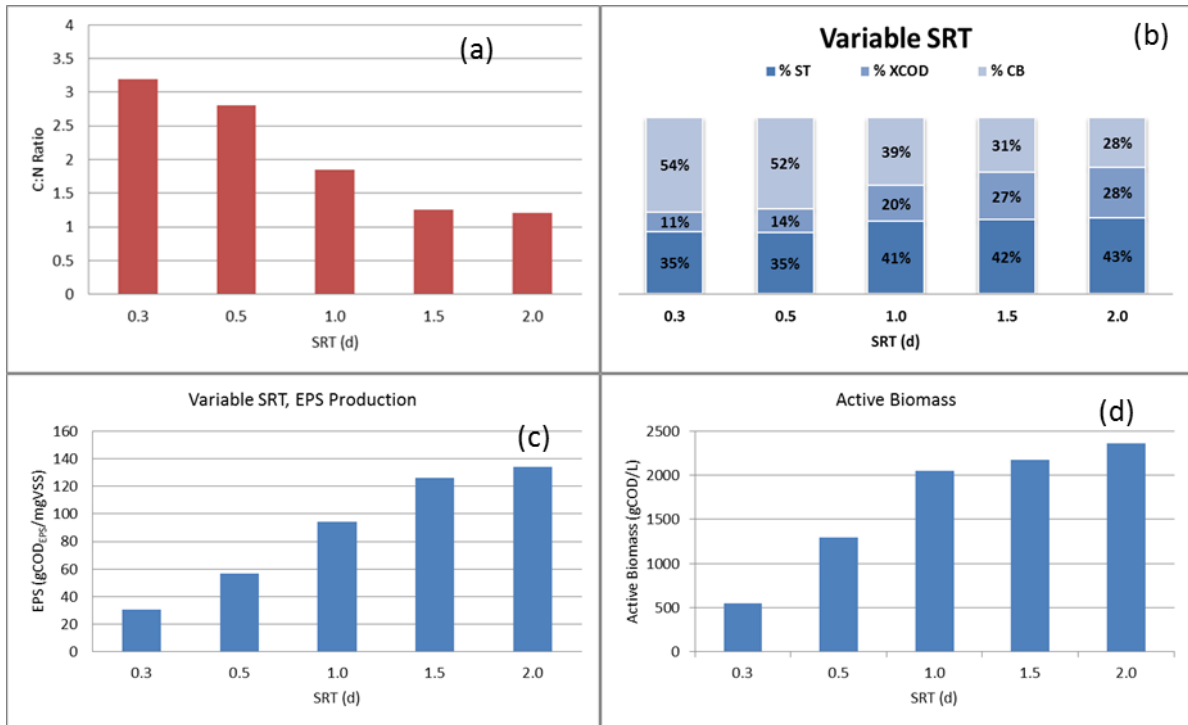


Figure 31: Effect of variable SRT on A-stage effluent COD:N ratios (a), TCOD fractions (b), EPS production (c) and active biomass concentration (d) (HRAS model), $S_T = S_U + S_{Bf} + S_{Bs}$ where S_U is the inert fraction.

The total COD fractions are shown in Figure 31b. At the lower SRTs the total COD consists primarily of colloidal and particulate COD (> 65 %), which, correlates well with the lower EPS production rate and active biomass concentration. These results suggest that operating at low SRTs and a DO > 1.0 mg/l, would increase the COD:N ratio to a value adequate to support the B-stage nitrification/denitrification process. In addition, the composition of the total COD in the A-stage effluent, has the highest percentage of colloidal COD, would be more suitable for the nitrification process (Regmi et al., 2013).

6.3.2 Variable Dissolved Oxygen

The effect of variable DO concentration in the reactor was evaluated at an SRT of 1.5 days and 0.13 days. The lower SRT (0.13 days) is more representative of the HRSD data set. Figure 32 shows COD:N ratios at variable DO for an SRT of 1.5 days. The results suggest that at lower DO's the COD:N ratio would be adequate to support a downstream nitrification process. This would largely be due to the lower removal efficiency of colloidal and particulate COD, although the soluble biodegradable COD concentration also increases at low SRTs (data not shown). Again, the higher percentage of colloidal and particulate COD correlates well with the EPS production rate and active biomass concentrations. Based on the literature these results would suggest that an adequate COD:N ratio would result at the lower DO concentrations with the total COD composition that would be ideal to support the nitrification process. At higher DO concentrations (≥ 1.0 mg/L) COD:N ratios are less than 3 suggesting that an insufficient amount of COD would be available; a supplemental source of carbon would be required.

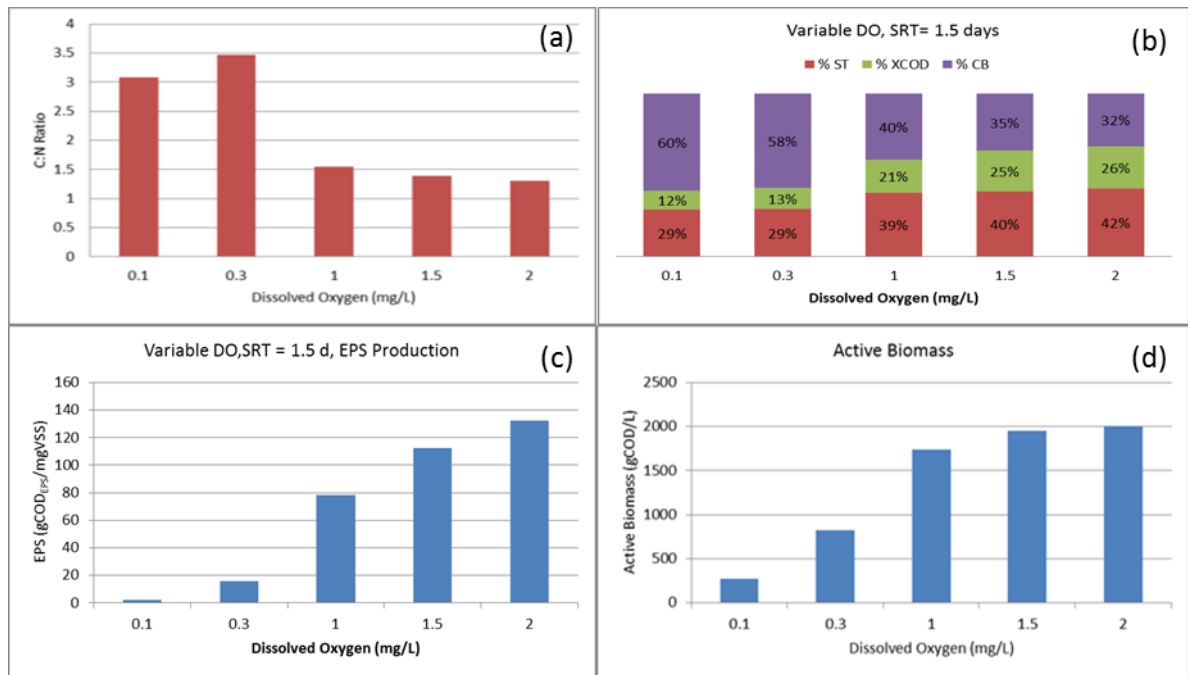


Figure 32: Effect of variable DO on A –stage effluent COD:N ratios (a), TCOD fractions (b), EPS production (c) and active biomass concentration (d) at SRT = 1.5 days (HRAS Model), $S_T = S_U + S_{BF} + S_{Bs}$ where S_U is the inert fraction.

Figure 33 shows COD:N ratios at variable DO's for an SRT of 0.13 days. The results suggest (Figure 33a) that the variable DO has minimal effect on the COD:N ratio at the lower SRT. The COD:N ratios are adequate to support downstream nitrification independent of the operating DO in the reactor. In addition, the soluble COD fraction is significantly higher; this would be attributed to the reduced removal efficiency of soluble substrate at these operating conditions supported by the very low EPS production (Figure 33c) and active biomass concentration (Figure 33d) in the reactor.

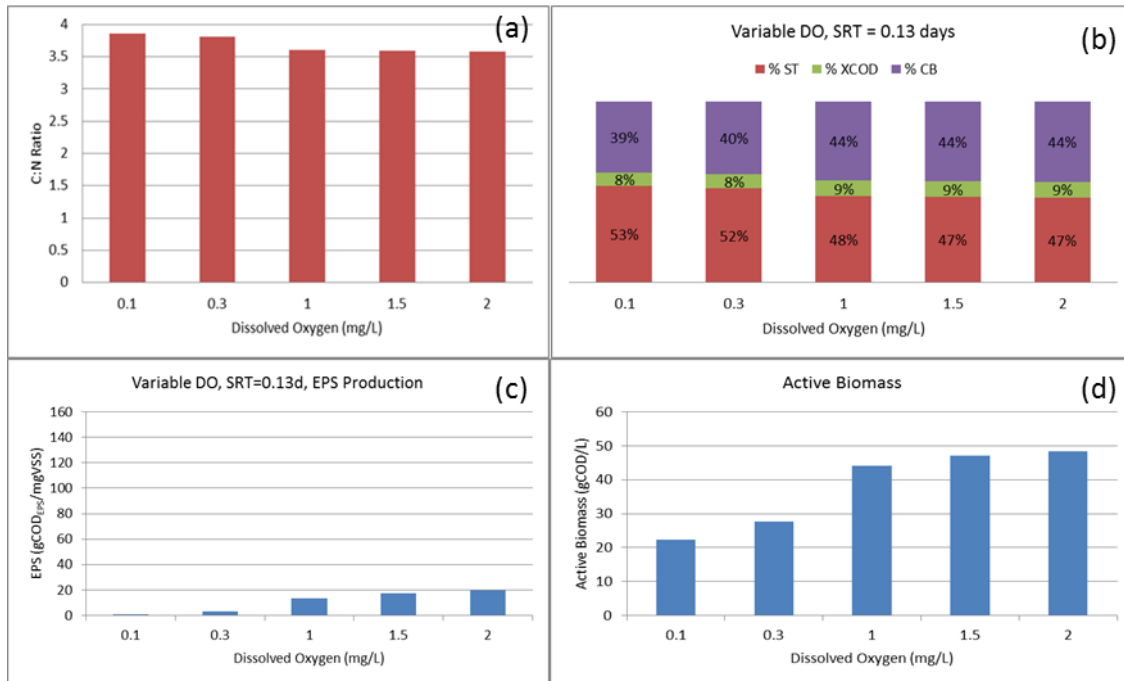


Figure 33: Effect of variable DO on effluent COD:N ratios (a), TCOD fractions (b), EPS production (c) and active biomass concentration (d) at SRT = 0.13 days (HRAS Model), $S_T = S_U + S_{Bf} + S_{Bs}$ where S_U is the inert fraction.

6.3.3 Effect of Storage

The HRAS model shunts a portion of the influent electrons to the formation of cellular storage products. At low DOs and SRT the HRAS model predicts soluble substrate removal as the accumulation of storage products (X_{STO}) in the cells (Third et al., 2003), which shunts electrons away from the production of EPS. Colloidal COD removal efficiency is a function of the EPS concentration in the reactor, hence lower EPS production rates result in a lower C_B removal efficiencies. As a result, the colloidal COD would account for a larger fraction of the effluent TCOD, as seen in Figure 31, Figure 32, and Figure 33.

For variable SRT and $DO > 1.0$ mg/L (i.e. Figure 34a), the model predicted a S_T removal efficiency of 60% at an SRT of 0.3 days. However, colloidal removals are low, and Figure 33c indicates that at low SRT, EPS production is very low, regardless of the DO level.

From Figure 34a it can be seen that the S_B removal efficiency may be attributed to an increase in X_{STO} which shunts electrons away from growth (Figure 31d) and EPS production (Figure 31c) resulting in reduced C_B removal efficiency. Even more significant is the effect of low DO (Figure 34b) which shows significant X_{STO} production as the DO decreases. In addition, we see low active biomass (Figure 32d) and EPS concentrations (Figure 32c) along with low C_B removal efficiencies.

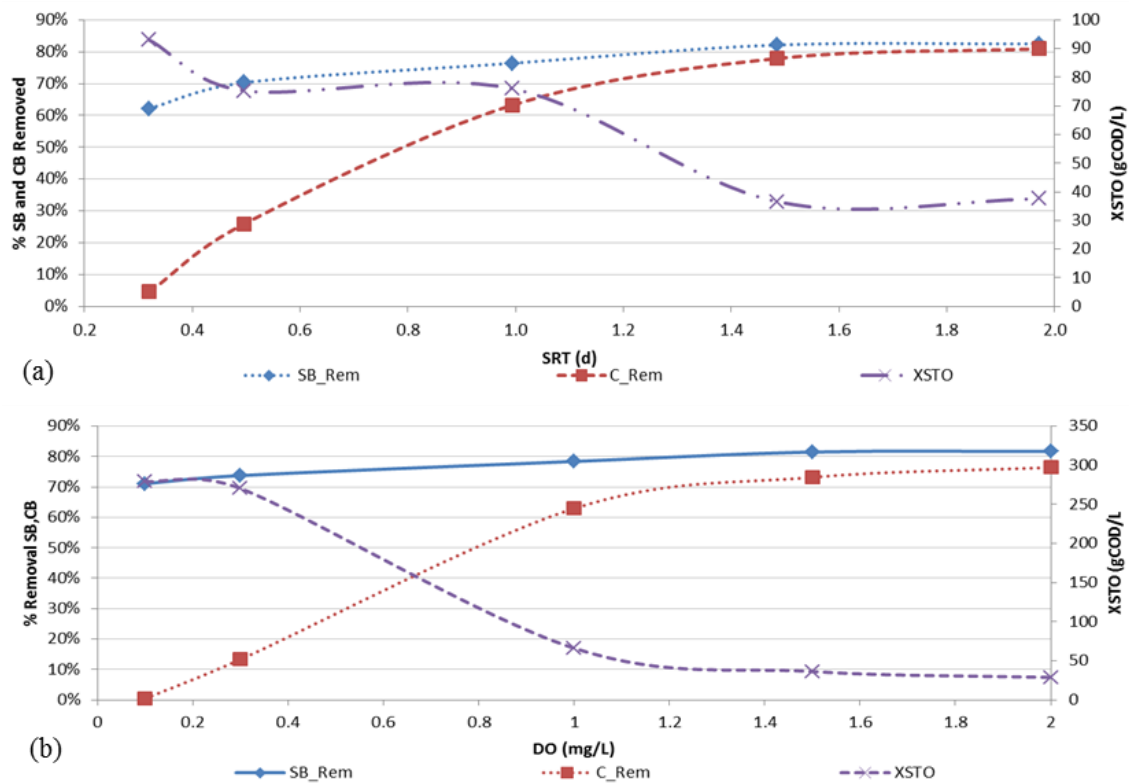


Figure 34: Comparison of the effect of variable SRT and DO on COD removal in the HRAS model (a) variable SRT DO > 1.0, (b) variable DO at SRT = 1.5 d. Influent TCOD = 301 mg/L

6.3.4 Temperature Effect on the COD:N Ratio

The effect of temperature was evaluated by running each of the above simulations at 20, 15 and 10 degrees Celsius. The results are summarized in Figure 35. As would be expected the COD:N ratio increases with a decrease in temperature. The variation is more significant at the lower SRT and DO concentration. The results show that temperature does not have a significant effect on A-stage effluent COD:N ratios.

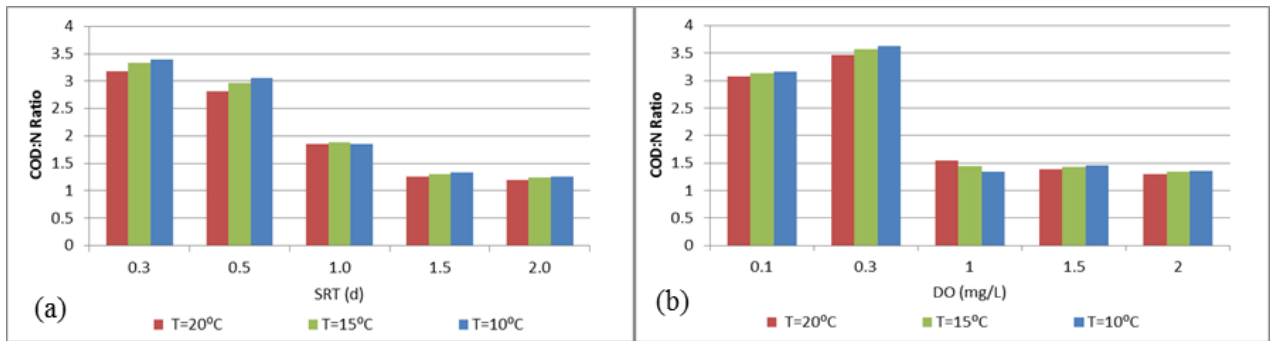


Figure 35: Effect of Temperature on COD:N ratio at (a) variable SRT, (b) SRT = 1.5 d and variable DO

6.3.5 Optimal HRAS Operating Parameters

The results presented to this point suggest that there would be a set of optimal operating parameters that would stabilize the A-stage effluent and consistently produce an effluent with a suitable COD:N for the type nitrogen removal process downstream. Figure 36 is a comparison of COD:N ratios at varying SRT and DO concentrations for the New Orleans data set having an influent COD:N ratio of 8.5. The results suggest an SRT in the range of 0.25 to 0.5 days would reliably produce an effluent COD:N ratio at or above 3.0, independent of the DO concentration (Figure 36a). At and SRT > 0.5 days the DO

concentration can significantly reduce the COD:N ratio due to heterotrophic biomass growth (Figure 36b,d). The soluble substrate removal at the lower SRTs (<0.25 d) can be more attributed the production of storage products than biomass growth, with an increase in X_{STO} at the lower DO (Figure 36c). The specific OUR (SOUR) data (Figure 36d) shows lower SOUR values at lower DO's which is consistent with the predicted increase in X_{STO} . Assimilation of soluble substrate and conversion to X_{STO} shunts electrons away from EPS production which results in lower colloidal COD removal (Figure 36e,f). As a result, the colloidal fraction of the TCOD in the effluent would increase as the SRT and DO decrease.

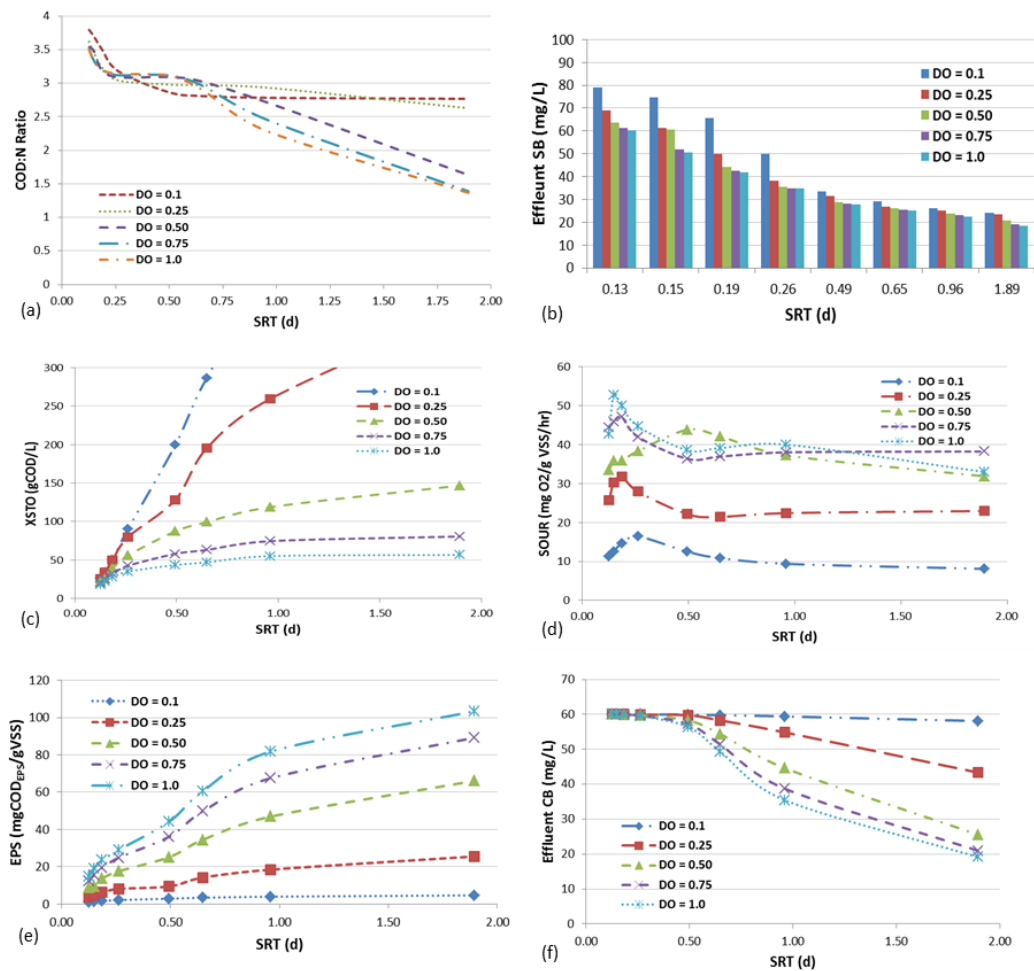


Figure 36: Comparison of COD:N ratios at constant SRT and variable DO, TCOD = 361 mg/L(), Influent COD:N ratio = 8.5:1 (HRAS model)

The results shown in Figure 36a suggest that the COD:N ratio would increase rapidly at very low SRTs. However, as the ratio approaches a threshold value, i.e., the influent COD:N ratio, the A-stage is no longer providing any operational value. Based on these model results the A-stage would begin to approach this threshold at an SRT at or below 0.2 days.

The effect of higher influent TCOD (TCOD = 600 mg/L, influent COD:N ratio of 15:1), which is representative of the HRSD data set, is shown in Figure 37. The increased influent TCOD generated higher COD:N ratios similar to the values seen by Lemaire et al. (2008) especially at SRTs < 0.25d (Figure 37a).

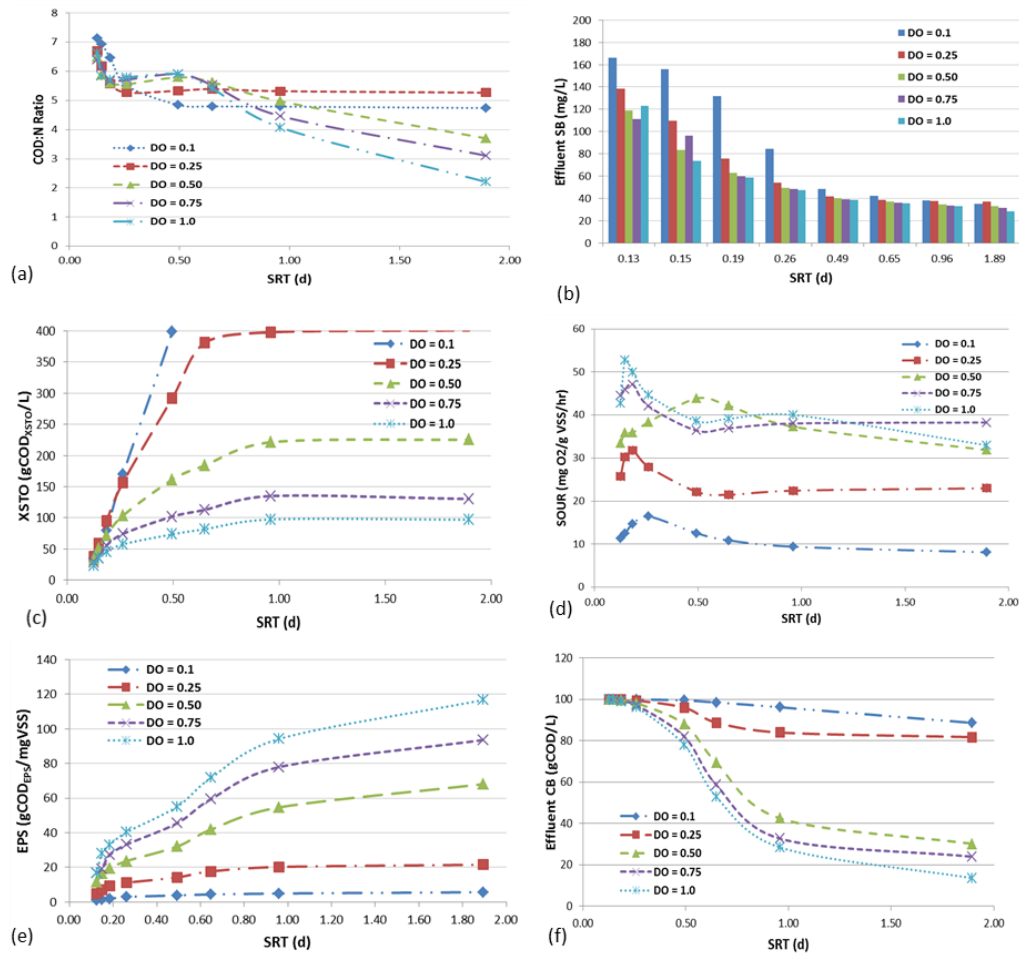


Figure 37: Comparison of COD:N ratios at constant SRT and variable DO, TCOD = 600 mg/L, influent COD:N = 15:1 (HRAS model)

Regmi et al. (2014) operated an A/B pilot to evaluate control strategies for mainstream nitrification/denitrification. The pilot was operated using intermittent aeration without oxidized nitrogen recycle and supplemental carbon addition. They used a novel aeration strategy based on set-points for reactor ammonia, nitrite and nitrate concentration having the goal of maintaining equal effluent ammonia and nitrite + nitrate (NO_x) concentrations. In addition, unique operational and process control strategies were developed to facilitate the out-selection of NOB including optimizing the influent COD, imposing transient anoxia, operating at an aggressive SRT towards AOB washout and high DO (> 1.5 mg/L). An A-stage effluent COD:N ratio of 7:1 was used to support the B-stage nitrification/denitrification. The model results from Figure 37 suggest that the A-stage pilot would have to operate at an SRT at or less than 0.25 d, independent of the reactor DO concentration, to produce an effluent with a COD:N ratio of 7:1.

A monthly average summary of the last 10 months of A-stage effluent COD: N ratios are shown in Figure 38 (influent COD:N= 13:1). The pilot consistently produced an effluent with a suitable COD:N ratio, at an SRT at or below 0.25 d, to support the downstream nitrification/denitrification process. Also, Figure 38 includes the HRAS model results for this period which show that COD:N ratios predicted by the model trend well with the pilot data.

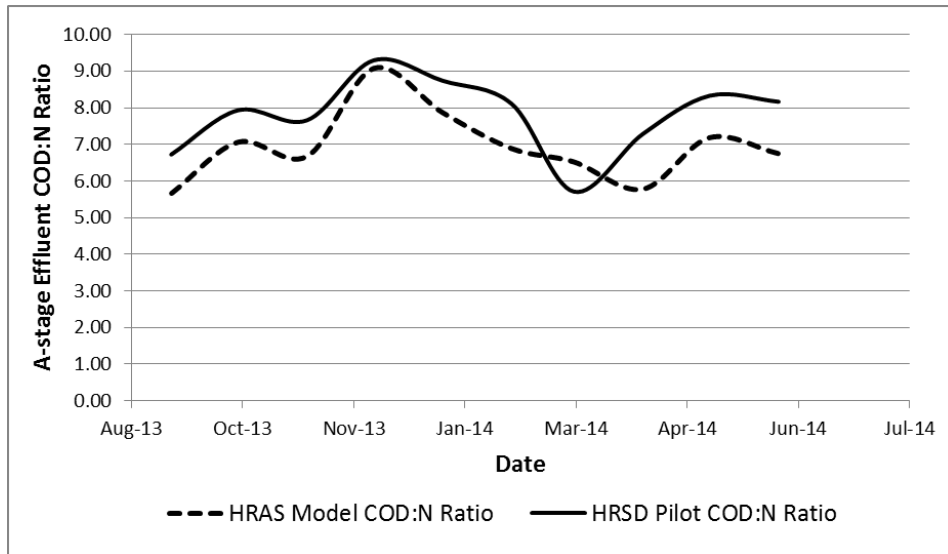


Figure 38: Comparison of A-stage effluent COD:N ratio

The average A-stage effluent TCOD fractions for this period are shown in Figure 39. A comparison of the results support that the predicted results from the HRAS model trends well with the HRSD pilot data. The majority of COD in the A-stage effluent is in the particulate and colloidal form consistent with the model results for low SRT and DO.

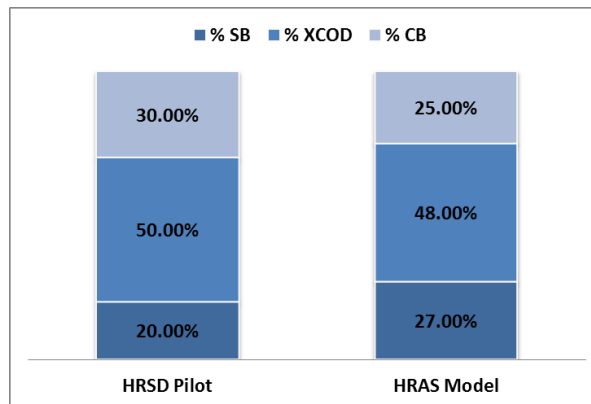


Figure 39: Comparison of TCOD fractions between the pilot data and the HRAS model

6.4 Conclusion

By using a model that integrates the kinetics of flocculation of the particulate and colloidal fractions of the influent COD in a HRAS process, the mechanisms for removal including enmeshment and bioflocculation can be added to the process matrix to accurately simulate the COD fractions in the effluent COD:N ratio. Based on the results of the model the findings are summarized as follows:

- A low SRT (<0.25 d) insures high effluent substrates (S_B and C_B), and elevated COD:N ratios consistent with NOB out-selection downstream.
- Temperature did not have a significant impact on the effluent TCOD:N ratio.
- At low SRTs (≤ 0.25 d) the COD:N ratio was not significantly affected by the DO concentration.
- The HRAS model was able to predict the measured higher fraction of C_B in the A-stage effluent at lower SRTs and DO concentrations.
- To achieve the benefits of operating an A-stage process, while maintaining an effluent COD:N ratio suitable for a downstream nitrification/denitrification process, an A-stage SRT in the range of 0.1 to 0.25 d should be maintained.

This will assist in developing control strategies that optimize the performance of the HRAS system to produce an effluent that supports the downstream nitrogen removal process.

CHAPTER 7
USING A STOICHIOMETRIC MASS BALANCE APPROACH TO IDENTIFY
SOLUBLE SUBSTRATE REMOVAL PATHWAYS IN THE HIGH RATE
ACTIVATED SLUDGE PROCESS

Note: The contents of this chapter will be submitted for publication in Water Science & Technology. Thomas M. Nogaj, Andrew A. Randall, Jose A. Jimenez, Imre Takacs, Charles B. Bott, Mark W. Miller, Sudhir Murthy and Bernhard Wett; Using a Stoichiometric Mass Balance Approach To Identify A-stage Soluble Substrate Removal Pathways.

7.1 Introduction

A-stage activated sludge systems are operated at low solids retention times (SRT), low hydraulic retention times (HRT) and low residual dissolved oxygen concentrations. The objective is the removal of soluble substrate and adsorption while minimizing oxidation of the organic carbon. The mechanisms for organic removal include bioflocculation of the particulate and colloidal fraction of the influent COD and intracellular storage of the soluble COD fractions of the influent COD (Beun et al., 2000; Carucci et al., 2001; Third et al., 2003). Research has shown that the bioflocculation of the colloidal COD fraction is a function of the amount of extracellular polymeric substances (EPS) produced by the bacterial cells (Jimenez et al., 2005). Past models assume instantaneous enmeshment whereas the data from Jimenez (2002) shows that this assumption may not be valid for A-stage systems with SRTs lower than 2 days.

Research has also shown that under certain operating conditions (low DO, high F:M ratio) the low DO limits biomass growth and most of the available DO is used by the bacterial cells to transport the soluble substrate into the cell (Third et al., 2003). This allows

the cells to preserve reducing power from influent chemical oxygen demand (COD) by using intracellular storage products such as poly- β -hydroxybutyrate (PHB) (Third et al., 2003). These soluble substrate removal pathways have been incorporated into an A-stage mathematical model (Nogaj et al., 2013) as illustrated in Figure 40. Although the current research supports the likelihood of the production of storage products in A-stage systems, this conclusion remains speculative due to the paucity of storage product data for A-stage systems.

Given that the A-stage operates a low SRT's (<1 d) this can affect the amount of substrate used for energy production and that used for synthesis. Considering the observed yield as a function of SRT based on Equation 20, the observed yield would decrease as the SRT increases (Grady et al., 2011).

$$Y_{OBS} = \frac{(1+f_D*b_H*SRT)*Y_H}{1+b_H*SRT} \quad (20)$$

Y_H = True growth yield (gCOD/gCOD)

b_H = Decay coefficient for heterotrophs (time⁻¹)

f_D = Fraction of active biomass contributing to biomass debris

SRT = Solids Retention Time (time⁻¹)

This is because longer SRT's provide greater opportunity for biomass decay requiring a greater need for maintenance energy. Shunting more carbon and electrons to CO₂ and H₂O leaves less carbon and electrons available for synthesis of new biomass and other removal mechanisms. At the lower SRT less maintenance energy is required (lower CO₂ production) leaving more electrons available for the formation of other bioproducts.

This study utilized two data sets; one based on an A/B pilot configuration at Hampton Roads Sanitation District (HRSD) (Miller et al., 2012) and the second dataset from the

University of New Orleans (NO) (Jimenez, 2002). Neither of these datasets included laboratory results on the production of PHAs and/or glycogen and only the NO dataset included EPS data. A stoichiometric procedure was developed based on mass balances to determine the most likely fate influent organic, i.e. mineralization to CO₂ and H₂O, biosynthesis, EPS, and storage products.

7.2 Objective

This paper will present an analysis using stoichiometry to determine the bio-products formed from soluble substrate removal in an A-stage reactor operating at low SRT (<1 day), low HRT (20 min), high F:M ratio (19 gCOD/gMLVSS.d), and no measurable DO (0.2 mg/L), providing pretreatment for a mainstream nitrogen removal activated sludge process. The results will be used to develop the process components and stoichiometric parameters to be used in the HRAS model.

7.3 Materials and Methods

Historical operating data from two pilot systems were evaluated to understand the organic substrate transformation mechanisms in A-stage systems and used to calibrate and validate the proposed process model. The data used during this study includes operating data from an A-stage (low SRT (SRT <1 day), HRT of 0.5 hrs) pilot plant owned and operated by the Hampton Roads Sanitation District (HRSD) (Miller et al., 2013) and from a (low SRT (SRT <2 day), HRT of 0.5 hrs) A-stage pilot plant operated at the University of New Orleans (Jimenez et al. unpublished data(Jimenez, 2002)).

The data set used from the HRSD pilot included the off-gas data collected from the A-stage which consisted of three A-stage reactors in series. These reactors were covered to collect the off-gas and analyzed using a Servomex Model 1440 gas analyzer. Data was collected at 10 second intervals included %CO₂, %O₂ and the standard airflow rates. By comparing this data to the ambient air concentrations, the change in CO₂ and O₂ concentrations in the off-gas were calculated. The change in CO₂ represented the CO₂ production rate (CO₂_PR) while the change in O₂ concentration represented the oxygen utilization rate (OUR).

The dataset used to calibrate the model was collected by Jimenez (unpublished data) and is referred to as the New Orleans (NO) dataset. The SRT and DO concentration were varied by Jimenez in order to evaluate the effect of these operating parameters on the production of EPS and the removal of organic substrate including colloids, and the same parameters were varied in the A-stage model referenced in this paper during calibration using the NO dataset. The process matrix used for this analysis was developed to model an A-stage system (Nogaj et al., 2013). The soluble substrate partitioning (Rittmann & McCarty, 2001) pathways incorporated into the model process configuration are shown in Figure 40. This process matrix (Table 17 and Table 18) includes mechanisms for flocculation or enmeshment of particulate and colloidal substrate, hydrolysis, and oxidation and storage of soluble biodegradable substrate. Extracellular Polymer Substance (EPS) production impacts the bioflocculation removal efficiency for particulate and colloidal substrate (Jimenez et al., 2005). This model includes mechanisms to predict the production of EPS associated with the aerobic growth of heterotrophic biomass. The low SRT (SRT < 1 day for the HRSD dataset

and an SRT < 2 days for the NO dataset) and no measurable DO (DO < 1.0 mg/L for the HRSD dataset and 1.0 mg/L < DO < 2.0 mg/L for the NO dataset) conditions in the A-stage reactor promote the formation of intracellular storage products. As such, a process component was added to the A-stage matrix to predict the formation of storage products. This pathway proved to be significant in closing the COD mass balances around the pilot reactors.

The process matrix developed by Nogaj et al. (2013) (Table 17) to describe the performance of an HRAS system established two state variables for soluble biodegradable substrate designated as S_{Bf} (S_B fast) and S_{Bs} (S_B slow). S_{Bf} is the soluble COD that is rapidly biodegradable in the A-stage. S_{Bs} is the slowly biodegradable soluble COD that is partially degraded in the HRAS system and also in the B stage. In the A-stage model S_{Bf} is biodegraded first, and it is only when S_{Bf} runs out that biodegradation of S_{Bs} becomes significant.

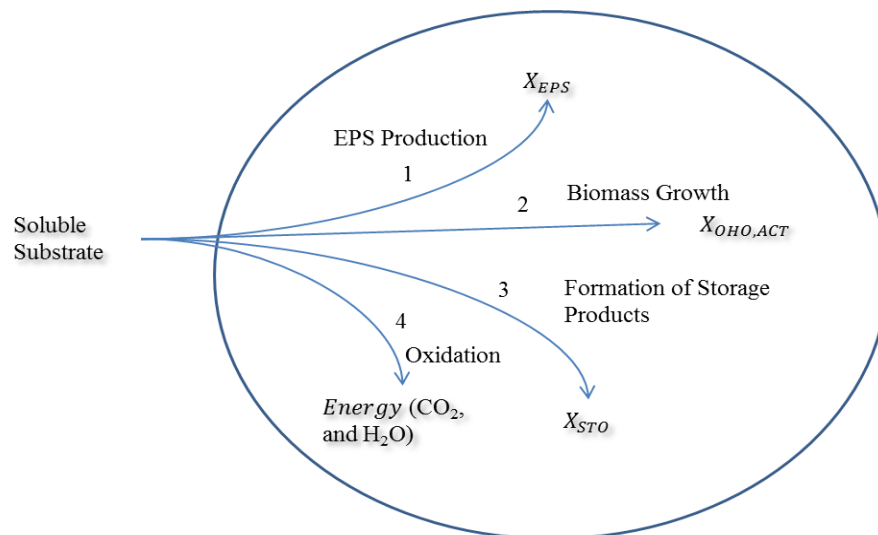


Figure 40: HRAS Model substrate partitioning pathways (for electron and carbon flow)

Each pathway is defined by a substrate partitioning coefficient with f_{eps} representing EPS production, f_{s} representing biosynthesis, f_{sto} representing the formation of storage products and f_{e} representing energy (conversion to CO_2 and H_2O , mineralization).

Table 17 Partial Peterson matrix processes and stoichiometric coefficients for the HRAS model

Name	S _{Bf}	S _{Bs}	C _B	C _U	X _B	X _U	X _{OHO, ACT}	X _{EPS}	X _{STO}
r1 Aerobic growth of X _{OHOs} – Fast	$-1/(Y_{OHO,AER} * (1 - k_{EPS,PC} - k_{STO,PC}))$						1	$k_{EPS,PC}/(Y_{OHO,AER} * (1 - k_{STO}/(Y_{OHO,AER} * (1 - k_{EPS,PC} - k_{STO,PC})))$	$k_{EPS,PC} - k_{STO,PC}$
r2 Aerobic growth of X _{OHOs} – Slow							1	$k_{EPS,PC}/(Y_{OHO,AER} * (1 - k_{STO}/(Y_{OHO,AER} * (1 - k_{EPS,PC} - k_{STO,PC})))$	$k_{EPS,PC} - k_{STO,PC}$
r3 Decay of heterotrophs					$1 - f_U$		-1		
r4 Hydrolysis of entrapped organics		1			-1				
r5 flocculation of colloidal substrate			-1		1				
r6 flocculation of colloidal inerts				-1		1			
r7 Hydrolysis of storage products		1							-1
r8 EPS hydrolysis		1						-1	

Table 18 Partial Peterson matrix process rate equations for the HRAS model

Name	Rate expression (r_i)
r1 Aerobic growth of heterotrophs - Fast	$\mu_{\text{OHO,Max}} \cdot (S_{\text{Bf}} / (K_{\text{Bf}} + S_{\text{Bf}})) \cdot (S_{\text{O}_2} / (K_{\text{O}_2,\text{OHO}} + S_{\text{O}_2})) \cdot (S_{\text{NH}_x} / (K_{\text{NH}_x,\text{nut}} + S_{\text{NH}_x})) \cdot X_{\text{OHO}}$
r2a Aerobic growth of heterotrophs - Slow	$\mu_{\text{OHO,Max}} \cdot (S_{\text{Bs}} / (K_{\text{Bs}} + S_{\text{Bs}})) \cdot (K_{\text{Bf}} / (K_{\text{Bf}} + S_{\text{Bf}})) \cdot (S_{\text{O}_2} / (K_{\text{O}_2,\text{OHO}} + S_{\text{O}_2})) \cdot (S_{\text{NH}_x} / (K_{\text{NH}_x,\text{nut}} + S_{\text{NH}_x})) \cdot X_{\text{OHO}}$
r2b Aerobic growth of heterotrophs - Slow	$\mu_{\text{OHO,max}} \cdot (S_{\text{Bs}} / (K_{\text{Bs}} + S_{\text{Bs}})) \cdot (S_{\text{O}_2} / (K_{\text{O}_2,\text{OHO}} + S_{\text{O}_2})) \cdot (S_{\text{NH}_x} / (K_{\text{NH}_x,\text{nut}} + S_{\text{NH}_x})) \cdot X_{\text{OHO}}$
r3 Decay of heterotrophs	$b_{\text{OHO}} \cdot X_{\text{OHO,ACT}}$
r4 Hydrolysis of entrapped organics	$q_{\text{XB,HYD}} \cdot ((X_{\text{B}} / X_{\text{OHO}}) / (K_{\text{B,HYD}} + X_{\text{B}} / X_{\text{OHO}})) \cdot ((S_{\text{O}_2} / (K_{\text{O}_2,\text{OHO}} + S_{\text{O}_2})) + \eta_{\text{HYD}} \cdot (K_{\text{O}_2,\text{OHO}} / (K_{\text{O}_2,\text{OHO}} + S_{\text{O}_2})) \cdot (S_{\text{NO}_x} / (K_{\text{NO}_x} + S_{\text{NO}_x}))) \cdot X_{\text{OHO}}$
r5 flocculation of colloidal substrate	$q_{\text{ADS}} \cdot C_{\text{B}} \cdot (X_{\text{OHO}} + X_{\text{ANO}}) \cdot (K_{\text{SL}} / ((C_{\text{B}} / (X_{\text{OHO}} + X_{\text{ANO}})) + K_{\text{SL}})) \cdot (X_{\text{EPS}} / (K_{\text{EPS}} + X_{\text{EPS}}))$
r6 flocculation of colloidal inerts	$q_{\text{ADS}} \cdot C_{\text{U}} \cdot (X_{\text{OHO}} + X_{\text{ANO}}) \cdot (K_{\text{SL}} / ((C_{\text{U}} / (X_{\text{OHO}} + X_{\text{ANO}})) + K_{\text{SL}})) \cdot (X_{\text{EPS}} / (K_{\text{EPS}} + X_{\text{EPS}}))$
r7 Hydrolysis of storage products	$q_{\text{STO,HYD}} \cdot (X_{\text{STO}} / X_{\text{OHO}}) / (K_{\text{STO,HYD}} + X_{\text{STO}} / X_{\text{OHO}}) \cdot (K_{\text{Bf}} / (K_{\text{Bf}} + S_{\text{Bf}})) \cdot (K_{\text{Bs}} / (K_{\text{Bs}} + S_{\text{Bs}})) \cdot (S_{\text{O}_2} / (K_{\text{O}_2,\text{OHO}} + S_{\text{O}_2})) \cdot X_{\text{OHO}}$
r8 EPS hydrolysis	$q_{\text{EPA,HYD}} \cdot X_{\text{EPS}}$

r2a corresponds to the Diauxic model, r2b corresponds to the Dual Substrate model

7.4 COD Mass Balance

One of the most important concepts in evaluating the validity of any experimental dataset is the mass balance. HRSD collected off-gas data from the HRAS system measuring the oxygen and carbon dioxide concentrations. This data was used to calculate the oxygen utilization rate (OUR) and CO₂ production rate (CO₂_PR) in the aerated reactors. The oxygen concentrations in both the off-gas and ambient air are calculated using the form of the ideal gas law shown in Equation 21 (Cooper & Alley, 2011).

$$O_2 \text{ Conc } \left(\frac{\text{mg}}{\text{L}} \right) = \frac{C_{ppm} * MW_{O_2} * 10^{-3}}{R_u T / P} \quad (21)$$

C_{ppm} = Oxygen concentration in parts per million (v/v)

MW_{O_2} = molecular weight of oxygen (32 g/mol)

R_u = 0.08208 atm·m³/kg·mole·K

T = Temperature °K

P = atmospheric pressure (1 atm)

The oxygen uptake rate (OUR) and the carbon dioxide production rate (CO₂_PR) are calculated based on the oxygen (O₂) and carbon dioxide (CO₂) concentrations in the reactor off-gas and ambient air containing 20.95 percent O₂ and 0.04 percent CO₂ using Equation 22 and Equation 31 respectively.

$$OUR \left(\frac{\text{mg}}{\text{L} \cdot \text{hr}} \right) = ((\text{Ambient } O_2 - \text{Off Gas } O_2) * (\text{Air Flow} * 60)) / (\text{Tanks Aerated} * V_{RTR}) \quad (22)$$

Ambient O₂ = Oxygen concentration in the ambient air (mg/L)

Off-Gas O₂ = Oxygen concentration in the reactor off-gas (mg/L)

Air Flow = Air flow rate to the reactors (standard liters per minute (SLPM))

Tanks Aerated = Number of tanks aerated in the pilot configuration

V_{RTR} = Volume of each reactor (L)

Using the HRSD dataset from September 2013 to January 2014, daily COD mass balances were calculated using Equation 23 (Melcer & Foundation, 2003).

$$Q * COD_{Inf} = Q * COD_{Eff} + q_w * X_{VSS} * f_{CV} + OUR * V_{AER} * 24 - 4.57 * S_{NO} * Q \quad (23)$$

Q= Influent flowrate

q_w = waste activated sludge flow

X_{VSS} = Reactor volatile suspended solids concentration

f_{CV} = COD/VSS ratio (1.48 g COD/g VSS)

OUR = oxygen utilization rate

V_{AER} = Aerated reactor volume

S_{NO} = Effluent nitrate concentration

The average COD percent recovery for this period is 99.79 % ± 1.25% (Figure 41).

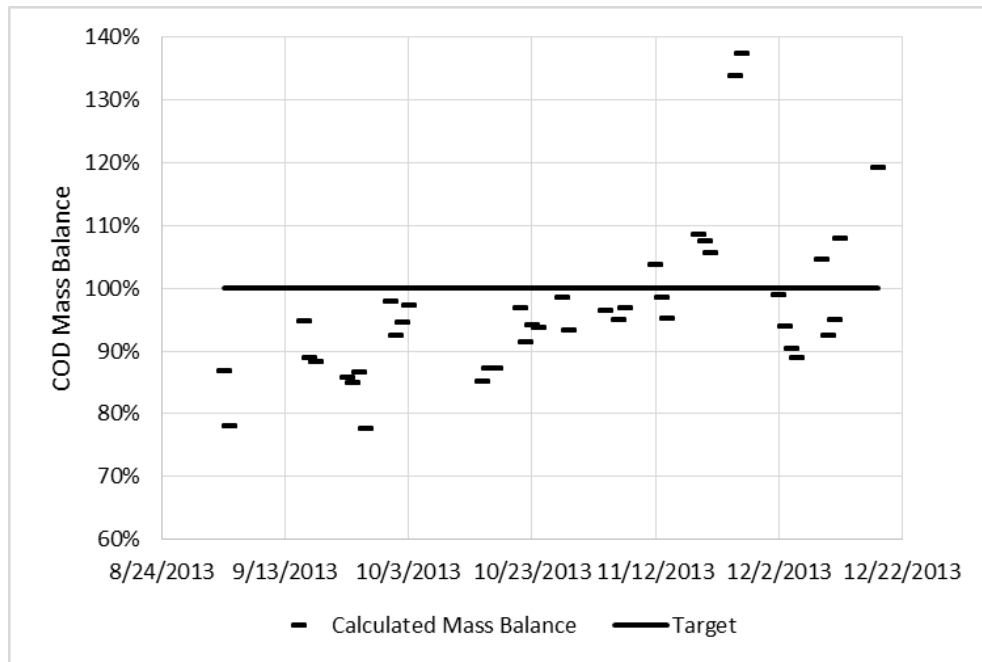


Figure 41: Calculated COD mass balances based on off-gas data

It was found that approximately 80 % of the COD mass balances calculated were < 100% (averaging 92%), suggesting that a portion of the COD leaving the system is

unaccounted for. Based on the biodegradable soluble substrate removal pathways identified in Figure 40, the one pathway that is not considered in the mass balance calculation is the formation of storage products. The COD removed through this would leave the system as effluent suspended solids or waste activated sludge. This would suggest that the solids COD/VSS ratio of 1.48 gCOD/gVSS does not take into account intracellular storage which would result in under predicting the COD being removed as suspended solids from the system. Evaluating the fraction of the dataset with COD mass balances less than 100% and applying Equation 24 resulted in an adjusted VSS/COD ratio of 1.86 is needed to close the mass balances.

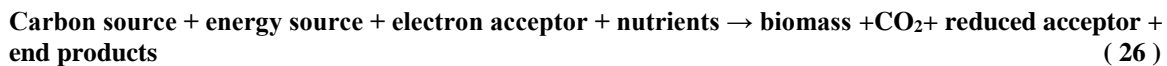
$$f_{CV_Actual} = \frac{Q * COD_{Infl} + 4.57 * S_{NO} * Q - Q * COD_{Eff} - OUR * V_{AER} * 24}{q_w * X_{VSS}} \quad (24)$$

Using f_{CV_Actual} , the target X_{STO} (gCOD/d) needed to close COD mass balances shown in Figure 41, were calculated using Equation 25

$$X_{STO_Target} = (q_w * WAS_{VSS}) * (f_{CV_Actual} - f_{CV}) \quad (25)$$

7.5 Stoichiometry

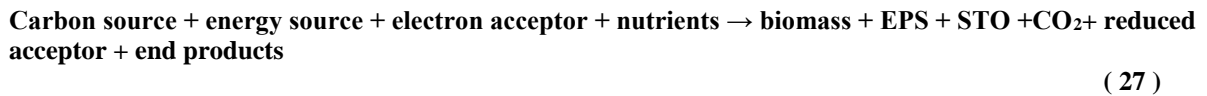
In a dynamic model of a conventional aerobic system (SRT >3 days, DO > 2 mg/L) the stoichiometry is typically represented by Equation 26.



In this system electrons are typically shunted along two pathways, either mineralization (f_e) or biosynthesis (f_s). Alternative pathways do not need to be modeled i.e. bioflocculation or the formation of storage products, since the SRT (>3 days) and HRT (> 4 hours) of these

system are long enough to allow for the development of a flocculated biomass (colloidal COD removal) and utilization of storage products. This type of system can be analyzed using the half reactions approach with the observed oxygen consumption as input for example. With an A-stage model the system operates at low SRT (< 1 day), low HRT (0.5 hrs), and no measurable DO, in this system alternative pathways may play a more significant role in modelling substrate removal making the evaluation of this system more complex and dynamic.

In the A-stage model, the primary removal mechanisms for colloidal COD is sequential and involves adsorption (facilitated by EPS), hydrolysis, and consumption for one of the four processes shown in Figure 40. The literature supports the production of extracellular polymeric substances (EPS) (Laspidou & Rittmann, 2002a; Ni, Zeng, et al., 2009) which aid in the adsorption mechanism and formation of storage products (Beun et al., 2002; Krishna & Van Loosdrecht, 1999; Ni & Yu, 2008; Third et al., 2003) which occur under high food/microorganism (F/M) ratios and low DO environments. These removal mechanisms can be represented by Equation 27.



To solve the stoichiometry in Equation 27 a computer based solution was developed, this method is referred as the substrate partitioning model. This method uses observed substrate utilization data and a calculated CO₂:O₂ ratio as input to a numerical solver (Excel Solver) with a series of applied constraints to generate a solution for the stoichiometric

coefficients and substrate partitioning fractions representing each substrate removal pathway. Since the substrate partitioning model is used to solve the A-stage stoichiometry represented in Equation 27, the half reaction model was modified to reflect the A-stage stoichiometry with the partitioning fractions from the substrate partitioning model as input to valid the results.

7.5.1 Half Reaction Approach

The generally accepted half reaction approach, in the absence of significant soluble microbial product formation, consists of two pathways for electrons and carbon; one for energy the other for biomass synthesis. These types of reactions consist of three half reactions: one for cell material (R_c), one for an electron donor (R_d , organic substrate for heterotrophic growth), and one for the electron acceptor (R_a , oxygen in an aerobic environment). The overall stoichiometric equation (R) is the sum of the half reactions (McCarty, 1975).

$$R = R_d - f_e * R_a - f_s * R_c \quad (28)$$

In order for Equation 28 to balance all the electrons originally in the donor must end up in either the electron acceptor or biomass:

$$f_e + f_s = 1 \quad (29)$$

To validate this hypothesis, the stoichiometry incorporating each pathway was evaluated using the $\text{CO}_2:\text{O}_2$ ratio as the observed parameter calculated from the off-gas data. McCarty (1975) was able to demonstrate that for suspended growth systems, the fraction of electrons going to mineralization (energy, f_e) increases as the sludge age (SRT) increases. This supports the hypothesis that the A-stage systems, operating at low sludge ages would shunt a higher fraction of the available electrons to the synthesis of new biomass (f_s). Using the half reaction approach, McCarty (1975) showed that, using domestic wastewater (Table 19) as the electron donor and oxygen as the electron acceptor, the production of CO_2 would decrease and the consumption of O_2 would also decrease as electrons are shunted away from energy production towards biosynthesis (Figure 42). Using the $\text{CO}_2:\text{O}_2$ ratio as an indicator as to the distribution of electrons, and Table 19 stoichiometry, if all the electrons are transported to the electron acceptor the $\text{CO}_2:\text{O}_2$ ratio would be 1.1 (Figure 42). As electrons are shunted away from energy production ($f_e \downarrow$) to synthesis of new biomass ($f_s \uparrow$) the $\text{CO}_2:\text{O}_2$ ratio decreases. This is due to the CO_2 produced decreasing at faster rate than the decrease of oxygen consumption.

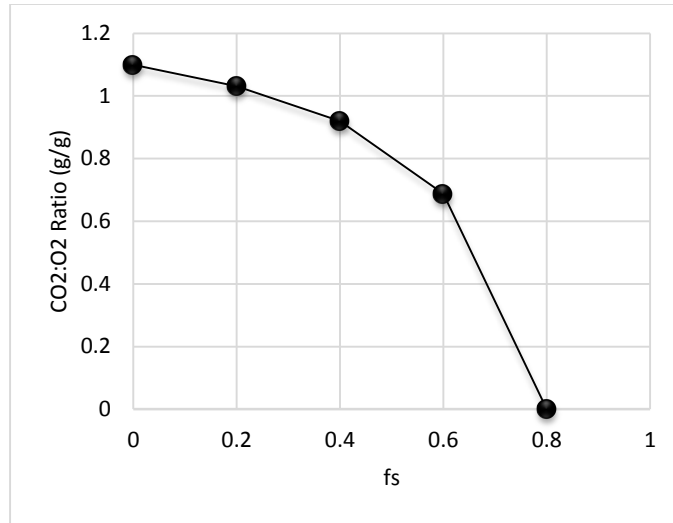


Figure 42: Rate of change in the CO₂:O₂ ratio as electrons are shunted away from fe and towards fs. Using domestic wastewater (S_{Bs}) as the electron donor (Table 19).

The stoichiometric molar ratio of CO₂:O₂ is equivalent to the ratio of the CO₂ production rate (CO₂_PR) to the oxygen utilization rate (OUR) (Equation 30).

$$\frac{CO_2}{O_2} \left(\frac{g}{g} \right) = \frac{dCO_2/dt}{dO_2/dt} = \frac{CO_2_PR}{OUR} \quad (30)$$

Using the HRSD off-gas data, the concentration for CO₂ produced can be determined from the calculated CO₂_PR and the concentration of O₂ consumed can be determined from the calculated OUR.. Equation 31 was used to calculate the CO₂ production rate (CO₂_PR).

$$CO_2_PR = ((Off\ Gas\ CO_2 - Ambient\ CO_2) * (Air\ Flow * 60)) / (Tanks\ Aerated * V_RTR) \quad (31)$$

- CO₂_PR = CO₂ production rate (mg/L·hr)
- Ambient CO₂ = Carbon dioxide concentration in the ambient air (mg/L)
- Off-Gas CO₂ = Carbon dioxide concentration in the reactor off-gas (mg/L)
- Air Flow = Air flow rate to the reactors (SLPM)
- Tanks Aerated = Number of tanks aerated in the pilot configuration
- V_RTR = Volume of each reactor (L)

This approach was used to establish baseline CO₂:O₂ ratios for varying A-stage operating conditions as well as to validate the stoichiometric coefficients determined from the substrate partitioning approach discussed in the next section.

7.5.2 Substrate Partitioning Approach

To account for significant product formation including the production of EPS and the formation of storage products (STO) Equation 28 was modified to incorporate each end product (Equation 32):

$$R = R_d - f_e * R_a - f_s * R_c - f_{eps} * R_{c,eps} - f_{sto} * R_{c,sto} \quad (32)$$

To balance this equation:

$$f_e + f_s + f_{eps} + f_{sto} = 1 \quad (33)$$

In an attempt to predict the performance of the HRAS system including all four pathways shown in Figure 40, a modified approach was taken to partition the substrate represented stoichiometrically by Equation 34.

$$aa(C_{N_{CS}}H_{m*N_{CS}}O_{n*N_{CS}}N_{p*N_{CS}} + aO_2 + bNH_3 \rightarrow cC_{N_{CB}}H_{q*N_{CB}}O_{r*N_{CB}}N_{s*N_{CB}} + dC_{N_{BP1}}H_{t*N_{BP1}}O_{u*N_{BP1}}N_{v*N_{BP1}} + eC_{N_{BP2}}H_{x*N_{BP2}}O_{y*N_{BP2}}N_{z*N_{BP2}} + fH_2O + gCO_2) \quad (34)$$

This is the basic equation used, NH₃ will show up as either a reaction product (b = negative) or reactant (b= positive) depending on the balanced constraint equations. The stoichiometric coefficients for CO₂ (g) and O₂ (a) are calculated from observed values as describe earlier for the CO₂_PR and OUR respectively. The subscript N_{CS} represents the electron donor, N_{CB} biomass synthesis; the equation includes the production of two bio-products, N_{BP1} representing EPS production and N_{BP2} the formation of STO.

The experimental dataset are based on aggregate samples representing the performance of the A-stage pilot. The stoichiometry used for the slow fraction of the readily biodegradable soluble substrate (S_{Bs}) is shown on Table 19. The stoichiometry shown for substrate, biomass, and EPS were obtained from McCarty (1975), the stoichiometry for STO, considered to be PHB for this study, was obtain from Dawes (1988) and Van Aalst-Van Leeuwen et al. (1997). S_{Bs} was calculated from observed data using ffCOD – VFA- S_U (B-stage effluent sCOD). This means S_{Bs} is equivalent to F-rbCOD from ASM2d.

Table 19 Stoichiometry for the slow fraction (S_{Bs}) of the readily biodegradable soluble substrate (i.e. equivalent to F-rbCOD from ASM2d)

Element		Substrate (N_{CS})		Biomass (N_{CB})		EPS (N_{BP1})		STO (N_{BP2})
C	N_{CS}	10	N_{CB}	5	N_{BP1}	16	N_{BP2}	4
H	$m \cdot N_{CS}$	19	$q \cdot N_{CB}$	7	$t \cdot N_{BP1}$	24	$x \cdot N_{BP2}$	6
O	$n \cdot N_{CS}$	3	$r \cdot N_{CB}$	2	$u \cdot N_{BP1}$	5	$y \cdot N_{BP2}$	2
N	$p \cdot N_{CS}$	1	$s \cdot N_{CB}$	1	$v \cdot N_{BP1}$	4	$z \cdot N_{BP2}$	0
MW		201		113		352		86
COD Mass Eq ¹		1.99		1.42		1.5		1.67
	m	1.9	q	1.4	t	1.5	x	1.5
	n	0.3	r	.4	u	.31	y	.5
	p	0.1	s	.2	v	.25	z	0

¹ COD Mass equivalents (gCOD/gSubstrate)

S_{Bf} was equal to the observed VFA values and its' stoichiometry is represented by the stoichiometry shown in Table 20 with acetate as the electron donor. The biomass formula was obtained from Rittmann and McCarty (2001) for biomass growth using acetate and ammonia in an aerobic environment.

Table 20 Stoichiometry for the fast fraction (S_{Bf}) of the readily biodegradable soluble substrate

Element		Substrate (N_{CS})		Biomass (N_{CB})		EPS (N_{BP1})		STO (N_{BP2})
C	N_{CS}	2	N_{CB}	7	N_{BP1}	16	N_{BP2}	4
H	$m*N_{CS}$	4	$q*N_{CB}$	12	$t*N_{BP1}$	24	$x*N_{BP2}$	6
O	$n*N_{CS}$	2	$r*N_{CB}$	4	$u*N_{BP1}$	5	$y*N_{BP2}$	2
N	$p*N_{CS}$	0	$s*N_{CB}$	1	$v*N_{BP1}$	4	$z*N_{BP2}$	0
MW		60		174		352		86
COD Mass Eq ¹		1.07		1.33		1.5		1.67
	m	2	q	1.4	t	1.5	x	1.5
	n	1	r	0.4	u	0.31	y	0.5
	p	0	s	0.2	v	0.25	z	0

¹ COD Mass equivalents (gCOD/gSubstrate)

The literature suggests that EPS consists of varying combinations of proteins and polysaccharides (Bala Subramanian et al., 2010; Frolund et al., 1996; Ni, Fang, et al., 2009; Park & Novak, 2007). However, protein is produced at a higher rate by a factor of 3 (Park & Novak, 2007). As such, the stoichiometric analysis for both fractions (S_{Bf} and S_{Bs}) were made with EPS (N_{BP1}) represented as a protein with the empirical formula $C_{16}H_{24}O_5N_4$ (McCarty, 1975).

The degrees of reduction (NCEES, 2011), which are the electrons available per unit of carbon was determined for the substrate, biomass, and both bio-products. This was used for developing the carbon, nitrogen, hydrogen, oxygen, electron, and energy balances (Table 21). This information was then input into excel solver to generate the COD based stoichiometric coefficients for oxygen consumption, biomass production (f_s), EPS production (f_{eps}), and storage product (expressed as PHB) formation (f_{sto}).

Table 21 Summary of equations used in the Substrate Partitioning Approach (NCEES, 2011)

Degrees of reduction - Available electrons per unit of carbon, a high degree of reduction denotes a low degree of oxidation			
	DR Equations	e ⁻ /unit of carbon Acetate	e ⁻ /unit of carbon Domestic WW
DR _{CS}	4 + m - 2n - 3p	4	5
DR _{CB}	4 + q - 2r - 3s	4	4
DR _{BP1}	4 + t - 2u - 3v	4.125	4.125
DR _{BP2}	4 + x - 2y - 3z	4.5	4.5
Excel Solver – Objective Function			
Element Balance	Balance Equations	Value	
Electron	$cDR_B N_{CB} + dDR_{BP_1} N_{BP_1} + eDR_{BP_2} N_{BP_2} - aaDR_S N_{CS} + 4a$	0	
Excel Solver - Constraints			
Carbon	$cN_{CB} + dN_{BP_1} + eN_{BP_2} + g - aaN_{CS}$	0	
Nitrogen	$csN_{CB} + dvN_{BP_1} + ezN_{BP_2} - aapN_{CS} - b$	0	
Hydrogen	$cqN_{CB} + dtN_{BP_1} + exN_{BP_2} + 2f - aamN_{CS} - 3b - h$	0	
Oxygen	$crN_{CB} + duN_{BP_1} + eyN_{BP_2} + f + 2g - aanN_{CS} - 2a$	0	
Energy ¹	$Q_o * (cDR_B N_{CB} + dDR_{BP_1} N_{BP_1} + eDR_{BP_2} N_{BP_2} - aaDR_S N_{CS} + 4a)$	0	
Determination of Stoichiometric Coefficients (S _{Bf} and S _{Bs})			
aa (observed substrate removed)	$\frac{S_{B_Removed}}{COD\ Mass\ Eq * MW * 1000}$		
a (oxygen consumed, dual substrate)	$(O_2\ Consumed)_{S_{Bs}} = \frac{OUR * Vol_{Aer} * 24}{F} - (O_2\ Consumed)_{S_{Bf}}$		
g (CO ₂ produced)	$(CO_2\ Produced)_{S_{Bs}} = \frac{CO_2_PR * Vol_{Aer} * 24}{F} - (CO_2\ Produced)_{S_{Bf}}$		

¹ Q_o Heat evolved per unit equivalent of available electrons = 26.9 kcal/mole O₂ consumed

For the purposes of this study the CO₂:O₂ ratio was a key parameter used to match the observed data to the model simulation and to understand the shunting of electrons along the different pathways. In developing this ratio, the HRSD pilot dataset used for this study

presented specific challenges. Given that the pilot plant is a continuous flow system, the experimental results represent an aggregate sample of all the biochemical reactions occurring in the reactor. No additional experiments were conducted to determine the contribution of each readily biodegradable soluble substrate fraction (S_{Bf} and S_{Bs}) to the aggregate oxygen utilization rate (OUR_{Sys}) or the aggregate CO_2 production rate ($CO_2_PR_{Sys}$). For the purpose of this study, in an attempt to match the X_{STO_target} value (Equation 25)), an iterative approach (Figure 43) was used to select a $CO_2:O_2$ ratio for the S_{Bf} fraction which best represented the contribution of the S_{Bf} fraction to the system OUR (Table 50 in Appendix G). Subtracting the S_{Bf} OUR and CO_2_PR values from the aggregate values resulted in the target OUR and CO_2_PR values for the S_{Bs} fraction. Using these values the target $CO_2:O_2$ ratio was calculated for the S_{Bs} fraction. The target $CO_2:O_2$ ratio along with the initial S_{Bs} removed were input into the substrate partitioning model and the contribution of S_{Bs} to the aggregate OUR_{Sys} and $CO_2_PR_{Sys}$ and the substrate partitioning fractions were determined (Figure 44).

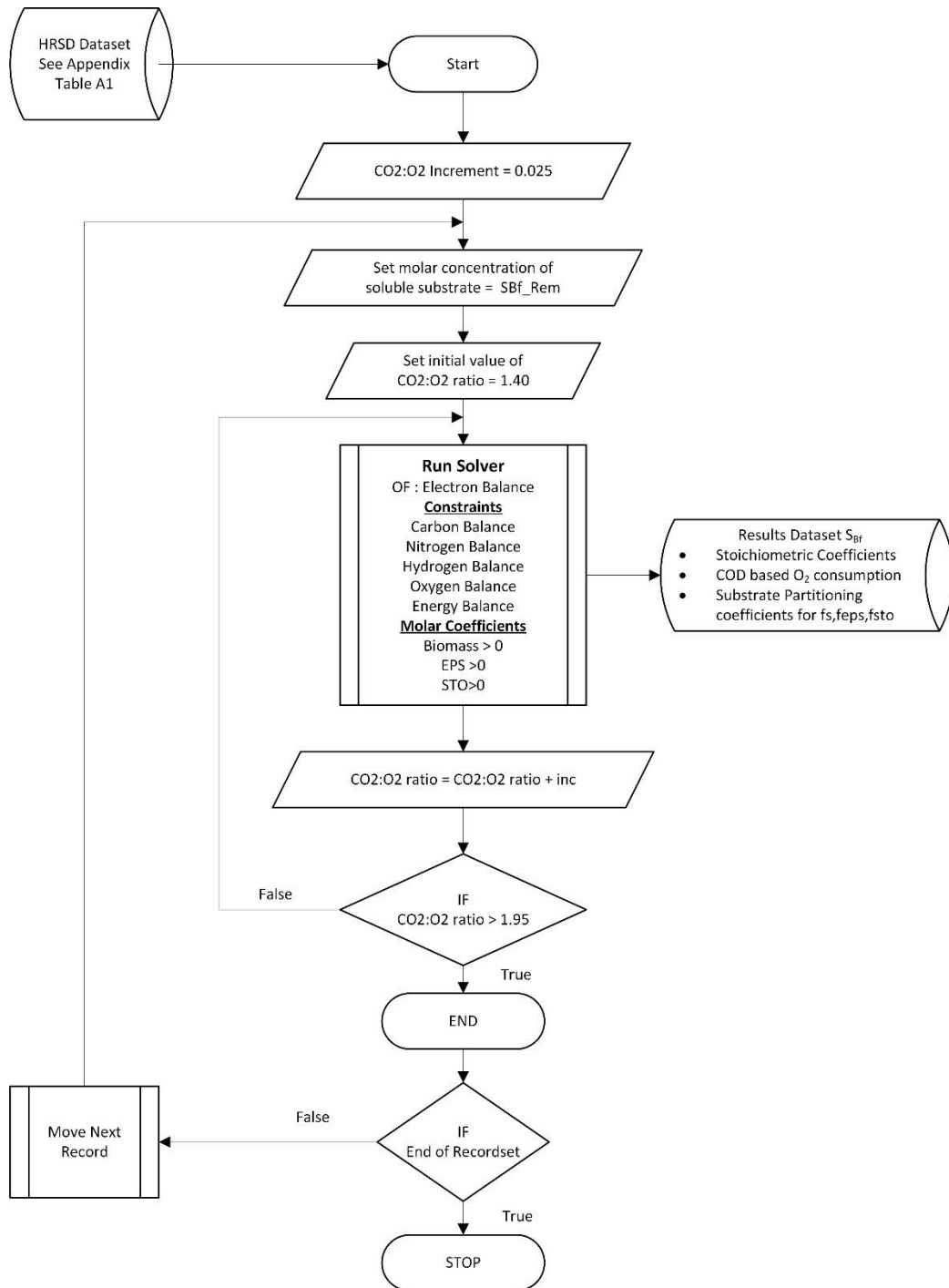


Figure 43: Procedure for determining stoichiometric coefficients for S_{Bf} at varying $CO_2:O_2$ ratios using the stoichiometry shown in Table 20.

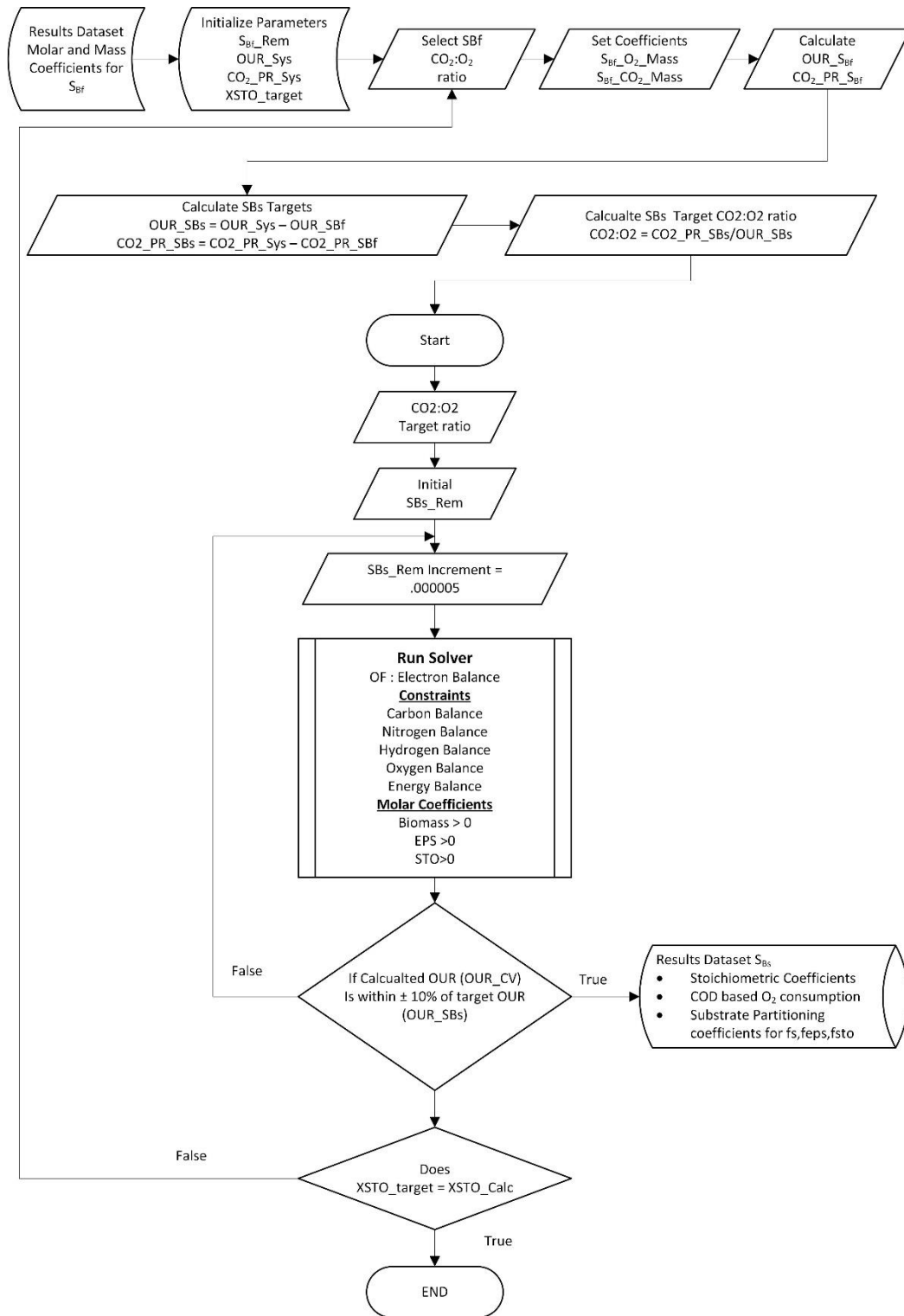


Figure 44: Procedure for determining stoichiometric coefficients for S_{Bs} using the stoichiometry shown in Table 19

7.6 Results and Discussion:

7.6.1 Dataset Analysis

7.6.1.1 Single Substrate

Figure 45 shows the observed $\text{CO}_2:\text{O}_2$ ratios for the pilot. Three dashed lines are superimposed over the pilot data. The upper line shows the predicted $\text{CO}_2:\text{O}_2$ ratio assuming the influent COD removed was metabolized like acetic acid (Table 20) and that $f_s = 0$. This gives a maximum $\text{CO}_2:\text{O}_2$ boundary, and it can be seen that the observed $\text{CO}_2:\text{O}_2$ ratios do not exceed it significantly. In contrast, 35% of the observed $\text{CO}_2:\text{O}_2$ ratios exceed the boundary if the COD removed is quantified like domestic wastewater (Table 19) stoichiometry. The lowest line uses Table 19 stoichiometry with $f_s = 0.63$.

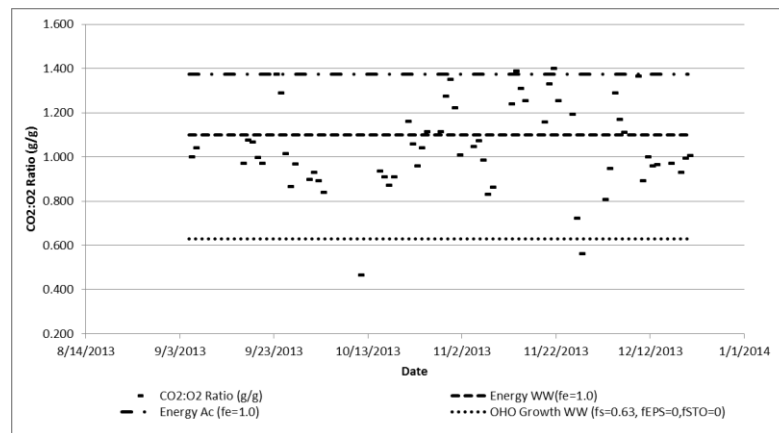


Figure 45: Comparison of off-gas $\text{CO}_2:\text{O}_2$ ratio to stoichiometric substrate partition fractions based on single substrate using stoichiometry defined in Table 19 and Table 20.

7.6.1.2 Mixed Substrate

Using the observed VFA (COD) removal and the stoichiometry of Table 20 (all treated as acetic acid) it was possible to calculate the oxygen consumption and CO₂ production resulting. The O₂ and CO₂ changes were then subtracted from the aggregate OURs and CO₂_PR observed. The remaining OURs and CO₂_PRs were due to non-VFA COD removed (i.e. Influent S_{Bs} plus hydrolyzed colloidal and particulate COD). In this way it was possible to input the non-VFA driven OUR and CO₂_PR into the Table 19 stoichiometry to back-calculate the quantity of S_{Bs} biodegraded. In addition, by using the stoichiometry from Table 19 and Table 20, it was possible to calculate the corresponding biomass, storage product (all treated as PHB) and EPS production.

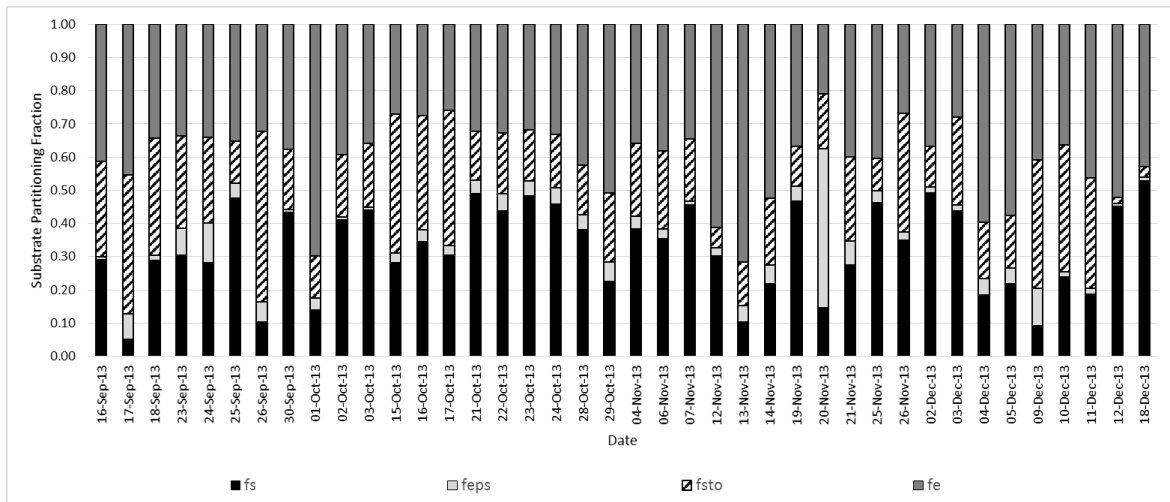


Figure 46: Composite substrate partition fractions based on combined S_{Bf} (acetic acid) and S_{Bs} (domestic wastewater) stoichiometry

The results in Figure 46 show a consistent portion of the electrons being shunted to biomass synthesis (f_s) over the entire dataset. The results suggest that the shunting of electrons to f_{eps} and f_{sto} is significant over the entire range. Consistently a higher fraction of

electrons are shunted to f_{sto} as opposed to f_{eps} . The results support the hypothesis that when operating an A-stage system at high F:M ratios and low SRT with no measurable DO that formation of storage products is possible which could account for the unidentified COD lost in the mass balance. In addition, the results also suggest that the four mechanisms incorporated into the A-stage model should effectively simulate the performance of this type of system. The variation in the partitioning coefficients could be due to specific operating parameters and conditions in the system, i.e. F:M ratio, SRT, temperature, DO. Further investigation would be required to determine the specific effect of any one or combination of the parameters, as well as, others not yet identified.

A summary of the stoichiometric yield coefficients generated for the study period using combined S_{Bf} and S_{Bs} stoichiometry (i.e. combined Table 19 and Table 20 stoichiometry) are summarized in Table 22.

Table 22 Average aggregate COD based stoichiometric yield coefficients based on combined stoichiometry

Substrate	f_s (gCOD/gCOD)	f_{EPS} (gCOD/gCOD)	f_{STO} (gCOD/gCOD)
S_{Bsys}	0.27	0.085	0.27

The results in Table 22 show that, based on the experimental constraints for OUR and $CO_2:O_2$ ratio, a significant portion of the readily biodegradable COD entering the reactor could be proportioned to one of the bio-products as either biomass synthesis (f_s), EPS production (f_{EPS}), or formation of STO (f_{STO}). The average stoichiometric maximum yield for biomass ($Y_{OHO,Max} = f_s / (1 - f_{EPS} - f_{STO})$), for the system ($S_{Bf} + S_{Bs}$), was 0.47 (gCOD/gCOD). Using the revised solids COD/VSS ratio, determined from the COD mass balances, the

calculated Y_{obs} would be 0.32 (gVSS/gCOD_{SB}); this value is comparable to the observed value of 0.4 (gVSS/gCOD_{SB}). A comparison of the X_{STO} calculated from stoichiometry and the COD mass balance showed that 38% of the data points were within $\pm 10\%$ and better than 60% were within $\pm 30\%$. This suggests that the stoichiometric approach supports the speculative hypothesis that in an A-stage system, the unaccounted for COD in the mass balances could be attributed to the formation of storage products.

7.7 Aggregate Stoichiometric Results

The calibration of the HRAS (A-stage) dynamic computer model using the NO dataset generated the results shown in Figure 47 for the proportionality coefficients for EPS production ($k_{EPS,PC}$, equivalent to f_{EPS}) and the formation of storage products ($k_{STO,PC}$, equivalent to f_{STO}).

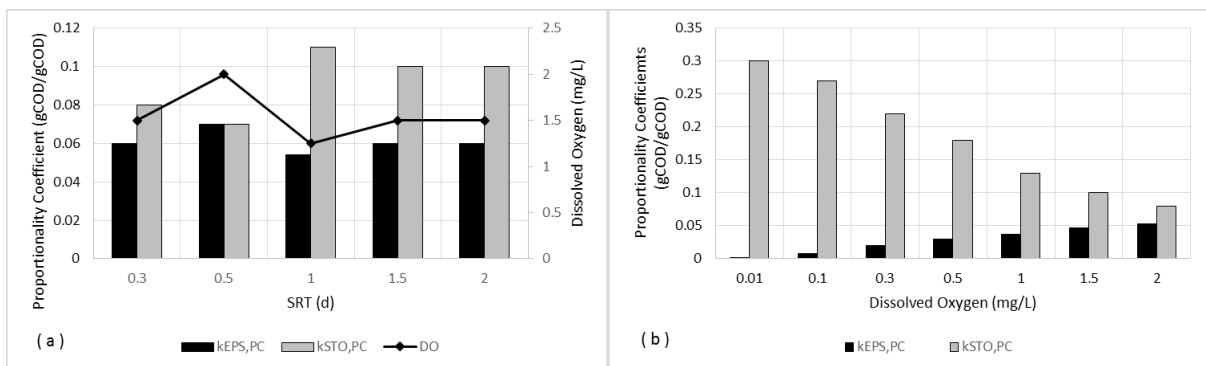


Figure 47: Substrate Partitioning coefficients $k_{EPS,PC}$ (f_{EPS}) and $k_{STO,PC}$ (f_{STO}) generated from the A-stage model at variable SRT and DO (SRT=1.5 days).

The results in Figure 47 suggest that as the SRT decreases, while maintaining a DO > 1.0 mg/l, the $k_{STO,PC}$ (f_{sto}) would increase slightly at an SRT ≥ 1.0 d and that $k_{EPS,PC}$ (f_{EPS}) would remain relatively constant. Dissolved Oxygen appears to have an inverse effect

with $k_{STO,PC}$ increasing with decreasing DO and $k_{EPS,PC}$ decreasing even at an SRT of 1.5 days. The average aggregate f_{EPS} ($k_{EPS,PC}$) and f_{sto} ($k_{STO,PC}$) values generated stoichiometrically (0.085 gCOD/gCOD, 0.27 gCOD/gCOD respectively) for the HRSD pilot operating at a low SRT (< 2 days) and low DO (<0.2 mg/L), are consistent with the NO pilot being operated at very low SRT (average 0.08 days) and low DO (average 0.10 mg/L). Operating at a low DO and SRT would suggest increased production of storage products and a decrease in the production of EPS. Steinbuchel (1996) has shown that oxygen limitation induces PHA biosynthesis.

7.8 Conclusions

The COD mass balance data and a stoichiometric approach are were consistent with the speculative hypothesis that storage products with significant associated oxygen demand were a significant part a A-stage COD removal. An independent dynamic computer model also implied that storage products should be significant at low DO concentrations. Future work should quantify storage products, EPS, and methane production potential of the waste activated sludge to better understand and optimize A-stage systems.

CHAPTER 8

CONCLUSIONS AND FUTURE RESEARCH

The purpose of this research was to simulate the performance of an HRAS (A-stage) system and simulate the probable mechanisms affecting the removal of soluble and particulate COD. Once these mechanisms were identified from the literature and pilot data, the objective was to develop a mathematical model framework that could effectively simulate the performance of this type of system. The task of developing the nitrogen removal model is being completed by other members of the research team.

8.1 Conclusions

1. It was observed that to effectively model an A-stage activated sludge system that the influent readily biodegradable soluble COD (rbCOD) must be subdivided into two fractions. One fraction (S_{BF}) representing the rapidly utilized fraction of the readily biodegradable COD which for this research were the volatile fatty acids (VFA) in the influent. The second fraction or slow fraction (S_{BS}) represented the remaining readily biodegradable COD which was only partially removed in the A-stage. This division of rbCOD into two state variables allowed the model to correctly simulate the higher effluent sCOD observed in the A-stage relative to the B-stage effluent sCOD.
2. Colloidal COD was observed to pass through the A-stage to the B-stage, indicating that enmeshment and hydrolysis of colloidal COD is not complete as assumed in current models (ASM1). This led to the addition of a new process component to the A-stage model matrix for flocculation. The reaction is represented by a first order reaction with respect to colloidal substrate concentration.

3. It was determined from review of the literature and analysis of the NO data that EPS production, which is essential for flocculation of colloidal COD, is a function of microbial growth on soluble substrate. EPS (X_{EPS}) production is defined in the A-stage model matrix as an end product of aerobic growth for both fast and slow fractions of the rbCOD. The adjustment of kinetic parameters (K_{EPS} , $q_{EPS,HYD}$, $K_{O,EPS}$) and the relevant stoichiometric coefficient ($k_{EPS,MAX}$) during the model calibration phase result in the model agreeing well with the NO dataset.
4. The calibration process simulated NO data best when the storage pathway was significant. Removal efficiencies for soluble substrate fractions and EPS production, were best simulated over the range of SRT (0.3 to 2 days) when storage product formation was significant. Preliminary calibration results eliminating this pathway did not capture the experimental trends as accurately as when the storage pathway was included. This affect was also observed during model validation using the HRSD dataset.
5. It was also observed that the model had difficulty simulating the HRAS performance when the influent biomass concentration was not considered. The results of the model simulation show that as the SRT increases above 0.3 d, the biomass concentration in the reactor approaches a condition where the influent biomass concentration no longer determines the reactor biomass concentration. However, at the lower SRT (typical of the HRSD pilot) the biomass concentration varies significantly depending on the influent biomass concentration. Therefore, the influent

- biomass concentration is essential to the model's ability to predict the MLVSS and the removal of soluble COD.
6. It was observed that a low SRT (<0.25 d) typical of an A-stage activated sludge system can produce high effluent substrate concentrations (S_B and C_B), and elevated effluent COD:N ratios which support NOB out-selection downstream since COD helps drive the creation of anoxic conditions (transient anoxia). It was also observed that temperature and DO did not have a significant impact on the effluent COD:N ratio at low SRTs (≤ 0.25 d). The A-stage model was able to predict the measured higher fraction of C_B in the A-stage effluent at these low SRTs and DO concentrations. To achieve the benefits of operating an A-stage process, while maintaining an effluent COD:N ratio suitable for a downstream nitrification/denitrification processes, an A-stage SRT in the range of 0.1 to 0.25 d should be maintained. The model was able to accurately simulate the elevated effluent colloidal COD and COD:N ratio by adding a process equation for flocculation of colloidal substrate (see also conclusion 2).
 7. The calculated COD mass balance using off-gas data suggests that, for better than 80 percent of the sampling events evaluated, a significant fraction of the COD is unaccounted for (mass balance $<100\%$). The consistent negative bias made it unlikely that the low COD mass balances were due to analytical error. To complete the mass balances, the COD in the solids fraction leaving the system was recalculated to be 1.86 gCOD/gVSS rather than the 1.48 gCOD/gVSS which is used for conventional systems. An independent stoichiometric analysis was also evaluated

and it also implied that there was probably significant storage product formation.

However, this hypothesis is speculative and future studies need to evaluate the role of storage products in A-stage systems.

8.2 Recommendations for Future Research

Future work should quantify storage products, EPS, and methane production potential of the waste activated sludge to better understand and optimize A-stage systems.

It was observed during the calibration/validation effort that the results were highly sensitive to changes in several parameters. Substrate consumption was controlled by varying the half saturation coefficients (K_{Bf} and K_{Bs}). Similar values were used ($K_{Bf} = 20$ and $K_{Bs} = 40$) for calibration and validation. The validation process is highly sensitive to the DO half saturation coefficient where a significantly lower value ($K_{O,OH_2} = 0.02$) was used as compared to the default value of 0.10 used for calibration. In addition, the formation of storage products had a significant effect on the A-stage models ability to simulate the removal of soluble substrate (S_{Bf} and S_{Bs}) for both validation and calibration. Future work should include a sensitivity analysis to identify the extent to which specific parameters affect the accuracy of the A-stage model. Future work should also determine if S_{Bf} is preferentially biodegradable relative to S_{Bs} .

APPENDIX A: STOICHIOMETRY SAMPLE CALCULATIONS

Chapter 4: Calculate the oxygen utilization rate (OUR) from the off-gas in mg/L·hr

1. Calculate the oxygen concentration in both the off-gas and ambient air used for aeration.

$$O_2 \text{ Conc } \left(\frac{\text{mg}}{\text{L}} \right) = \frac{C_{ppm} * MW_{O_2} * 10^{-3}}{R_u T / P}$$

C_{ppm} = Oxygen concentration in parts per million (v/v)

MW_{O_2} = molecular weight of oxygen (32 g/mol)

R_u = 0.08208 atm·m³/kg·mole·K

T = Temperature °K

P = atmospheric pressure (1 atm)

- a. Using an off-gas oxygen concentration of 19.47% or $C_{ppm} = 194,700$ ppm v/v

$$O_2 \text{ Conc } \left(\frac{\text{mg}}{\text{L}} \right) = \frac{194700 * 32 * 10^{-3}}{0.08208 * 293 / 1.0} = 259 \text{ mg/L}$$

- b. Using an ambient air oxygen concentration of 20.95% or $C_{ppm} = 209,500$ ppm v/v

$$O_2 \text{ Conc } \left(\frac{\text{mg}}{\text{L}} \right) = \frac{209500 * 32 * 10^{-3}}{0.08208 * 293 / 1.0} = 279 \text{ mg/L}$$

- c. Using these values calculate the OUR

$$\text{OUR} \left(\frac{\text{mg}}{\text{L} \cdot \text{hr}} \right) = ((\text{Ambient } O_2 - \text{Off Gas } O_2) * (\text{Air Flow} * 60)) / (\text{Tanks Aerated} * V_{\text{RTR}})$$

Air Flow = 82 SLPM @ 25°C, 66 SLPM @ 20°C

V_{RTR} = Reactor Volume @ Three reactors 170L each

Tanks Aerated = 2

- d. $\text{OUR} \left(\frac{\text{mg}}{\text{L} \cdot \text{hr}} \right) = ((279 - 259) * (66 * 60)) / (2 * 170) = 233 \text{ mg/L} \cdot \text{hr}$

2. Calculate the Carbon Dioxide concentration in both the off gas and ambient air used for aeration.

$$\text{CO}_2\text{Conc} \left(\frac{\text{mg}}{\text{L}} \right) = \frac{C_{\text{ppm}} * \text{MW}_{\text{CO}_2} * 10^{-3}}{R_u T / P}$$

C_{ppm} = Carbon Dioxide concentration in parts per million (v/v)

MW_{CO_2} = molecular weight of oxygen (44 g/mol)

R_u = 0.08208 atm·m³/kg·mole·K

T = Temperature °K

P = atmospheric pressure (1 atm)

- a. Using an off-gas Carbon Dioxide concentration of 1.05% or $C_{\text{ppm}} = 10,500$ ppm v/v

$$\text{CO}_2\text{Conc} \left(\frac{\text{mg}}{\text{L}} \right) = \frac{10,500 * 44 * 10^{-3}}{0.08208 * 293 / 1.0} = 19 \text{ mg/L}$$

- b. Using an ambient air Carbon Dioxide concentration of .04% or $C_{\text{ppm}} = 400$ ppm v/v

$$\text{CO}_2\text{Conc} \left(\frac{\text{mg}}{\text{L}} \right) = \frac{400 * 44 * 10^{-3}}{0.08208 * 293 / 1.0} = 0.73 \text{ mg/L}$$

- c. Using these values calculate the CO₂ production rate CO₂_PR

$$\text{CO}_2\text{-PR} = ((\text{Off Gas CO}_2 - \text{Ambient CO}_2) * (\text{Air Flow} * 60)) / (\text{Tanks Aerated} * V_{\text{RTR}})$$

Air Flow = 82 SLPM @ 25°C, 66 SLPM @ 20°C

V_RTR = Reactor Volume @three reactors 170 L each

Tanks Aerated = 2

$$\text{CO}_2 \left(\frac{\text{mg}}{\text{L}\cdot\text{hr}} \right) = ((19 - .73) * (66 * 60)) / (2 * 170) = 213 \text{ mg/L}\cdot\text{hr}$$

3. The Observed ratio of Carbon Dioxide produced to oxygen consumed would be:

$$\frac{\text{CO}_2}{\text{O}_2} = \frac{\text{CO}_2\text{-PR}}{\text{OUR}} = \frac{213}{233} = 0.91 \frac{\text{gCO}_2}{\text{gO}_2}$$

4. Calculate the COD mass balance

- a. Using the following mass balance equation to represent the HRAS system.

$$Q * COD_{Inf} = Q * COD_{Eff} + q_w * X_{VSS} * f_{CV} + OUR * V_{AER} * 24 - 4.57 * S_{NO} * Q$$

$COD_{Inf} = Q * COD_{Inf}$ = Total mass of COD in the influent (gCOD/m³)

$COD_{Eff} = Q * COD_{Eff}$ = Total mass of COD in the Effluent (gCOD/m³)

$COD_{WAS} = q_w * X_{VSS} * f_{CV}$ = Mass of COD in the waste activated sludge (gCOD/m³)

$COD_{OUR} = OUR * V_{AER} * 24$ = Mass of COD removed through mineralization (gCOD/m³)

$COD_N = 4.57 * S_{NO} * Q$ = Oxygen utilized for nitrification, assumed to be zero for the HRAS system.

- b. Calculate the COD percent recovery using the following parameter values:

$$Q = 24.53 \text{ m}^3/\text{d}, q_w = 0.87 \text{ m}^3/\text{d}, COD_{inf} = 520 \text{ gCOD}/\text{m}^3$$

$$COD_{eff} = 204 \text{ gCOD}/\text{m}^3, WAS_TSS = 4733 \text{ gTSS}/\text{m}^3$$

$$VSS \text{ fraction} = 0.74, f_{CV} = 1.48 \text{ gCOD}/\text{gVSS}$$

$$\text{Volume} = 0.17 \text{ m}^3, \text{No. of reactors aerated} = 2$$

$$OUR = 225 \text{ g}/\text{m}^3 \cdot \text{hr}$$

$$COD_{Inf} = 24.53 * 520 = 12,756 \text{ gCOD}/\text{m}^3$$

$$COD_{Eff} = (24.53 - 0.87) * 204 = 4,827 \text{ gCOD}/\text{m}^3$$

$$COD_{WAS} = (0.87 * 4733 * 0.74 * 1.48) = 4510 \text{ gCOD}/\text{m}^3$$

$$COD_{OUR} = ((0.17 * 2) * 225 * 24) = 1,836 \text{ gCOD}/\text{m}^3$$

$$\text{COD \% Recovery} = \frac{\text{COD}_{\text{Eff}} + \text{COD}_{\text{WAS}} + \text{COD}_{\text{OUR}} - \text{COD}_{\text{N}}}{\text{COD}_{\text{Inf}}}$$

$$\text{COD \% Recovery} = \frac{4,827 + 4,510 + 1,836 - 0}{12,756} * 100 = 87.6\%$$

- c. Calculate the revised f_{CV} required to close the COD mass balance.

$$f_{\text{CV-Actual}} = \frac{Q * \text{COD}_{\text{Inf}} + 4.57 * S_{\text{NO}} * Q - Q * \text{COD}_{\text{Eff}} - \text{OUR} * V_{\text{AER}} * 24}{q_w * X_{\text{VSS}}}$$

$$f_{\text{CV-Actual}} = \frac{12,756 + 0 - 4,828 - 1,836}{0.87 * 4733 * 0.74} = 2.0$$

- d. Estimated production of storage product (X_{STO}) based on the revised f_{CV} .

$$X_{\text{STO}} = \text{COD}_{\text{WAS}} * (f_{\text{CV}_{\text{Actual}}} - f_{\text{CV}})$$

$$X_{\text{STO}} = 4510 * (2.0 - 1.48) = 2,345 \text{ gCOD/m}^3$$

**APPENDIX B:
HRAS MODEL FRAMEWORK – DUAL SUBSTRATE**

Table 23 HRAS model framework

j	Symbol	Name	S_U	S_{Br}	S_{Bs}	C_B	X_U	X_B	$X_{OHO,ACT}$	X_{ANO}	X_E	S_{O2}	S_{NOx}	S_{NHx}	S_{NB}	X_{NB}	S_{ALK}	S_{N2}	X_{INORG}	X_{EPS}	X_{STO}
1	r1	Aerobic growth of heterotrophs - Fast		$\frac{1}{(Y_{OHO,AER} \cdot R \cdot (1 - \frac{k_{EPS,PC}}{k_{STO,PC}}))}$					1			$-\frac{(1 - Y_{OHO,AER})}{(Y_{OHO,AER})}$		$-i_{N,XB}$			$-i_{N,XB} \cdot i_{Charge_SNHx}$			$\frac{k_{EPS,PC}}{(1 - k_{EPS,PC} - k_{STO,PC})} \cdot (Y_{OHO,AER})^*$	$\frac{k_{STO,PC}}{(1 - k_{EPS,PC} - k_{STO,PC})} \cdot (Y_{OHO,AER})^*$
2	r2	Aerobic growth of heterotrophs - Slow		$\frac{1}{(Y_{OHO,AER} \cdot (1 - \frac{k_{EPS,PC}}{k_{STO,PC}}))}$					1			$-\frac{(1 - Y_{OHO,AER})}{(Y_{OHO,AER})}$		$-i_{N,XB}$			$-i_{N,XB} \cdot i_{Charge_SNHx}$			$\frac{k_{EPS,PC}}{(1 - k_{EPS,PC} - k_{STO,PC})} \cdot (Y_{OHO,AER})^*$	$\frac{k_{STO,PC}}{(1 - k_{EPS,PC} - k_{STO,PC})} \cdot (Y_{OHO,AER})^*$
3	r3	Anoxic growth of heterotrophs -Fast		$\frac{1}{Y_{OHO,ANOX}}$					1				$-\frac{(1 - Y_{OHO,ANOX})}{(i_{NO3,N2} \cdot Y_{OHO,ANOX})}$	$-i_{N,XB}$			$-\frac{(1 - Y_{OHO,ANOX})}{(i_{NO3,N2} \cdot Y_{OHO,ANOX})} \cdot i_{Charge_e_SNOx} - i_{N,XB} \cdot i_{Charge_SNHx}$	$\frac{(1 - Y_{OHO,ANOX})}{(i_{NO3,N2} \cdot Y_{OHO,ANOX})} \cdot Y_O$			
4	r4	Anoxic growth of heterotrophs -Slow		$-1/Y_{OHO,ANOX}$					1				$-\frac{(1 - Y_{OHO,ANOX})}{(i_{NO3,N2} \cdot Y_{OHO,ANOX})}$	$-i_{N,XB}$			$-\frac{(1 - Y_{OHO,ANOX})}{(i_{NO3,N2} \cdot Y_{OHO,ANOX})} \cdot i_{Charge_e_SNOx} - i_{N,XB} \cdot i_{Charge_SNHx}$	$\frac{(1 - Y_{OHO,ANOX})}{(i_{NO3,N2} \cdot Y_{OHO,ANOX})} \cdot Y_O$			
5	r5	Aerobic growth of autotrophs								1		$-\frac{(i_{COD_NO3} - Y_{ANO})}{Y_{ANO}}$	$1/Y_{ANO}$	$-i_{N,XB} - 1/Y_{ANO}$				$(i_{N,XB} + 1/Y_{ANO}) \cdot i_{Charge_SNHx} + (1/Y_{ANO}) \cdot i_{Charge_SNOx}$			
6	r6	Decay of heterotrophs						$1 - f_U$	-1		f_U					$i_{N,XB} - f_U \cdot i_{N,XU}$					
7	r7	Decay of autotrophs						$1 - f_U$		-1	f_U					$i_{N,XB} - f_U \cdot i_{N,XU}$					
8	r8	Ammonification of soluble organic nitrogen												1	-1		i_{Charge_SNHx}				
9	r9	Hydrolysis of entrapped organics			1			-1													
10	r10	Hydrolysis of entrapped organic nitrogen													1	-1					
11	r11	flocculation of colloidal substrate				-1		1													
12	r12	Hydrolysis of storage products			1																-1
13	r13	Enmeshment /storage of S_{NB}													-1	1					
14	r14	EPS hydrolysis			1															-1	

Elemental composition																					
COD	1	1	1	1	1	1	1	1	1	1	-1	i_{COD_NO3}	0	0	0	0	0	i_{COD_N2}	0	1	1
N	0	0	0	0	0	0	$i_{N,XB}$	$i_{N,XB}$	$i_{N,XU}$	0	0	1	1	1	1	0	0	1	0	0	0
Charge	0	0	0	0	0	0	0	0	0	0	0	i_{Charge_SNOx}	i_{Charge_SNHx}	0	0	0	-1	0	0	0	0

j	Symbol	Name	S _U	S _{Br}	S _{Bs}	C _B	X _U	X _B	X _{OH₂ACT}	X _{ANO}	X _E	S _{O2}	S _{NOx}	S _{NHx}	S _{NB}	X _{NB}	S _{ALK}	S _{N2}	X _{INOR_G}	X _{EPS}	X _{STO}
1	r1	Aerobic growth of heterotrophs - Fast	0	- 1.5787473 22	0	0	0	0	1	0	0	-0.492537313	0	-0.086	0	0	-0.006142857	0	0	0.070422535	0.015787473
2	r2	Aerobic growth of heterotrophs - Slow	0	0	- 1.578747322	0	0	0	1	0	0	-0.492537313	0	-0.086	0	0	-0.006142857	0	0	0.070422535	0.015787473
3	r3	Anoxic growth of heterotrophs -Fast	0	- 1.8518518 52	0	0	0	0	1	0	0	0	-0.298148148	-0.086	0	0	0.015153439	0.298148148	0	0	0
4	r4	Anoxic growth of heterotrophs -Slow	0	0	- 1.851851852	0	0	0	1	0	0	0	-0.298148148	-0.086	0	0	0.015153439	0.298148148	0	0	0
5	r5	Aerobic growth of autotrophs	0	0	0	0	0	0	0	1	0	-18.04761905	4.166666667	- 4.25266 6667	0	0	-0.601380952	0	0	0	0
6	r6	Decay of heterotrophs	0	0	0	0	0	0.92	-1	0	0.08	0	0	0	0	0.0812	0	0	0	0	0
7	r7	Decay of autotrophs	0	0	0	0	0	0.92	0	-1	0.08	0	0	0	0	0.0812	0	0	0	0	0
8	r8	Ammonification of soluble organic nitrogen	0	0	0	0	0	0	0	0	0	0	0	1	-1	0	0.071428571	0	0	0	0
9	r9	Hydrolysis of entrapped organics	0	0	1	0	0	-1	0	0	0	0	0	0	0	0	0	0	0	0	0
10	r10	Hydrolysis of entrapped organic nitrogen	0	0	0	0	0	0	0	0	0	0	0	0	1	-1	0	0	0	0	0
11	r11	flocculation of colloidal substrate	0	0	0	-1	0	1	0	0	0	0	0	0	0	0	0	0	0	0	0
12	r12	Hydrolysis of storage products	0	0	1	0	0	0	0	0	0	0	0	0	0	0	0	0	0	0	0
13	r13	enmeshment/storage of S _{NB}	0	0	0	0	0	0	0	0	0	0	0	0	-1	1	0	0	0	0	0
14	r14	EPS hydrolysis	0	0	1	0	0	0	0	0	0	0	0	0	0	0	0	0	0	-1	0

Elemental composition																					
COD	1	1	1	1	1	1	1	1	1	1	1	-1	-4.57	0	0	0	0	-1.714285714	0	1	1
N	0	0	0	0	0	0	0.086	0.086	0.06	0	0	0	1	1	1	1	0	1	0	0	0
Charge	0	0	0	0	0	0	0	0	0	0	0	0	-0.071	0.071	0	0	-1	0	0	0	0

Table 24 HRAS model framework rate expressions

j	Symbol	Name	Rate expression (rj)	rj value
1	r1	Aerobic growth of heterotrophs - Fast	$\mu_{\text{OHO},T} * (S_{\text{Bf}} / (K_{\text{Bf}} + S_{\text{Bf}})) * (S_{\text{O}_2} / (K_{\text{O},\text{OHO}} + S_{\text{O}_2})) * (S_{\text{NH}_x} / (K_{\text{NH}_x,\text{nut}} + S_{\text{NH}_x})) * X_{\text{OHO},\text{ACT}}$	43.29
2	r2	Aerobic growth of heterotrophs - Slow	$\mu_{\text{OHO},T} * (S_{\text{Bs}} / (K_{\text{Bs}} + S_{\text{Bs}})) * (K_{\text{Bf}} / (K_{\text{Bf}} + S_{\text{Bf}})) * (S_{\text{O}_2} / (K_{\text{O},\text{OHO}} + S_{\text{O}_2})) * (S_{\text{NH}_x} / (K_{\text{NH}_x,\text{nut}} + S_{\text{NH}_x})) * X_{\text{OHO},\text{ACT}}$	8.66
3	r3	Anoxic growth of heterotrophs -Fast	$\mu_{\text{OHO},T} * (S_{\text{Bf}} / (K_{\text{Bf}} + S_{\text{Bf}})) * (K_{\text{O},\text{OHO}} / (K_{\text{O},\text{OHO}} + S_{\text{O}_2})) * (S_{\text{NO}_x} / (K_{\text{NO}_x} + S_{\text{NO}_x})) * (S_{\text{NH}_x} / (K_{\text{NH}_x,\text{nut}} + S_{\text{NH}_x})) * \eta_{\text{GRO},\text{ANOX}} * X_{\text{OHO},\text{ACT}}$	3.38
4	r4	Anoxic growth of heterotrophs -Slow	$\mu_{\text{OHO},T} * (S_{\text{Bs}} / (K_{\text{Bs}} + S_{\text{Bs}})) * (K_{\text{Bf}} / (K_{\text{Bf}} + S_{\text{Bf}})) * (K_{\text{O},\text{OHO}} / (K_{\text{O},\text{OHO}} + S_{\text{O}_2})) * (S_{\text{NO}_x} / (K_{\text{NO}_x} + S_{\text{NO}_x})) * (S_{\text{NH}_x} / (K_{\text{NH}_x,\text{nut}} + S_{\text{NH}_x})) * \eta_{\text{GRO},\text{ANOX}} * X_{\text{OHO},\text{ACT}}$	0.68
5	r5	Aerobic growth of autotrophs	$\mu_{\text{ANO}} * (S_{\text{NH}_x} / (K_{\text{NH}_x} + S_{\text{NH}_x})) * (S_{\text{O}_2} / (K_{\text{O},\text{ANO}} + S_{\text{O}_2})) * X_{\text{ANO}}$	22.86
6	r6	Decay of heterotrophs	$b_{\text{O}_2,\text{OHO},T} * X_{\text{OHO},\text{ACT}}$	6.20
7	r7	Decay of autotrophs	$b_{\text{ANO}} * X_{\text{ANO}}$	12.00
8	r8	Ammonification of soluble organic nitrogen	$q_{\text{AMM}} * S_{\text{NB}} * X_{\text{OHO},\text{ACT}}$	0.80
9	r9	Hydrolysis of entrapped organics	$q_{\text{XB},\text{HYD}} * ((X_{\text{B}} / X_{\text{OHO},\text{ACT}}) / (K_{\text{B},\text{HYD}} + X_{\text{B}} / X_{\text{OHO},\text{ACT}})) * ((S_{\text{O}_2} / (K_{\text{O},\text{OHO}} + S_{\text{O}_2})) + \eta_{\text{HYD}} * (K_{\text{O},\text{OHO}} / (K_{\text{O},\text{OHO}} + S_{\text{O}_2})) * (S_{\text{NO}_x} / (K_{\text{NO}_x} + S_{\text{NO}_x}))) * X_{\text{OHO},\text{ACT}}$	25.90
10	r10	Hydrolysis of entrapped organic nitrogen	$q_{\text{XB},\text{HYD}} * (X_{\text{NB}} / X_{\text{B}}) * ((X_{\text{B}} / X_{\text{OHO},\text{ACT}}) / (K_{\text{B},\text{HYD}} + X_{\text{B}} / X_{\text{OHO},\text{ACT}})) * ((S_{\text{O}_2} / (K_{\text{O},\text{OHO}} + S_{\text{O}_2})) + \eta_{\text{HYD}} * (K_{\text{O},\text{OHO}} / (K_{\text{O},\text{OHO}} + S_{\text{O}_2})) * (S_{\text{NO}_x} / (K_{\text{NO}_x} + S_{\text{NO}_x}))) * X_{\text{OHO},\text{ACT}}$	0.52
11	r11	flocculation of colloidal substrate	$q_{\text{ADS}} * C_{\text{B}} * (X_{\text{OHO},\text{ACT}} + X_{\text{ANO}}) * (K_{\text{SL}} / ((C_{\text{B}} / (X_{\text{OHO},\text{ACT}} + X_{\text{ANO}})) + K_{\text{SL}})) * (X_{\text{EPS}} / (K_{\text{EPS}} + X_{\text{EPS}}))$	0.00
12	r12	Hydrolysis of storage products	$q_{\text{STO},\text{HYD}} * (X_{\text{STO}} / X_{\text{OHO},\text{ACT}} / (K_{\text{STO},\text{HYD}} + X_{\text{STO}} / X_{\text{OHO},\text{ACT}})) * (K_{\text{Bf}} / (K_{\text{Bf}} + S_{\text{Bf}})) * (K_{\text{Bs}} / (K_{\text{Bs}} + S_{\text{Bs}})) * (S_{\text{O}_2} / (K_{\text{O},\text{OHO}} + S_{\text{O}_2})) * X_{\text{OHO},\text{ACT}}$	3.78

j	Symbol	Name	Rate expression (rj)	rj value
13	r13	enmeshment/storage of S _{NB}	$q_{STO} * S_{NB} / S_{Bf} * (S_{Bf} / (K_{B,STO} + S_{Bf})) * (S_{O2} / (K_{O,OHO} + S_{O2})) * X_{OHO,ACT}$	1.82
14	r14	EPS hydrolysis	$q_{EPS,HYD} * X_{EPS}$	0.00

Table 25 HRAS model state variables

Symbol	Name	Influent	Initial concentration	Unit
S _U	Soluble undegradable organics	10	25	g COD.m ⁻³
S _{Bf}	Soluble biodegradable organics	60	5	g COD.m ⁻³
S _{Bs}	Slowly biodegradable organics	30	10	g COD.m ⁻³
C _B	Colloidal biodegradable organics	40	1	g COD.m ⁻³
X _U	Particulate undegradable organics from the influent	30	700	g COD.m ⁻³
X _B	Particulate biodegradable organics	150	100	g COD.m ⁻³
X _{OHO,ACT}	Active Ordinary heterotrophic organisms	10	10	g COD.m ⁻³
X _{ANO}	Autotrophic nitrifying organisms (NH ₄ ⁺ to NO ₃ ⁻)	1	80	g COD.m ⁻³
X _E	Particulate undegradable endogenous products	0	200	g COD.m ⁻³
S _{O2}	Dissolved oxygen	0	1	g O ₂ .m ⁻³
S _{NOx}	Nitrate and nitrite (NO ₃ + NO ₂)	0	20	g N.m ⁻³
S _{NHx}	Ammonia (NH ₄ + NH ₃)	35	1	g N.m ⁻³
S _{NB}	Soluble biodegradable organic N	5	1	g N.m ⁻³
X _{NB}	Particulate biodegradable organic N	10	2	g N.m ⁻³

Symbol	Name	Influent	Initial concentration	Unit
S _{ALK}	Alkalinity	6	3	meq/L
S _{N2}	Dissolved nitrogen	16	16	g N.m ⁻³
X _{INORG}	Inorganic suspended solids	40	350	g TSS.m ⁻³
X _{EPS}	Extracellular Polymer Substances	10	0	g COD.m ⁻³
X _{STO}	Storage Polymer Substances	10	50	g COD.m ⁻³
S _{CO2}	Total inorganic carbon	351.00	250.00	g CO ₂ .m ⁻³

Table 26 HRAS model kinetic parameters for Hydrolysis

Symbol	Name	Default	Unit
$K_{B,HYD}$	Saturation coefficient for X_B/X_{OHO}	0.03	$g\ X_{CB}.g\ X_{OHO}^{-1}$
η_{HYD}	Correction factor for hydrolysis under anoxic conditions	0.4	-
$q_{EPS,HYD}$	EPS hydrolysis	0.16	
K_{EPS}	Half-saturation coefficient for EPS	100	
$K_{EPS,HYD}$	Hydrolysis Half-saturation coefficient for EPS	0.05	
$q_{XB,HYD}$	Rate Constant	2.75	
$q_{STO,HYD}$	Storage Hydrolysis Rate Constant	3	
$K_{STO,HYD}$	Hydrolysis Half-saturation coefficient for STO	0.15	
$K_{O,EPS}$	EPS Half-saturation coefficient for S_{O_2}	0.70	$g\ S_{O_2}.m^{-3}$

Table 27 HRAS model kinetic parameters for Heterotrophic growth and decay

Symbol	Name	Default	Unit
μ_{OHO}	Maximum growth rate of X_{OHO}	8	d^{-1}
$\eta_{GRO,ANOX}$	Reduction factor for anoxic growth of X_{OHO}	0.8	-
K_{Bf}	Half-saturation coefficient for S_B	20	$g\ S_{Bf}.m^{-3}$
K_{Bs}	Half-saturation coefficient for S_{Bs}	40	$g\ S_{Bs}.m^{-3}$
b_{OHO}	Decay rate for X_{OHO}	0.62	d^{-1}
$K_{O,OHO}$	Half-saturation coefficient for S_{O_2}	.015	$g\ S_{O_2}.m^{-3}$
K_{NOx}	Half-saturation coefficient for S_{NOx}	0.5	$g\ S_{NOx}.m^{-3}$
$K_{NHx,nut}$	Nutrient half-saturation coefficient	0.05	$g\ S_{NHx}.m^{-3}$
q_{STO}	Rate constant for growth on X_{STO}	2	d^{-1}
$K_{B,STO}$	Half-saturation coefficient for storage of S_B	5	-
$K_{O,STO}$	Half-Saturation Coefficient STO for S_{O_2}	0.7	$g\ SO_2.m^{-3}$

Table 28 HRAS model kinetic parameters for Autotrophic growth and decay

Symbol	Name	Default	Unit
μ_{ANO}	Maximum growth rate of X_{ANO}	0.8	d^{-1}
K_{NHx}	Substrate Half-saturation coefficient for ANOs	1	$g\ S_{NHx}.m^{-3}$
$K_{O,ANO}$	Half-saturation coefficient for S_{O_2}	0.4	$g\ S_{O_2}.m^{-3}$
b_{ANO}	Decay rate for X_{ANO}	0.15	d^{-1}

Table 29 HRAS model kinetic parameters for other conversion reactions

Symbol	Name	Default	Unit
q_{AMM}	Rate constant for ammonification	0.08	$m^3.g\ X_{C,B,N}^{-1}.d^{-1}$
q_{ADS}	Rate constant for adsorption	0.06	d^{-1}
K_{SL}	Half-saturation coefficient for surface limitation	0.009	-

Table 30 HRAS model kinetic parameters for temperature dependency

Symbol	Name	Default	Unit
θ_{μ,OH_0}	Arrhenius coefficient	1.04	-
θ_{b,O_2,OH_0}	Arrhenius coefficient	1.03	-

Table 31 HRAS model kinetic parameters for operational inputs

Symbol	Name	Default	Unit
T	Temperature	20.0	C°
Tbase	Arrhenius base temperature	20.0	C°

Table 32 HRAS model stoichiometric parameters for growth yields

Symbol	Name	Default	Unit
$Y_{OH_0,AER}$	Yield for aerobic X_{OH_0} growth	0.67	$g\ X_{OH_0}.g\ S_B^{-1}$
$Y_{OH_0,ANOX}$	Yield for anoxic X_{OH_0} growth	0.54	$g\ X_{OH_0}.g\ S_B^{-1}$
Y_{STO}	Yield for S_B storage and enmeshment	0.9	$g\ X_B.g\ S_B^{-1}$
Y_{ANO}	Yield of X_{ANO} growth per S_{NO_3}	0.24	$g\ X_{AUT}.g\ S_{NO_3}^{-1}$
f_U	Fraction of X_U generated in biomass decay	0.08	$g\ X_U.g\ X_{Bio}^{-1}$

Table 33 HRAS model stoichiometric parameters for nitrogen fractions

Symbol	Name	Default	Unit
$i_{N,XB}$	N content of biomass (X_{OHO} , X_{PAO} , X_{ANO})	0.086	g N.g X_{Bio}^{-1}
$i_{N,XU}$	N content of products from biomass	0.06	g N.g X_{UE}^{-1}
$i_{N,EPS}$	N content EPS	0.12	g N.g X_{EPS}^{-1}

Table 34 HRAS model stoichiometric parameters for charge and electron equivalence

Symbol	Name	Default	Unit
$i_{NO3,N2}$	NO ₃ reduction to N ₂ electron equivalence	2.857	g COD.g N ⁻¹
$i_{COD,NO3}$	NH ₃ to NO ₃ oxidation electron equivalence	-4.571	g COD.g N ⁻¹
$i_{COD,N2}$	NH ₃ to N ₂ oxidation electron equivalence	-1.714285714	g COD.g N ⁻¹
$i_{Charge,SNHx}$	Conversion factor for NH _x in charge	0.071	Charge.g N ⁻¹
$i_{Charge,SNOx}$	Conversion factor for NO ₃ in charge	-0.071428571	Charge.g N ⁻¹

Table 35 HRAS model stoichiometric parameters for calculated variable conversions

Symbol	Name	Default	Unit
i_{CV}	Particulate COD to VSS ratio	1.86	g COD.g VSS ⁻¹
i_{CB}	Biomass COD to VSS ratio	1.42	g COD.g VSS ⁻¹

Table 36 HRAS model stoichiometric parameters for EPS and Storage Products (STO)

Symbol	Name	Default	Unit
$k_{EPS,MAX}$	EPS formation coefficient	0.2	g COD _{EPS} .g VSS ⁻¹
$k_{STO,MAX}$	Maximum Production Rate for Storage Polymers	0.56	g X_{STO} .g S_{Br}^{-1}
f_{STO}	Fraction of STO in the biomass	0.15	

Table 37 Calculated stoichiometric parameter values for oxygen demands

Symbol	Name	Expression	Value	Unit
X_{COD}	Particulate COD	$X_U + X_B + X_{OHO} + X_{ANO} + X_E + X_{EPS} + X_{STO}$	1140.0	g COD.m ⁻³
S_{TOC}	Total Soluble (Dissolved) Organic Carbon	$S_U + S_{Bf} + S_{Bs}$	40.0	g COD.m ⁻³
C_{TOC}	Total Carbon	$X_{COD} + S_{TOC} + C_B$	1181	g COD.m ⁻³

Table 38 Calculated stoichiometric parameter values for suspended solids

Symbol	Name	Expression	Value	Unit
X_{VSS}	VSS	X_{COD}/i_{CV}	770.3	g.m ⁻³
X_{TVSS}	TVSS	$X_{VSS} + X_{INORG}$	1120.3	g.m ⁻³

Table 39 Calculated stoichiometric parameter values for other variables

Symbol	Name	Expression	Value	Unit
X_{OHO}	OHO's	$X_{OHO,ACT}$	10.0	g COD.m ⁻³
S_{TKN}	Total Kjeldahl Nitrogen	$S_{NB} + S_{NHx}$	2.0	g N.m ⁻³
S_{TIN}	Total Inorganic Nitrogen	$S_{NHx} + S_{NOx}$	21.0	g N.m ⁻³
S_{TN}	Total Soluble Nitrogen	$S_{NHx} + S_{NOx} + S_{NB}$	22.0	g N.m ⁻³
N_{TN}	Total Nitrogen	$S_{TN} + X_{NB}$	24.0	g N.m ⁻³
R_{CtoN}	Carbon to Nitrogen ratio	C_{TOC}/N_{TN}	49.2	gCOD/g N
P_{EPS}	EPS Production	$(X_{EPS}/X_{VSS}) * 1000$	0.0	
R_{CtoAmm}	TCOD to Ammonia Ratio	C_{TOC}/S_{NHx}	1181.0	
R_{STO}	Ratio X_{STO} to X_{COD}	X_{STO}/X_{COD}	0.0	

Table 40 Calculated kinetic parameter values for OUR and Temperature dependency

Symbol	Name	Expression	Value	Unit
OUR	Oxygen Uptake Rate	$-(v1_S_{O2}*r1+v2_S_{O2}*r2+v5_S_{O2}*r5)/24$	18.7	mg/l/hr
$\mu_{OHO,T}$		$\mu_{OHO} * Arrh(\theta_{\mu,OHO}; T; Tbase)$	7.00	d ⁻¹
$b_{O2,OHO,T}$		$b_{OHO} * Arrh(\theta_{b,O2,OHO}; T; Tbase)$	0.62	d ⁻¹

Table 41 Calculated kinetic parameter values for Growth Rate and Proportionality Coefficients

Symbol	Name	Expression	Value	Unit
μ	Actual Growth Rate	$\mu_{OHO,T} * (S_{Bf} / (K_{Bf} + S_{Bf})) * (S_{O2} / (K_{O,OHO} + S_{O2})) * (S_{NHx} / (K_{NHx,nut} + S_{NHx}))$	4.3	d ⁻¹
$f_{STO,max}$	STO saturation capacity of biomass	$(-.783 * ((\mu) / 24)) + 0.39$	0.249	
$Y_{PC,O2}$	STO yield adjusted for DO concentration	$(Y_{STO}) * (K_{O,STO} / (K_{O,STO} + S_{O2}))$	0.371	g X_{OHO} .g S_B^{-1}
$k_{STO,PC}$	STO Proportionality Coefficient	$Max(.01; Y_{PC,O2} * (1 - (f_{STO} / f_{STO,max})))$	0.010	g COD_{STO} .g COD_{SBf}^{-1}
$k_{EPS,SC}$	EPS Stoichiometric Coefficient	$(k_{EPS,MAX} / i_{CB}) * (S_{O2} / (K_{O,EPS} + S_{O2}))$	0.070	g COD_{EPS} .g COD_{XOHO}^{-1}
$k_{EPS,PC}$	EPS Proportionality Coefficient	$((k_{EPS,SC} * Y_{OHO,AER}) * (1 - k_{STO,PC})) / (1 + (k_{EPS,SC} * Y_{OHO,AER}))$	0.045	g COD_{EPS} .g COD_{SBf}^{-1}

Table 42 Calculated kinetic parameter values for saturation concentrations

Symbol	Name	Expression	Value	Unit
$G_{O2,sat,eq,field}$	Oxygen saturation concentration	9.1	9.1	mol.L ⁻¹ .bar ⁻¹
$G_{O2,sat,eq,st}$	Oxygen saturation concentration	9.1	9.1	mol.L ⁻¹ .bar ⁻¹

APPENDIX C: NO DATASET CALIBRATION RESULTS

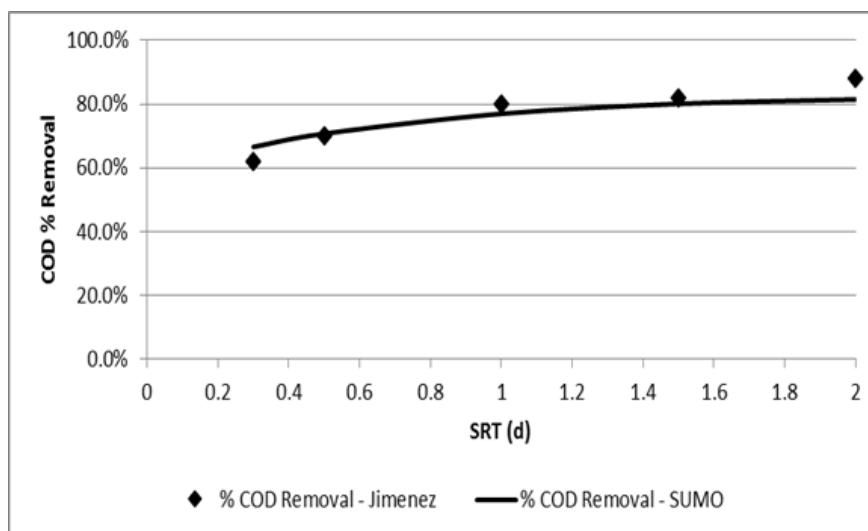
Effect of Variable SRT

Readily Biodegradable COD

Modeling Results

Influent	10	60	30
SRT	S_U	S_{BF}	S_{BS}
0.3	10	2.9	20.5
0.5	10	1.25	18
1	10	0.4	12.6
1.5	10	0.3	9.6
2	10	0.2	8.32

SRT (days)	% COD Removal – Observed Data	% COD Removal – A-stage Model
0.3	62.0%	66.6%
0.5	70.0%	70.8%
1	80.0%	77.0%
1.5	82.0%	80.1%
2	88.0%	81.5%

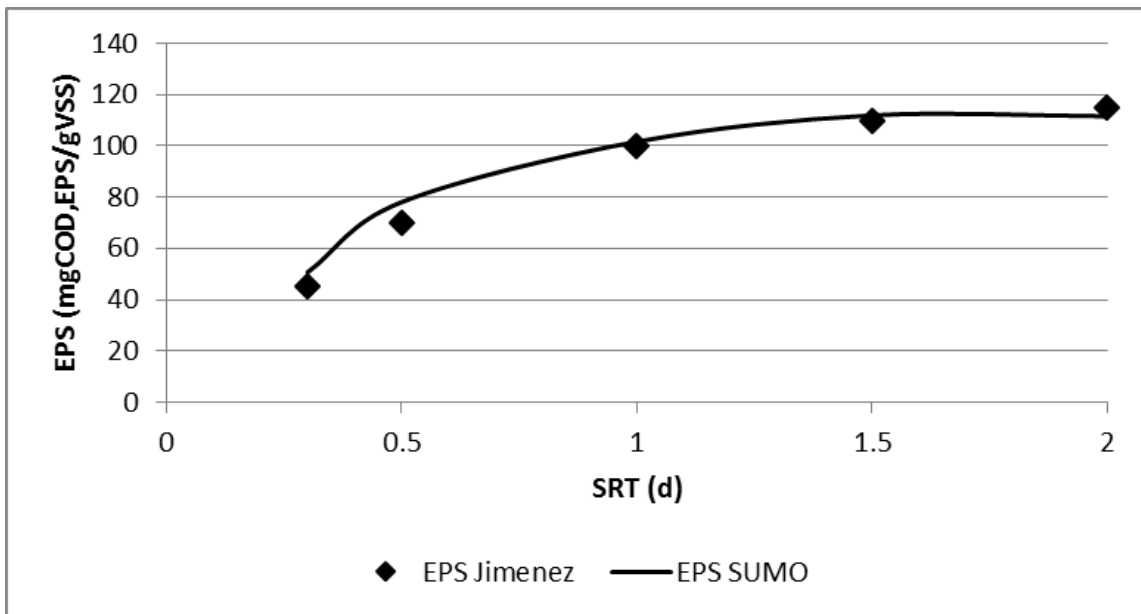


EPS Production

Modeling Results

SRT	X_{EPS}	X_{VSS}
0.3	80.2	1582
0.5	185	2369
1	228	2242
1.5	223	1992
2	288	2581

SRT (days)	EPS Production Rate	
	Observed Data (mgCOD/g _{VSS})	EPS Production Rate A-stageModel (mgCOD/g _{VSS})
0.3	45	50.70
0.5	70	78.09
1	100	101.69
1.5	110	111.95
2	115	111.58

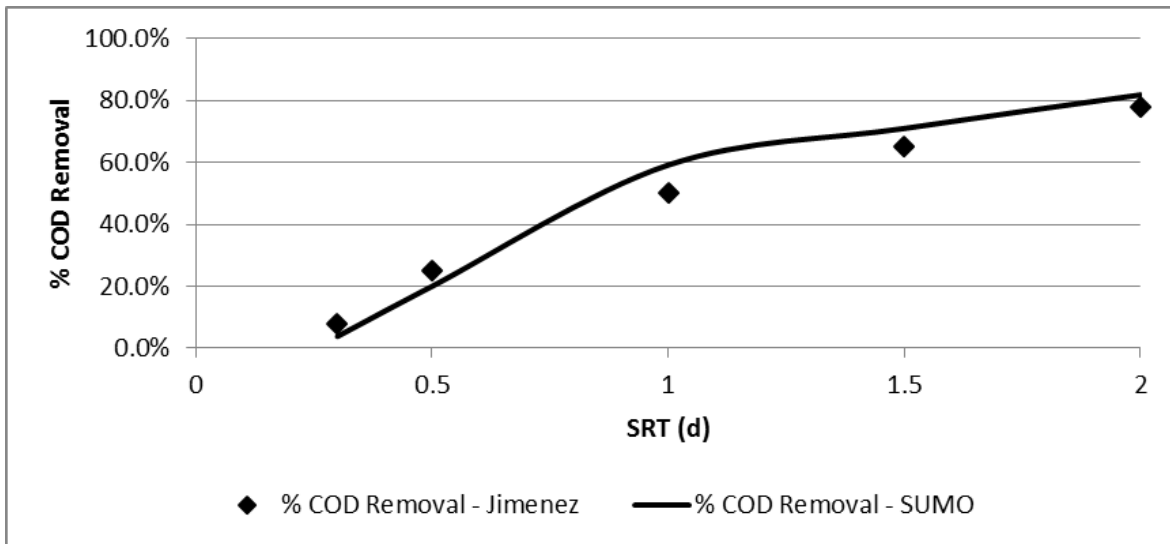


Colloidal COD Removal Efficiency

Modeling Results

Influent	0	60
SRT	C_U	C_B
0.3	0	57.7
0.5	0	48
1	0	24.5
1.5	0	17.4
2	0	10.9

SRT (days)	% COD Removal – Observed Data	% COD Removal – A-stage Model
0.3	8.0%	3.8%
0.5	25.0%	20.0%
1	50.0%	59.2%
1.5	65.0%	71.0%
2	78.0%	81.8%



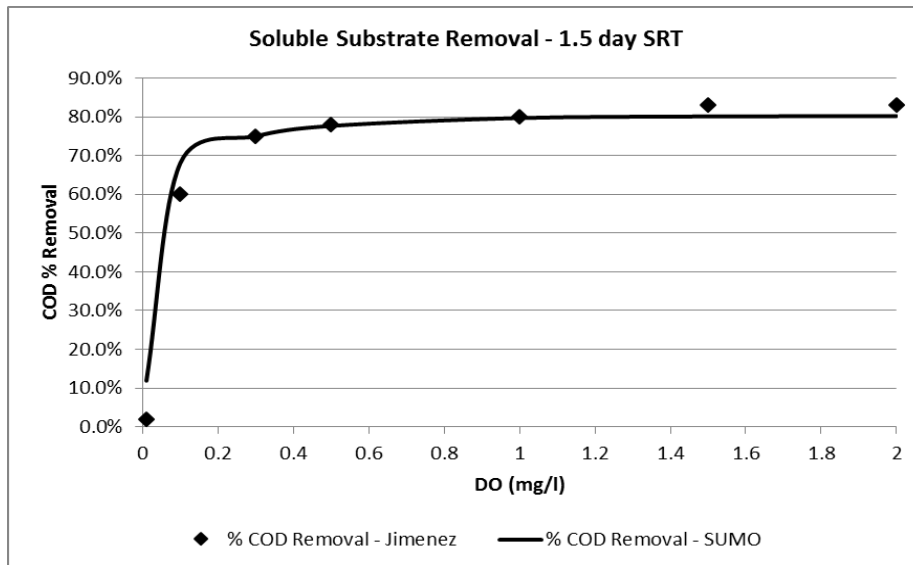
Effect of Variable DO

Readily Biodegradable COD

Modeling Results

Influent	10	60	30
DO	S_U	S_{BF}	S_{BS}
0.01	10	49.8	28.3
0.1	10	1.5	20.4
0.3	10	0.4	14.6
0.5	10	0.32	12
1	10	0.28	10
1.5	10	0.28	9.6
2	10	0.28	9.5

DO (mg/l)	% COD Removal – Observed Data	% COD Removal – A-stage Model
0.01	2.0%	11.9%
0.1	60.0%	68.1%
0.3	75.0%	75.0%
0.5	78.0%	77.7%
1	80.0%	79.7%
1.5	83.0%	80.1%
2	83.0%	80.2%

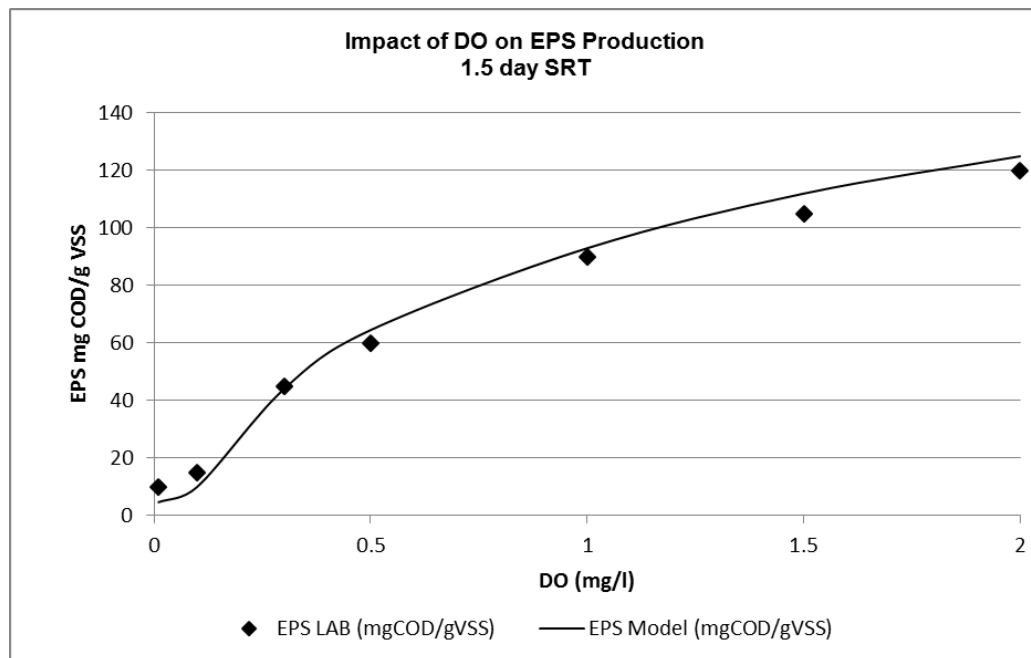


EPS Production

Modeling Results

DO (mg/l)	X_{EPS}	X_{VSS}
0.01	8	2053
0.1	20.4	2424
0.3	86.5	2066
0.5	125.7	2036
1	182.5	2038
1.5	221.2	2059
2	249	2078

DO (mg/l)	EPS Production Rate Observed Data (mgCOD/gVSS)	EPS Production Rate A-stage Model (mgCOD/gVSS)
0.01	10	4.60
0.1	15	10.00
0.3	45	44.00
0.5	60.0	64.50
1	90.0	93.00
1.5	105.0	112.00
2	120.0	125.00

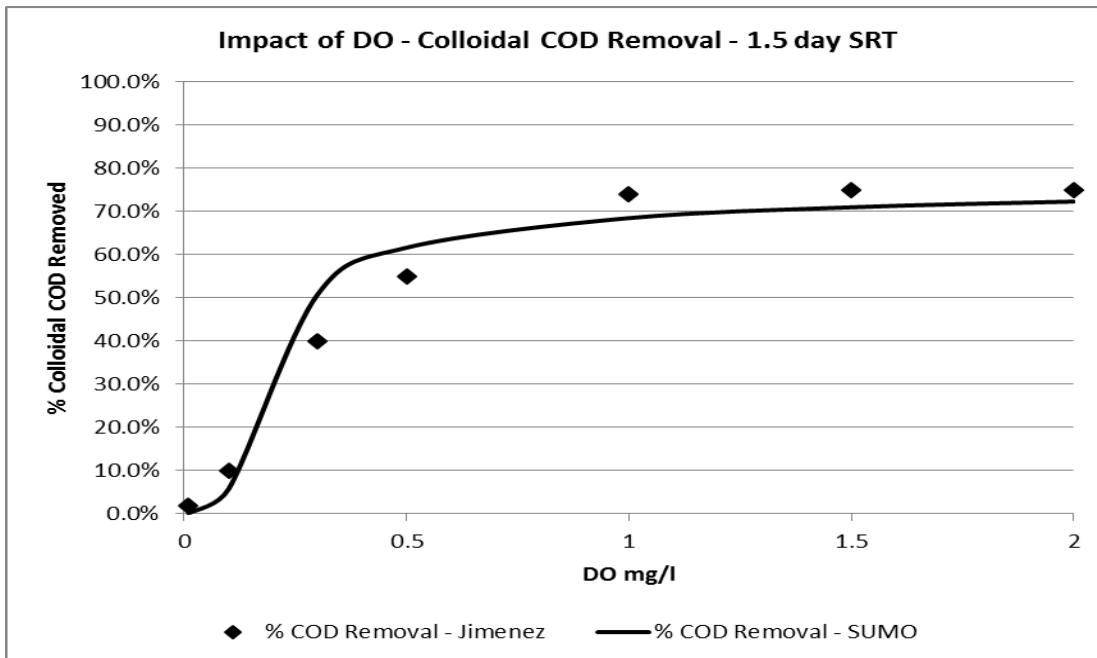


Colloidal COD Removal Efficiency

Modeling Results

Influent	0	60
DO (mg/l)	C_U	C_B
0.01	0	59.9
0.1	0	56.5
0.3	0	29.5
0.5	0	23
1	0	18.9
1.5	0	17.4
2	0	16.6

DO (mg/l)	% COD Removal - Observed Data	% COD Removal - A-stage Model
0.01	2.0%	0.2%
0.1	10.0%	5.8%
0.3	40.0%	50.8%
0.5	55.0%	61.7%
1	74.0%	68.5%
1.5	75.0%	71.0%
2	75.0%	72.3%



Modified Parameter Values

Table 43 NO calibration modified parameter list

Symbol	Name	Default	Value	Unit
μ_{OHO}	Maximum growth rate of X_{OHO}	3	8	d^{-1}
K_{Bf}	Half-saturation coefficient for S_{B}	2	20	$\text{g } S_{\text{Bf}} \cdot \text{m}^{-3}$
K_{Bs}	Half-saturation coefficient for S_{Bs}	10	40	$\text{g } S_{\text{Bs}} \cdot \text{m}^{-3}$
$K_{\text{O,OHO}}$	Half-saturation coefficient for S_{O_2}	0.1	0.15	$\text{g } S_{\text{O}_2} \cdot \text{m}^{-3}$
$q_{\text{EPS,HYD}}$	EPS hydrolysis	0.16	0.25	
q_{ADS}	Rate constant for adsorption	0.07	0.065	d^{-1}
K_{SL}	Half-saturation coefficient for surface limitation	0.002	0.009	-
$k_{\text{EPS,MAX}}$	EPS formation coefficient	0.2	0.225	$\text{g COD}_{\text{EPS}} \cdot \text{gVSS}^{-1}$

APPENDIX D: HRSD STATE VARIABLE DATASET

Table 44 HRSD pilot influent state variables

Date	Time	Inf Q (m ³ /d)	Q WAS (m ³ /d)	Inf S _U (gCOD/m ³)	Inf S _{Bf} (gCOD/m ³)	Inf S _{Bs} (gCOD/m ³)	Inf C _B (gCOD/m ³)	Inf X _U (gCOD/m ³)	Inf X _B (gCOD/m ³)	Inf X _{OHO_ACT} (gCOD/m ³)	Inf S _{NHx} (gN/m ³)	Inf X _{NB} (gN/m ³)	Inf VSS (gVSS/m ³)	Temp (°C)
03-Sep-13	0	24.53	0.87	38.22	53.50	88.13	37.15	170.00	220.00	23.41	42.01	12.74	207.30	26.80
04-Sep-13	1	24.53	0.87	32.30	45.21	74.49	44.00	137.00	180.00	19.79	35.50	10.77	175.20	26.70
09-Sep-13	2	24.53	0.87	30.77	47.89	66.10	85.24	48.00	210.00	18.82	36.48	9.41	177.04	26.50
10-Sep-13	3	24.53	0.87	33.80	52.60	72.60	41.00	106.00	230.00	20.68	40.07	10.34	194.45	26.80
11-Sep-13	4	24.53	0.87	30.96	48.18	66.50	61.35	74.00	210.00	18.94	36.71	9.47	178.13	26.90
12-Sep-13	5	24.53	0.87	36.95	57.51	79.37	26.17	136.00	250.00	22.60	43.81	11.30	212.59	26.90
16-Sep-13	6	24.53	0.87	27.35	50.90	96.41	60.34	54.00	230.00	20.02	37.97	12.28	167.68	26.70
17-Sep-13	7	24.53	0.87	27.40	51.00	96.60	28.00	87.00	230.00	20.06	38.04	12.30	168.00	26.50
18-Sep-13	8	24.53	0.87	31.30	58.26	110.35	35.10	99.00	260.00	22.91	43.45	14.05	191.91	26.50
23-Sep-13	9	24.53	0.87	30.51	56.79	87.80	83.90	100.00	220.00	22.33	40.86	10.64	198.74	26.00
24-Sep-13	10	24.53	0.87	28.40	52.86	81.73	62.00	114.00	200.00	20.79	38.04	9.91	185.01	26.00
25-Sep-13	11	24.53	0.87	30.14	56.10	86.74	51.02	128.00	220.00	22.06	40.37	10.51	196.33	25.70
26-Sep-13	12	24.53	0.87	34.94	65.03	100.54	11.50	201.00	250.00	25.57	46.79	12.18	227.57	25.70
30-Sep-13	13	24.53	1.01	32.73	37.01	100.34	63.92	114.00	220.00	21.91	44.54	12.24	173.60	25.50
01-Oct-13	14	24.53	1.01	30.60	34.60	93.80	56.00	116.00	200.00	20.48	41.64	11.44	162.29	25.30
02-Oct-13	15	24.53	1.01	31.81	35.97	97.51	74.71	102.00	210.00	21.29	43.28	11.90	168.71	25.20
03-Oct-13	16	24.53	1.08	33.08	37.40	101.40	79.12	103.00	220.00	22.14	45.01	12.37	175.44	25.20
07-Oct-13	17	24.53	1.08	33.48	48.99	68.99	72.54	87.00	270.00	22.41	38.35	8.09	220.19	25.80
08-Oct-13	18	24.53	1.08	28.29	41.40	58.31	73.00	60.00	230.00	18.94	32.41	6.83	186.08	25.30
09-Oct-13	19	24.53	1.08	31.00	45.36	63.89	35.75	112.00	250.00	20.75	35.51	7.49	203.89	25.10
10-Oct-13	20	24.53	1.08	28.24	41.32	58.19	31.26	101.00	230.00	18.90	32.34	6.82	185.70	24.50
15-Oct-13	21	24.53	1.08	21.70	52.20	72.10	58.00	66.00	230.00	19.29	36.41	5.89	183.88	24.30
16-Oct-13	22	24.53	1.08	23.39	56.27	77.72	40.61	91.00	250.00	20.79	39.26	6.35	198.22	24.10
17-Oct-13	23	24.53	1.08	23.83	57.32	79.17	85.69	53.00	250.00	21.18	39.98	6.47	201.90	24.20
21-Oct-13	24	24.53	1.08	22.46	53.06	57.81	98.67	77.00	210.00	20.02	38.52	12.52	193.04	24.30
22-Oct-13	25	24.53	1.08	25.10	59.30	64.60	48.00	153.00	230.00	22.37	43.05	13.99	215.73	24.00
23-Oct-13	26	24.53	1.08	23.37	55.21	60.14	62.28	129.00	210.00	20.83	40.08	13.02	200.85	24.00
24-Oct-13	27	24.53	1.08	24.41	57.66	62.82	57.11	142.00	220.00	21.76	41.86	13.60	209.78	23.60
28-Oct-13	28	24.53	1.08	15.45	46.89	81.17	108.50	109.00	160.00	20.10	38.21	11.79	169.68	22.90
29-Oct-13	29	24.53	1.08	16.90	51.30	88.80	51.00	192.00	170.00	21.99	41.80	12.90	185.64	22.90
04-Nov-13	30	24.53	0.79	17.82	49.21	82.07	59.89	102.00	290.00	20.00	39.74	14.28	212.02	22.50
06-Nov-13	31	24.53	0.79	17.91	49.46	82.48	52.15	102.00	300.00	20.10	39.94	14.35	213.08	22.40
07-Nov-13	32	24.53	0.79	17.49	48.31	80.57	56.62	97.00	290.00	19.63	39.02	14.02	208.14	22.40
12-Nov-13	33	24.53	0.87	23.66	54.40	70.53	70.41	117.00	230.00	18.84	38.84	10.75	140.06	21.50
13-Nov-13	34	24.53	0.87	24.20	55.65	72.15	55.00	142.00	230.00	19.27	39.73	11.00	143.28	21.20
14-Nov-13	35	24.53	0.87	23.66	54.40	70.53	65.41	122.00	230.00	18.84	38.84	10.75	140.06	21.10
18-Nov-13	36	24.53	0.94	24.03	66.80	94.03	56.14	114.00	220.00	18.00	41.38	5.51	198.98	21.00
19-Nov-13	37	24.53	0.94	21.19	58.90	82.91	65.00	79.00	200.00	15.87	36.49	4.86	175.44	20.80
20-Nov-13	38	24.53	0.94	21.19	58.90	82.91	55.00	89.00	200.00	15.87	36.49	4.86	175.44	20.80
21-Nov-13	39	24.53	1.01	23.99	66.68	93.87	39.46	130.00	220.00	17.97	41.31	5.50	198.63	20.60
25-Nov-13	40	24.53	1.01	24.33	67.61	95.17	75.89	99.00	220.00	18.22	40.91	5.58	201.40	20.00
26-Nov-13	41	24.53	1.01	23.95	66.57	93.70	52.78	116.00	220.00	17.94	40.27	5.49	198.28	20.20
02-Dec-13	42	24.53	0.87	21.44	55.51	93.41	92.65	104.00	190.00	17.44	39.20	9.53	181.36	18.70

Date	Time	Inf Q (m ³ /d)	Q WAS (m ³ /d)	Inf S _U (gCOD/m ³)	Inf S _{Bf} (gCOD/m ³)	Inf S _{Bs} (gCOD/m ³)	Inf C _B (gCOD/m ³)	Inf X _U (gCOD/m ³)	Inf X _B (gCOD/m ³)	Inf X _{OHO,ACT} (gCOD/m ³)	Inf S _{NHx} (gN/m ³)	Inf X _{NB} (gN/m ³)	Inf VSS (gVSS/m ³)	Temp (°C)
03-Dec-13	43	24.53	0.87	22.40	58.00	97.60	59.00	145.00	200.00	18.22	40.95	9.95	189.50	18.60
04-Dec-13	44	24.53	0.87	21.40	55.41	93.24	78.95	117.00	190.00	17.41	39.12	9.51	181.04	18.80
05-Dec-13	45	24.53	0.79	23.79	61.59	103.64	65.99	143.00	220.00	19.35	43.49	10.57	201.23	18.90
09-Dec-13	46	24.53	0.79	23.98	22.97	104.48	78.58	241.00	300.00	34.00	45.87	17.33	274.14	18.70
10-Dec-13	47	24.53	0.79	19.00	18.20	82.80	68.00	183.00	240.00	26.94	36.35	13.73	217.25	18.40
11-Dec-13	48	24.53	0.87	17.04	16.32	74.26	87.37	133.00	220.00	24.17	32.60	12.32	194.85	18.10
12-Dec-13	49	24.53	0.94	15.98	15.31	69.65	107.05	106.00	200.00	22.67	30.58	11.55	182.76	18.20
18-Dec-13	50	24.53	1.04	12.69	35.72	58.99	113.60	129.00	200.00	24.25	31.97	11.26	175.27	17.40
30-Dec-13	51	24.53	1.04	13.89	39.09	64.56	111.45	153.00	220.00	26.55	35.79	14.70	203.75	17.10
02-Jan-14	52	24.53	1.04	14.70	41.37	68.32	154.62	128.00	230.00	28.09	37.87	15.55	215.60	17.00
06-Jan-14	53	24.53	1.04	13.20	52.17	121.33	50.31	55.00	280.00	25.22	36.53	6.29	204.27	16.70
07-Jan-14	54	24.53	1.04	9.97	39.40	91.63	78.00	1.00	212.00	19.05	27.59	4.75	154.28	16.90
08-Jan-14	55	24.53	1.04	13.64	53.90	125.36	11.10	97.00	290.00	26.06	37.75	6.50	211.06	16.10
09-Jan-14	56	24.53	1.04	12.88	50.89	118.36	22.88	73.00	280.00	24.61	35.64	6.14	199.27	16.30
13-Jan-14	57	24.53	1.04	10.22	40.40	49.90	116.47	6.00	220.00	18.00	26.97	1.85	158.20	16.00
14-Jan-14	58	24.53	1.04	12.00	47.43	58.57	81.00	61.00	260.00	21.13	31.66	2.17	185.70	15.90
15-Jan-14	59	24.53	1.04	11.61	45.88	56.66	80.86	58.00	250.00	20.44	30.62	2.10	179.63	16.50
16-Jan-14	60	24.53	1.04	13.06	51.62	63.76	52.56	105.00	280.00	23.00	34.46	2.36	202.13	16.10
21-Jan-14	61	24.53	0.87	13.66	38.60	82.08	124.66	83.00	250.00	19.21	30.67	7.48	166.18	16.20
23-Jan-14	62	24.53	0.84	15.07	42.58	90.53	63.82	171.00	270.00	21.19	33.83	8.25	183.30	15.40
27-Jan-14	63	24.53	0.84	17.49	49.42	105.09	68.99	207.00	310.00	31.00	37.74	20.35	313.73	14.80
30-Jan-14	64	24.53	0.87	14.19	40.10	85.27	76.44	149.00	250.00	25.15	30.62	16.51	254.54	14.10
03-Feb-14	65	24.53	0.87	22.11	30.54	102.33	74.02	159.00	200.00	24.05	35.79	12.01	255.43	14.30
04-Feb-14	66	24.53	0.87	19.40	26.80	89.80	75.00	135.00	170.00	21.10	31.41	10.54	224.15	14.20
05-Feb-14	67	24.53	0.87	16.92	23.37	78.31	74.40	107.00	150.00	18.40	27.39	9.19	195.48	14.30
06-Feb-14	68	24.53	0.87	21.62	29.86	100.07	48.45	185.00	190.00	23.52	35.00	11.74	249.78	14.20
10-Feb-14	69	24.53	0.87	25.54	40.58	72.32	99.57	118.00	150.00	20.69	31.62	3.13	219.14	14.20
11-Feb-14	70	24.53	0.87	21.40	34.00	60.60	98.00	90.00	120.00	17.34	26.50	2.63	183.62	14.00
12-Feb-14	71	24.53	0.87	29.27	46.51	82.90	36.32	215.00	170.00	23.72	36.25	3.59	251.18	14.00
13-Feb-14	72	24.53	0.87	24.73	39.29	70.03	30.94	185.00	140.00	20.04	30.62	3.04	212.21	13.20
17-Feb-14	73	24.53	0.87	23.96	40.60	93.13	59.30	226.00	230.00	42.00	36.76	18.29	255.53	13.90
18-Feb-14	74	24.53	0.87	19.30	32.70	75.00	98.00	137.00	180.00	33.82	29.61	14.73	205.79	14.30
19-Feb-14	75	24.53	0.87	22.04	37.35	85.65	77.96	186.00	210.00	38.63	33.81	16.82	235.03	14.20
20-Feb-14	76	24.53	0.94	22.47	38.07	87.32	94.15	179.00	210.00	39.38	34.47	17.15	239.58	14.50
24-Feb-14	77	24.53	0.94	23.06	54.72	72.59	93.63	80.00	230.00	22.00	31.62	3.03	161.61	14.90
25-Feb-14	78	24.53	1.01	20.40	48.40	64.20	95.00	52.00	210.00	19.46	27.97	2.68	142.94	14.90
26-Feb-14	79	24.53	1.01	21.69	51.46	68.26	74.59	85.00	220.00	20.69	29.74	2.85	151.99	14.80
27-Feb-14	80	24.53	1.01	33.89	80.40	106.65	103.06	150.00	340.00	32.32	46.46	4.45	237.46	15.10
06-Mar-14	81	24.53	1.01	30.48	63.10	62.68	52.74	343.00	180.00	29.07	38.01	8.20	215.57	14.40
10-Mar-14	82	24.53	1.01	15.09	22.94	97.59	85.37	168.00	230.00	17.00	33.58	15.24	218.58	14.40
11-Mar-14	83	24.53	1.01	14.80	22.50	95.70	62.00	192.00	220.00	16.67	32.93	14.94	214.34	14.50
12-Mar-14	84	24.53	1.08	14.65	22.28	94.75	67.31	182.00	220.00	16.51	32.60	14.80	212.22	14.90
13-Mar-14	85	24.53	1.08	14.58	22.17	94.28	82.97	164.00	220.00	16.42	32.44	14.72	211.16	15.00
17-Mar-14	86	24.53	1.15	17.38	26.69	77.76	94.18	155.00	170.00	14.86	31.06	12.10	171.30	15.00

Date	Time	Inf Q (m ³ /d)	Q WAS (m ³ /d)	Inf S _U (gCOD/m ³)	Inf S _{Bf} (gCOD/m ³)	Inf S _{Bs} (gCOD/m ³)	Inf C _B (gCOD/m ³)	Inf X _U (gCOD/m ³)	Inf X _B (gCOD/m ³)	Inf X _{OHO,ACT} (gCOD/m ³)	Inf S _{NHx} (gN/m ³)	Inf X _{NB} (gN/m ³)	Inf VSS (gVSS/m ³)	Temp (°C)
18-Mar-14	87	24.53	1.23	16.80	25.80	75.17	52.23	193.00	160.00	14.36	30.02	11.70	165.60	14.80
19-Mar-14	88	24.53	1.30	16.99	26.10	76.03	56.88	183.00	170.00	14.53	30.37	11.83	167.50	14.60
24-Mar-14	89	24.53	1.44	19.84	41.85	62.44	102.88	97.00	270.00	16.31	36.58	12.16	197.13	15.30
25-Mar-14	90	24.53	1.44	18.20	38.40	57.29	90.11	91.00	250.00	14.97	33.56	11.16	180.87	15.40
26-Mar-14	91	24.53	1.44	16.66	35.16	52.45	86.73	78.00	230.00	13.70	30.73	10.22	165.61	14.90
27-Mar-14	92	24.53	1.44	17.93	37.84	56.44	86.79	98.00	240.00	14.75	33.07	11.00	178.22	15.20
31-Mar-14	93	24.53	1.59	16.13	33.84	74.96	87.06	78.00	220.00	14.01	32.22	8.76	174.06	15.50
01-Apr-14	94	24.53	1.73	17.30	36.30	80.40	61.00	122.00	230.00	15.02	34.56	9.40	186.69	15.70
02-Apr-14	95	24.53	1.73	18.66	39.15	86.72	47.47	148.00	250.00	16.20	37.27	10.14	201.37	15.80
03-Apr-14	96	24.53	1.73	17.93	37.63	83.34	57.10	131.00	240.00	15.57	35.82	9.74	193.52	16.00
07-Apr-14	97	24.53	1.08	17.34	43.65	80.78	76.24	146.00	200.00	15.49	35.33	10.55	198.98	16.80
08-Apr-14	98	24.53	1.08	17.00	42.80	79.20	62.00	152.00	200.00	15.19	34.64	10.35	195.10	16.70
09-Apr-14	99	24.53	1.08	15.74	39.63	73.33	87.31	116.00	180.00	14.06	32.07	9.58	180.63	17.00
10-Apr-14	100	24.53	1.01	18.94	47.68	88.22	40.16	201.00	220.00	16.92	38.59	11.53	217.32	16.90
14-Apr-14	101	24.53	1.01	17.31	45.73	77.50	80.46	178.00	210.00	16.73	36.23	15.24	297.51	18.10
15-Apr-14	102	24.53	1.01	17.00	44.90	76.10	64.00	186.00	210.00	16.42	35.58	14.96	292.13	18.20
16-Apr-14	103	24.53	1.01	14.19	37.47	63.50	45.85	168.00	170.00	13.70	29.69	12.49	243.77	17.70
17-Apr-14	104	24.53	1.01	13.79	36.42	61.72	59.08	144.00	170.00	13.32	28.86	12.14	236.93	17.90
21-Apr-14	105	24.53	1.01	18.35	43.87	107.49	40.30	153.00	200.00	15.46	38.21	8.42	175.56	17.60
22-Apr-14	106	24.53	1.01	17.86	42.70	104.62	26.82	166.00	190.00	15.05	37.19	8.20	170.88	17.80
23-Apr-14	107	24.53	1.01	16.00	38.26	93.74	61.00	112.00	170.00	13.48	33.33	7.35	153.10	17.90
24-Apr-14	108	24.53	1.01	18.64	44.57	109.21	43.58	156.00	200.00	15.71	38.82	8.56	178.36	18.00
29-Apr-14	109	24.53	1.15	17.00	49.30	60.70	60.00	136.00	160.00	13.26	30.20	7.55	170.71	18.50
30-Apr-14	110	24.53	1.15	18.41	53.38	65.73	51.48	164.00	170.00	14.36	32.70	8.18	184.84	18.60
05-May-14	111	24.53	1.15	20.30	45.67	91.35	64.68	218.00	170.00	16.75	37.97	12.64	187.77	19.40
07-May-14	112	24.53	0.87	20.00	44.99	90.01	82.00	194.00	170.00	16.51	37.41	12.45	185.00	19.70
08-May-14	113	24.53	0.87	18.27	41.10	82.22	69.41	188.00	150.00	15.08	34.17	11.37	168.99	19.80
12-May-14	114	24.53	0.72	18.87	40.94	72.26	110.93	94.00	230.00	15.57	37.91	11.38	206.37	20.50
13-May-14	115	24.53	1.01	21.43	46.50	82.07	71.00	163.00	260.00	17.69	43.06	12.93	234.40	20.90
15-May-14	116	24.53	0.87	18.90	41.01	72.38	82.70	123.00	230.00	15.60	37.98	11.40	206.74	21.30
19-May-14	117	24.53	1.15	19.30	41.88	72.24	79.58	137.00	230.00	15.93	34.27	11.14	189.43	21.50
20-May-14	118	24.53	1.15	19.07	41.37	71.37	66.19	145.00	230.00	15.74	33.85	11.01	187.14	21.50
21-May-14	119	24.53	1.15	20.83	45.20	77.97	32.00	200.00	250.00	17.19	36.98	12.02	204.45	21.60
22-May-14	120	24.53	1.01	17.94	38.92	67.13	71.01	124.00	220.00	14.80	31.84	10.35	176.04	21.90
27-May-14	121	24.53	0.79	20.17	43.76	98.08	55.00	169.00	220.00	20.30	36.91	8.57	236.89	22.70
28-May-14	122	24.53	0.79	18.50	40.15	89.99	48.37	149.00	210.00	18.63	33.86	7.86	217.34	22.70
29-May-14	123	24.53	0.79	19.50	42.31	94.84	16.35	193.00	220.00	19.63	35.69	8.28	229.07	22.90
02-Jun-14	124	24.53	0.94	19.47	52.61	91.23	62.70	179.00	180.00	19.60	39.19	7.81	192.92	22.70
03-Jun-14	125	24.53	0.94	18.84	50.90	88.26	74.00	154.00	180.00	18.96	37.92	7.55	186.65	22.80
04-Jun-14	126	24.53	0.94	17.30	46.76	81.09	80.84	134.00	160.00	17.42	34.84	6.94	171.48	23.10
05-Jun-14	127	24.53	0.94	19.60	52.97	91.85	29.58	215.00	180.00	19.73	39.46	7.86	194.24	23.20
09-Jun-14	128	24.53	1.08	19.40	58.76	89.23	65.62	140.00	210.00	19.53	38.81	6.72	200.11	23.50
10-Jun-14	129	24.53	1.15	17.04	51.60	78.36	60.00	125.00	180.00	17.15	34.08	5.90	175.74	23.80
11-Jun-14	130	24.53	1.15	16.97	51.40	78.06	56.57	127.00	180.00	17.09	33.95	5.88	175.05	24.00

Date	Time	Inf Q (m ³ /d)	Q WAS (m ³ /d)	Inf S _U (gCOD/m ³)	Inf S _{Bf} (gCOD/m ³)	Inf S _{Bs} (gCOD/m ³)	Inf C _B (gCOD/m ³)	Inf X _U (gCOD/m ³)	Inf X _B (gCOD/m ³)	Inf X _{OHO,ACT} (gCOD/m ³)	Inf S _{NHx} (gN/m ³)	Inf X _{NB} (gN/m ³)	Inf VSS (gVSS/m ³)	Temp (°C)
12-Jun-14	131	24.53	1.15	20.50	62.08	94.28	18.14	201.00	220.00	20.64	41.01	7.10	211.44	24.10
16-Jun-14	132	24.53	1.15	18.44	55.83	84.79	70.94	124.00	200.00	18.56	37.22	6.38	190.16	24.30
17-Jun-14	133	24.53	1.15	18.67	56.54	85.86	72.93	127.00	200.00	18.79	37.69	6.46	192.56	24.60

Table 45 HRSD pilot reactor state variables

Date	Time	TK105 SO2 (g/m³)	TK106 SO2 (g/m³)	TK107 SO2 (g/m³)	TK107 XTSS (gTSS/m³)	TK107 XVSS (gVSS/m³)	WAS TSS (gTSS/m³)	XTSS target (gTSS/m³)	fr1_Q
03-Sep-13	0	0.02	1.75	2.93	248.48	244.03	2559.45	127.15	0.04
04-Sep-13	1	0.04	1.63	3.20	210.00	174.30	2163.09	91.88	0.04
09-Sep-13	2	0.06	0.45	1.06	2683.50	2320.38	4333.70	87.34	0.04
10-Sep-13	3	0.30	0.46	0.86	2947.45	2799.30	4759.97	72.72	0.04
11-Sep-13	4	0.25	0.33	0.96	2700.00	2349.00	4360.35	76.10	0.04
12-Sep-13	5	0.13	0.32	0.87	3222.40	3061.28	5204.00	80.97	0.04
16-Sep-13	6	0.07	0.60	1.72	2271.72	1667.30	4724.38	75.00	0.04
17-Sep-13	7	0.11	0.37	1.52	2276.09	1673.73	4733.48	68.00	0.04
18-Sep-13	8	0.02	0.21	1.05	2600.00	2184.00	5407.09	67.33	0.04
23-Sep-13	9	0.14	4.19	5.87	1012.24	922.16	1989.90	158.28	0.04
24-Sep-13	10	0.07	3.54	4.92	942.31	799.15	1852.42	145.76	0.04
25-Sep-13	11	0.07	1.55	1.76	1000.00	900.00	1965.84	148.59	0.04
26-Sep-13	12	0.11	0.80	1.10	1159.09	1101.14	2278.59	133.25	0.04
30-Sep-13	13	0.09	1.31	1.75	1317.10	1192.64	3024.68	135.54	0.04
01-Oct-13	14	0.08	1.04	1.47	1231.30	1042.33	2827.65	118.18	0.04
02-Oct-13	15	0.07	1.50	1.70	1280.00	1126.40	2939.48	127.68	0.04
03-Oct-13	16	0.07	1.87	1.87	1331.01	1217.97	3056.63	133.06	0.04
07-Oct-13	17	0.10	1.87	1.77	1220.32	1106.99	2302.81	156.10	0.04
08-Oct-13	18	0.13	2.95	4.48	1031.28	790.60	1946.09	131.25	0.04
09-Oct-13	19	0.10	1.80	1.66	1130.00	949.20	2132.38	131.72	0.04
10-Oct-13	20	0.08	0.66	1.05	1029.18	787.38	1942.13	130.79	0.04
15-Oct-13	21	0.10	0.65	0.68	1307.98	897.87	2353.79	128.97	0.04
16-Oct-13	22	0.07	1.46	1.60	1410.00	1043.40	2537.39	147.33	0.04
17-Oct-13	23	0.06	0.42	2.40	1436.16	1082.48	2584.47	146.36	0.04
21-Oct-13	24	0.27	0.74	1.16	1595.44	1334.06	2201.23	141.64	0.04
22-Oct-13	25	0.06	0.79	0.67	1782.96	1666.08	2459.95	142.43	0.04

Date	Time	TK105 SO2 (g/m ³)	TK106 SO2 (g/m3)	TK107 SO2 (g/m3)	TK107 XTSS (gTSS/m ³)	TK107 XVSS (gVSS/m ³)	WAS TSS (gTSS/m ³)	XTSS target (gTSS/m ³)	fr1_Q
23-Oct-13	26	0.06	0.34	0.34	1660.00	1444.20	2290.30	140.07	0.04
24-Oct-13	27	0.07	0.46	0.46	1733.78	1575.43	2392.09	145.56	0.04
28-Oct-13	28	0.07	1.61	2.06	1601.59	1344.36	2344.47	150.43	0.04
29-Oct-13	29	0.04	0.60	0.59	1752.22	1609.12	2564.97	148.00	0.04
04-Nov-13	30	0.07	0.35	0.32	3044.80	2544.93	5677.87	92.68	0.03
06-Nov-13	31	0.05	0.21	0.22	3060.00	2570.40	5706.21	87.58	0.03
07-Nov-13	32	0.06	0.23	0.19	2989.07	2452.62	5573.95	86.38	0.03
12-Nov-13	33	0.06	0.20	0.19	2482.97	2063.14	5524.16	109.08	0.04
13-Nov-13	34	0.06	0.20	0.27	2540.00	2159.00	5651.04	100.69	0.04
14-Nov-13	35	0.06	0.22	0.27	2482.97	2063.14	5524.16	92.65	0.04
18-Nov-13	36	0.01	0.24	0.15	1939.35	1935.52	4245.15	99.63	0.04
19-Nov-13	37	0.05	0.88	0.58	1710.00	1504.80	3743.12	96.39	0.04
20-Nov-13	38	0.06	0.50	0.32	1710.00	1504.80	3743.12	98.16	0.04
21-Nov-13	39	0.01	0.68	0.57	1935.98	1928.80	4237.77	96.68	0.04
25-Nov-13	40	0.05	1.19	1.25	1962.96	1864.81	6833.13	93.73	0.04
26-Nov-13	41	0.09	1.19	1.24	1932.60	1922.08	6727.46	93.44	0.04
02-Dec-13	42	0.09	3.32	4.90	1051.89	958.94	1978.73	140.89	0.04
03-Dec-13	43	0.47	4.19	6.51	1099.10	1046.95	2067.55	137.56	0.04
04-Dec-13	44	0.05	3.98	5.93	1050.00	955.50	1975.18	131.23	0.04
05-Dec-13	45	0.06	2.77	4.40	1167.09	1108.73	2195.44	140.89	0.03
09-Dec-13	46	0.08	4.44	6.71	3629.89	3448.40	6467.83	139.73	0.03
10-Dec-13	47	0.06	0.51	0.54	2876.61	2758.29	5125.61	99.03	0.03
11-Dec-13	48	0.08	0.23	0.30	2580.00	2218.80	4597.11	95.64	0.04
12-Dec-13	49	0.05	0.30	0.46	2419.93	1952.02	4311.89	111.92	0.04
18-Dec-13	50	0.07	1.37	1.83	2020.00	1858.40	4691.42	122.79	0.04
30-Dec-13	51	0.03	1.18	1.21	2210.98	2100.43	5354.40	86.76	0.04
02-Jan-14	52	0.09	1.01	1.09	2339.53	2222.55	5665.70	92.00	0.04

Date	Time	TK105 SO2 (g/m ³)	TK106 SO2 (g/m3)	TK107 SO2 (g/m3)	TK107 XTSS (gTSS/m ³)	TK107 XVSS (gVSS/m ³)	WAS TSS (gTSS/m ³)	XTSS target (gTSS/m ³)	fr1_Q
06-Jan-14	53	0.02	1.41	1.72	987.21	869.48	4228.29	119.14	0.04
07-Jan-14	54	0.10	1.50	2.35	745.58	495.95	3193.39	108.34	0.04
08-Jan-14	55	0.08	1.42	2.17	1020.00	928.20	4368.74	115.54	0.04
09-Jan-14	56	0.08	0.81	1.12	963.05	827.44	4124.80	123.07	0.04
13-Jan-14	57	0.08	1.18	1.10	1673.36	1296.90	3339.30	103.58	0.04
14-Jan-14	58	0.08	0.92	0.96	1964.21	1786.93	3919.72	108.00	0.04
15-Jan-14	59	0.08	0.57	0.59	1900.00	1672.00	3791.58	107.32	0.04
16-Jan-14	60	0.07	0.85	0.90	2137.97	2117.06	4266.47	108.34	0.04
21-Jan-14	61	3.52	3.48	3.77	2241.07	1933.40	4638.33	85.43	0.04
23-Jan-14	62	0.16	0.13	0.35	2471.99	2352.37	5116.27	80.81	0.03
27-Jan-14	63	0.04	0.01	0.10	2869.48	2726.01	7057.83	79.98	0.03
30-Jan-14	64	0.06	0.03	0.39	2328.14	2086.55	5726.34	67.00	0.04
03-Feb-14	65	0.11	0.08	0.08	2456.53	2333.71	7172.08	97.26	0.04
04-Feb-14	66	0.04	0.08	0.51	2155.73	2047.95	6293.87	79.54	0.04
05-Feb-14	67	0.10	0.08	0.02	1880.00	1673.20	5488.84	72.94	0.04
06-Feb-14	68	0.07	0.17	0.44	2402.22	2282.11	7013.52	75.72	0.04
10-Feb-14	69	0.05	0.03	0.01	2303.17	1828.48	8801.69	70.75	0.04
11-Feb-14	70	0.02	0.06	0.11	1929.93	1283.87	7375.33	58.54	0.04
12-Feb-14	71	0.02	0.03	0.11	2640.00	2402.40	10088.90	57.98	0.04
13-Feb-14	72	0.03	0.07	1.72	2230.34	1714.67	8523.38	52.71	0.04
17-Feb-14	73	0.13	0.13	0.13	2511.52	2385.94	8253.16	66.91	0.04
18-Feb-14	74	0.18	0.11	0.11	2022.65	1647.07	6646.67	62.39	0.04
19-Feb-14	75	1.05	0.12	0.12	2310.00	2148.30	7590.94	64.05	0.04
20-Feb-14	76	0.11	0.11	0.11	2354.78	2232.40	7738.10	68.34	0.04
24-Feb-14	77	0.12	0.11	0.11	1892.74	1831.49	5986.21	53.18	0.04
25-Feb-14	78	0.14	0.14	0.14	1674.09	1432.78	5294.66	48.54	0.04
26-Feb-14	79	0.42	0.45	0.45	1780.00	1619.80	5629.63	55.50	0.04

Date	Time	TK105 SO2 (g/m ³)	TK106 SO2 (g/m3)	TK107 SO2 (g/m3)	TK107 XTSS (gTSS/m ³)	TK107 XVSS (gVSS/m ³)	WAS TSS (gTSS/m ³)	XTSS target (gTSS/m ³)	fr1_Q
27-Feb-14	80	2.21	2.21	2.21	2781.04	2641.98	8795.62	99.21	0.04
06-Mar-14	81	1.71	1.71	1.71	2736.66	2709.54	5022.77	78.28	0.04
10-Mar-14	82	2.13	2.13	2.13	3264.94	2925.57	6276.51	49.86	0.04
11-Mar-14	83	1.80	1.80	1.80	3201.65	2813.24	6154.84	48.77	0.04
12-Mar-14	84	2.21	2.21	2.21	3170.00	2757.90	6094.00	46.59	0.04
13-Mar-14	85	2.52	2.52	2.52	3154.18	2730.44	6063.58	48.22	0.04
17-Mar-14	86	2.19	2.19	2.19	2403.31	2162.89	4960.32	53.12	0.05
18-Mar-14	87	3.85	3.85	3.85	2323.35	2021.35	4795.28	43.90	0.05
19-Mar-14	88	3.82	3.82	3.82	2350.00	2068.00	4850.30	51.53	0.05
24-Mar-14	89	0.82	0.82	0.82	2583.13	2453.97	4850.36	60.68	0.06
25-Mar-14	90	0.45	0.45	0.45	2370.04	2226.13	4450.25	49.37	0.06
26-Mar-14	91	0.19	0.26	0.23	2170.00	1866.20	4074.63	40.11	0.06
27-Mar-14	92	0.90	0.90	0.90	2335.25	2161.25	4384.92	47.57	0.06
31-Mar-14	93	0.35	0.39	1.07	2498.14	1878.68	3815.07	53.99	0.07
01-Apr-14	94	0.24	0.27	0.58	2679.37	2161.16	4091.85	52.78	0.07
02-Apr-14	95	0.12	0.15	0.25	2890.00	2514.30	4413.51	49.46	0.07
03-Apr-14	96	0.25	0.31	0.89	2777.34	2322.09	4241.46	51.27	0.07
07-Apr-14	97	0.09	0.19	0.22	2225.16	2181.52	4220.49	73.49	0.04
08-Apr-14	98	0.09	0.40	0.42	2181.76	2097.26	4138.17	64.95	0.04
09-Apr-14	99	0.09	0.27	0.30	2020.00	1797.80	3831.36	59.55	0.04
10-Apr-14	100	0.09	0.23	0.33	2430.31	2308.80	4609.61	56.63	0.04
14-Apr-14	101	0.09	0.13	0.18	2947.83	2800.44	5559.54	110.22	0.04
15-Apr-14	102	0.08	0.11	0.14	2894.59	2876.30	5459.12	106.84	0.04
16-Apr-14	103	0.10	0.22	0.28	2415.38	2002.77	4555.35	86.22	0.04
17-Apr-14	104	0.10	0.22	1.53	2347.62	1891.97	4427.54	83.98	0.04
21-Apr-14	105	0.09	0.19	0.23	2166.39	1972.23	4589.64	86.74	0.04
22-Apr-14	106	0.10	0.20	0.19	2108.67	1868.53	4467.36	80.05	0.04

Date	Time	TK105 SO2 (g/m ³)	TK106 SO2 (g/m3)	TK107 SO2 (g/m3)	TK107 XTSS (gTSS/m ³)	TK107 XVSS (gVSS/m ³)	WAS TSS (gTSS/m ³)	XTSS target (gTSS/m ³)	fr1_Q
23-Apr-14	107	0.09	0.17	0.18	1889.34	1500.04	4002.69	79.77	0.04
24-Apr-14	108	0.11	0.15	0.17	2201.02	2035.78	4663.01	82.00	0.04
29-Apr-14	109	0.11	1.68	2.96	1647.88	1379.99	3044.83	76.53	0.05
30-Apr-14	110	0.09	0.35	0.38	1784.34	1618.03	3296.99	70.02	0.05
05-May-14	111	0.14	1.11	1.52	2455.64	2332.86	5081.56	91.43	0.05
07-May-14	112	0.12	2.20	3.52	2419.41	2397.95	5006.58	98.42	0.04
08-May-14	113	0.14	2.30	3.20	2210.08	2000.95	4573.40	99.54	0.04
12-May-14	114	0.10	0.33	0.34	1825.85	1603.07	4438.45	134.34	0.03
13-May-14	115	0.14	2.10	3.67	2073.80	2068.03	5041.20	125.74	0.04
15-May-14	116	0.14	2.22	3.77	1829.07	1608.73	4446.28	120.33	0.04
19-May-14	117	2.19	2.19	3.03	2266.89	2141.73	4169.91	137.75	0.05
20-May-14	118	6.04	6.81	7.15	2239.53	2090.34	4119.59	119.34	0.05
21-May-14	119	5.52	6.13	6.26	2446.67	2324.34	4500.63	117.57	0.05
22-May-14	120	4.29	4.42	4.08	2106.64	1849.63	3875.14	106.59	0.04
27-May-14	121	1.79	1.23	0.36	3287.68	2975.41	7783.57	99.77	0.03
28-May-14	122	1.65	1.48	1.78	3016.42	2504.67	7141.37	93.05	0.03
29-May-14	123	1.12	0.91	2.56	3179.17	2782.25	7526.69	85.62	0.03
02-Jun-14	124	0.17	0.11	0.80	3396.42	3029.56	6936.97	101.74	0.04
03-Jun-14	125	0.17	0.11	0.80	3286.11	2835.96	6711.67	98.77	0.04
04-Jun-14	126	0.17	0.11	0.79	3019.04	2393.72	6166.20	93.15	0.04
05-Jun-14	127	0.21	0.21	0.24	3419.65	3071.13	6984.41	86.22	0.04
09-Jun-14	128	1.58	1.93	1.41	1981.29	1882.22	3094.75	98.00	0.04
10-Jun-14	129	3.18	4.17	4.31	1740.00	1600.80	2717.86	98.00	0.05
11-Jun-14	130	3.72	4.91	4.84	1733.20	1588.32	2707.25	101.53	0.05
12-Jun-14	131	3.26	4.13	4.20	2093.44	1988.77	3269.93	100.89	0.05
16-Jun-14	132	3.01	3.75	3.80	1882.73	1874.20	2612.62	98.00	0.05
17-Jun-14	133	2.33	2.68	2.41	1906.52	1811.20	2645.64	95.11	0.05

Table 46 HRS D pilot effluent state variables

Date	Time	Eff SU (gCOD/m ³)	Eff S _{Br} (gCOD/m ³)	Eff S _{Bs} (gCOD/m ³)	Eff C _B (gCOD/m ³)	Eff X _U (gCOD/m ³)	Eff X _B (gCOD/m ³)	Eff TSS (gTSS/m ³)	Eff TVSS (gVSS/m ³)	Eff VSS (gVSS/m ³)	Eff Filtered COD (gCOD/m ³)
03-Sep-13	0	38.22	39.00	25.18	84.60	136.00	70.00	127.15	120.79	134.22	137.00
04-Sep-13	1	32.30	28.18	13.52	57.00	103.00	50.00	91.88	88.59	96.99	99.00
09-Sep-13	2	30.77	1.04	41.44	45.74	54.00	60.00	87.34	82.79	84.53	91.28
10-Sep-13	3	33.80	0.87	26.33	45.00	38.00	50.00	72.72	57.40	70.38	76.00
11-Sep-13	4	30.96	0.91	31.96	43.17	46.00	50.00	76.10	62.85	73.65	79.53
12-Sep-13	5	36.95	0.97	30.00	34.08	64.00	50.00	80.97	71.15	78.36	84.62
16-Sep-13	6	27.35	1.30	24.29	72.06	20.00	80.00	75.00	69.49	72.69	70.59
17-Sep-13	7	27.40	1.18	19.42	55.00	31.00	70.00	68.00	57.12	65.91	64.00
18-Sep-13	8	31.30	1.17	15.06	82.47	2.00	70.00	67.33	56.01	65.26	63.37
23-Sep-13	9	30.51	2.27	67.12	106.10	86.00	100.00	158.28	150.37	134.55	128.13
24-Sep-13	10	28.40	2.09	61.51	76.00	103.00	90.00	145.76	138.48	123.91	118.00
25-Sep-13	11	30.14	2.13	61.51	67.22	117.00	90.00	148.59	141.16	126.31	120.29
26-Sep-13	12	34.94	1.91	47.26	39.90	126.00	80.00	133.25	126.58	113.27	107.87
30-Sep-13	13	32.73	0.57	29.77	75.92	69.00	120.00	135.54	128.76	100.25	81.43
01-Oct-13	14	30.60	0.50	23.90	68.00	63.00	100.00	118.18	94.71	87.41	71.00
02-Oct-13	15	31.81	0.54	27.07	77.58	62.00	110.00	127.68	110.55	94.44	76.71
03-Oct-13	16	33.08	0.56	28.28	83.08	57.00	120.00	133.06	126.40	98.42	79.94
07-Oct-13	17	33.48	1.25	16.41	78.86	43.00	160.00	156.10	148.29	126.20	59.46
08-Oct-13	18	28.29	1.05	13.66	66.00	31.00	140.00	131.25	106.50	106.11	50.00
09-Oct-13	19	31.00	1.05	11.10	73.85	24.00	140.00	131.72	107.27	106.49	50.18
10-Oct-13	20	28.24	1.05	13.56	65.15	31.00	140.00	130.79	105.74	105.73	49.82
15-Oct-13	21	21.70	0.83	18.47	69.00	37.00	120.00	128.97	98.83	98.19	47.68
16-Oct-13	22	23.39	0.95	22.50	66.16	52.00	140.00	147.33	128.96	112.17	54.46
17-Oct-13	23	23.83	0.94	21.76	63.47	53.00	140.00	146.36	127.28	111.43	54.11
21-Oct-13	24	22.46	13.13	35.02	99.39	81.00	110.00	141.64	134.56	134.27	85.53
22-Oct-13	25	25.10	13.20	32.70	76.00	106.00	110.00	142.43	135.30	135.02	86.00

Date	Time	Eff SU (gCOD/m3)	Eff S _{Bf} (gCOD/m3)	Eff S _{Bs} (gCOD/m3)	Eff C _B (gCOD/m3)	Eff X _U (gCOD/m3)	Eff X _B (gCOD/m3)	Eff TSS (gTSS/m3)	Eff TVSS (gVSS/m3)	Eff VSS (gVSS/m3)	Eff Filtered COD (gCOD/m3)
23-Oct-13	26	23.37	12.98	33.48	70.17	107.00	110.00	140.07	133.07	132.79	84.58
24-Oct-13	27	24.41	13.49	34.67	72.44	106.00	120.00	145.56	138.29	137.99	87.90
28-Oct-13	28	15.45	19.31	44.52	106.72	86.00	100.00	150.43	142.90	121.15	99.61
29-Oct-13	29	16.90	19.00	42.10	77.00	111.00	100.00	148.00	140.60	119.20	98.00
04-Nov-13	30	17.82	0.71	32.63	67.84	80.00	110.00	92.68	82.04	109.01	62.41
06-Nov-13	31	17.91	0.67	29.77	92.66	51.00	100.00	87.58	73.26	103.01	58.98
07-Nov-13	32	17.49	0.66	29.53	85.32	55.00	100.00	86.38	71.27	101.60	58.17
12-Nov-13	33	23.66	6.13	27.63	107.58	87.00	60.00	109.08	93.39	77.21	73.67
13-Nov-13	34	24.20	5.66	23.14	84.00	91.00	60.00	100.69	79.58	71.27	68.00
14-Nov-13	35	23.66	5.21	19.90	90.23	76.00	50.00	92.65	67.37	65.58	62.57
18-Nov-13	36	24.03	0.80	27.89	124.28	81.00	80.00	99.63	94.65	116.96	78.56
19-Nov-13	37	21.19	0.77	29.04	107.00	99.00	70.00	96.39	91.57	113.16	76.00
20-Nov-13	38	21.19	0.78	29.96	102.06	109.00	70.00	98.16	93.25	115.23	77.39
21-Nov-13	39	23.99	0.77	26.39	143.84	63.00	70.00	96.68	91.85	113.50	76.23
25-Nov-13	40	24.33	0.75	24.52	123.40	75.00	70.00	93.73	89.05	110.04	73.91
26-Nov-13	41	23.95	0.75	24.74	102.56	95.00	70.00	93.44	88.77	109.70	73.68
02-Dec-13	42	21.44	36.15	48.93	132.48	144.00	40.00	140.89	133.84	137.73	100.37
03-Dec-13	43	22.40	35.30	46.30	85.00	184.00	40.00	137.56	130.68	134.48	98.00
04-Dec-13	44	21.40	33.68	44.14	108.78	156.00	30.00	131.23	124.67	128.29	93.49
05-Dec-13	45	23.79	36.15	46.58	95.48	181.00	40.00	140.89	133.84	137.73	100.37
09-Dec-13	46	23.98	0.70	28.94	142.38	66.00	150.00	139.73	132.74	146.49	97.76
10-Dec-13	47	19.00	0.50	18.50	93.00	51.00	110.00	99.03	77.79	103.82	69.29
11-Dec-13	48	17.04	0.48	19.18	85.30	50.00	110.00	95.64	72.55	100.27	66.92
12-Dec-13	49	15.98	0.56	26.40	102.05	65.00	120.00	111.92	106.32	117.34	78.31
18-Dec-13	50	12.69	4.87	48.57	86.87	86.00	120.00	122.79	116.65	114.41	86.08
30-Dec-13	51	13.89	4.72	45.49	103.89	60.00	120.00	86.76	82.43	117.78	83.44
02-Jan-14	52	14.70	5.01	48.27	114.03	67.00	120.00	92.00	87.40	124.89	88.47
06-Jan-14	53	13.20	12.98	47.50	116.32	54.00	120.00	119.14	113.18	129.99	92.37

Date	Time	Eff SU (gCOD/m3)	Eff S _{Bf} (gCOD/m3)	Eff S _{Bs} (gCOD/m3)	Eff C _B (gCOD/m3)	Eff X _U (gCOD/m3)	Eff X _B (gCOD/m3)	Eff TSS (gTSS/m3)	Eff TVSS (gVSS/m3)	Eff VSS (gVSS/m3)	Eff Filtered COD (gCOD/m3)
07-Jan-14	54	9.97	11.80	45.23	94.00	60.00	110.00	108.34	102.92	118.21	84.00
08-Jan-14	55	13.64	12.58	45.23	94.55	67.00	120.00	115.54	109.76	126.06	89.58
09-Jan-14	56	12.88	13.40	49.83	81.89	98.00	120.00	123.07	116.92	134.28	95.42
13-Jan-14	57	10.22	0.83	31.14	128.80	44.00	90.00	103.58	88.42	108.92	58.51
14-Jan-14	58	12.00	0.87	31.13	103.00	71.00	100.00	108.00	102.60	113.56	61.00
15-Jan-14	59	11.61	0.86	31.25	93.28	79.00	100.00	107.32	101.95	112.85	60.62
16-Jan-14	60	13.06	0.87	30.20	80.86	94.00	100.00	108.34	102.92	113.92	61.19
21-Jan-14	61	13.66	0.69	21.48	79.16	104.00	40.00	85.43	76.82	72.70	49.68
23-Jan-14	62	15.07	0.65	18.18	72.10	109.00	30.00	80.81	68.74	68.77	47.00
27-Jan-14	63	17.49	0.71	18.47	121.33	57.00	50.00	79.98	91.65	109.68	50.83
30-Jan-14	64	14.19	0.59	15.93	93.28	58.00	40.00	67.00	64.32	91.88	42.58
03-Feb-14	65	22.11	0.84	22.29	84.76	90.00	60.00	97.26	107.91	121.63	61.14
04-Feb-14	66	19.40	0.69	16.91	81.00	61.00	50.00	79.54	72.18	99.48	50.00
05-Feb-14	67	16.92	0.63	16.38	63.07	73.00	40.00	72.94	60.70	91.22	45.85
06-Feb-14	68	21.62	0.66	12.95	64.78	68.00	50.00	75.72	65.41	94.70	47.60
10-Feb-14	69	25.54	1.18	44.58	89.70	64.00	30.00	70.75	82.20	110.43	76.14
11-Feb-14	70	21.40	0.98	36.62	81.00	41.00	30.00	58.54	56.28	91.38	63.00
12-Feb-14	71	29.27	0.97	28.20	61.56	59.00	30.00	57.98	55.22	90.51	62.40
13-Feb-14	72	24.73	0.88	27.51	52.87	54.00	30.00	52.71	45.63	82.28	56.73
17-Feb-14	73	23.96	0.82	24.56	83.66	108.00	40.00	66.91	60.27	106.69	70.79
18-Feb-14	74	19.30	0.76	25.94	101.00	85.00	30.00	62.39	52.39	99.48	66.00
19-Feb-14	75	22.04	0.78	24.41	117.77	64.00	40.00	64.05	55.23	102.14	67.76
20-Feb-14	76	22.47	0.83	27.09	119.61	77.00	40.00	68.34	62.87	108.97	72.30
24-Feb-14	77	23.06	0.70	28.82	129.41	63.00	30.00	53.18	40.05	80.22	77.79
25-Feb-14	78	20.40	0.64	26.96	114.00	59.00	30.00	48.54	33.37	73.22	71.00
26-Feb-14	79	21.69	0.73	32.46	109.12	93.00	30.00	55.50	43.62	83.72	81.18
27-Feb-14	80	33.89	1.31	62.91	200.90	164.00	50.00	99.21	94.24	149.65	145.11
06-Mar-14	81	30.48	0.73	48.14	46.65	109.00	40.00	78.28	76.79	80.99	77.79

Date	Time	Eff SU (gCOD/m3)	Eff S _{Bf} (gCOD/m3)	Eff S _{Bs} (gCOD/m3)	Eff C _B (gCOD/m3)	Eff X _U (gCOD/m3)	Eff X _B (gCOD/m3)	Eff TSS (gTSS/m3)	Eff TVSS (gVSS/m3)	Eff VSS (gVSS/m3)	Eff Filtered COD (gCOD/m3)
10-Mar-14	82	15.09	1.00	20.71	64.20	42.00	40.00	49.86	45.88	64.62	52.14
11-Mar-14	83	14.80	0.98	20.22	58.00	45.00	40.00	48.77	43.90	63.21	51.00
12-Mar-14	84	14.65	0.94	18.80	60.61	36.00	40.00	46.59	40.06	60.38	48.72
13-Mar-14	85	14.58	0.97	20.05	57.40	44.00	40.00	48.22	42.92	62.50	50.43
17-Mar-14	86	17.38	1.17	23.80	58.64	6.00	60.00	53.12	47.13	52.88	54.46
18-Mar-14	87	16.80	0.97	17.23	52.00	1.00	50.00	43.90	32.18	43.70	45.00
19-Mar-14	88	16.99	1.14	22.96	38.91	22.00	60.00	51.53	44.35	51.29	52.83
24-Mar-14	89	19.84	0.81	30.98	65.38	59.00	60.00	60.68	64.26	78.32	60.23
25-Mar-14	90	18.20	0.66	23.14	73.00	27.00	50.00	49.37	42.53	63.72	49.00
26-Mar-14	91	16.66	0.54	16.92	61.88	20.00	40.00	40.11	28.08	51.77	39.81
27-Mar-14	92	17.93	0.64	21.90	68.53	26.00	50.00	47.57	39.49	61.40	47.21
31-Mar-14	93	16.13	0.90	25.93	69.04	37.00	30.00	53.99	47.92	61.09	51.14
01-Apr-14	94	17.30	0.88	23.82	59.00	54.00	20.00	52.78	45.80	59.73	50.00
02-Apr-14	95	18.66	0.82	19.88	41.64	63.00	20.00	49.46	40.22	55.97	46.86
03-Apr-14	96	17.93	0.85	22.01	53.20	56.00	20.00	51.27	43.22	58.02	48.57
07-Apr-14	97	17.34	1.03	35.94	81.69	121.00	70.00	73.49	69.81	115.37	67.89
08-Apr-14	98	17.00	0.91	30.09	84.00	97.00	60.00	64.95	61.90	101.96	60.00
09-Apr-14	99	15.74	0.83	27.44	97.99	63.00	60.00	59.55	52.05	93.49	55.02
10-Apr-14	100	18.94	0.79	22.12	92.15	68.00	50.00	56.63	47.07	88.91	52.32
14-Apr-14	101	17.31	6.32	40.32	114.04	66.00	50.00	110.22	107.32	143.62	70.15
15-Apr-14	102	17.00	6.13	38.87	98.00	75.00	50.00	106.84	100.85	139.23	68.00
16-Apr-14	103	14.19	4.95	30.90	58.96	81.00	40.00	86.22	65.68	112.36	54.88
17-Apr-14	104	13.79	4.82	30.12	64.27	71.00	40.00	83.98	62.30	109.43	53.45
21-Apr-14	105	18.35	1.39	36.81	102.45	92.00	60.00	86.74	84.02	96.98	80.47
22-Apr-14	106	17.86	1.28	33.04	92.82	92.00	50.00	80.05	71.56	89.49	74.26
23-Apr-14	107	16.00	1.28	34.72	97.00	87.00	50.00	79.77	71.06	89.18	74.00
24-Apr-14	108	18.64	1.31	33.50	106.55	84.00	50.00	82.00	75.09	91.68	76.07
29-Apr-14	109	17.00	2.17	19.83	92.00	56.00	60.00	76.53	56.86	87.30	45.00

Date	Time	Eff SU (gCOD/m3)	Eff S _{Bf} (gCOD/m3)	Eff S _{Bs} (gCOD/m3)	Eff C _B (gCOD/m3)	Eff X _U (gCOD/m3)	Eff X _B (gCOD/m3)	Eff TSS (gTSS/m3)	Eff TVSS (gVSS/m3)	Eff VSS (gVSS/m3)	Eff Filtered COD (gCOD/m3)
30-Apr-14	110	18.41	1.99	15.29	85.32	45.00	60.00	70.02	47.60	79.87	41.17
05-May-14	111	20.30	2.08	49.15	89.47	86.00	80.00	91.43	86.86	100.66	89.18
07-May-14	112	20.00	2.24	54.76	116.00	79.00	80.00	98.42	93.50	108.35	96.00
08-May-14	113	18.27	2.26	57.34	92.13	96.00	90.00	99.54	94.57	109.58	97.09
12-May-14	114	18.87	20.62	45.87	95.64	131.00	110.00	134.34	127.62	153.60	102.24
13-May-14	115	21.43	19.30	39.17	96.10	119.00	100.00	125.74	119.46	143.77	95.70
15-May-14	116	18.90	18.47	39.09	78.54	123.00	100.00	120.33	114.32	137.58	91.58
19-May-14	117	19.30	19.01	28.01	93.68	109.00	120.00	137.75	130.87	127.05	81.67
20-May-14	118	19.07	16.47	21.92	86.55	93.00	100.00	119.34	113.37	110.06	70.75
21-May-14	119	20.83	16.22	19.55	71.40	104.00	100.00	117.57	111.69	108.43	69.70
22-May-14	120	17.94	14.71	18.67	67.68	92.00	90.00	106.59	84.70	98.31	63.19
27-May-14	121	20.17	13.78	12.65	84.40	81.00	70.00	99.77	91.65	110.23	59.40
28-May-14	122	18.50	12.85	12.11	72.54	77.00	70.00	93.05	79.71	102.81	55.40
29-May-14	123	19.50	11.82	8.66	62.01	80.00	60.00	85.62	67.49	94.60	50.97
02-Jun-14	124	19.47	0.91	23.20	96.43	98.00	70.00	101.74	90.62	101.57	50.47
03-Jun-14	125	18.84	0.88	22.58	102.70	94.00	60.00	98.77	85.41	98.60	49.00
04-Jun-14	126	17.30	0.83	21.76	93.11	89.00	60.00	93.15	75.97	93.00	46.21
05-Jun-14	127	19.60	0.77	16.56	88.08	76.00	60.00	86.22	65.08	86.07	42.77
09-Jun-14	128	19.40	1.37	33.13	108.10	63.00	80.00	98.00	84.28	104.69	70.10
10-Jun-14	129	17.04	1.37	35.49	89.10	82.00	80.00	98.00	84.28	104.69	70.10
11-Jun-14	130	16.97	1.42	37.45	90.16	90.00	80.00	101.53	96.46	108.46	72.63
12-Jun-14	131	20.50	1.41	33.58	70.51	108.00	80.00	100.89	95.85	107.78	72.17
16-Jun-14	132	18.44	1.37	34.09	91.10	80.00	80.00	98.00	84.28	104.69	70.10
17-Jun-14	133	18.67	1.33	32.31	74.69	89.00	80.00	95.11	79.38	101.60	68.03

APPENDIX E: HYDROLYSIS

Hydrolysis

Bacteria can only utilize low molecular weight organic compounds. Many high molecular weight, colloidal and particulate substrates, which are typically present in domestic wastewater, cannot be utilized directly by microorganisms. These substrates must be made available through external enzymatic reactions that produce low molecular weight compounds that can be transported across the cell membrane. These reactions are referred to as hydrolysis (Henze et al., 2000).

Lysis Regrowth

The HRAS model incorporates the Lysis-regrowth concept to depict the loss of viability and biomass in biochemical operations. Based on the assumption that only active, viable biomass is present; it is viewed as continually undergoing death and lysis, yielding particulate substrate (X_B) and biomass debris. Once converted to X_B , it enters the hydrolysis cycle where it is converted to S_{Bs} and available as substrate for growth. This process is illustrated in Figure 48 for the HRAS model.

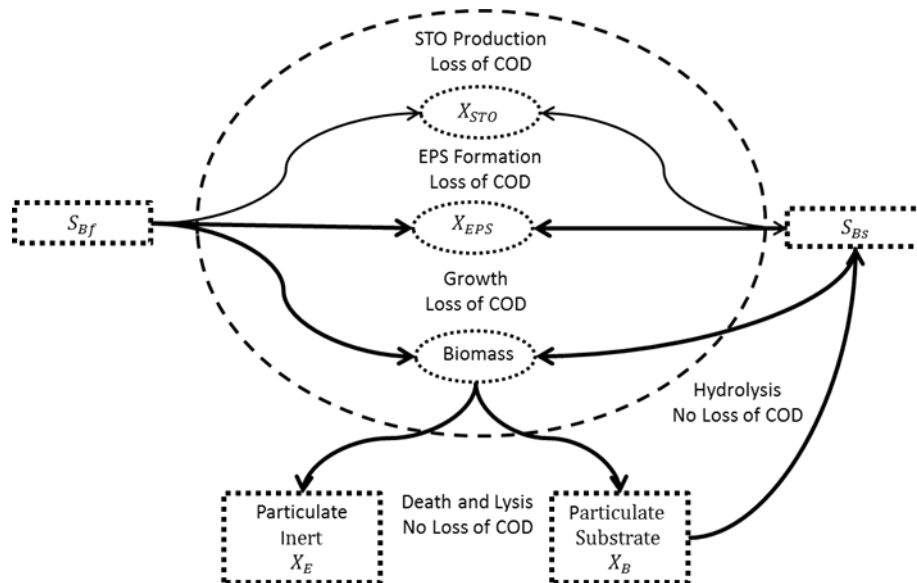


Figure 48: Schematic representation of the lysis: regrowth approach to modeling biomass decay

The A-stage model includes several hydrolysis processes shown in Table 23 including;

- Hydrolysis of entrapped organics to form slowly biodegradable substrate ($X_B \rightarrow S_{Bs}$)
- Hydrolysis of storage products to readily biodegradable substrate ($X_{STO} \rightarrow S_{Bf}$)
- Hydrolysis of EPS to readily biodegradable substrate ($X_{EPS} \rightarrow S_{Bf}$)

These processes play a significant role in the calibration of the model and ultimately the ability of the model to effectively predict system performance over a wide range of operating conditions.

APPENDIX F: PARTIAL PETERSON MATRIX

Table 47 Partial Peterson matrix processes and stoichiometric coefficients for the HRAS model

Name	S_{Bf}	S_{Bs}	C_B	C_U	X_B	X_U	$X_{OHO, ACT}$	X_{EPS}	X_{STO}
r1 Aerobic growth of X_{OHOs} – Fast	$-1/(Y_{OHO,AER}*(1-k_{EPS,PC}-k_{STO,PC}))$						1	$k_{EPS,PC}/(Y_{OHO,AER}*(1-k_{EPS,PC}-k_{STO,PC}))$	$k_{STO,PC}/(Y_{OHO,AER}*(1-k_{EPS,PC}-k_{STO,PC}))$
r2 Aerobic growth of X_{OHOs} – Slow		$-1/(Y_{OHO,AER}*(1-k_{EPS,PC}-k_{STO,PC}))$					1	$k_{EPS,PC}/(Y_{OHO,AER}*(1-k_{EPS,PC}-k_{STO,PC}))$	$k_{STO,PC}/(Y_{OHO,AER}*(1-k_{EPS,PC}-k_{STO,PC}))$
r3 Decay of heterotrophs					$1-f_U$		-1		
r4 Hydrolysis of entrapped organics		1			-1				
r5 flocculation of colloidal substrate			-1		1				
r6 flocculation of colloidal inerts				-1		1			
r7 Hydrolysis of storage products		1							-1
r8 EPS hydrolysis		1						-1	

Table 48 Partial Peterson matrix process rate equations for the HRAS model

Name	Rate expression (r_j)
r1 Aerobic growth of heterotrophs - Fast	$\mu_{OHO,Max} * (S_{Bf}/(K_{Bf}+S_{Bf})) * (S_{O_2}/(K_{O_2,OHO}+S_{O_2})) * (S_{NH_4}/(K_{NH_4,nut}+S_{NH_4})) * X_{OHO}$
r2a Aerobic growth of heterotrophs - Slow	$\mu_{OHO,Slow,Max} * (S_{Bs}/(K_{Bs}+S_{Bs})) * (K_{Bf}/(K_{Bf}+S_{Bf})) * (S_{O_2}/(K_{O_2,OHO}+S_{O_2})) * (S_{NH_4}/(K_{NH_4,nut}+S_{NH_4})) * X_{OHO}$
r2b Aerobic growth of heterotrophs - Slow	$\mu_{OHO,max} * (S_{Bs}/(K_{Bs}+S_{Bs})) * (S_{O_2}/(K_{O_2,OHO}+S_{O_2})) * (S_{NH_4}/(K_{NH_4,nut}+S_{NH_4})) * X_{OHO}$
r3 Decay of heterotrophs	$b_{OHO} * X_{OHO,ACT}$
r4 Hydrolysis of entrapped organics	$q_{XB,HYD} * ((X_B/X_{OHO})/(K_{B,HYD}+X_B/X_{OHO})) * ((S_{O_2}/(K_{O_2,OHO}+S_{O_2})) + \eta_{HYD} * (K_{O_2,OHO}/(K_{O_2,OHO}+S_{O_2})) * (S_{NO_3}/(K_{NO_3}+S_{NO_3}))) * X_O$ H_O
r5 flocculation of colloidal substrate	$q_{ADS} * C_B * (X_{OHO}+X_{ANO}) * (K_{SL}/((C_B/(X_{OHO}+X_{ANO}))+K_{SL})) * (X_{EPS}/(K_{EPS}+X_{EPS}))$
r6 flocculation of colloidal inerts	$q_{ADS} * C_U * (X_{OHO}+X_{ANO}) * (K_{SL}/((C_U/(X_{OHO}+X_{ANO}))+K_{SL})) * (X_{EPS}/(K_{EPS}+X_{EPS}))$
r7 Hydrolysis of storage products	$q_{STO,HYD} * (X_{STO}/X_{OHO}/(K_{STO,HYD}+X_{STO}/X_{OHO})) * (K_{Bf}/(K_{Bf}+S_{Bf})) * (K_{Bs}/(K_{Bs}+S_{Bs})) * (S_{O_2}/(K_{O_2,OHO}+S_{O_2})) * X_{OHO}$
r8 EPS hydrolysis	$q_{EPA,HYD} * X_{EPS}$

r2a corresponds to the Diauxic model, r2b corresponds to the Dual Substrate model

Table 49 Partial list of default parameter values for the mass-balance equations

Symbol	Name	Value	Unit
$K_{B,HYD}$	Saturation coefficient for X_B/X_{OHO}	0.03	$g X_B/g X_{OHO}$
$\mu_{OHO,Max}$	Maximum growth rate of X_{OHO} on S_{Bf}	7.0	d^{-1}
$\mu_{OHO,Slow,Max}^1$	Maximum growth rate of X_{OHO} on S_{Bs}	3.0	d^{-1}
K_{Bf}	Half-saturation coefficient for $S_{Bf}(X_{OHO})$	5.0	$g S_{Bf}.m^{-3}$
K_{Bs}	Half-saturation coefficient for $S_{Bs}(X_{OHO})$	40	$g S_{Bs}.m^{-3}$
b_{OHO}	Decay rate for X_{OHO}	0.62	d^{-1}
$K_{O,OHO}$	Half-saturation coefficient for $S_{O_2}(X_{OHO})$	0.1	$g S_{O_2}.m^{-3}$
q_{ADS}	Rate constant for adsorption	0.07	d^{-1}
K_{SL}	Half-saturation coefficient for surface limitation	0.002	-
q_{STO}	Rate constant for growth on $X_{STO}(X_{OHO})$	2.0	d^{-1}
$k_{EPS,MAX}$	EPS formation coefficient	0.25	$g COD_{EPS}.gVSS^{-1}$
$q_{EPS,HYD}$	EPS hydrolysis	0.12	d^{-1}
K_{EPS}	Half-saturation coefficient for EPS (X_{OHO})	50	$gX_{EPS}.m^{-3}$
$q_{XB,HYD}$	Particulate COD Hydrolysis Rate Constant	3.5	d^{-1}
$k_{STO,MAX}$	Maximum Production Yield for Storage Polymers	.65	$g X_{STO}.gS_{Bf}^{-1}$
$f_{Shunt,Max}$	Fraction of X_{STO} in the Active Biomass	.30	-
$q_{STO,HYD}$	Storage Hydrolysis Rate Constant	3.0	d^{-1}
$K_{STO,HYD}$	Hydrolysis Half-saturation coefficient for $X_{STO}(X_{OHO})$	0.15	$gX_{STO}.gX_{OHO}^{-1}$
$K_{O_2,EPS}$	Half-saturation coefficient for S_{O_2}	1.5	$g S_{O_2}.m^{-3}$
$K_{O_2,STO}$	Half-saturation coefficient STO for S_{O_2}	1.0	$gS_{O_2}.m^{-3}$
$K_{EPS,HYD}$	Saturation Coefficient X_{EPS}	0.05	$gX_{EPS}.gX_{OHO}^{-1}$

APPENDIX G: STOICHIOMETRY TABLES

Table 50 Stoichiometry dataset

Date	COD Mass Balance	OUR (mg/L·hr)	CO ₂ _PR (mg/L·hr)	CO ₂ :O ₂ Ratio	Aerobic SRT (d)	Temp (°C)	f _{CV} Calculated (gCOD/gVSS)	Influent Biomass (gCOD/m ³)
9/16/2013	89%	247.8	240.8	0.98	0.1	26.7	1.79	20.02
9/17/2013	91%	224.49	241.7	1.08	0.1	26.5	2.02	20.06
9/18/2013	86%	250.63	228.59	1.07	0.12	26.5	1.97	22.91
9/23/2013	74%	67.14	92.97	1.38	0.05	26	2.79	22.33
9/24/2013	75%	75.26	97.18	1.31	0.05	26	2.99	20.79
9/25/2013	96%	127.11	129.02	1.05	0.05	25.7	2.8	22.06
9/26/2013	84%	189.31	164.32	0.87	0.07	25.7	3.89	25.57
9/30/2013	102%	199.96	171.76	0.92	0.06	25.5	1.66	21.91
10/1/2013	95%	188.38	175.62	0.94	0.06	25.3	1.97	20.48
10/2/2013	86%	184	164.44	0.9	0.06	25.2	1.83	21.29
10/3/2013	94%	186.48	156.26	0.84	0.06	25.2	1.65	22.14
10/15/2013	94%	171.08	149.15	0.9	0.06	24.3	2.64	19.29
10/16/2013	82%	150.83	137.35	0.92	0.06	24.1	2.38	20.79
10/17/2013	78%	164.62	143.76	0.88	0.06	24.2	2.38	21.18
10/21/2013	89%	104.56	98.97	1.18	0.07	24.3	1.71	20.02
10/22/2013	79%	96.53	102.35	1.07	0.08	24	1.98	22.37
10/23/2013	103%	104.58	100.58	0.96	0.07	24	1.87	20.83
10/24/2013	103%	92.9	96.97	1.05	0.07	23.6	1.86	21.76
10/28/2013	93%	83.93	90.33	1.12	0.07	22.9	1.58	20.1
10/29/2013	99%	83.97	106.9	1.28	0.08	22.9	1.85	21.99
11/4/2013	91%	152.9	150.56	1.04	0.11	22.5	1.64	20
11/6/2013	96%	175.08	172.62	0.99	0.11	22.4	1.7	20.1
11/7/2013	101%	204.15	170.2	0.83	0.11	22.4	1.64	19.63
11/12/2013	108%	139.64	172.72	1.26	0.09	21.5	1.35	18.84
11/13/2013	99%	128.38	178.53	1.39	0.09	21.2	1.52	19.27
11/14/2013	91%	131.36	172.24	1.32	0.09	21.1	1.65	18.84

Date	COD Mass Balance	OUR (mg/L·hr)	CO ₂ _PR (mg/L·hr)	CO ₂ :O ₂ Ratio	Aerobic SRT (d)	Temp (°C)	f _{CV} Calculated (gCOD/gVSS)	Influent Biomass (gCOD/m ³)
11/19/2013	110%	139.91	144.55	1.13	0.07	20.8	1.16	15.87
11/20/2013	112%	112.76	150.35	1.33	0.07	20.8	1.18	15.87
11/21/2013	96%	109.84	153.9	1.41	0.08	20.6	1.28	17.97
11/25/2013	145%	172.73	181.01	1.3	0.06	20	0.87	18.22
11/26/2013	117%	225.59	163.57	0.74	0.06	20.2	0.7	17.94
12/2/2013	94%	129.57	104.67	0.8	0.05	18.7	1.66	17.44
12/3/2013	81%	121.74	86.1	1.03	0.05	18.6	2.06	18.22
12/4/2013	90%	79.67	102.76	1.3	0.05	18.8	2.36	17.41
12/5/2013	100%	94.78	110.95	1.18	0.05	18.9	2.77	19.35
12/9/2013	60%	118.28	120.93	1.4	0.13	18.7	1.77	34
12/10/2013	109%	140.57	125.59	0.9	0.12	18.4	1.77	26.94
12/11/2013	108%	124.74	124.96	1.01	0.11	18.1	1.68	24.17
12/12/2013	113%	119.33	114.53	0.97	0.09	18.2	1.18	22.67
12/18/2013	129%	129.51	120.66	0.93	0.07	17.4	0.89	24.25

Table 51 S_{Bf} substrate partition fractions

Date	CO ₂ :O ₂ Ratio	$x_{S_{Bf_calc}}$ (gO ₂ /gCOD _{S_{Bf}})	Y _{OHO,MAX} (gCOD _{OHO} /gCOD _{S_{Bf}})	Y _{OHO} (gCOD _{OHO} /gCOD _{S_{Bf}})	Y _{EPS} (gCOD _{EPS} / gCOD _{S_{Bf}})	Y _{STO} (gCOD _{STO} /gCOD _{S_{Bf}})
9/16/2013	1.4	0.795	0.079	0.068	0.038	0.098
9/17/2013	1.45	0.556	0.233	0.168	0.077	0.200
9/18/2013	1.425	0.654	0.160	0.125	0.064	0.158
9/23/2013	1.975	0.132	0.751	0.397	0.105	0.366
9/24/2013	1.975	0.132	0.751	0.397	0.105	0.366
9/25/2013	1.525	0.381	0.400	0.254	0.095	0.270
9/26/2013	1.975	0.132	0.751	0.397	0.105	0.365
9/30/2013	1.4	0.797	0.078	0.067	0.035	0.100
10/1/2013	1.975	0.132	0.751	0.397	0.104	0.367
10/2/2013	1.4	0.798	0.078	0.067	0.035	0.100
10/3/2013	1.4	0.797	0.078	0.068	0.035	0.100
10/15/2013	1.875	0.154	0.713	0.383	0.105	0.357
10/16/2013	1.975	0.132	0.751	0.397	0.105	0.366
10/17/2013	1.925	0.142	0.733	0.391	0.105	0.362
10/21/2013	1.975	0.132	0.751	0.397	0.104	0.366
10/22/2013	1.975	0.132	0.751	0.397	0.105	0.366
10/23/2013	1.975	0.132	0.751	0.397	0.105	0.366
10/24/2013	1.65	0.250	0.566	0.327	0.102	0.322
10/28/2013	1.8	0.177	0.676	0.369	0.102	0.351
10/29/2013	1.975	0.132	0.750	0.397	0.104	0.367
11/4/2013	1.6	0.290	0.512	0.304	0.100	0.306
11/6/2013	1.5	0.426	0.352	0.231	0.090	0.252
11/7/2013	1.4	0.795	0.079	0.068	0.038	0.099
11/12/2013	1.4	0.795	0.079	0.068	0.038	0.099
11/13/2013	1.425	0.654	0.160	0.125	0.063	0.158
11/14/2013	1.975	0.132	0.751	0.397	0.105	0.366

Date	CO ₂ :O ₂ Ratio	x_{SBf_calc} (gO ₂ /gCOD _{SBf})	Y _{OHO,MAX} (gCOD _{OHO} /gCOD _{SBf})	Y _{OHO} (gCOD _{OHO} /gCOD _{SBf})	Y _{EPS} (gCOD _{EPS} / gCOD _{SBf})	Y _{STO} (gCOD _{STO} /gCOD _{SBf})
11/19/2013	1.5	0.426	0.352	0.231	0.091	0.252
11/20/2013	1.45	0.555	0.233	0.169	0.077	0.199
11/21/2013	1.975	0.132	0.751	0.397	0.106	0.365
11/25/2013	1.45	0.555	0.233	0.169	0.078	0.199
11/26/2013	1.45	0.555	0.233	0.169	0.078	0.199
12/2/2013	1.525	0.380	0.402	0.255	0.098	0.267
12/3/2013	1.975	0.132	0.751	0.398	0.107	0.364
12/4/2013	1.975	0.132	0.751	0.398	0.107	0.364
12/5/2013	1.975	0.132	0.751	0.398	0.107	0.364
12/9/2013	1.975	0.132	0.751	0.398	0.107	0.364
12/10/2013	1.75	0.196	0.647	0.359	0.106	0.340
12/11/2013	1.55	0.344	0.444	0.274	0.100	0.281
12/12/2013	1.4	0.790	0.082	0.070	0.045	0.095
12/18/2013	1.4	0.799	0.077	0.067	0.033	0.101
	Average		0.474	0.270	0.085	0.269
	Std Dev		0.277	0.133	0.027	0.106
	Minimum		0.077	0.067	0.033	0.095
	Maximum		0.751	0.398	0.107	0.367

APPENDIX H: HRSD PILOT OFF-GAS DATA

Table 52 HRSD pilot off-gas data

Date	OUR mg/L.hr	CO₂_PR mg/L.hr	CO₂:O₂ Ratio
9/3/2013	55.87	76.98	1.37
9/4/2013	89.22	108.80	1.40
9/5/2013	124.65	125.24	0.99
9/6/2013	113.93	118.64	1.03
9/16/2013	247.80	240.80	0.98
9/17/2013	224.49	241.70	1.08
9/18/2013	229.19	231.33	1.07
9/19/2013	223.56	223.08	1.00
9/20/2013	211.88	207.35	0.98
9/23/2013	69.25	95.10	1.38
9/24/2013	75.26	97.18	1.31
9/25/2013	128.03	130.38	1.05
9/26/2013	189.31	164.32	0.87
9/27/2013	146.33	142.51	0.92
9/30/2013	206.77	173.62	0.92
10/1/2013	188.38	175.62	0.94
10/2/2013	184.00	164.44	0.90
10/3/2013	186.48	156.26	0.84
10/11/2013	69.48	31.41	0.26
10/15/2013	179.12	154.42	0.90
10/16/2013	150.87	137.39	0.92
10/17/2013	164.62	143.76	0.88
10/18/2013	137.43	125.28	0.91
10/21/2013	105.39	102.56	1.18
10/22/2013	96.53	102.35	1.07
10/23/2013	104.58	100.58	0.96
10/24/2013	92.90	96.97	1.05
10/25/2013	83.35	92.92	1.03
10/28/2013	83.95	93.59	1.12

Date	OUR mg/L.hr	CO₂_PR mg/L.hr	CO₂:O₂ Ratio
10/29/2013	83.97	106.90	1.28
10/30/2013	86.22	116.61	1.38
10/31/2013	92.39	113.00	1.23
11/1/2013	104.19	105.24	0.97
11/4/2013	156.78	163.13	1.04
11/5/2013	163.83	176.15	1.08
11/6/2013	175.08	172.62	0.99
11/7/2013	204.15	170.20	0.83
11/8/2013	171.23	148.23	0.83
11/12/2013	142.32	176.48	1.26
11/13/2013	128.55	178.54	1.39
11/14/2013	131.51	172.28	1.32
11/15/2013	112.19	141.03	1.17
11/19/2013	148.81	145.89	1.13
11/20/2013	112.94	150.37	1.33
11/21/2013	110.14	154.11	1.41
11/22/2013	128.13	160.79	1.26
11/25/2013	172.45	183.34	1.30
11/26/2013	225.59	163.57	0.74
11/27/2013	249.62	142.39	0.55
12/2/2013	133.09	106.14	0.80
12/3/2013	124.12	91.30	1.03
12/4/2013	79.67	102.76	1.30
12/5/2013	95.41	111.29	1.18
12/6/2013	103.11	114.88	1.13
12/9/2013	92.87	119.93	1.40
12/10/2013	140.57	125.59	0.90
12/11/2013	124.78	125.00	1.01
12/12/2013	119.33	114.53	0.97

Date	OUR mg/L.hr	CO₂_PR mg/L.hr	CO₂:O₂ Ratio
12/13/2013	109.23	105.67	0.98
12/16/2013	144.32	126.29	0.97
12/18/2013	129.51	120.66	0.93
12/19/2013	109.93	108.45	0.99
12/20/2013	118.03	119.36	1.01
3/24/2014	201.89	74.03	0.37
3/25/2014	148.46	119.44	0.83
3/26/2014	129.55	130.40	1.02
3/27/2014	113.12	139.09	1.23
3/28/2014	123.29	126.39	1.00
3/31/2014	155.64	142.39	0.92
4/1/2014	148.04	158.05	1.07
4/2/2014	141.88	148.88	1.05
4/3/2014	145.77	147.97	1.02
4/4/2014	131.13	118.13	0.89
4/7/2014	145.10	148.03	0.92
4/8/2014	171.00	172.39	1.01
4/9/2014	150.71	167.48	1.12
4/10/2014	106.64	135.70	1.27
4/11/2014	120.80	137.45	1.17
4/14/2014	150.11	158.95	1.09
4/15/2014	151.89	138.60	0.90
4/16/2014	94.06	129.89	1.41
4/17/2014	77.48	136.17	1.80
4/22/2014	145.55	130.46	0.85
4/23/2014	160.78	155.55	0.98
4/24/2014	149.26	153.98	1.04
4/25/2014	157.43	144.92	0.93
4/28/2014	154.26	158.56	1.03

Date	OUR mg/L.hr	CO₂_PR mg/L.hr	CO₂:O₂ Ratio
4/29/2014	130.41	136.72	1.05
4/30/2014	129.34	131.95	1.03
5/1/2014	151.76	142.56	0.94
5/2/2014	146.52	137.13	0.93
5/5/2014	151.63	152.92	1.03
5/6/2014	151.29	148.52	0.98
5/7/2014	143.65	166.80	1.16
5/8/2014	146.30	167.45	1.17
5/9/2014	148.37	172.92	1.18
5/12/2014	148.90	193.37	1.31
5/13/2014	152.03	180.63	1.21
5/14/2014	144.38	174.05	1.21
5/15/2014	148.85	160.17	1.08

REFERENCES

- Bala Subramanian, S., Yan, S., Tyagi, R. D., & Surampalli, R. Y. (2010). Extracellular polymeric substances (EPS) producing bacterial strains of municipal wastewater sludge: Isolation, molecular identification, EPS characterization and performance for sludge settling and dewatering. *Water Research*, 44(7), 2253-2266. doi: <http://dx.doi.org/10.1016/j.watres.2009.12.046>
- Beun, J. J., Dircks, K., Van Loosdrecht, M. C. M., & Heijnen, J. J. (2002). Poly- β -hydroxybutyrate metabolism in dynamically fed mixed microbial cultures. *Water Research*, 36(5), 1167-1180. doi: [http://dx.doi.org/10.1016/S0043-1354\(01\)00317-7](http://dx.doi.org/10.1016/S0043-1354(01)00317-7)
- Beun, J. J., Paletta, F., Van Loosdrecht, M. C. M., & Heijnen, J. J. (2000). Stoichiometry and kinetics of poly--hydroxybutyrate metabolism in aerobic, slow growing, activated sludge cultures. *Biotechnology and Bioengineering*, 67(4), 379-389. doi: 10.1002/(SICI)1097-0290(20000220)67:4<379::AID-BIT1>3.0.CO;2-2
- Boehnke, B., Diering, B., & Zuckut, S. W. (1997). Cost-effective wastewater treatment process for removal of organics and nutrients. *Water Engineering and Management*, 144(5), 5pp-5pp.
- Bohnke, B., & Diering, B. (1986). United States Patent No. 4,568,462. U. S. P. a. T. Office.
- Bott, C. B. (2012). *Nitrogen Removal 3.0: Installation of Full-Scale Sidestream Deammonification and Piloting Mainstream Deammonification*. Powerpoint Presentation. Hampton Roads Sanitation District.

- Carucci, A., Dionisi, D., Majone, M., Rolle, E., & Smurra, P. (2001). Aerobic storage by activated sludge on real wastewater. *Water Research*, 35(16), 3833-3844. doi: 10.1016/S0043-1354(01)00108-7
- Clark, D. P. M., Michael T.; Martinko, John M.; Stahl, David A. (2012). *Brock Biology of Microorganisms 13th edition* (Kindle Edition ed.): Benjamin Cummings.
- Cooper, C. D., & Alley, F. C. (2011). *Air pollution control : A design approach* (4th ed. ed.). Long Grove, Ill: Waveland Press.
- Daigger, G. T., Sanjines, P., Pallansch, K., Sizemore, J., & Wett, B. (2011). Implementation of a full-scale anammox-based facility to treat an anaerobic digestion sidestream at the alexandria sanitation authority water resource facility. *Water Practice and Technology*, 6(2). doi: 10.2166/wpt.2011.033
- Dawes, E. A. (1988). Polyhydroxybutyrate: an intriguing biopolymer. *Bioscience reports*, 8(6), 537-547.
- De Silva, D. G. V., & Rittmann, B. E. (2000). Nonsteady-state modeling of multispecies activated-sludge processes. *Water Environment Research*, 72(5), 554-565.
- Desloover, J., De Clippeleir, H., Boeckx, P., Du Laing, G., Colsen, J., Verstraete, W., & Vlaeminck, S. E. (2011). Floc-based sequential partial nitrification and anammox at full scale with contrasting N₂O emissions. *Water Research*, 45(9), 2811-2821. doi: <http://dx.doi.org/10.1016/j.watres.2011.02.028>
- Dold, P. L., Ekama, G. A., & Marais Van, G. R. (1980). A general model for the activated sludge process. *Progress in water technology*, 12(6), 47-77.

- Ehlers, G. A. C., & Turner, S. J. (2011). Evaluation of extracellular biopolymer and its impact on bioflocculation in activated sludge bioreactors. *Water Science and Technology*, 63(4), 689-694. doi: 10.2166/wst.2011.112
- Ekama, G. A., Dold, P. L., & Marais Van, G. R. (1986). Procedure for determining influent COD fractions and the maximum specific growth rate of heterotrophs in activated sludge systems. *Water Science & Technology*, 18(6), 91-114.
- Flemming, H. C., & Wingender, J. (2001). *Relevance of microbial extracellular polymeric substances (EPSs) - Part I: Structural and ecological aspects*.
- Frolund, B., Griebe, T., & Nielsen, P. H. (1995). Enzymatic activity in the activated-sludge floc matrix. *Applied Microbiology and Biotechnology*, 43(4), 755-761.
- Frolund, B., Palmgren, R., Keiding, K., & Nielsen, P. H. (1996). Extraction of extracellular polymers from activated sludge using a cation exchange resin. *Water Research*, 30(8), 1749-1758. doi: 10.1016/0043-1354(95)00323-1
- Garrido, J. M., van Benthum, W. A. J., van Loosdrecht, M. C. M., & Heijnen, J. J. (1997). Influence of dissolved oxygen concentration on nitrite accumulation in a biofilm airlift suspension reactor. *Biotechnology and Bioengineering*, 53(2), 168-178. doi: 10.1002/(SICI)1097-0290(19970120)53:2<168::AID-BIT6>3.0.CO;2-M
- Grady, C. P. L., Daigger, G. T., & Lim, H. C. (2011). *Biological wastewater treatment* (3rd ed. ed.). Boca Raton, FL: IWA Pub./CRC Press.
- Guisasola, A., Jubany, I., Baeza, J. A., Carrera, J., & Lafuente, J. (2005). Respiriometric estimation of the oxygen affinity constants for biological ammonium and nitrite

- oxidation. *Journal of Chemical Technology and Biotechnology*, 80(4), 388-396. doi: 10.1002/jctb.1202
- Gujer, W., & Henze, M. (1991). *Activated sludge modelling and simulation*. Proceedings of Proceedings of the 15th Biennial Conference of the International Association on Water Pollution Research and Control, July 29, 1990 - August 3, 1990, Kyoto, Jpn.
- Gujer, W., Henze, M., Mino, T., & Vanloosdrecht, M. (1999). Activated Sludge Model No. 3. *Water Science and Technology*, 39(1), 183-193. doi: 10.1016/s0273-1223(98)00785-9
- Haider, S., Svardal, K., Vanrolleghem, P. A., & Kroiss, H. (2003). The effect of low sludge age on wastewater fractionation (SS, SI). *Water Science and Technology*, 47, 203-209.
- Hanada, S., Satoh, H., & Mino, T. (2002). *Measurement of microorganisms with PHA production capability in activated sludge and its implication in activated sludge model No. 3*.
- Hellinga, C., Schellen, A. A. J. C., Mulder, J. W., van Loosdrecht, M. C. M., & Heijnen, J. J. (1998). SHARON process: an innovative method for nitrogen removal from ammonium-rich waste water. *Water Science and Technology*, 37(9), 135-142. doi: 10.1016/S0273-1223(98)00281-9
- Henze, M., Gujer, W., Mino, T., Matsuo, T., Wentzel, M. C., Marais, G. V. R., & Van, L. M. C. M. (1999). Activated sludge model no.2d, ASM2d. *Water Science and Technology*, 39(1), 165-182. doi: 10.1016/S0273-1223(98)00829-4
- Henze, M., Gujer, W., Mino, T., & Van, L. M. C. M. (2000). *Activated Sludge Models ASM1, ASM2, ASM2d and ASM3* (I. Publisher Ed.). London: IWA Publishing.

- Higgins, M. J., & Novak, J. T. (1997). Characterization of exocellular protein and its role in bioflocculation. *Journal of Environmental Engineering*, 123(5), 479-485.
- Hingley, D. (2012). *HRSD - Chesapeake-Elizabeth Treatment Plant Nutrient Removal Pilot Testing*. Technical Memorandum. HDR.
- Insel, G., Yavasbay, A., Ozcan, O., & Cokgor, E. U. (2012). Modeling of simultaneous growth and storage kinetics variation under unsteady feast conditions for aerobic heterotrophic biomass. *Bioprocess and Biosystems Engineering*, 35(8), 1445-1454. doi: 10.1007/s00449-012-0733-1
- Jenni, S., Vlaeminck, S. E., Morgenroth, E., & Udert, K. M. (2014). Successful application of nitrification/anammox to wastewater with elevated organic carbon to ammonia ratios. *Water Research*, 49, 316-326. doi: 10.1016/j.watres.2013.10.073
- Jimenez, J. A. (2002). *Kinetics of COD Removal in the Activated Sludge Process Including Bioflocculation*. (Doctor of Philosophy), University of New Orleans, umi:3084238.
- Jimenez, J. A. (2013). [Personal Communication].
- Jimenez, J. A. (2014). *HRAS Pilot Plant Data*. The Department of Civil and Environmental Engineering. University of New Orleans. Unpublished.
- Jimenez, J. A., Bott, C. B., Murthy, S., Nogaj, T., Randall, A., & Wett, B. (2013). Removal of organic substrate in the high-rate activated sludge process and its kinetics implications. *Submitted to Water Research*.
- Jimenez, J. A., La Motta, E. J., & Parker, D. S. (2005). Kinetics of removal of particulate chemical oxygen demand in the activated-sludge process. *Water Environment Research*, 77(5), 437-446. doi: 10.2175/106143005X67340

- Jimenez, J. A., La Motta, E. J., & Parker, D. S. (2007). Effect of operational parameters on the removal of particulate chemical oxygen demand in the activated sludge process. *Water Environment Research*, 79(9), 984-990. doi: 10.2175/106143007X175717
- Jorand, F., Zartarian, F., Thomas, F., Block, J. C., Bottero, J. Y., Villemin, G., Urbain, V., & Manem, J. (1995). Chemical and structural (2D) linkage between bacteria within activated sludge flocs. *Water Research*, 29(7), 1639-1639. doi: 10.1016/0043-1354(94)00350-G
- Jubany, I., Lafuente, J., Baeza, J. A., & Carrera, J. (2009). Total and stable washout of nitrite oxidizing bacteria from a nitrifying continuous activated sludge system using automatic control based on Oxygen Uptake Rate measurements. *Water Research*, 43(11), 2761-2772.
- Krishna, C., & Van Loosdrecht, M. C. M. (1999). Substrate flux into storage and growth in relation to activated sludge modeling. *Water Research*, 33(14), 3149-3161. doi: 10.1016/S0043-1354(99)00031-7
- Laspidou, C. S., & Rittmann, B. E. (2002a). Non-steady state modeling of extracellular polymeric substances, soluble microbial products, and active and inert biomass. *Water Research*, 36(8), 1983-1992. doi: [http://dx.doi.org/10.1016/S0043-1354\(01\)00414-6](http://dx.doi.org/10.1016/S0043-1354(01)00414-6)
- Laspidou, C. S., & Rittmann, B. E. (2002b). A unified theory for extracellular polymeric substances, soluble microbial products, and active and inert biomass. *Water Research*, 36(11), 2711-2720. doi: [http://dx.doi.org/10.1016/S0043-1354\(01\)00413-4](http://dx.doi.org/10.1016/S0043-1354(01)00413-4)
- Lemaire, R., Marcelino, M., & Yuan, Z. (2008). Achieving the nitrite pathway using aeration phase length control and step-feed in an SBR removing nutrients from abattoir

wastewater. *Biotechnology and Bioengineering*, 100(6), 1228-1236. doi:
10.1002/bit.21844

Li, X. Y., & Yang, S. F. (2007). Influence of loosely bound extracellular polymeric substances (EPS) on the flocculation, sedimentation and dewaterability of activated sludge. *Water Research*, 41(5), 1022-1030. doi:
<http://dx.doi.org/10.1016/j.watres.2006.06.037>

Mamais, D., Jenkins, D., & Pitt, P. (1993). A rapid physical-chemical method for the determination of readily biodegradable soluble COD in municipal wastewater. *Water Research*, 27(1), 195-197.

McCarty, P. L. (1975). Stoichiometry Of Biological Reactions. *Progress in water technology*, 7(1), 157-172.

Melcer, H., & Foundation, W. E. R. (2003). *Methods for Wastewater Characterization in Activated Sludge Modeling*: Water Environment Research Foundation.

Miller, M. (2013). HRSD Pilot Sampling Plan. In C. B. P. M. SP (Ed.), *Microsoft Excel*.

Miller, M. W., Jimenez, J., Murthy, S., Kinnear, D., Wett, B., & Bott, C. B. (2013). *Mechanisms of COD Removal in the Adsorption Stage of the A/B Process*. Proceedings of weftec 2013, Chicago, Illinois.

Miller, M. W., Regmi, P., Bunce, R., Hingley, D. M., Kinnear, D., Wett, B., Murthy, S., & Bott, C. B. (2012). *A/B Process Pilot Optimized for Nitrite Shunt: High Rate Carbon Removal Followed by BNR with Ammonia-Based Cyclic Aeration Control*. Proceedings of weftec 2012, New Orleans, Louisiana.

- Narang, A., Konopka, A., & Ramkrishna, D. (1997). Dynamic analysis of the cybernetic model for diauxic growth. *Chemical Engineering Science*, 52(15), 2567-2578. doi: [http://dx.doi.org/10.1016/S0009-2509\(97\)00073-0](http://dx.doi.org/10.1016/S0009-2509(97)00073-0)
- NCEES. (2011). *Fundamentals of Engineering* (8th ed.). Clemson, S.C: National Council of Examiners for Engineering and Surveying.
- Ni, B.-J., Fang, F., Xie, W.-M., Sun, M., Sheng, G.-P., Li, W.-H., & Yu, H.-Q. (2009). Characterization of extracellular polymeric substances produced by mixed microorganisms in activated sludge with gel-permeating chromatography, excitation-emission matrix fluorescence spectroscopy measurement and kinetic modeling. *Water Research*, 43(5), 1350-1358. doi: 10.1016/j.watres.2008.12.004
- Ni, B.-J., & Yu, H.-Q. (2008). Simulation of heterotrophic storage and growth processes in activated sludge under aerobic conditions. *Chemical Engineering Journal*, 140(1-3), 101-109. doi: 10.1016/j.cej.2007.09.017
- Ni, B.-J., Zeng, R. J., Fang, F., Xu, J., Sheng, G.-P., & Yu, H.-Q. (2009). A novel approach to evaluate the production kinetics of Extracellular Polymeric Substances (EPS) by activated sludge using weighted nonlinear least-squares analysis. *Environmental Science and Technology*, 43(10), 3743-3750. doi: 10.1021/es9001289
- Nogaj, T. M., Randall, A. A., Jimenez, J. A., Takacs, I., Bott, C. B., Miller, M. W., Murthy, S., & Wett, B. (2013). *Mathematical Modeling of Carbon Removal in the High-Rate Activated Sludge System: Model Presentation and Application*. Proceedings of weftec 2013 Chicago, Illinois.

- Pala-Ozkok, I., Rehman, A., Kor-Bicakci, G., Ural, A., Schilhabel, M. B., Ubay-Cokgor, E., Jonas, D., & Orhon, D. (2013). Effect of sludge age on population dynamics and acetate utilization kinetics under aerobic conditions. *Bioresource Technology*, *143*, 68-75.
- Park, C., & Novak, J. T. (2007). Characterization of activated sludge exocellular polymers using several cation-associated extraction methods. *Water Research*, *41*(8), 1679-1688. doi: <http://dx.doi.org/10.1016/j.watres.2007.01.031>
- Peterson, E. E. (1965). *Chemical Reaction Analysis*. Englewood Cliffs, NJ.: Prentice-Hall.
- Pollice, A., Tandoi, V., & Lestingi, C. (2002). Influence of aeration and sludge retention time on ammonium oxidation to nitrite and nitrate. *Water Research*, *36*(10), 2541-2546. doi: 10.1016/S0043-1354(01)00468-7
- Regmi, P., Holgate, B., Miller, M. W., Bunce, R., Park, H., Chandran, K., Wett, B., Murthy, S., & Bott, C. B. (2013). *NOB out-selection in mainstream makes two-stage deammonification and nitrite-shunt possible*. Proceedings of Proceedings of the WEF/IWA Nutrient Removal and Recovery Conference and Exhibition, Vancouver, BC July 28 - 31.
- Regmi, P., Miller, M. W., Bunce, R., Hingley, D. M., Kinnear, D., Wett, B., Murthy, S., & Bott, C. B. (2012). Nitrogen Removal 3.0: A Pilot Study to Evaluate the Feasibility of Mainstream Deammonification. *Water Environment Federation*.
- Regmi, P., Miller, M. W., Holgate, B., Bunce, R., Park, H., Chandran, K., Wett, B., Murthy, S., & Bott, C. B. (2014). Control of aeration, aerobic SRT and COD input for

mainstream nitrification/denitrification. *Water Research*, 57, 162-171. doi:

10.1016/j.watres.2014.03.035

Rittmann, B. E., & McCarty, P. L. (2001). *Environmental biotechnology : principles and applications*. Boston: McGraw-Hill.

Roels, J. A. (1983). *Energetics and kinetics in biotechnology*: ELSEVIER BIOMEDICAL, AMSTERDAM (NETHERLANDS).

Ruiz, G., Jeison, D., & Chamy, R. (2003). Nitrification with high nitrite accumulation for the treatment of wastewater with high ammonia concentration. *Water Research*, 37(6), 1371-1377. doi: [http://dx.doi.org/10.1016/S0043-1354\(02\)00475-X](http://dx.doi.org/10.1016/S0043-1354(02)00475-X)

Schulze-Rettmer, R., & Zuckut, S. W. (1998). Treatment of textile dyeing wastewater by adsorption/bio-oxidation process. *Textile Chemist and Colorist*, 30(5), 19-23.

Sherrard, J. H., & Schroeder, E. D. (1976). Stoichiometry of industrial biological wastewater treatment. *Journal of the Water Pollution Control Federation*, 48(4), 742-747.

Sin, G., Guisasola, A., De Pauw, D. J. W., Baeza, J. A., Carrera, J., & Vanrolleghem, P. A. (2005). A new approach for modelling simultaneous storage and growth processes for activated sludge systems under aerobic conditions. *Biotechnology and Bioengineering*, 92(5), 600-613. doi: 10.1002/bit.20741

Smolders, G. J. F., Van Loosdrecht, M. C. M., & Heijnen, J. J. (1995). *A metabolic model for the biological phosphorus removal process*, Tarrytown, NY, United States.

Steinbüchel, A. (1996). PHB and Other Polyhydroxyalkanoic Acids in Biotechnology. In M. Roehr (Ed.), *Products of Primary Metabolism* (Vol. 6). New York, New York: VCH.

- Strous, M., Heijnen, J. J., Kuenen, J. G., & Jetten, M. S. M. (1998). The sequencing batch reactor as a powerful tool for the study of slowly growing anaerobic ammonium-oxidizing microorganisms. *Applied Microbiology and Biotechnology*, 50(5), 589-596.
- Strous, M., Kuenen, J. G., & Jetten, M. S. M. (1999). Key physiology of anaerobic ammonium oxidation. *Applied and Environmental Microbiology*, 65(7), 3248-3250.
- Takacs, I. (2013). SUMO: Dynamita Inc.
- Third, K. A., Newland, M., & Cord-Ruwisch, R. (2003). The effect of dissolved oxygen on PHB accumulation in activated sludge cultures. *Biotechnology and Bioengineering*, 82(2), 238-250. doi: <http://dx.doi.org/10.1002/bit.10564>
- Van Aalst-Van Leeuwen, M. A., Pot, M. A., Van Loosdrecht, M. C. M., & Heijnen, J. J. (1997). Kinetic modeling of poly(beta-hydroxybutyrate) production and consumption by *Paracoccus pantotrophus* under dynamic substrate supply. *Biotechnology and Bioengineering*, 55(5), 773-782.
- Van Loosdrecht, M. C. M., & Heijnen, J. J. (2002). *Modelling of activated sludge processes with structured biomass*.
- Wett, B. (2007). Development and implementation of a robust deammonification process. *Water Science and Technology*, 56(7), 81-88. doi: 10.2166/wst.2007.611
- Wett, B., Omari, A., Podmirseg, S. M., Han, M., Akintayo, O., Gomez Brandon, M., Murthy, S., Bott, C., Hell, M., Takacs, I., Nyhuis, G., & O'Shaughnessy, M. (2013). Going for mainstream deammonification from bench to full scale for maximized resource efficiency. *Water Science and Technology*, 68(2), 283-289. doi: 10.2166/wst.2013.150